SHEAR TRANSFER IN CRACKED REINFORCED CONCRETE

by

S. G. Millard, B.Sc., C.Eng., M.I.C.E.

Department of Engineering, University of Warwick

A dissertation submitted to the University of Warwick

for the degree of Doctor of Philosophy

1983

PREFACE

This dissertation is based upon the research of the author in the Engineering Department of the University of Warwick from September 1978 until September 1981.

The author is indebted to Professor R. P. Johnson for his stimulating guidance and advice during the course of this study.

Thanks are also due to Mr. A. Redhead and his staff in the structures laboratory for their able assistance in the experimental work, to Miss M. A. Revell for her efficient typing and arrangement of this thesis and to Mrs B. Cotgreave for her assistance with the figures.

Finally the author would like to thank the Science and Engineering Research Council and the Transport and Road Research Laboratory, without whose financial support this study could not have been carried out.

The contents of this dissertation are original except where specific reference is made to the work of others. No part of it has been submitted for a degree or diploma at any other university.

PUBLICATIONS

A discussion of some of the results from this study has been published.

MILLARD, S. G.

'On aggregate interlock mechanism in reinforced concrete plates with extensive cracking'.

Studi e Ricerche, Vol. 3, Corso di Perfezionamento per le Costruzioni in Cemento Armato

Fratelli Pesenti del Politecnico di Milano, Milan 1982

SUMMARY

The objective of this research was to determine the in-plane shear stiffness and strength of a reinforced concrete specimen, which had first been cracked in uniaxial tension. This information could then lead to a more accurate analysis of reinforced concrete structures using the finite element method.

Tests were devised that enabled the effects of aggregate interlock and of dowel action in slab type specimens to be studied independently. As the aggregate interlock and dowel action specimens were similar and were loaded in the same way, a direct comparison of the test results could be made. The composite effects of aggregate interlock and dowel action were then studied by applying the same shear loading to cracked reinforced concrete specimens.

The shear stiffness and strength due to aggregate interlock were typically found to be two to four times as great as those due to dowel action. It was also observed that the crack in the aggregate interlock tests tended to widen as shear slip occurred. This is an effect which has received very little attention in the past. The stiffness normal to the crack that restrains crack widening, and the initial crack width were both observed to have a significant influence on the aggregate interlock shear stiffness. The behaviour of the reinforced concrete specimens was similar to that which was expected from the results of the dowel action and aggregate interlock tests, if the additional effects of local bond were taken into consideration.

Several analytical models of the micro mechanisms of shear resistance within the specimens were studied and formulae were derived to predict their behaviour. A matrix equation for the material properties for cracked concrete was derived and used in a finite element analysis in an attempt to model the behaviour of a reinforced concrete structure.

C O N T E N T S

N O M E N C L A T U R E

A_s	cross section area of reinforcement
E_s	elastic modulus of reinforcement
F_d	dowel force on reinforcement
F_{du}	ultimate dowel force
F_c	direct compressive force in concrete
F_t	tensile force
G_f	foundation modulus
G_o	shear modulus of uncracked concrete
$\bar{G}$	averaged shear modulus of cracked r.c. specimen
K_i	initial stiffness
K_n	axial stiffness normal to crack
K_s	shear stiffness across crack
M_p	plastic moment
P	applied force
V_d	dowel force
C_w	width of crack
f_{ct}	tensile strength of concrete
f_y	yield stress of reinforcement
f_r	relative rib area of reinforcement
ℓe	length of finite element
$\bar{\gamma}$	averaged shear strain of r.c. specimen
Δ_s	shear slip across crack
ϵ_s	strain in reinforcement
μ	coefficient of friction
η, ξ	elemental coordinate factors
ν_c	Poisson ratio for concrete
ρ	reinforcement ratio
σ_s	tensile stress in steel
σ_c	compressive stress in concrete

τ_s shear stress

τ_{ult} ultimate shear stress

ϕ bar diameter

CHAPTER ONE

INTRODUCTION

1.1 Historical background

For over a thousand years concrete has been used as a construction material. It was originally used, like masonry, to withstand compressive forces and also, like masonry, it was found to be weak in tension. The use of concrete as a flexural material, withstanding compression and tension, was developed by the French, over a hundred years ago, by the addition of reinforcing steel, embedded within the tension zone of the concrete. The concrete still cracks at a relatively low tensile stress, but by a redistribution of internal forces, the reinforcing steel carries most of the tensile portion of the applied flexural load. Reinforcement is most commonly used today in the form of deformed steel bars of high-yield steel. There is a complex interface interaction between the concrete and the reinforcement in a cracked tension zone.

Since the 1960s there have been considerable advances in the use of matrix methods of analysis. One of the most versatile of these methods is the finite element method. This method models a structure of continuous form by dividing it into a number of discrete elements. Each element is assigned physical properties which approximate to those of the real structure and is connected to adjacent elements at nodal points. Constraints are placed upon the possible displacement field within each element so that the boundaries of adjacent elements always remain coincident. Using the displacement method, a stiffness matrix for each element can be formulated, relating the nodal forces to their respective nodal displacements. An overall stiffness matrix can then be assembled, incorporating the stiffness matrix for each finite element. For a given

nodal load matrix the nodal displacements can then be determined by inverting the stiffness matrix or otherwise solving the sets of simultaneous equations.

The development of matrix methods of analysis has been paralleled by the development of computer hardware and software capable of manipulating matrices of large magnitude and hence the use of the finite element method for solving structural analysis problems has become increasingly popular. Initially the physical properties of structures under investigation were assumed to be linear and elastic. Research was directed into the development of higher order elements which modelled complex element shapes and stress distributions with greater accuracy. More recently, however attention has been focussed on the use of iterative methods, combined with the finite element method to model the behaviour of structures with non linear physical properties within the working load range. However unless the material properties of the structure are realistically modelled there is little point in using more sophisticated analysis techniques in an attempt for greater accuracy.

1.2 Modelling of the material properties of reinforced concrete

The ability to use finite element methods of analysis for structures with non linear physical properties makes it particularly suitable for analysing reinforced concrete structures. The non linear physical properties of both concrete and reinforcing steel have been well investigated in the past and several models have been developed (1, 2, 3) describing their respective behaviour. Concrete is neither homogeneous nor isotropic but on the macro scale may be considered as such. Methods are available for smoothing out the effects of the reinforcement or otherwise including it into the structural stiffness matrix. However,

once tensile cracking has occurred, there is a complex interaction between the concrete and the reinforcing steel for which no accurate model is yet available.

Because concrete is relatively weak in tension, tensile cracking may well occur at a quite low level of loading. This cracking results in a large change in the axial stiffness of the reinforced concrete. The concrete between cracks still carries some tensile forces, which are transmitted through the reinforcing steel by bond action between the surfaces of the two materials. Research (4, 5) has shown that this bond action is primarily a mechanical keying by the deformed surface of the reinforcing steel with the concrete. At higher stress levels, the bonding gradually breaks down until finally the axial stiffness of the reinforced concrete becomes that of the reinforcing steel alone. Post-cracking interaction of this kind between concrete and reinforcing steel is known as tension stiffening. An accurate knowledge of the tension stiffening effect is needed to model the post-cracking direct stiffness of reinforced concrete using the finite element method. However it may also be needed in order to model the behaviour of cracked reinforced concrete under shear loading.

Cracks form and propagate in reinforced concrete in a direction normal to the direction of principal tensile stress. If the crack surface were plane and the cracks opened normal to these surfaces, there would be no shear transfer across the cracks. However, shear transfer does occur in practice and so a value for the stiffness in shear of a cracked region is needed for use in a numerical analysis. Three areas where shear transfer across cracks does occur have been identified.

1. Anisotropy of the structural material may cause the directions of principal stress and principal strain not to coincide. For example reinforcement crossing a crack at an oblique angle may transfer shear forces even though a direct load normal to the plane of cracking is applied.

2. Tensile cracking of the concrete may result in a redistribution of the internal forces, causing a shear force to be transferred across the cracks, even though the applied load is unaltered. In a simply supported beam with a central concentrated load flexural/shear cracks propagate from the beam soffit towards the neutral axis. Taylor (6) has demonstrated that up to 75% of the shear carried in the beam may be transferred across the cracks. This is only possible if the internal forces have been modified by the cracking.

3. If the directions, the relative magnitudes or the points of application of the external loadings are altered subsequent to tensile cracking then shear will be transferred across the cracks. One example of this could occur in a composite steel/concrete bridge deck. Once the concrete slab has been cast onto steel I-beams the falsework is removed and transverse hogging cracks may occur over the support regions. In a long span bridge the neutral axis is several slab thicknesses below the slab and hence the cracks are effectively axial tensile cracks. When the bridge deck is subsequently subjected to lateral wind loading, this shear loading must be transferred across the cracks to the supports.

1.3 Mechanisms of shear transfer in cracked reinforced concrete

The micro mechanisms involved in transferring shear across cracks in reinforced concrete are complex and not well understood. In the past

many simple approximations have been used for the shear stiffness of cracked reinforced concrete. When the analytical techniques were also quite simple, this was adequate. However, now that intricate structures with complex stress distributions and non linear physical properties can be analysed, a deeper understanding of the internal mechanisms and the distribution of forces is required.

Shear forces will be transmitted across a crack by any material projecting from one side of the crack to the other. The reinforcing steel is primarily intended to carry axial tensile forces. If the reinforcing steel crosses the crack obliquely, there will be a component of its axial force, F_t, parallel to the crack, which will transmit shear force, (Figure 1.1). The stiffness of this mechanism of shear transfer will depend upon the anchorage stiffness of the reinforcing bars, the reinforcement ratio and the angle at which the reinforcing steel intersects the crack.

Shear can also be transferred across a crack by a shear force, F_d, on the reinforcing steel normal to the longitudinal axis. This mechanism, known as dowel action, may be activated when there is a shear slip between the two crack faces. The reinforcing steel acts as a dowel, keying the two faces together. The shear stiffness of the dowel action mechanism will depend upon the flexural and shear stiffness of the reinforcing steel, together with the bearing stiffness of the material supporting the dowel bar reinforcement, adjacent to each crack face.

The third mechanism of the transfer of shear across a crack is the contact and interlocking of aggregate particles and surface roughness of the crack. When reinforced concrete cracks in tension, the line of weakness is usually the interface between the cement matrix and the

aggregate particles. Aggregate particles are thus left embedded in each crack face, with their respective "pockets" on the opposite face. A shear force across the crack causes interlocking of these asperities (Figure 1.2). The degree of contact will depend upon such factors as the initial crack width, the size of the aggregate particles and the degree of embedment. As the crack faces slip across each other, there will be a tendency for the faces to both crush and slide apart. This increase in the crack width will cause an increase in the tensile forces in the reinforcing steel, and hence cause normal compressive forces on the crack face due to equilibrium. Thus it is to be expected that both the degree of crack widening and the axial stiffness provided by the reinforcing steel, normal to the crack, will influence the shear stiffness due to aggregate interlock. Hence the breakdown of local bond between the reinforcement and the concrete will influence the shear stiffness of cracked reinforced concrete, as well as the direct stiffness.

The shear stiffness of a cracked reinforced concrete element must depend upon the spacing and width of the cracks which might be expected to occur. Much work has been done (7, 8) on the study and prediction of the spacing and width of cracks on the surface of reinforced concrete with respect to corrosion of the reinforcing steel and the visual impact of the surface. However, for examining the effects of dowel action and aggregate interlock attention must be focussed upon the variation of the crack width beneath the surface of the concrete. It is to be expected that the entire crack width profile beneath the surface of the concrete will influence the shear stiffness of the reinforced concrete and hence it is necessary to investigate the form of this profile.

The relative effects of aggregate interlock and dowel action will also depend upon the type of structure under load and the configuration and sequence of loading. In a beam, without vertical shear stirrups, one would not expect the effects of dowel action to be significant. The concrete supporting the reinforcement has little bearing stiffness (Figure 1.3). Once horizontal dowel cracking is initiated it will propagate quickly and the dowel action stiffness then becomes negligible.

In a beam with shear stirrups or in a slab under in-plane shear loading, the support to the reinforcing steel acting as dowel bars is more substantial and the effects of dowel action may be more significant. It is necessary therefore, to decide upon the probable application of the investigation before designing test specimens and a loading arrangement.

1.4 Scope of the research

The research programme was planned to investigate the transfer of in-plane shear forces in cracked reinforced concrete slabs and membranes. This was to supplement a continuing programme of research at the University of Warwick on steel-concrete composite beams.

It was decided to limit the area of interest to the study of shear transfer across a single crack with the reinforcement always normal to the plane of cracking. It was considered that, until this simple problem was fully understood, there was little point in extending the research to cover more complex problems. Only increasing monotonic loading was to be used, for the same reasons.

It is often difficult or inappropriate to compare or combine test results from different experiments, where the type of loading, the shape

and size of the test specimen and the physical properties of the materials used in the construction of the specimens may all differ. The research program was planned to examine the separate effects of aggregate interlock and of dowel action, using similar test specimens and loading configurations. Tests on specimens of normal reinforced concrete were then planned, to discover if the stiffness of cracked reinforced concrete could be predicted from the separate stiffnesses due to aggregate interlock and dowel action.

The axial stiffness of the reinforcing steel, insitu in the cracked reinforced concrete specimens, and the variation of the crack width beneath the surface of a reinforced concrete specimen were also investigated. This was because it was thought that the axial stiffness and the crack width profile of the aggregate interlock specimens might differ substantially from those of the reinforced concrete specimens and hence invalidate a direct comparison.

This study of shear in cracked specimens was planned in association with another research programme at the Transport and Road Research Laboratory, for the design, construction and testing, to serviceability and ultimate failure, of a half scale model of a typical motorway bridge deck. Details of this bridge deck are to be found in Chapter 7. It was intended that the results of the present tests would lead to a better understanding and prediction of the behaviour of this half scale model. A finite element analysis of the model was planned, using information about the material properties of cracked elements derived from the small scale test results.

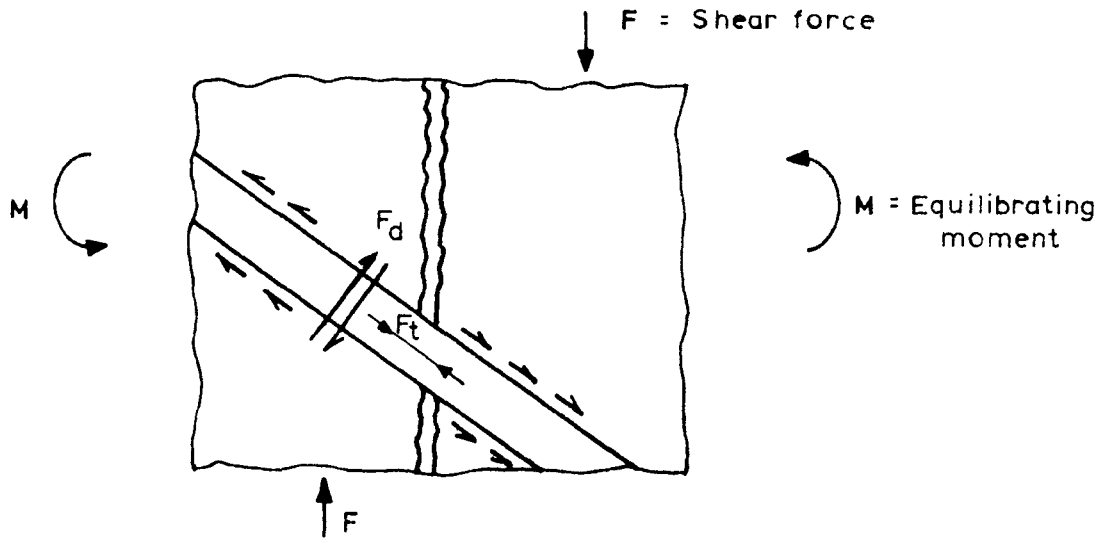

FIGURE 1.1. SHEAR TRANSFER BY THE REINFORCING BARS.

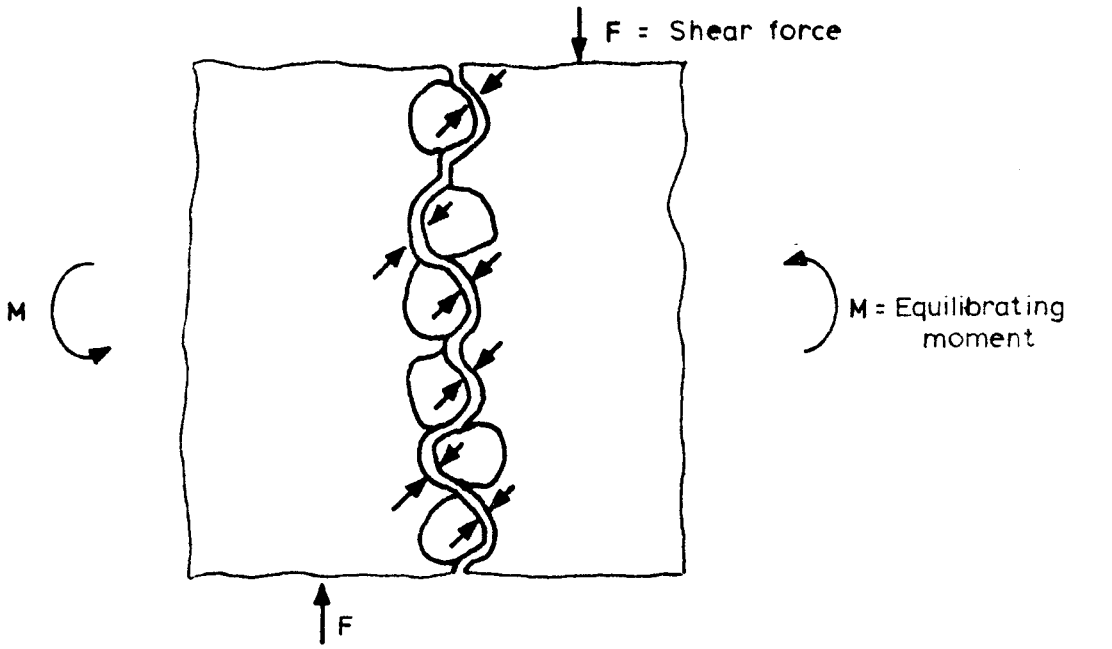

FIGURE 1.2. SHEAR TRANSFER BY THE AGGREGATE PARTICLES.

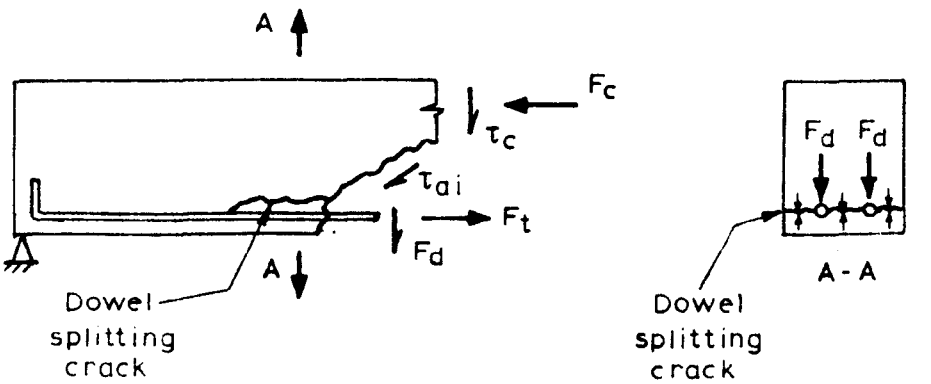

FIGURE 1.3. DOWEL ACTION IN A BEAM, WITHOUT SHEAR LINKS.

CHAPTER TWO

REVIEW OF PREVIOUS RESEARCH

2.1 Methods of analysis of cracked reinforced concrete

2.1.1 Modelling of discrete cracks

During serviceability loading of a reinforced concrete structure tensile cracking can occur, which will cause a significant change in the shear stiffness of the structure. There have been several attempts at modelling this change in stiffness using the finite element method.

One method of modelling cracking is to disconnect the nodes of adjacent elements when the tensile strength of the material has been exceeded. Thus the two elements have nodes with the same spatial coordinates and joined together with a spring linkage which represents the physical properties of the crack. Ngo and Scordelis (9) used this method to model the behaviour of a simply supported reinforced concrete beam. Linear horizontal springs were used to represent bond slip between the reinforcement and the concrete. Rigid vertical links were used to represent the normal interaction between the reinforcement and the concrete (Figure 2.1). There were no linkages connecting opposite sides of the cracked concrete.

This model is not very realistic for several reasons. The linear bond slip stiffness is an oversimplification. There is no modelling of the softening of the concrete beneath the reinforcement due to high bearing stresses, nor is shear interaction across the crack considered. There is no shear transmitted across the cracks, by aggregate interlock, whereas Taylor (6) has shown this to make the greatest contribution to the shear transfer. However the most serious limitation is that the

crack position and orientation are limited to element boundaries, which are fixed when the problem is formulated. In Figure 2.1 the element boundaries follow the approximate paths that flexural and shear cracks would be expected to follow. This would not necessarily be the case in a more general problem. Moreover, the cracks in Figure 2.1 were located in the structure at the beginning of the analysis instead of being progressively formed as the principal tensile stress in each element reached the tensile strength of the concrete.

Nilson (11) also used the method of disconnecting nodes in a finite element analysis to model the tensile cracking of reinforced concrete. A non linear spring linkage was used to model the degradation of bond between the reinforcement and the concrete. A non linear expression was also used for the stiffness of the concrete. Cracking was modelled progressively by disconnecting two elements when the mean value of the principal tensile stress in the two elements reached the tensile strength of the concrete. This meant that a new elemental mesh for the structure was defined. The structure was then reloaded incrementally until another crack was formed.

Using this method of analysis, the behaviour of an eccentric reinforced concrete tensile member was predicted quite closely. However, there were still two drawbacks with the method described. The crack pattern is still restricted to the initial element mesh selected and hence the solution is dependent upon this mesh. Secondly, no interaction across the cracks was allowed for. This did not affect the solution of the tensile member chosen because shear or direct forces would not be expected to be transferred across the cracks. However, in a more general problem the solution may not be so accurate.

Houde (10) improved upon the methods of analysis already discussed by using spring linkages across the cracks in concrete to represent the transfer of shear by aggregate interlock. Similar springs connected the reinforcement to the concrete and represented bond action and dowel action. This method was then used to analyse a simply supported beam (Figure 2.2), where it is known that a significant transfer of shear across the cracks occurs (6). Although the predicted behaviour of the beam was close to the observed behaviour of a test beam the method lacks general applicability. The location of the shear crack was predetermined before the analysis was carried out and was present from zero loading. Any further cracking during the loading was modelled by reducing the entire stiffness of the element concerned to zero, instead of disconnecting further nodes. In a structure with significant compressive stresses parallel to the direction of cracking this method would predict a more flexible behaviour than would realistically occur.

The representation of discrete cracks by disconnecting the nodes of adjacent elements is not a method which readily lends itself to modelling the progressive formation of cracks in any position or direction. The solutions given by the various methods discussed are all dependent upon the original choice of finite element mesh. Cracks are restricted in position and direction to the boundaries of the elements. Gergely and White (12) have recently reported on a method which simulates progressive cracking by redefining the elemental mesh configuration as cracking occurs. Hence the crack path is not restricted to the original element boundaries (Figure 2.3). However, this method must require sophisticated programming and a computer capacity in excess of that which is usually available to solve even the simplest of problems. It is unlikely therefore that this method will become used in structural design.

2.1.2 Modelling of smeared cracking

An alternative method of modelling the cracking of reinforced concrete using the finite element method is to modify the material properties of an element to simulate cracking within the element. Hence the effects of cracking are smoothed throughout the element instead of being represented discretely. In a similar manner the stiffness due to the reinforcement can be smeared uniformly through the element if the spacing of the bars is relatively small.

One method of modelling tensile cracking, used by Isenberg and Adham (13), is to reduce the direct stiffness of an element, normal to the direction of principal tensile stress, when this stress exceeds the tensile strength of the material. The direct stiffness parallel to the direction of cracking and the shear stiffness remained unchanged. Hence,

$$\begin{Bmatrix} \sigma_1 \\ \sigma_2 \\ \tau_{12} \end{Bmatrix} = \begin{bmatrix} D_{11} & \beta D_{12} & 0 \\ \beta D_{21} & \alpha D_{22} & 0 \\ 0 & 0 & D_{33} \end{bmatrix} \begin{Bmatrix} \varepsilon_1 \\ \varepsilon_2 \\ \gamma_{12} \end{Bmatrix} \qquad (2.1)$$

describes the behaviour of the material subsequent to cracking in parallel to the 1 axis. The terms α and β were taken to be constants between unity and zero. When the direction of cracking is not orthogonal to the global axis the material stiffness matrix must be transformed from the local cracking axis 1, 2 to the global axis.

One criticism of this method is that the shear modulus, D_{33}, is left unaltered after cracking has occurred. Thus the crack is modelled as "locking up" in shear, which is not necessarily true in practice. The more usual approach is to use

$$D_{33} = \eta \cdot G_o \qquad (2.2)$$

where $0 < \eta < 1$

when cracking has occurred. Lin and Scordelis (14) and Hand et al. (15) both used a value for η which remained constant for all post-cracking strains.

Cedolin and Dei Poli(78) extended this method to improve the modelling of actual cracks by making η inversely proportional to the tensile strain, normal to the direction of cracking. This was based upon the result that for greater crack widths, the amount of aggregate interlocking across the crack is reduced and hence the shear stiffness is less. It would be possible to modify this even further by making η also a function of the shear strain, γ, to model degradation of the crack faces for high strains. However, it is clear that none of these methods is likely to model accurately the transfer of shear across cracks until a deeper understanding of the basic mechanisms involved is obtained. It is probable that parameters other than the normal and shear strains may affect the transfer of shear across cracks.

2.2 The influence of local bond upon the direct and shear stiffness of cracked reinforced concrete

2.2.1 Crack dilatancy

One effect which has received very little attention in the literature reviewed is the relationship between the direct stress and the shear strain in a cracked reinforced concrete element. When shear strain occurs the rough crack faces tend to slide over each other and cause the crack to widen. This in turn will cause increasing tensile forces in the reinforcing bars crossing the crack and hence compressive forces

in the concrete in a direction normal to the crack, restraining further crack widening. Thus the material stiffness matrix [D] should contain an off-diagonal term, D_{13}, relating the direct stress to the shear strain.

The tendency for the crack to widen, or dilate, as shear slip occurs might also be expected to influence the shear stiffness term, D_{33}. If there was, for some reason, a greater tendency for the crack to widen or if there was an increased stiffness normal to the crack restraining crack widening, this would tend to increase the resistance of the crack faces to sliding and hence to increase the shear stiffness.

To evaluate the effect of crack dilatancy it is first necessary to study the anchorage of the reinforcing bars in concrete, which provide the normal restraint to crack widening. Equilibrium is maintained between the tensile reinforcement forces and the compressive concrete forces via local bond at the concrete-steel interface. It is the shear stiffness of this local bonding which will determine the axial stiffness of the reinforcement crossing the crack. If the reinforcement is inclined to the plane of cracking, the axial stiffness will also provide a component which directly resists shear across the crack.

2.2.2 Extensional stiffness of cracked reinforced concrete

Bresler and Bertero (16) carried out an early investigation into the nature of bond between reinforcing steel and concrete. Experiments were carried out on cylindrical concrete specimens, reinforced with a single, central reinforcing bar (Figure 2.4a). A tensile load was applied to the ends of the reinforcing bar, which had been fitted with a series of internal strain gauges. A groove was cut around the circumference of the cylinder, at the centre of the specimen to

predetermine the location of the crack.

The results of the test, after cracking, showed that high stress concentrations were present in the reinforcement at the ends and at the central crack. (Figure 2.4b). Between these points, tension is transferred into the concrete by bond action and was evaluated by subtracting the force in the reinforcement from the applied load. These results were correlated with an axisymmetric finite element analysis, using a technique developed by Clough and Rashid (17).

Using these results Nilson (11) derived values for the displacements of the steel and the concrete at any point along the bar. From this an empirical third order polynomial equation was formulated relating the local bond slip to the bond stress. This equation was used to represent the stiffness of the bond slip spring linkages, described earlier. The analysis carried out by Nilson predicted that a reinforced concrete specimen still has a considerably greater stiffness than that of a free bar, at steel stresses several times that required to cause the concrete to crack. This effect is known as tension stiffening.

Nilson carried out similar tests to Bresler and Bertero in a later paper (18). Strain gauges embedded in the concrete confirmed the strain distribution in the concrete, which had previously been obtained indirectly. The peak bond stress was observed to be dependent upon the strength of the concrete. However, the relationship between the local bond stress and the slip was also observed to be dependent upon the distance from the free crack surface, where the load is applied (Figure 2.5). This result has not yet been confirmed by further tests, but if true will make implementation in a finite element analysis difficult. It implies that the stiffness of a bond spring linkage or the direct

stiffness of a crack element is not unique but must depend upon the position of the link or element within the structure with respect to the crack positions.

Houde and Mirza (19) also conducted tests on similar specimens to those described in reference 16 and obtained stress distributions in the steel similar to those shown in Figure 2.5. However, the authors were able to find a polynomial relationship between the bond stress and the slip which was independent of the distance from the crack face. It is reported that the distance to the nearest crack face only influenced the descending branch of this curve. The initial slope of the curve is also seen to be half of that proposed by Nilson (18) which suggests that there must be more parameters influencing the bond stress-slip relationship than just the magnitude of the local slip.

In a later paper (20) Mirza and Houde studied the effects of varying the cover to the concrete upon the local bond. It was observed that increasing the cover caused an increase in the amount of end slip for the same stress in the reinforcement. However, this was not observed to affect the local bond stress-slip relationship. The larger section specimens were also observed to carry a greater resultant tensile force in the concrete for a given steel stress than the smaller specimens i.e. more tension stiffening occurs in the larger specimens.

Clark and Speirs (21) investigated tension stiffening in reinforced concrete flexural members on a macroscopic level. Tests were devised to determine the area of concrete associated with each tensile reinforcing bar and the rate of decrease of tension within this concrete area due to increasing breakdown of the bond with the reinforcement at higher strains.

It was found that the maximum tension stiffening force increased with increasing concrete strength and with an increasing area of concrete below the neutral axis. This agrees with the findings of Houde and Mirza (20). However, a study of the local bond effect at a microscopic level would be expected to be a more fruitful direction to follow. If the fundamental nature of local bond and slip is investigated this should lead to an understanding and an accurate predictive model of the axial stiffness of an embedded reinforcing bar.

2.2.3 The mechanism of local bond

Lutz and Gergely (5) studied the problems of tension stiffening, anchorage and cracking of reinforced concrete at a microscopic level by observing the behaviour of a bar with a single rib. It was deduced that bond is comprised of three components:

a) chemical adhesion,

b) friction,

c) mechanical keying of the surface deformations of the reinforcement.

The first two components are the principal mechanism of bond for plain bars, while the third component is the principal mechanism for deformed bars.

The angle of the rib face of deformed reinforcement, (Figure 2.6), was only found to influence the bond properties of the reinforcement if it was less than 40°. The ribs then tend to wedge the concrete apart and cause splitting in the concrete. When the angle of the rib face is greater than 40°, bond slip was said to occur in the following way. First, there is a progressive crushing of the porous concrete paste in

front of each rib. This does not appear to produce significant wedging action until considerable crushing has occurred. The crushed concrete powder then becomes compacted in front of each rib and moves with it. This effectively reduces the rib face angle to 30° to 40° and wedging of the intact concrete then occurs, with resulting splitting cracks along the axis of the bar.

An elastic finite element analysis was carried out to model a single bar centrally embedded in a cylinder of concrete. Separation of the reinforcement and the concrete was assumed, over a length of 1.5 times the bar diameter from each end. Over this region the concrete slip was constrained to move along a rib face angle of 59° (Figure 2.7a). The resulting deformation of the concrete (Figure 2.7b) suggests that the crack width varies significantly below the surface of the concrete.

It is not clear why the authors constrained the ratio of bond slip and separation to an angle of 59° when it was deduced from the test results that 40° was the effective angle of the rib face. The internal profile of the crack width will inevitably be influenced by the amount of bond slip and separation between the concrete and the reinforcement and this topic warrants further investigation.

Goto (22) investigated the formation of internal cracks in a cylindrical reinforced concrete specimen by injecting red ink down a small hole, adjacent to the reinforcement. Primary cracks were initiated by cutting notches around the circumference of the specimen at various spacings. It was discovered that when using parallel ribbed reinforcement, each rib initiated an internal radial crack which was inclined towards the closest primary crack (Figure 2.8). The height of the internal crack from the surface of the bar diminished as the distance to the nearest

primary crack increased and the crack direction became more normal to the reinforcement.

The cracks closed up when the steel stress was reduced and so it was not possible to obtain an accurate profile of the primary crack width from the test results. However, the presence of internal cracks at each reinforcement rib suggests that bond slip may occur by bending of the internal cantilevers formed by these cracks instead of or in addition to sliding and crushing of the concrete.

It was also reported that at higher steel stresses, an internal crack, close to a primary crack, may propagate and reach the surface of the concrete and so become a "secondary crack". Unlike the primary cracks, the secondary cracks were not normal to the reinforcement and the adjacent internal cracks were not inclined towards them. It was found that these secondary cracks were less likely to form if the ribs on the reinforcement were not normal to the longitudinal axis.

The theory that bond slip was accomplished by internal cracking and subsequent bending of the internal cantilevers formed, rather than by crushing and sliding of the concrete over the reinforcement, was supported by Mirza and Houde (20). In tensile tests similar to Goto's, but using different specimen dimensions, it was observed that on cutting the specimens open with a diamond saw, a clearly defined imprint of the reinforcement remained in the concrete. There was no evidence of crushed concrete adjacent to the ribs or of polishing of the concrete due to sliding.

Experiments on the effect of the inclination of the reinforcement ribs to the bar surface on the bond slip properties of the reinforcement

were carried out by Soretz and Hölzenbein (23). It was found that ribbing closer to 90° to the axis of the reinforcement gave an increased bond slip stiffness. However, the relative rib area, defined as the ratio of the area of the rib face to the surface area of the reinforcement between two ribs, was observed to have a much greater influence upon the bond slip stiffness. It was confirmed that the angle of the rib face did not affect the bond properties of the reinforcement, if it was between 45° and 90°. The internal mechanism for bond slip with different rib patterns was, unfortunately, not investigated.

The relative rib area, f_r, is commonly used on the Continent to define the bond properties of reinforcement. Experiments by Martin (24) on reinforcing bars embedded over a short length in concrete have resulted in the empirical expression

$$\frac{\tau_x}{f'_{cc}} = a_o + b_o \Delta_s^{1/\beta} \qquad (2.3)$$

where τ_x = the shear stress on the surface of the reinforcement

f'_{cc} = the compressive strength of a concrete cylinder

Δ_s = the shear slip in cm.

a_o, b_o, β are constant for a given relative rib area, f_r

From equilibrium the change of stress in the steel over a length dx is equal to the shear transferred to the concrete.

$$\frac{d\sigma_s}{dx} = \frac{\Sigma u}{A_s} \cdot \tau_x \qquad (2.4)$$

and from comptibility of deformations

$$\frac{d\Delta_s}{dx} = \frac{\sigma_{sx}}{E_s}\left(1 - \frac{\sigma_{cx}}{\sigma_{sx}} \cdot \frac{E_s}{E_c}\right) \qquad (2.5)$$

where σ_{sx}, σ_{cx} = steel and concrete stresses at a distance x from the primary crack face

Σu = circumference of reinforcement

A_s = area of reinforcement

The values of a_o, b_o and β, found experimentally by Martin, are given in Table 2.1.

A numerical solution of equations 2.4 and 2.5 gives the results shown in Figure 2.9. It is important to note that the equation 2.3 is based upon the concept of bond slip being a frictional sliding mechanism which deteriorates at high values of shear slip. The solution of these equations utilizes the assumption, made by Schiessl (27), that strain in the concrete is negligible. Hence the shear slip at the end face is equivalent to the elongation of the steel. Equation 2.3 does not involve the geometry of the concrete in which the reinforcement is embedded, because it is assumed to be rigid. However, this assumption cannot be completely valid because it has been shown (21) that altering the size of the specimen results in a different tension stiffening effect in the concrete.

2.2.4 Internal crack widths

The local bond between the concrete and the reinforcement will not only affect the shear stiffness of a crack by influencing the direct tensile stiffness normal to the crack. The local bond may also influence the

width of a crack within a reinforced concrete specimen and hence affect the interlocking of the aggregate particles.

One of the first studies of internal cracks was carried out by Broms (26). Using a similar testing procedure to that later used by Goto (22), the author injected coloured epoxy resin into internal cracks. When the resin had hardened, the tensile force on the reinforcing bar was removed. The specimen was then cut open adjacent to the bar to reveal the cracks. It was not possible to corroborate Goto's findings, that each reinforcement rib initiated an internal crack, because the reinforcing bar itself was not visible. The author was more interested in the relationship between the spacing and the length of internal cracks. For the cracks in the specimens which did propagate to the surface of the specimen, the author measured the surface crack width to be about three times that of the width at the surface of the reinforcement.

However, Broms did not find any secondary cracks reaching the surface adjacent to primary cracks. The largest internal cracks tended to be those furthest from the primary cracks, which was the opposite of the results found by Goto. The theory which Broms (26) used to explain his results seems oversimplified. All the tensile force in the reinforcement is assumed to be transferred to the concrete at the primary crack face. There is assumed to be no internal interaction between the reinforcement and the concrete. Disparity between the test results and those of Goto may be due to the differing geometry of the test specimens. By using crack initiators, Goto forced his primary cracks to form at almost the maximum spacing normally found to occur. Broms did nothing to predetermine the location of primary cracks and this may explain why secondary cracks did not appear on the surface.

The tests of Goto were repeated by Illston and Stevens (27), using reinforcement with ribs inclined to the axis of the bar instead of normal to the axis as previously used. A resin injection technique, similar to that developed by Broms, was used to examine the internal cracking. The results differed from those of Goto in several respects. Cracks were not in general found to be initiated by reinforcement ribs and were far less numerous. No secondary cracks were observed and primary cracks were found to have significant widths at the surface of the reinforcement. The ratio of the widths at the surface of the concrete and at the surface of the reinforcement was about two to one.

It is possible that, like Broms, Illston and Stevens did not observe secondary cracking because the use of surface crack initiators, to obtain the maximum possible crack spacing, is not reported. If the crack spacing is large, the longitudinal displacement of the steel relative to the concrete adjacent to a primary crack face will be high. Hence an adjacent internal crack may propagate to the surface of the concrete. However, it is also probable that the use of inclined ribbed reinforcement in place of lateral ribbed reinforcement had an influence upon the test results. The inclined ribbing may cause a reduction in the local bond stresses and a greater tendency for slipping instead of internal cracking. This would explain the absence of internal cracks at every rib, as found by Goto, and also the high crack widths at the surface of the reinforcement.

An attempt to model the shape of a crack by carrying out a three dimensional finite element analysis of a tensile reinforced concrete specimen is reported by Johnson (28). The displacement of the end faces, which can be considered as crack faces, is shown on Figure 2.10. This analysis has not yet been extended to include bond slip or any type

of internal cracking and hence the crack profile obtained is probably unrealistically narrow close to the reinforcement.

Bresler and Bertero (16) carried out an axisymmetric finite element analysis to model a cylindrical reinforced concrete tensile specimen. Adjacent to the reinforcement the Young's modulus of the concrete elements was reduced to model bond slip. This had the effect of changing the tapered crack, obtained without bond slip, into a crack which was of nearly uniform width, (Figure 2.36). The crack shape is closer to that found by Illston and Stevens, using inclined ribbing, than by Broms, using lateral ribbing. It can be inferred that slip between the concrete and the reinforcement does influence the internal crack width and the geometry of the rib may affect the degree of slip.

It is apparent from this review that the problem of predicting crack widths has not been completely resolved. The type of reinforcement used does seem to influence the variation of the crack width beneath the surface of the concrete and also the formation of internal cracks, between the principal cracks. None of the investigations into internal crack width variation has considered the use of double helical ribbed reinforcement, e.g. GKN Torbar. As this is one of the most common rib patterns used in the United Kingdom, it was chosen for use in this project and hence it will be necessary to determine how its use influences the internal crack width profile. It is also not clear whether the relative rib area is a useful parameter to describe the anchorage properties of this type of bar. It will certainly be necessary to correlate the axial tensile stiffness of this type of reinforcement embedded in concrete with the existing formulae described, before they may be used with confidence.

2.3 Dowel action in cracked reinforced concrete

2.3.1 Mechanisms of dowel action

Dowel action is the transferring of shear forces by reinforcing bars which cross a crack and resist flexural or shear forces normal to the axis of the bars. Paulay, Park and Phillips (29) identified three separate mechanisms by which shear can be transferred across a crack by the reinforcement.

1. Direct shear of the reinforcement

This is the primary deformation mode which occurs when the span to depth ratio of a fixed-ended beam is less than unity, (Figure 2.11a). The ultimate shear capacity of a circular bar is given as

$$V_d = \frac{A_s f_y}{\sqrt{3}} \qquad (2.6)$$

Although the bar diameter may be two orders of magnitude greater than the crack width, direct shear is not considered to be an important mode of deformation. The concrete surrounding the bar is not rigid and hence the effective span of the bar will be much greater than the crack width. Failure is more likely to occur by crushing of the concrete beneath the bar or by tensile splitting rather than a shear failure of the steel.

2. Kinking of the reinforcement

If the shear slip causes a large deformation of the reinforcement, the component of the axial reinforcement force parallel to the crack will resist shear (Figure 2.11b). If the reinforcement is not normal to the direction of cracking there will be considerable shear transfer through axial forces in the reinforcement, without kinking, and a knowledge of

the axial stiffness of a bar embedded in concrete, discussed in section 2.2.1, becomes important. However there has been controversy over whether sufficient kinking of the reinforcement across a crack does occur to be significant.

In his original yield line theory Johansen (30) ignored kinking of reinforcement passing obliquely across a crack. Wood (31) found that this assumption gave over-conservative results for the ultimate strength of a reinforced concrete one-way slab and proposed a "complete kinking" theory. Hence the ultimate force normal to the crack was given by $A_s f_y$ and not $A_s f_y \cos \theta$ as suggested by Johansen.

Further tests by Kwiecinski (32), Prince and Kemp (33) and Mills (34) suggest that there is a partial kinking of the reinforcement across cracks. Morley (35) did not find significant distortion of the reinforcement across cracks but suggested that this might be because the crack often tends to travel parallel to the reinforcement when it is close to the reinforcement. Thus for a given crack width, the distortion of the reinforcement from its original orientation becomes insignificant.

All these studies have been carried out by observing the flexural behaviour of a slab with reinforcement oblique to the axis of principal moment. In a situation where tensile forces cause cracking in a slab and shear is subsequently applied to the crack, kinking may be more significant. However, it is necessary to develop large shear displacements across the crack before the reinforcement will deviate substantially from its original line. This will again be limited by the concrete strength and, like shearing, kinking is not generally considered to be an important mode of shear transfer.

3. Flexure of the reinforcement

This deformation mode becomes significant when the span of a fixed-ended beam is greater than its depth, (Figure 2.11c). The relatively low stiffness of concrete means that this is probably the most important mode of behaviour of a dowel bar. Friberg (36) identified three components of deflection due to bending of the bar.

$$\Delta_{total} = \Delta_o + \frac{d\,\Delta_o}{dx} \cdot w + \Delta_w \qquad (2.7)$$

where Δ_o is the bending deflection within the concrete,

w is the crack width

and Δ_w is the bending deflection across the crack.

However, the size of a crack is usually so small that only the first term in this equation is important.

2.3.2 Modes of failure of dowel bars

The ultimate failure of a dowel bar will depend upon the type of specimen tested. Jimenez, Gergely and White (37) identified the following different types of failure.

A dowel bar will initially follow the load-deflection curve A in Figure 2.12. At a fairly low load level internal radial cracks form in the concrete due to the localised bearing stresses. If the concrete is well restrained or there is a high cover to the dowel bar these cracks will not propagate to the surface. Failure will ultimately occur by crushing of the concrete beneath the bar or by yielding of the bar in bending.

Where there is little support given to the reinforcement once cracking has commenced, the crack will propagate along the bar and failure will be immediate. This is a typical mode of failure in an over-reinforced beam without shear links and is shown by curve B on Figure 2.12.

Stanton (38) carried out a plane stress elastic analysis to model a dowel bar embedded in concrete. The circumferential tensile stress σ_ψ was given by

$$\sigma_\psi = \mu \cdot \frac{F_d}{\pi R} \qquad (2.8)$$

where F_d is the dowel force per unit length of bar

and R is the radius of the bar.

μ is a parameter dependent upon the location of the point of interest.

e.g. $\mu = 0.688$ beneath the dowel bar

and $\mu = 1.274$ on a radius perpendicular to the applied force vector

Thus a radial splitting crack which is normal to the direction of the dowel force will occur unless confinement of the concrete or a local plane of weakness causes radial cracking in another direction.

If shear links or lateral reinforcement are provided which give support to the reinforcement then curve C will describe the load-displacement response. Failure will then occur when the dowel bars yield or when the secondary steel yields or fails in shear itself. It can be seen from these curves that dowel bars in a beam will behave quite differently from those in a cracked slab under in-plane shear loading. The results of tests on beam type specimens are only relevant to the present study at loads below that which causes dowel cracking along the axis of the bar.

The authors also reported that the presence of an axial tensile force in the reinforcement caused the beam type of specimen to split at a lower load (curve D). It is not clear however what would be the effect of an axial force on a dowel specimen which was not prone to splitting.

2.4 Dowel action tests

The tests on dowel action which have been carried out can be subdivided into three groups

- Divided beam tests, in which the central part of the beam is cast separately from the rest of the beam. Dowel forces are applied by loading the central region (Figure 2.13a).

- Beam end tests, in which a specimen is cast and loaded to simulate the state of stress in the end of a beam after shear cracking has occurred (Figure 2.13b).

- Direct shear tests, in which the dowel bars are embedded in slab type specimens and then loaded with in-plane shear (Figure 2.13c).

2.4.1 Divided beam tests

The divided beam test has been used by a number of research workers (39, 40) studying the dowel action mechanism. The test applies simultaneous shear and axial tension to the reinforcing bars. The relative proportions of these forces is determined by the geometry of the beam and the centre section.

All the divided beam specimens failed ultimately by the formation of a splitting crack, propagating along the axis of the reinforcing bar. This crack would occur on the side or the soffit of the beam depending

upon the relative cover in each direction. It is only the behaviour of these specimens before splitting cracks occurred which is of relevance to this study.

It was observed that increasing the tension in the reinforcement tended to "soften" the concrete and hence reduce the shear stiffness of the dowel mechanism. Krefield and Thurston (39) discovered that with a very large concrete cover to the reinforcement, the splitting of the concrete was more gradual and the shear stiffness before splitting failure was greater. Increasing the diameter of the reinforcement resulted in a greater dowel stiffness before cracking occurred but the ultimate load was in fact lower. This is probably because the area of concrete resisting splitting was reduced by using larger diameter bars. Empirical formulae were derived by both authors to describe the behaviour of dowel bars. However, these would appear to be limited in their applicability to specimens of similar geometry.

2.4.2 Beam end tests

In a beam end test there is again very little concrete supporting the bar (Figure 2.13b) and the failure mechanism is the tensile splitting of concrete around the reinforcement. A greater degree of control is available over the axial tensile stresses in the reinforcement than with the divided beam tests. The beam end test can also be used to examine the anchorage properties of reinforcement with or without dowel forces present.

Houde (10) carried out a number of tests on beam-end specimens and observed similar results to those of the tests on divided beams. It was also observed that the dowel capacity was not influenced by the axial force in the reinforcement if this was less than 60% of the

ultimate axial force. The influence of the axial force upon the dowel stiffness before cracking was unfortunately not examined.

Beam end tests by Fenwick and Paulay (41) revealed the importance of the orientation and position of the reinforcement during casting upon the dowel stiffness. During placing and compaction of the concrete air and excess water tends to become trapped beneath the reinforcement and this results in a layer of softer and weaker concrete. This effect is more significant for bars close to the upper surface. If the dowel loading is subsequently applied such that the bars are supported by this weaker region (Figure 2.14), the dowel stiffness can be reduced by up to 40%.

2.4.3 Direct dowel tests

In the direct dowel tests the reinforcement is embedded in a slab and is subjected to in-plane shear. The splitting stresses in the concrete are the same as before but the major difference is that when splitting starts to occur, there is sufficient concrete beneath the reinforcement to permit a redistribution of the internal forces. The bearing stress beneath the reinforcement increases, but the splitting crack does not propagate. Failure is either by yielding of the reinforcement or by bearing failure of the concrete.

During an investigation of construction joints, Paulay, Park and Phillips (29) tested a few direct shear specimens with a smooth, waxed interface, so that only dowel bars resisted the shear. The results indicated that the ultimate dowel load was proportional to the area of cross section of the reinforcement, irrespective of the diameter of bar used. From the three models of dowel action examined (Figure 2.11) it was deduced that the mechanism of shear transfer must be due to

kinking or direct shear of the bars. This deduction is not in agreement with the results and theories of other research discussed in this Chapter. However, Walraven (42) has shown that if the model of a beam on elastic foundations is used to describe the behaviour of dowel bar bending, instead of the fully fixed, free-spanning beam in Figure 2.11c, the results in Figure 2.15 are compatible with this theory.

Den Hartog (45) analysed a semi-infinite beam on an elastic foundation (B.E.F.) with a point load, F_d, at the end (Figure 2.16). The end deflection was given by

$$\Delta_o = \frac{2 \beta F_d}{k} \qquad (2.9)$$

where $\beta = \left(\frac{k}{4 E_s I_s}\right)^{1/4}$,

and k is the stiffness of the spring foundation, per unit length of beam. Now if the beam is considered as a cylindrical bar,

$$I_s = \frac{\pi \phi^4}{64}$$

If G_f is the foundation modulus for concrete (in units of force x length^{-3}),

then $k = G_f \phi$

Hence

$$F_d = C \Delta_o \phi^{1.75} G_f^{0.75} E_s^{0.25} . \qquad (2.10)$$

This would explain why the curves in Figure 2.15 have similar initial stiffnesses. However, the model predicts a linear load-deflection

behaviour and hence will not predict the failure mode or the ultimate load of a dowel bar.

Elliott (46), Stanton (38) and Jimenez, Gergely and White (37) all used direct shear specimens to study the effects of dowel action. In each test series it was noted that the early part of the load-deflection curve for dowel bars could be modelled quite closely by the B.E.F. analysis. However, this analysis was in each case found to give a poor correlation with experimental results after the onset of concrete crushing beneath the dowel bars.

A simplified B.E.F. model was developed by Dulacska (43, 44) to predict the ultimate failure load of a series of direct shear tests (Figure 2.17a). The B.E.F. theory predicts that the distribution of reaction loads supporting the beam is that of a damped sinusoid (Figure 2.17b). This was simplified by the author to a triangular distribution (Figure 2.17c). Furthermore, where the concrete stress has exceeded the crushing stress the concrete was assumed to behave plastically. Ultimate failure occurs when the plastic moment in the bar is reached. The ultimate dowel force was given by

$$F_{du} = 0.2\ \phi^2\ f_{sy}\ \sin\theta\left(\left[1 + \frac{f_{cc}}{0.03\ f_{sy}\ \sin^2\theta}\right]^{1/2} - 1\right)$$

where f_{sy} = yield stress of the steel

θ = angle of inclination of the dowel bar

f_{cc} = cylinder crushing strength of concrete.

When $\theta = 0$, this equation simplifies to

$$F_{du} = 1.16\ \phi^2\ f_{sy}^{1/2}\ f_{cc}^{1/2} \qquad (2.11)$$

The nearly elastic-plastic behaviour of the test specimens (Figure 2.18) was consistent with the proposed theory of failure. However the concept of plasticity in concrete once the ultimate compressive stress is attained is not very credible. This probably explains why the author was unable to derive a fundamental relationship for the load-deflection response of a dowel bar before ultimate loading was reached. Instead an empirical expression was found to fit the test data.

A similar expression to equation 2.11 was derived by Rasmussen (47) to predict the ultimate capacity of reinforcement or bolts embedded in concrete. The stiffness of the concrete is assumed to diminish once the compressive strength is reached at the face of the crack. The load is therefore redistributed to the concrete further away from the crack (Figure 2.19) until a plastic hinge ultimately forms in the bar at some distance remote from the crack face.

The theoretical model of dowel failure proposed by Dulacska and Rasmussen agrees quite closely with the experimental results. However it should be realised that this type of failure will only occur if the concrete is sufficiently well restrained not to fail first in splitting. The model does not consider what the predicted failure load will be if the dowel force is combined with axial tension, as will usually occur in practice. It is clear that the ultimate plastic moment of the bar will be reduced by an axial force. It is reasonable to expect however that the axial tension in the bar may also damage the concrete supporting the bar. This would cause a more rapid redistribution of the bearing stress resultant away from the crack and hence cause a reduction in the initial dowel stiffness and in the ultimate dowel force.

White and Gergely (48) carried out some direct dowel tests with superimposed axial tension in the reinforcement. It was observed that with zero axial stress a foundation modulus of 820 N/mm^3 was present. As the axial stress was increased, the foundation modulus decreased linearly, until with an axial stress of 350 N/mm^2 the foundation modulus was 410 N/mm^3.

Walraven (42) argued that, as well as softening of the concrete foundation beneath the reinforcement, a tensile force in the bar may cause internal cracking of the type discovered by Goto (22), (Figure 2.8). If the internal cracks adjacent to the primary crack propagate and meet it, the effective free length of the reinforcement unsupported by concrete will be considerably greater than the measured crack width. Flexure of the reinforcing bar over this unsupported length will also reduce the dowel stiffness.

An empirical expression for the dowel force as a function of the shear slip and the crack width was proposed, based upon the test data from reference (29) and (46)

$$F_d = 10(C_w + 0.2)^{-1} \Delta_s^{0.36} \phi^{1.75} f_{cu}^{0.38} \qquad (2.12)$$

where F_d is the dowel force in Newtons

Δ_s and C_w are the shear slip and the crack width in mm

f_{cu} is the crushing strength of concrete in N/mm^2 and ϕ is the bar diameter in mm.

To summarise the research work presented, it would seem that the B.E.F. model can predict with a reasonable accuracy the initial stiffness of a dowel bar whilst the concrete is still elastic. However, once the

concrete starts to crush or split locally the model is no longer realistic. It may be possible to model this localised damage by reducing the overall foundation modulus for the concrete, but at best this will only be an empirical approximation which is unlikely to be generally applicable. In the absence of tensile splitting causing ultimate failure, equation 2.11 gives a reasonable prediction of the ultimate dowel force. This equation has the advantage that its derivation does not rely upon any assumptions about the stiffness of locally damaged concrete. More information is required upon the shape of the load-deflection curve for a dowel bar once non linearity starts to occur and up to ultimate loading. The effects of axial loading upon the dowel stiffness and upon the ultimate dowel force also need to be studied.

2.5 Aggregate interlock in cracked concrete

When reinforced concrete cracks in tension the resulting crack faces are rough and irregular. The aggregate particles will either remain embedded in the concrete and project across the crack or they may be fractured by the crack. The degree of fracture must depend upon the relative strengths of the concrete mortar and the aggregate and also upon the strength of the bond between these two constituents.

If there is a subsequent displacement of the two crack faces, parallel to the plane of cracking, the crack asperities will interlock with the opposite crack face and resist the displacement. The interlocking faces are unlikely to be normal to the plane of cracking and so there is a tendency for the crack to wedge open. Reinforcement crossing the crack will provide a restraint to this crack widening.

2.5.1 Tests on aggregate interlock

One of the early investigations into aggregate interlock, was carried out by Fenwick and Paulay (41). A concrete specimen was cracked by applying an indirect tensile splitting force. A direct shear load was then applied incrementally to the crack (Figure 2.20a). After each increment of loading the crack width was restored to its initial value by applying a compressive force normal to the crack.

It was observed that the crack width had a large influence over the shear stiffness of the crack (Figure 2.20b). The strength of the concrete also influenced the shear stiffness, but to a lesser degree (Figure 2.20c). All the specimens failed ultimately by additional cracking of the specimen, caused by undesirable bending moments remote from the crack. It is unfortunate that the normal force, required to maintain the constant crack width, is not reported. Hence it is not known what tendency there was for the crack to widen. An empirical expression was found to describe the shear stiffness of the cracked specimens.

Using a similar testing arrangement, Houde and Mirza (19) observed similar trends and also observed that varying the size of the aggregate did not influence the shear stiffness. Again an empirical, dimensionally inconsistent expression was derived to describe the aggregate interlock shear stiffness.

The tests of Houde (19) and Fenwick and Paulay (41) are limited to values of shear stress less than 1.5 N/mm^2 because the specimens were prone to flexural failure in both cases. However, within this range of specimens tested, Houde had a significantly higher shear stiffness, especially for specimens with small initial cracks. It is not

clear why this difference occurred. It may have been due to differences in the casting of the specimens or in the stiffness of the test rig used. However it does highlight the problems in using test results from a particular experiment to derive predictive formulae for general application, without an understanding of the fundamental mode of behaviour.

The specimens used by Paulay and Loeber (50) were not prone to flexural failure and the ultimate load was reached when the concrete on each crack face began to crush. A bilinear force-displacement curve was obtained, when the crack width was held constant, (Figure 21). The authors attributed this to a "no load slip", during which the crack faces were coming into contact with each other. Houde (10) disputed this hypothesis and argued that at high stress levels the localised crushing of concrete on each crack face would increase the area of contact. This could increase the shear stiffness of the specimen and explain the strain hardening results obtained. However, this would depend upon how the shear forces were being resisted. If the mechanism is primarily a frictional one, then the shear stiffness would be independent of the area of contact.

It was confirmed by Paulay and Loeber that altering the size of the aggregate did not significantly influence the aggregate interlock shear stiffness. Tests were also carried out using both angular and rounded aggregates but no great difference in the test results were observed.

Tests were then carried out in which the crack width was allowed to increase proportionally with the applied shear stress. The resulting shear stress-displacement curve was then compared to that which could

be predicted using the constant crack width test results (Figure 2.21b). The assumption made in making this comparison was that the aggregate interlock action is independent of its history i.e. the shear stress obtained by opening a crack and then applying a shear displacement will be the same as that obtained by shearing the crack at constant crack width and then subsequently widening the crack. It can be seen from Figure 2.21b that the mean experimental result is rather lower than predicted which implies that there may be some history dependence.

Taylor (6) designed a test rig that imposed a predetermined ratio of crack widening to shear slip, in order to simulate the flexural widening of a tensile crack, resisting shear in a beam. Shear loading with an externally applied crack widening is not directly comparable with in-plane shear in a slab, where the crack widening is caused by internal overriding of the crack faces. However, there were some results from this work which are of relevance to in-plane shear in slabs.

It was observed that the ultimate shear capacity increased with increasing concrete strength. However, if the concrete strength was greater than that of the aggregate used, the ultimate shear strength was considerably lower than if a weaker mix was used. The explanation for this behaviour was that, for a strong concrete mix, the aggregate particles themselves failed in tension and hence there was little aggregate interlock action over the resulting smooth crack face. With a weaker concrete, the crack followed the aggregate-cement paste interface and the resulting aggregate particles protruding from each crack face generated a high level of interlock.

Over the last ten years there has been a continuous programme of research into shear transfer across cracks in reinforced concrete at Cornell University, New York. The main focus of attention has been into cyclic shear loading, such as that occurring during an earthquake. However, the results of the first cycle of loading are relevant to this project and are reviewed here.

In the aggregate interlock tests conducted by White and Holley (52), the crack was allowed to widen as shear slip and overriding occurred. The stiffness normal to the crack resisting overriding was held constant by using external clamping bars (Figure 2.22a). External bars such as these have no bond with the concrete and so their effective axial stiffness remains constant until the yield stress is reached.

The specimens were cracked by the application of transverse splitting forces to a central notch and the initial crack width was preset by adjusting the external clamping bars. Typical results are shown in Figure 2.22b. It was observed that decreasing the initial crack width or increasing the normal restraint stiffness resulted in a higher shear stiffness and ultimate load. However, contrary to the observations of Houde (10) and Paulay (50), the use of larger aggregates was found to reduce the shear stiffness. This could possibly be attributed to the fact that the different sized aggregates originated from different sources and perhaps had different strengths. Alternatively this difference could be due to the fact that the authors tested specimens with very large crack widths (0.75 to 2.5 mm), where the use of larger aggregates would be expected to have an effect.

In all the tests, there was little visible damage to the crack faces.

Only when the specimens were loaded monotonically to their ultimate capacity (2 - 3 N/mm^2) was crushed concrete powder and aggregate visible inside the crack.

This work was later extended by Laible, White and Gergely (53) to study a wider range of parameters. Both the shear slip and the crack width were found to be proportional to the applied shear load in the first load cycle, which was at a quite low stress intensity (1.2 N/mm^2). The normal force restraining the crack from widening was always observed to be less than 65% of the applied shear force. It was noted that the shear stiffness of the specimens was sensitive to changes in the initial crack width but that the ultimate strength was less dependent upon the crack width but more dependent upon the compressive force normal to the plane of cracking.

2.5.2 Theories of aggregate interlock

2.5.2.1 Local/global roughness

Based upon their experimental results Laible, White and Gergely (53) put forward a theory that aggregate interlock was comprised of two separate modes of behaviour. It was suggested that the roughness of a crack face contained a local and a global roughness (Figure 2.23). The local roughness was said to resist shear through a bearing or a crushing mode of behaviour. The global roughness was said to resist shear through a frictional mode of behaviour. It was also argued that when the initial crack width was less than 0.25 mm, the bearing mode of behaviour predominated. Thus the shear stiffness was sensitive to the initial crack width but there was little tendency for the crack to wedge open and so the shear stiffness was not very sensitive to the normal restraint stiffness. For an initial crack width of 0.5 mm or greater, the friction mode of behaviour predominated and hence

the shear stiffness was not particularly sensitive to the crack width. However, there was a tendency for the crack to widen with shear slip and hence cause a greater stress normal to the crack plane. Therefore the shear stiffness at this stage was sensitive to changes in the normal stiffness.

It was also observed by the authors that the size and the strength of the aggregate did influence the shear stiffness of the specimens, but that the strength of the concrete did not. This is not consistent with the findings of the other research discussed but it can be argued that it is in accordance with the local/global roughness theory. All the previous tests considered only specimens with crack widths of less than 0.5 mm. If this is the area where aggregate interlock is a bearing action, then the concrete strength would be expected to influence the shear stiffness. However in Laible's tests the crack width is usually greater than 0.5 mm. If this is where aggregate interlock is a frictional mechanism, the shear stiffness would not be expected to be influenced by the concrete strength unless it is sufficiently strong as to cause a change in the shape of the crack, as discussed.

2.5.2.1 Sawtooth crack model

In a later paper, Jimenez, Gergely and White (37) presented an analytical model to explain the results obtained. The crack profile was modelled as a sawtooth with a mean slope of θ (Figure 2.24). Hence:

$$V = A_o(\sigma_n \sin\theta + \tau \cos\theta) \qquad (2.13)$$

$$\Delta p = A_o(\sigma_n \cos\theta - \tau \sin\theta) \qquad (2.14)$$

V = total shear force across crack

σ_n = normal stress at the contact area

τ = frictional stress at the contact area

Θ = angle of inclination of contact plane

A_o = contact area

Δp = change in reinforcement tension due to increase in crack width

Eliminating σ_n gives

$$V = \Delta p \tan\Theta + \frac{A_o \tau}{\cos\Theta} \qquad (2.15)$$

The authors then state that the increase in the normal force with crack widening was observed to be small and hence the first term in equation 2.15 can be ignored. The shear slip is then related to the friction and bearing stresses described by Laible et al. (53) using

$$\Delta_s = A_o(\beta_1 \tau + \beta_2 \sigma_n)$$

where β_1 and β_2 are empirically derived flexibility coefficients for the friction and bearing actions.

A dimensionally inconsistent expression was then formulated relating the aggregate interlock shear stiffness to the crack width and the stiffness normal to the plane of cracking.

The elimination of the first term in equation 2.15 is not a rational assumption to make. In aggregate interlock tests the reinforcement is unbonded and hence the stiffness restraining crack widening will be quite low. However, in reinforced concrete the normal stiffness

will be much higher, for the same reinforcement ratio, because of the effects of local anchorage and hence the term Δp can be quite large.

However, one of the strongest criticisms of the sawtooth model of aggregate interlock is that it is assumed that the crack faces are rigid. Thus the ratio of crack widening to shear slip is constant, regardless of the forces restraining the crack from widening. This clearly does not match the experimental evidence. A further point is that even if the crack faces were perfectly rigid, the ratio of crack widening to shear slip would be expected to be influenced by the crack width. Using rounded aggregates the mean angle of contact between the two crack faces would diminish as the crack width increased.

2.5.2.3 Parabolic crack profile model

Fardis and Buyukozturk (54) developed a more sophisticated model for shear friction than the sawtooth model. It was assumed that there was no shear resistance due to aggregate interlock until two particles of protruding aggregate came into contact. At this point there was a frictional sliding between the rigid crack faces. The shear force, V, was then given by

$$V = N \tan(\theta + \phi) \qquad (2.16)$$

where N is the force normal to the crack

θ is the contact angle

ϕ is the angle of internal friction

ϕ was said to have two components ϕ_μ and $\phi_\ell(n)$, where ϕ_μ is a constant angle of internal friction and $\phi_\ell(n)$ is a component of friction due to local roughness. $\phi_\ell(n)$ degrades with cycling and is written as a decreasing function of the number of load cycles, n.

The shape of the crack face was expressed as a series of parabolic segments given by

$$y = a_k - b_k + b\{1 - \frac{2(x_k - x)}{\ell_k}\}^2 \text{ for } x_k - \frac{\ell_k}{2} < x < x_k$$

and

$$y = a_k + b_k - b_k\{1 - \frac{2(x - x_k)}{\ell_k}\}^2 \text{ for } x_k < x < x_k + \frac{\ell_k}{2}$$

This function is plotted in Figure 2.25.

For a two dimensional model there will be only two points of contact over a finite crack length. The tangent of the upper and lower curve will have the same slope at each contact point.

From the overall equilibrium and the geometric shape of the two crack faces an expression is derived for the shear stiffness. For a two dimensional case, where the crack width is uniform, this may be expressed as

$$V = A_d\,\delta x + b_a\,A_n\,c_o + e'\,A_n\,\delta x \qquad (2.18)$$

where A_d and A_n are the dowel and extensional stiffnesses of the reinforcement, δx is the shear slip, c_o is the initial crack width and b_a and e' are frictional terms derived from equation 2.17.

It was then argued that because any crack path is inherently stochastic, it is not possible to evaluate the terms in equation 2.17 and hence b_a and e'. However, it was inferred from the qualitative form of the expression that an increase in the initial crack width will result in a decrease in the shear stiffness. An increase in the axial tensile force applied normal to the plane of cracking will also cause a reduction in the shear stiffness. These trends agree with the experimental observations.

Having developed the model but being unable to evaluate it, the authors then suggest that the shear stress-slip relationship is a bilinear one. At low slip values, when the crack surfaces have not made contact, only dowel action is resisting shear. At higher values of shear slip a linear aggregate interlock stiffness is proposed. However this proposal is inconsistent with the fundamental aggregate interlock model described. The shear stiffness is dependent upon the contact angle between the two surfaces (equation 2.16 and Figure 2.25c). As shear slip occurs the contact angle must diminish and hence cause a reduction in the aggregate interlock shear stiffness.

2.5.2.4 Two phase model

In a recent paper, Walraven (42) has developed a more plausible theoretical model for aggregate interlock action. Concrete is modelled as a two phase material with rigid aggregates and rigid-plastic cement paste. If a shear and normal force are applied to a single spherical aggregate particle there is a combination of crushing and sliding between the aggregate and the cement paste until equilibrium is reached. (Figure 2.26). The resultant normal and shear forces are given by,

$$F_\sigma = 2R\ \sigma_{pu}\ \sin\Theta$$

$$F_\tau = 2R\ \tau_{pu}\ \sin\Theta$$

where $\tau_{pu} = \mu\ \sigma_{pu}$ and Θ is the angle of the contact segment. The projected areas of contact in the x and y directions are given by,

$$a_x = 2R\ \sin\Theta\ \sin\alpha$$

$$a_y = 2R\ \sin\Theta\ \cos\alpha$$

Hence the forces in the x and y directions are given by

$$F_x = \sigma_{pu}(a_y + \mu\ a_x) \tag{2.19}$$

$$F_y = \sigma_{pu}(ax - \mu\ a_y) \tag{2.20}$$

For a given aggregate grading, a set of curves were then derived (Figure 2.27) relating the total projected contact areas per unit area of crack plane to the crack width, c_w, and the shear slip, Δ_s. Hence, using equations 2.19 and 2.20 the normal and shear stresses were obtained.

Tests were then carried out by the author on aggregate interlock specimens with external restraint bars (Figure 2.28a). The results fitted the theoretically predicted results quite closely (Figure 2.28b).

The theoretical model was then used to show that for large values of shear slip the frictional forces on the aggregate contributed to about 50% of the total shear resistance. For low shear slip the friction

did not contribute much and most of the shear resistance was due to bearing action and crushing of the cement paste (Figure 2.29).

Other conclusions reached, from varying different parameters in the theoretical model, were that the entire range of aggregate particle sizes contributed to the interlock stiffness, but for a smaller initial crack width, the smaller particles contributed the greater part of this stiffness. Similarly, an increase in the maximum aggregate size only had a significant effect on the shear stiffness for large crack widths and shear slips. It is interesting to note that the only research workers claiming that increasing the aggregate size had the effect of increasing the aggregate interlock stiffness were the Cornell University group, who were testing specimens with large initial crack widths, i.e. 0.5 mm and over.

These expressions derived to give the projected contact areas in Figure 2.27 are complex and so the following linear regression equations were derived to describe the experimental results

$$\tau = -\frac{f_{cu}}{30} + (1.8\, c_w^{-0.80} + [0.234\, c_w^{-0.707} - 0.2]\, f_{cu})\, \Delta_s \qquad \text{for } \tau \geq 0 \qquad (2.21)$$

$$\sigma = -\frac{f_{cu}}{20} + (1.35\, c_w^{-0.63} + [0.191\, c_w^{-0.552} - 0.15]\, f_{cu})\, \Delta_s \qquad \text{for } \sigma \geq 0 \qquad (2.22)$$

where f_{cu} is the concrete strength (N/mm^2) and c_w and Δ_s are in mm. A comparison of these equations with the experimental results is shown in Figure 2.30.

These equations may be used to predict the shear stress-shear slip curve and the crack width-shear slip curve in the following manner. For a given specimen, the concrete strength and the axial stiffness normal to the plane of cracking must be known. A crack width is then selected and the resulting compression across the crack face (tension in the reinforcement) is found from the axial stiffness. From equation 2.22, or from the lower half of Figure 2.30, the shear slip necessary to provide this compressive force is found. Hence, using equation 2.21 or the upper half of Figure 2.30, the shear stress consistent with this shear slip and the crack width chosen is found. This can be repeated for different crack widths to obtain the shear stress-slip curve and the crack width-shear slip curve.

2.5.3 Summary of aggregate interlock research

Summarizing the work on aggregate interlock, the following points have been observed:

1. Aggregate interlock is dependent upon the crack width and the shear slip across the crack.

2. The relative strengths of the aggregate and the concrete can exert a major influence on the interlock stiffness but the absolute strengths are of lesser importance.

3. As slip occurs across the crack there is an overriding action which forces the crack open. This is resisted by the reinforcement crossing the crack. The axial stiffness of this reinforcement has a large influence upon the interlock stiffness.

4. The aggregate shape and size does not appear to have a great

influence upon the interlock stiffness until the crack width or shear slip becomes quite large.

5. Laible et al. (53) have presented a simple model of aggregate interlock as a combination of crushing and friction. The relative importance of these actions is said to depend upon the initial crack width.

6. Walraven (42) has presented a more sophisticated and detailed model considering concrete as a two phase material with rigid and rigid/plastic components. The results predicted by this model seem to correlate well with experimental results.

2.6 Shear transfer in cracked reinforced concrete

If the mechanisms of aggregate interlock and dowel action are understood, it should be possible to combine these two effects and predict the behaviour of cracked reinforced concrete under shear loading. However, there are several reasons why the interaction of these two effects make this task more complex than it might at first appear.

In the dowel action tests, aggregate interlock is removed by the artificial creation of a smooth crack face and hence there is no tendency for the crack faces to override. In reinforced concrete, the aggregate interlock effect does cause overriding. This overriding causes widening of the crack and there is a resultant axial tensile force in the reinforcement. This has been shown to cause local tensile damage to the concrete and hence soften the dowel stiffness. However there are also compressive forces over the whole crack face, balancing the tensile force in the reinforcement, which may also influence the dowel stiffness. These compressive forces are not

present on dowel action tests with a simultaneous axial tensile force in the reinforcement.

In aggregate interlock tests, dowel action is removed either by placing a soft sleeve around the reinforcement or by removing the reinforcement from the concrete altogether and providing an external restraint, normal to the plane of cracking. The difficulty with both these methods is that, in removing the dowel action effects, the local bond between the reinforcement and the concrete has also been removed. One problem this causes is that the axial restraint stiffness of sleeved or external reinforcement is much less than that of fully bonded reinforcement. It is necessary to compare the results of aggregate interlock tests, using a normal restraint stiffness similar to that of the fully bonded reinforcement in the cracked reinforced concrete tests, to obtain a meaningful result.

Another problem caused by the removal of local bond in the aggregate interlock tests is that the crack width will be of uniform thickness throughout the section. The literature reviewed in section 2.2.2 suggests that the width of the crack tends to taper towards the reinforcement. Clearly, if the aggregate interlock stiffness is a function of the crack width, two cracks with the same surface widths cannot be expected to have the same shear stiffness if one is of uniform width internally and the other tapers considerably towards the reinforcement.

2.6.1 Tests on cracked reinforced concrete

Some early work on shear across joints or cracks in reinforced concrete was done by Birkeland and Birkeland (55). Dowel action was assumed to contribute a negligible proportion of the shear stiffness and

the aggregate interlock stiffness was visualised as a series of frictionless sawtooth ramps of slope $\tan\phi$ (Figure 2.31). Thus the shear stiffness is directly proportional to the reinforcement ratio. Hence,

$$v = \rho f_s \tan\phi \qquad (2.23)$$

where $\tan\phi = 1.7$ for monolithic concrete.
The ultimate shear stress was reached when the reinforcement yielded in tension.

There has been an extensive study of shear transfer in cracked and uncracked reinforced concrete at the University of Washington, U.S.A. Using several types of "push-off" test, the effects of the reinforcement, the aggregate size, the concrete strength, etc. were studied. Attention was focussed mainly upon predicting the ultimate shear stress attained rather than the shear stiffness of the specimens.

A series of shear tests on cracked and uncracked reinforced concrete specimens, with additional compressive forces normal to the place of cracking, were carried out by Hofbeck et al. (56). The results tended to confirm the shear friction model. However a more accurate fit to the experimental results was obtained if a cohesion term was added to equation 2.23 and the angle of the sawtooth was reduced from 60° to 39°. Increasing the normal compressive stress, σ_n was found to have exactly the same effect as increasing the parameter ρf_y. Hence,

$$v_u = 2.75 + 0.8(\rho f_y + \sigma_n) \qquad (2.24)$$

was used to predict the mean ultimate shear stress.

The units of each term in this equation are N/mm^2. The equation was claimed to be applicable for $\rho f_y < 0.15 f_{cu}$ and for $f_{cu} < 28 N/mm^2$.

It was observed by the authors that the concrete strength did not influence the ultimate shear stress of cracked reinforced concrete specimens with low values of ρf_y. If ρf_y was increased, however, there came a point when the concrete strength did influence the shear strength of the specimens (Figure 2.32). From this result it was inferred that when there is a small reinforcement ratio the specimens failed ultimately by yielding of the steel. For higher reinforcement ratios failure was said to occur by crushing of the concrete. The dowel action was estimated to contribute 20% to 30% of the total shear strength and hence the assumption that this proportion was negligible made in reference 55 is not valid.

In a later paper, Mattock and Hawkins (57) discovered that direct stresses parallel to the plane of cracking had little effect upon the shear strength. The reinforcement diameter and yield stress were also found not to affect the shear strength, as long as the magnitude of ρf_y was held constant.

Mattock (58) also investigated the effect of combined shear with tensile forces, normal to the crack plane. Equation 2.24 was still found to give a close estimate of the ultimate shear stress. However, this result is somewhat suspect because the shear and tension loading parts of the test rig are not independent. The shear stiffness of that part of the loading rig inducing tension into the specimen appears to be contributing to the shear strength of the specimen itself. The influence of a tensile force upon the shear stiffness of the specimen was not investigated, but it was observed that the ratio of

crack widening to shear slip was independent of the initial crack width.

However, in another study Mattock (59) concluded that the ratio of crack widening to shear slip was influenced by the sand fraction of the concrete and by the reinforcement size. It was observed that crack opening direction (Figure 2.33) was not changed if the ratio between the strength of the large aggregate particles and the strength of the concrete was altered. However the crack opening direction was influenced by the ratio of the strength of the sand to the strength of the concrete. This implies that if the crack path intersects the large aggregate particles, the crack opening direction is the same as when the crack passes around the edge of the aggregate. If, however, the crack path intersects the sand particles, then the crack opening direction is affected. This result tends to support the aggregate interlock theory of Laible et al. (53) but is not consistent with the work of Walraven (42).

It was also found that the use of larger reinforcing bars tended to increase the angle of the crack opening direction. Mattock (60) attributed this result to the fact that the larger bars were used with larger specimens and hence the crack had more freedom to deviate from the mean plane of cracking. This argument is inconsistent with his earlier theory that the crack opening direction is controlled by local and not global roughness, and warrants further study before any conclusions can be drawn.

Walraven (42) found that there were a number of major differences between the behaviour of aggregate interlock specimens and that of reinforced concrete specimens. With aggregate interlock specimens,

the crack opening direction was dependent upon the stiffness restraining the crack from widening. With reinforced concrete specimens there was a characteristic crack opening direction which was quite steep and was independent of the amount of reinforcement crossing the crack. The stiffness of the reinforced concrete specimens was found to be greater than the stiffness obtained by summing the separate components of aggregate interlock and dowel action. The only exception to this was when the reinforcement ratio was very low. In this case the crack opening direction, in the aggregate interlock test, was similar to the characteristic crack opening direction, in the reinforced concrete tests, and the stiffness of the reinforced concrete specimen could be predicted by summing the separate components (Figure 2.34).

The following hypothesis was presented by the author to explain these observations. It was argued that when the reinforced concrete specimens crack in tension, internal cracks, of the type observed by Goto (22), were initiated by reinforcement ribs adjacent to the primary crack. If these internal cracks propagate to the primary crack, a conical region of loose concrete is formed (Figure 2.35a). If there is a subsequent shear displacement with a low level of crack widening, this conical region will "lock up" and form a strut which forces the crack to open in a characteristic direction (Figure 2.35b). The strut is considered to be rigid and hence the amount of reinforcement does not affect the characteristic crack opening direction. The strut also provides the compressive force required to complete the equilibrium of internal and external forces (Figure 2.35c). If the reinforcement ratio is low, the crack opening direction, caused by the ordinary aggregate interlock, is steeper than the characteristic path and hence the conical region of damaged concrete does not "lock up" and form a strut.

In support of this theory was the evidence that when reinforced concrete shear specimens were opened after testing, a conical region of concrete on each crack face, adjacent to the reinforcement was observed to be extensively damaged. To confirm the theory a series of reinforced concrete specimens were tested in which the reinforcement had been provided with a short, soft sleeve adjacent to the crack face. The intention was to prevent tensile damage in the concrete in this region. The results followed the trends of the aggregate interlock tests in that the direction of crack opening was sensitive to the reinforcement ratio and the shear stiffness was similar to the result predicted from aggregate interlock and dowel action tests.

2.6.2 Summary of research on cracked reinforced concrete

It is possible to note the following points from the tests on cracked reinforced concrete specimens:

1. The shear friction model presents a simple model which does not attempt to describe the mechanism of shear transfer but gives a reasonably close fit for the type and range of specimens tested. It is important to note that the ultimate shear stress will only be accurately predicted if the concrete fails through axial yielding of the reinforcement. When the reinforcement ratio is high, failure may be caused by crushing of the concrete or by tensile splitting around the reinforcement, as reported in ref. 29 and ref. 37.

2. The marked difference in behaviour between a crack in plain concrete and one in reinforced concrete observed by Walraven was a surprising result. It is possible that this had not been previously

noted because the many inherent differences between the two types of tests make it difficult to correlate the test results. Walraven's effective theoretical treatment of aggregate interlock makes this task easier. However, it would appear that the effects of any differences in crack width variation, within the concrete, between the two types of tests still need to be included before a worthwhile comparison can be made. Walraven has not considered that the crack width may get smaller closer to the steel, in reinforced concrete specimens, and it may be this effect, rather than the "locking up" of crushed particles, which caused the difference in behaviour.

TABLE 2.1

Values for the constants in the bond stress-slip equation 2.3 from reference [24]

f_r	a_o	b_o	β
0.005	0.0320	0.129	2.34
0.010	0.0317	0.300	2.00
0.025	0.0317	0.680	1.85
0.050	0.0314	0.827	2.10
0.100	0.0315	1.135	2.31
0.200	0.0322	1.353	2.53
0.400	0.0316	1.308	2.85

Note: f_r is the 'relative rib area' of the reinforcement.

Typically for ϕ = 8mm, f_r = 0.050

for ϕ > 12mm, f_r = 0.065

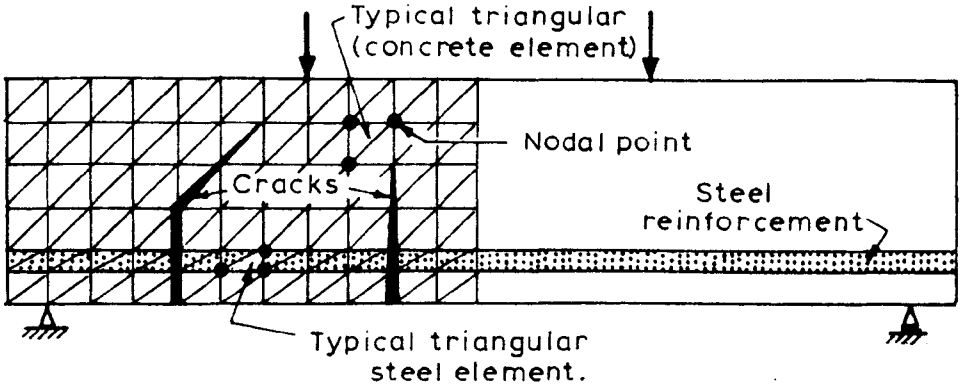

FIGURE 2.1. REINFORCED CONCRETE BEAM MODELLED IN [9].

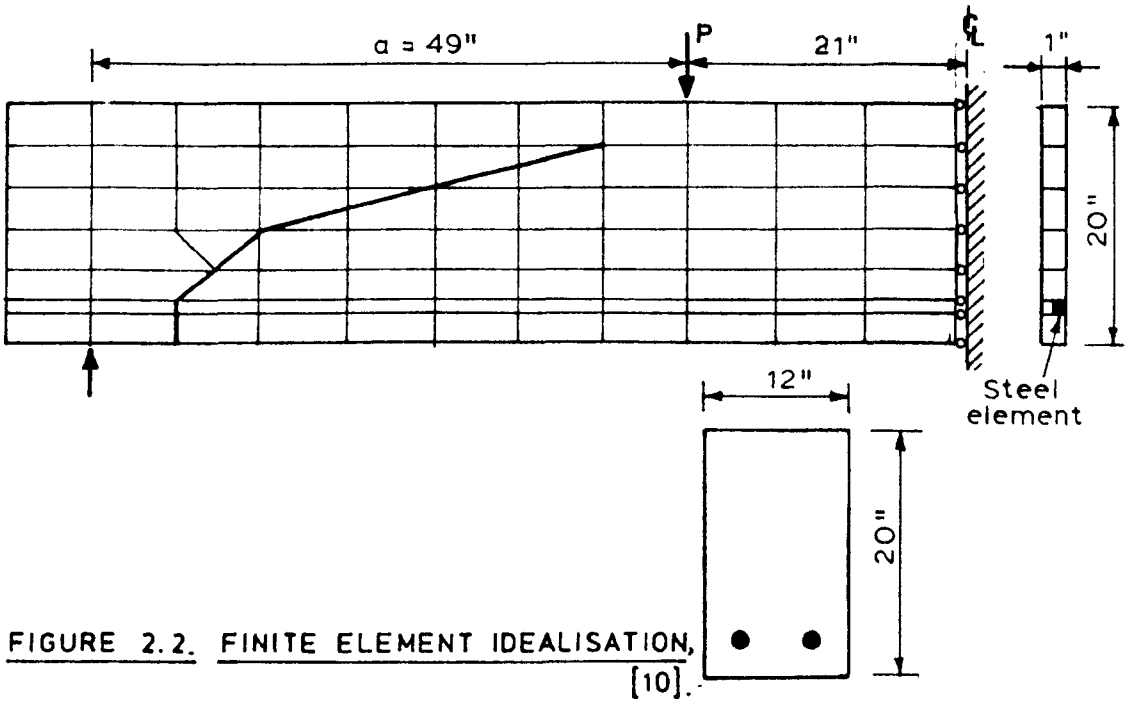

FIGURE 2.2. FINITE ELEMENT IDEALISATION, [10].

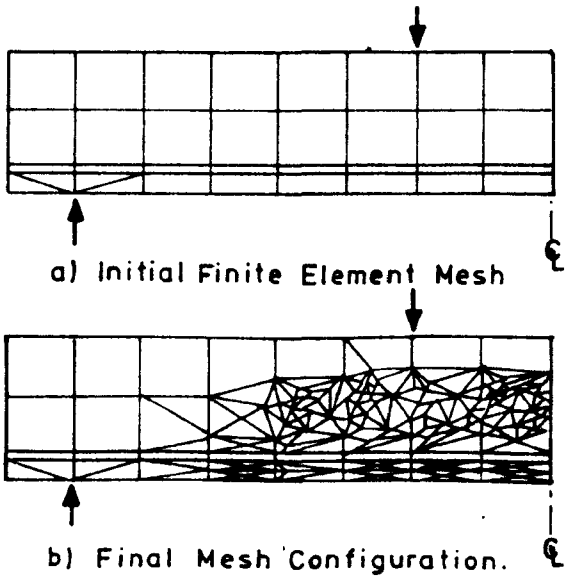

FIGURE 2.3. MODELLING OF PROGRESSIVE CRACK FORMATION,[12]

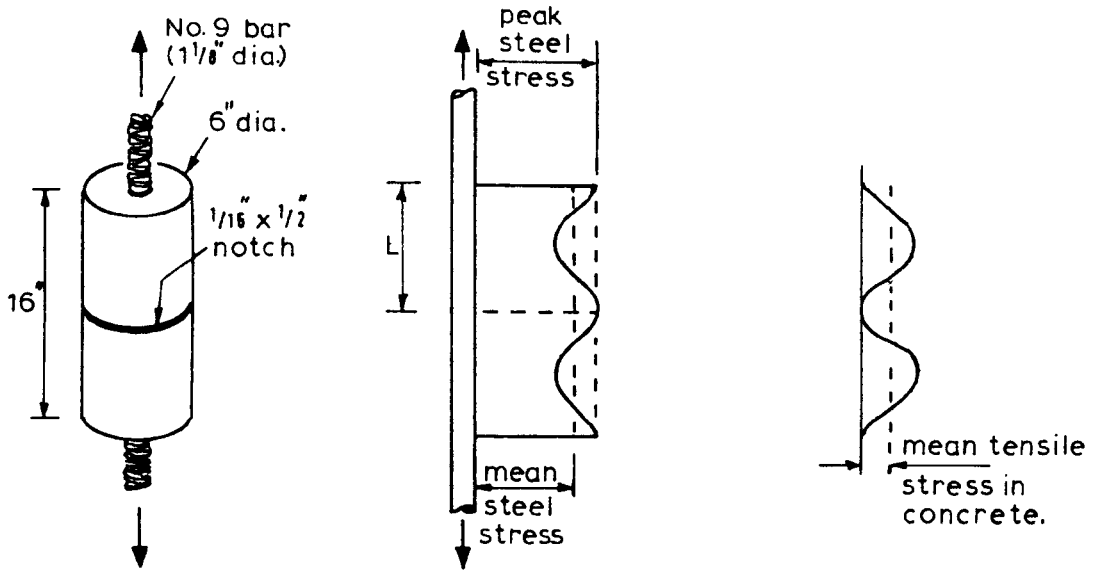

FIGURE 2.4. TEST SPECIMEN AND RESULTS FROM [16].

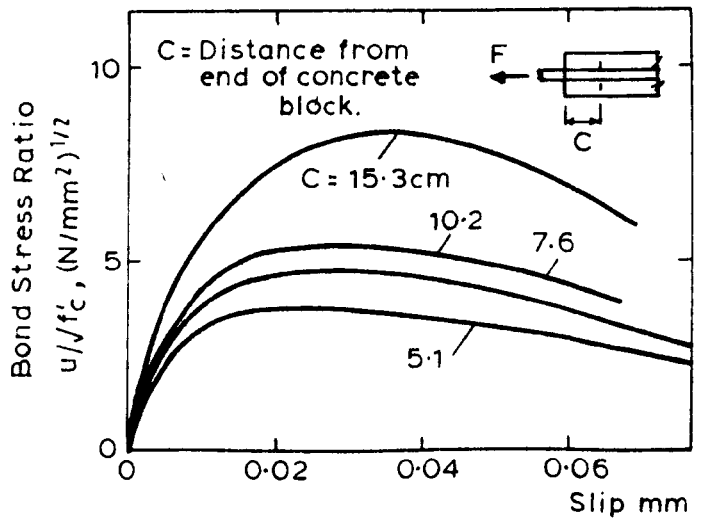

FIGURE 2.5. BOND STRESS - SLIP RELATIONSHIP [18].

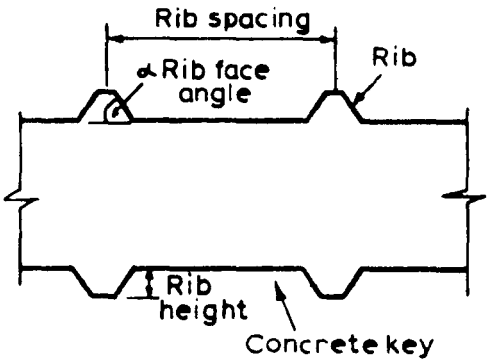

FIGURE 2.6. GEOMETRY OF BAR DEFORMATION.

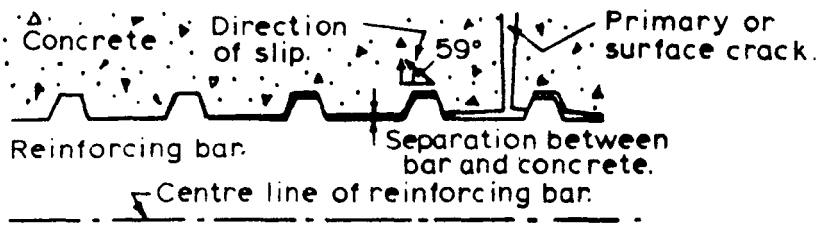

FIGURE 2.7a. SECTION THROUGH REINFORCING BAR AND CONCRETE SHOWING SEPARATION THAT OCCURS NEAR A PRIMARY CRACK.

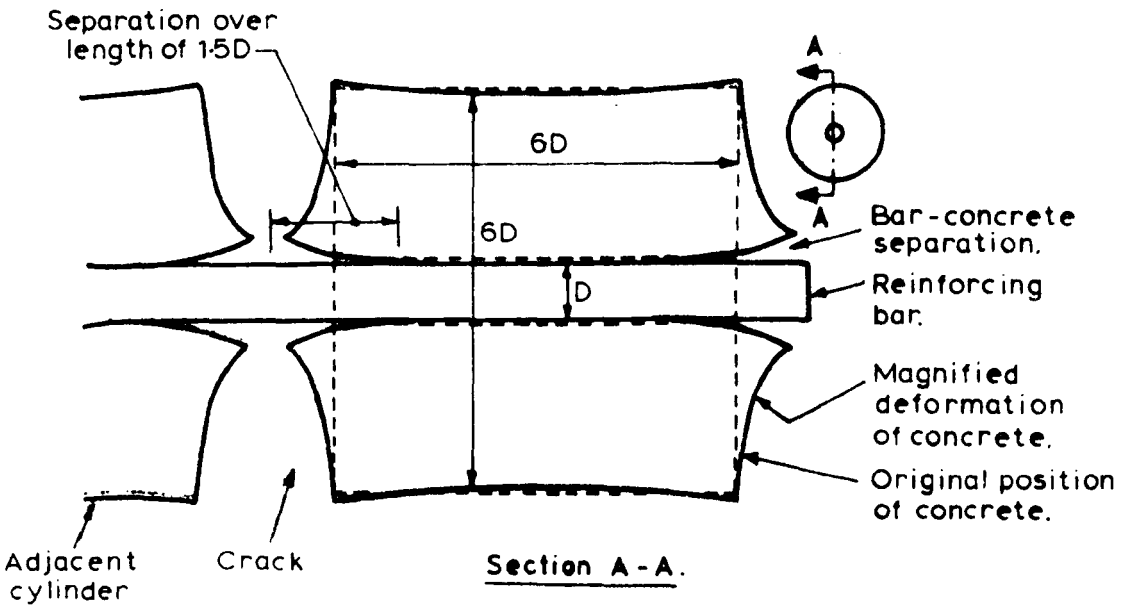

FIGURE 2.7b. MAGNIFIED DEFORMATION OF A PRISM FROM A FINITE ELEMENT ANALYSIS, [25].

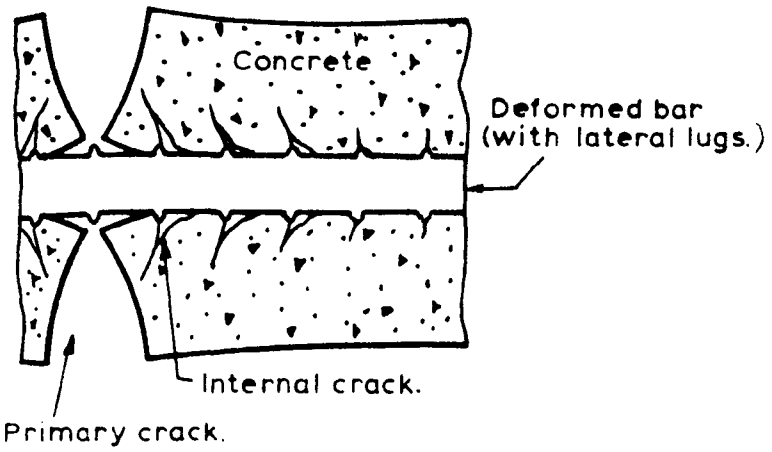

FIGURE 2.8. INTERNAL CRACK PATTERN ACCORDING TO [22]

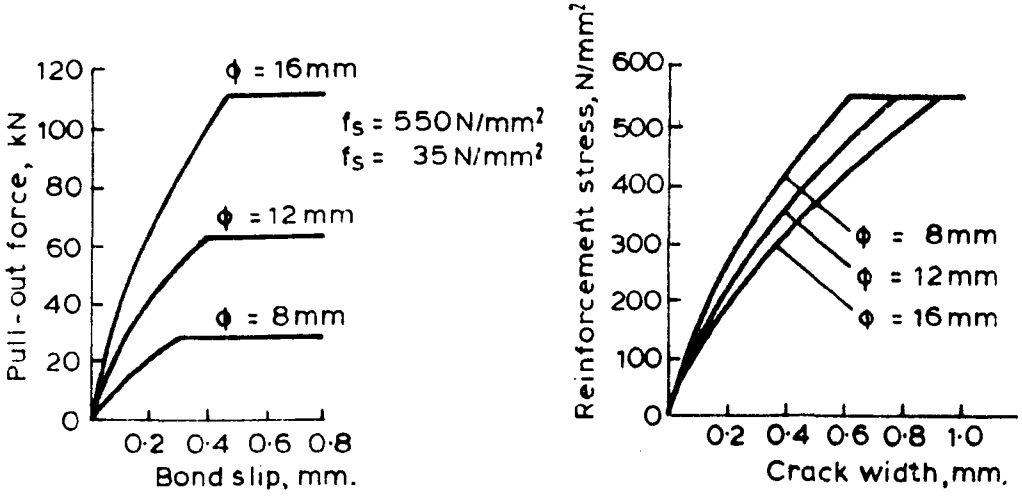

FIGURE 2.9. ANCHORAGE PROPERTIES OF DEFORMED REINFORCEMENT [24]

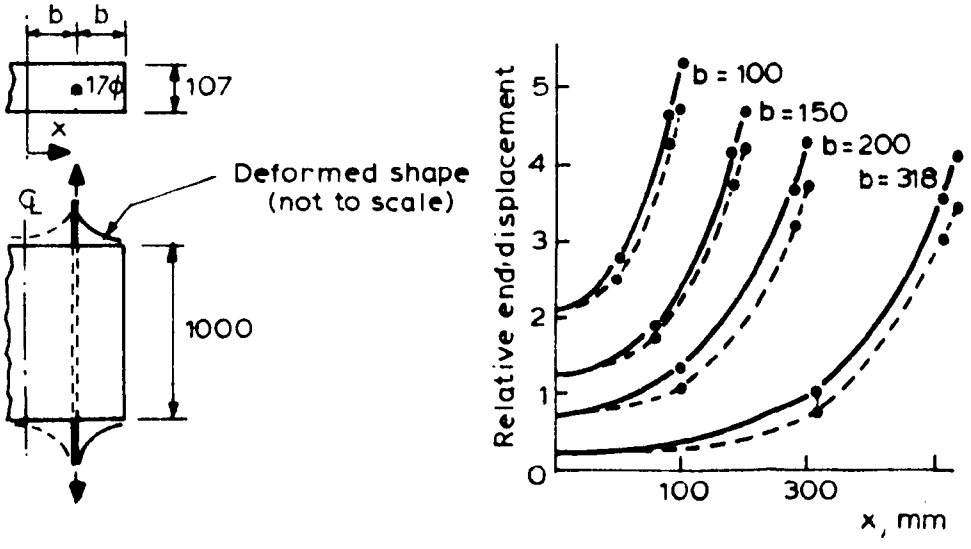

FIGURE 2.10. FINITE ELEMENT STUDIES OF CRACK WIDTH [28]

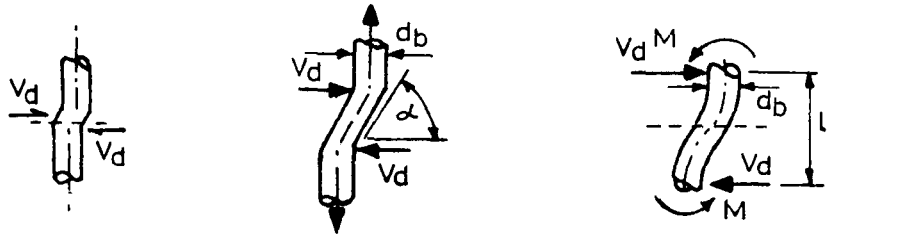

FIGURE 2.11. THE MECHANISM OF DOWEL ACTION.

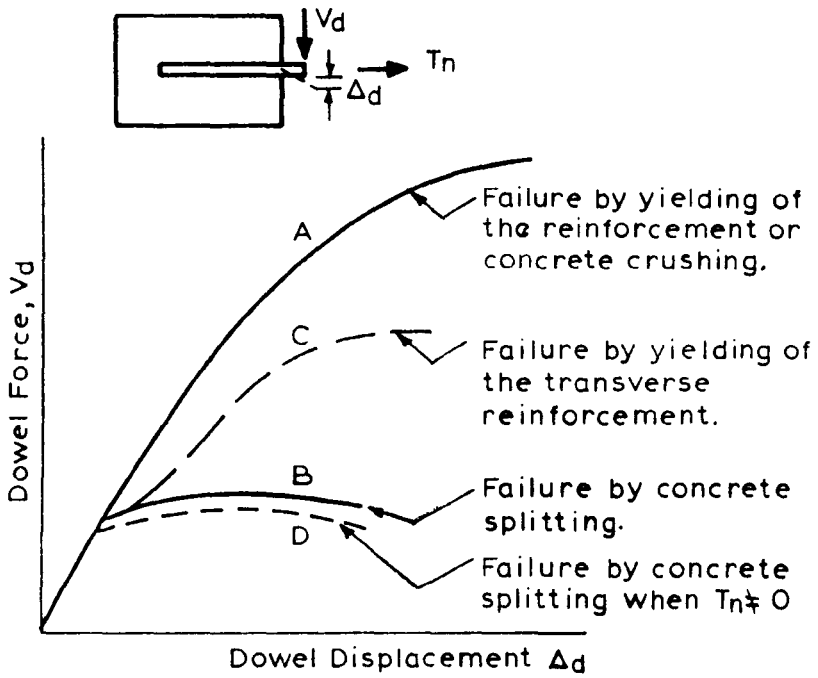

FIGURE 2.12. POSSIBLE RELATIONSHIP BETWEEN DOWEL FORCE AND DISPLACEMENT.

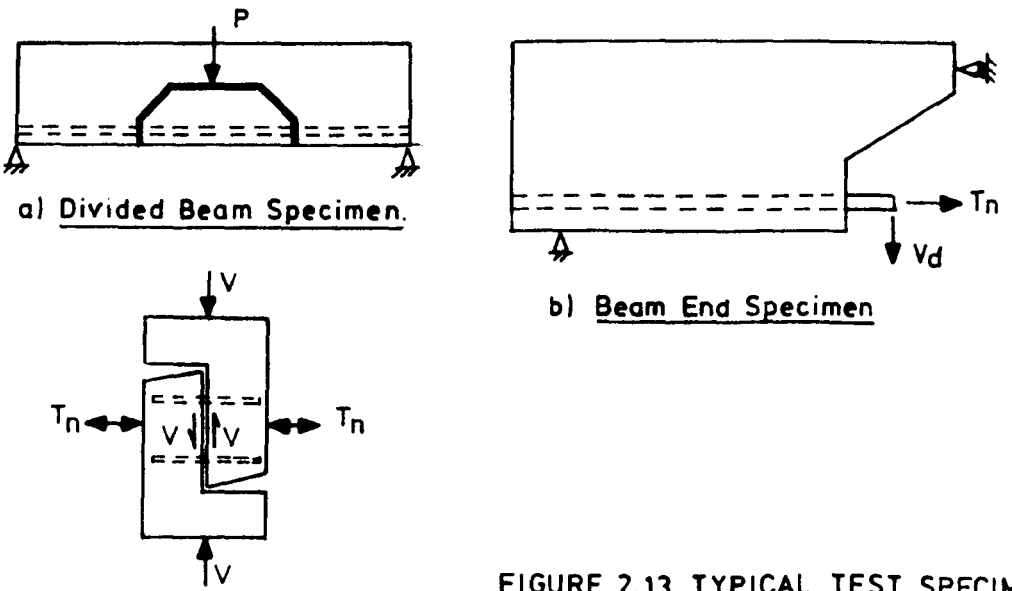

FIGURE 2.13. TYPICAL TEST SPECIMENS FOR DOWEL TESTS.

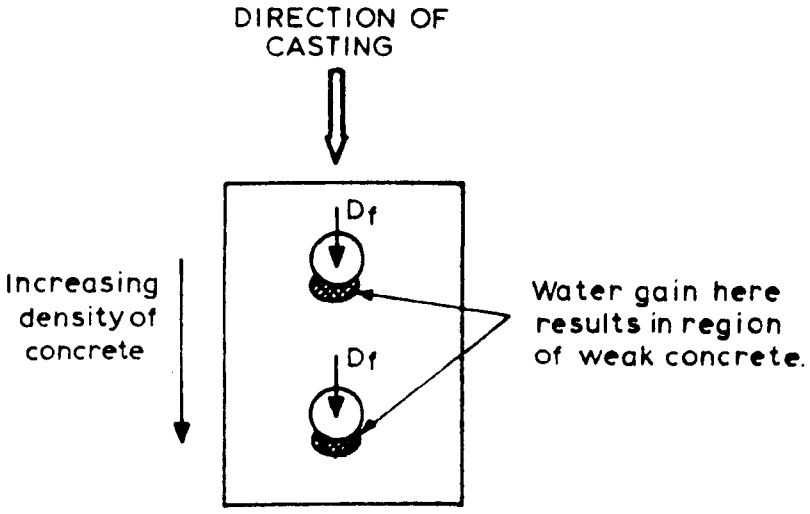

a) Direction of Casting and Loading results in Low Dowel Stiffness.

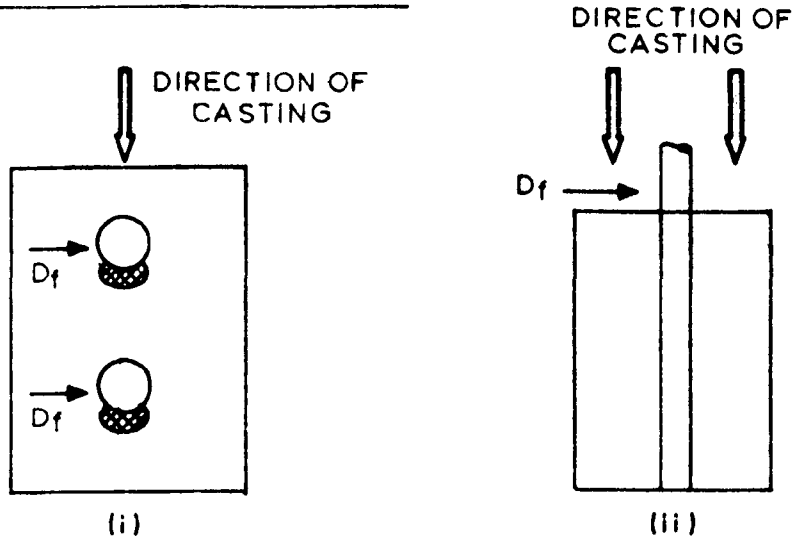

b) Dowel Stiffness not affected by Water Gain.

FIGURE 2.14. EFFECTS OF METHOD OF MANUFACTURE OF SPECIMENS UPON DOWEL STIFFNESS.

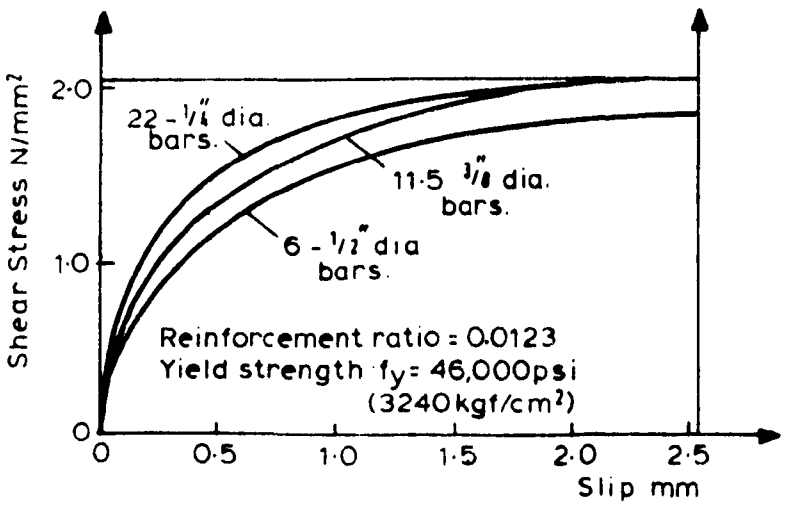

FIGURE 2.15. DOWEL ACTION FOR CONSTANT REINFORCEMENT RATIO [29].

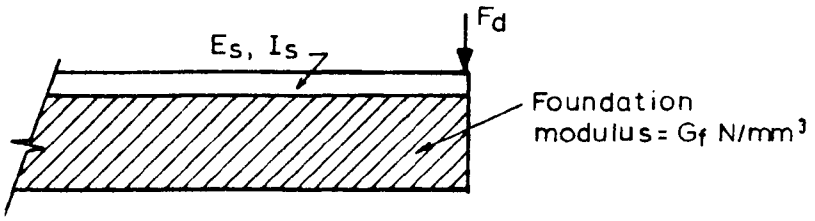

a) Beam on an elastic foundation (B.E.F).

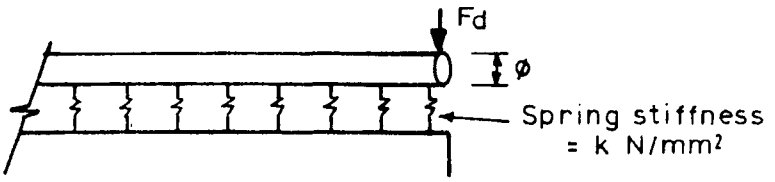

b) Conceptual model.

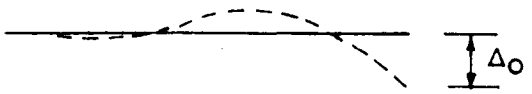

c) Deflected shape.

FIGURE 2.16. DOWEL ACTION MODEL.

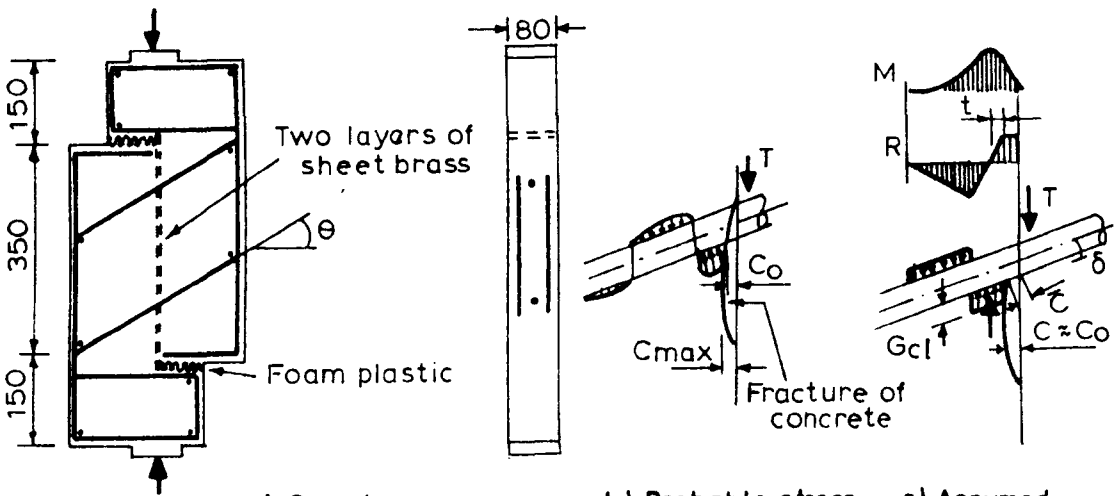

a) Specimen

b) Probable stress distribution.

c) Assumed stress distribution.

FIGURE 2.17. TEST SPECIMEN AND MODEL OF BEHAVIOUR. [43]

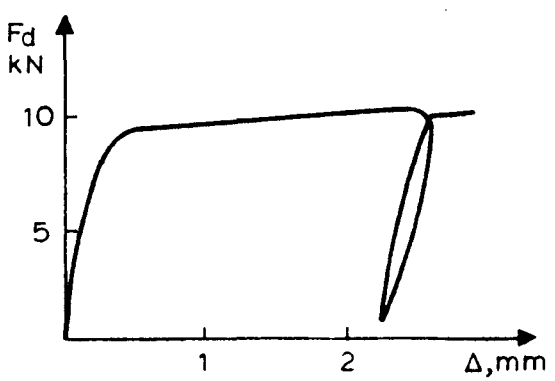

FIGURE 2.18. TYPICAL DOWEL LOAD - SLIP CURVE [44]

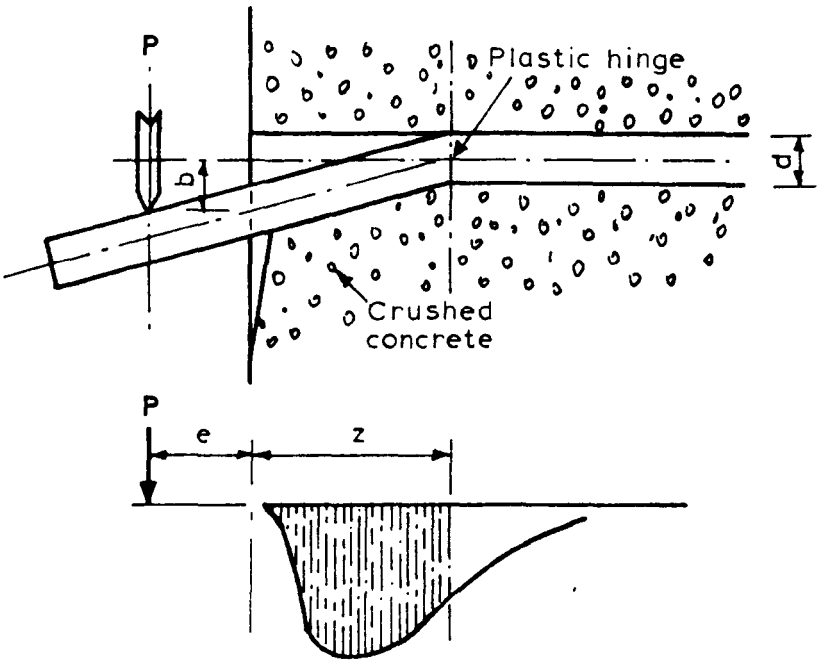

a) Deformation at ultimate loading.

b) Re-distributed reaction.

FIGURE 2.19. MECHANISM TO DESCRIBE THE BEARING CAPACITY FOR A DOWEL, [47]

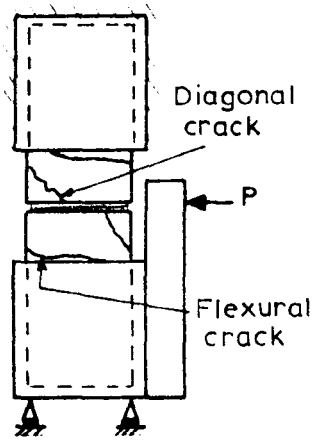

a) Test rig.

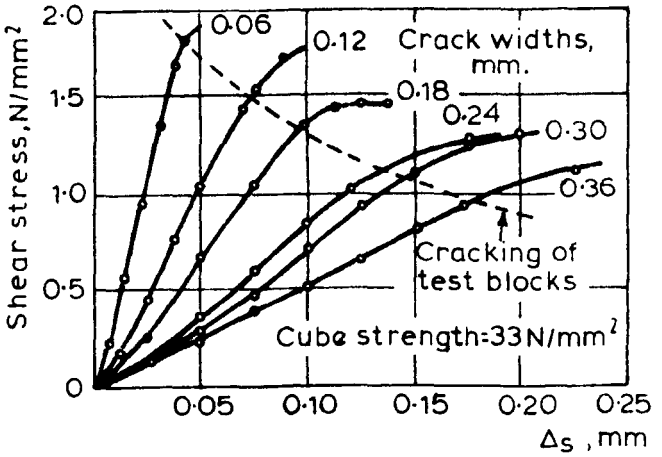

b) Effect of crack width upon aggregate interlock.

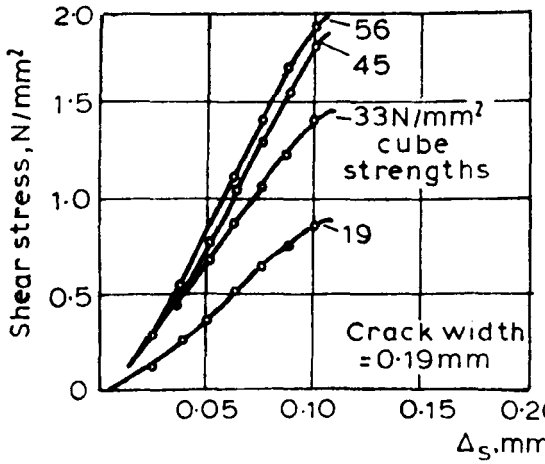

c) Effect of concrete strength upon aggregate interlock.

FIGURE 2.20. AGGREGATE INTERLOCK TESTS, [49]

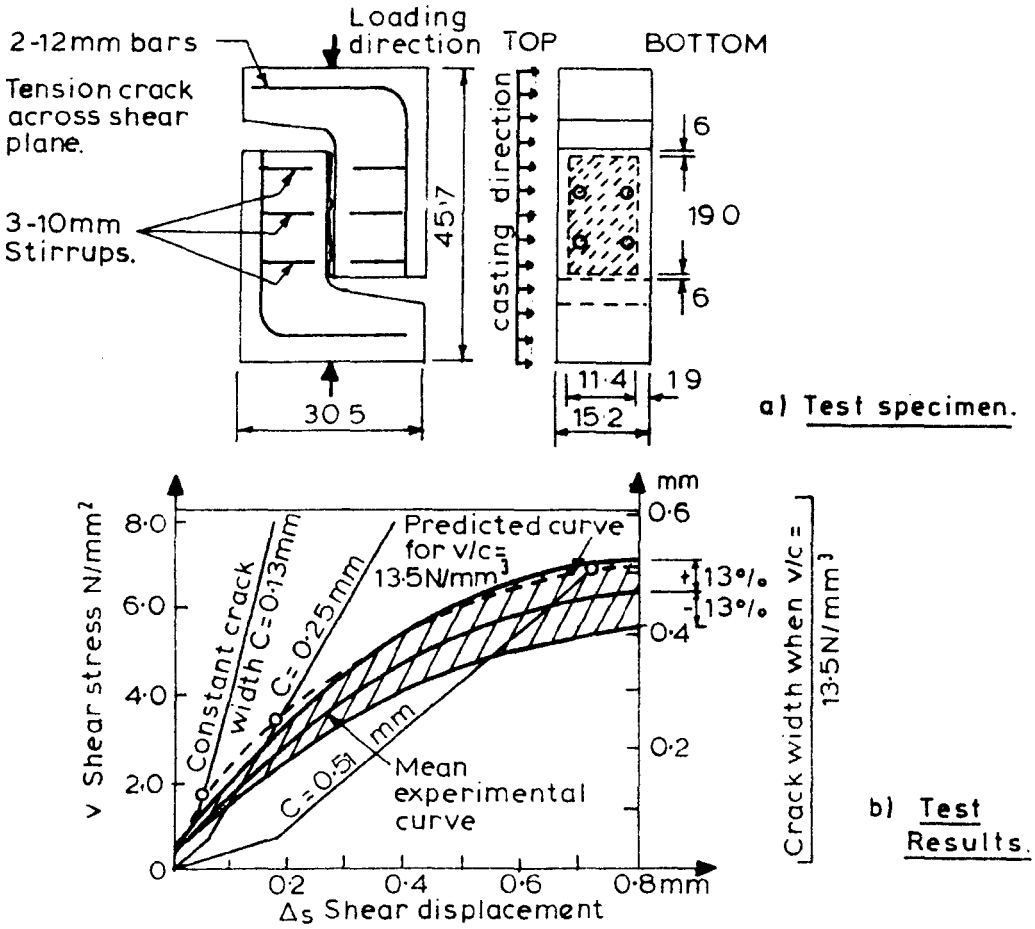

FIGURE 2.21. AGGREGATE INTERLOCK TESTS. [50]

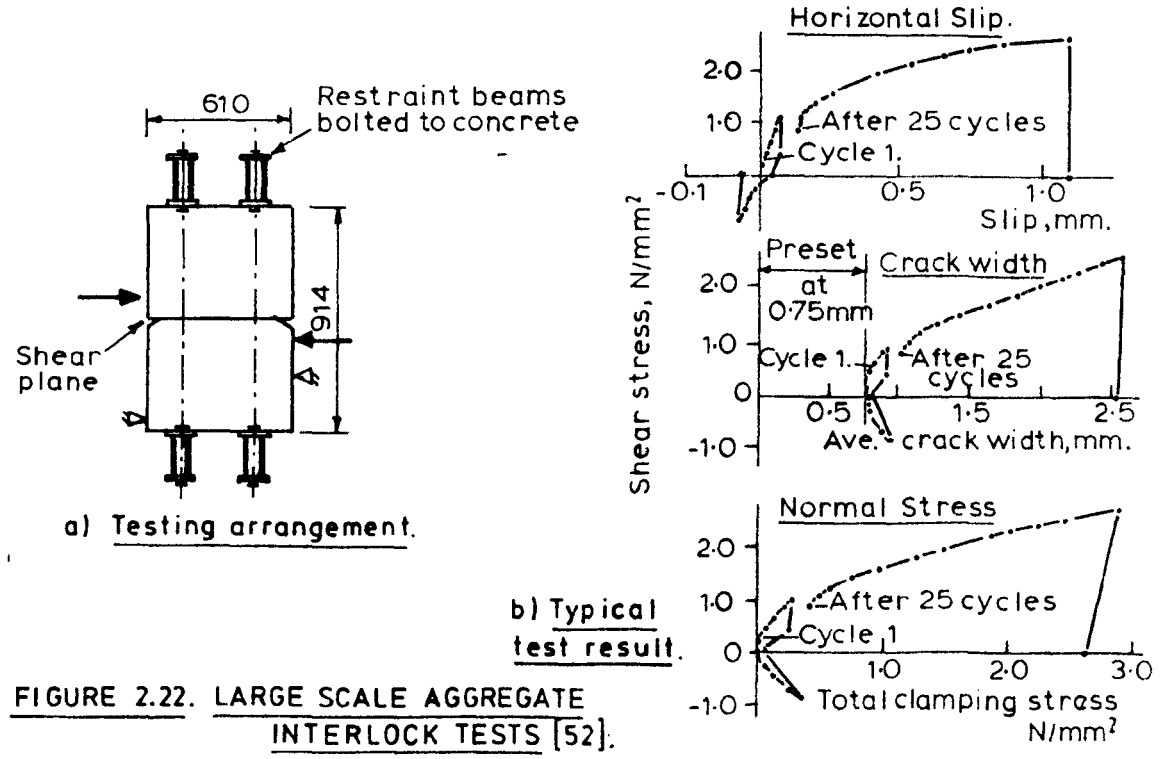

FIGURE 2.22. LARGE SCALE AGGREGATE INTERLOCK TESTS [52].

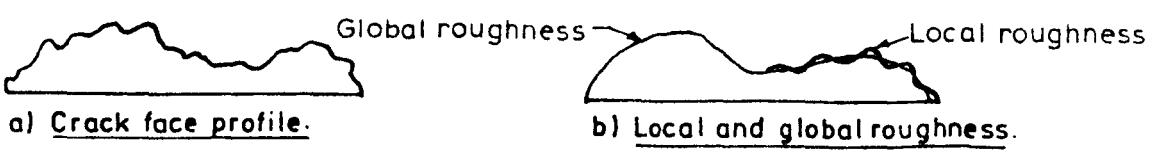

FIGURE 2.23. SUBDIVISION OF ROUGHNESS [53].

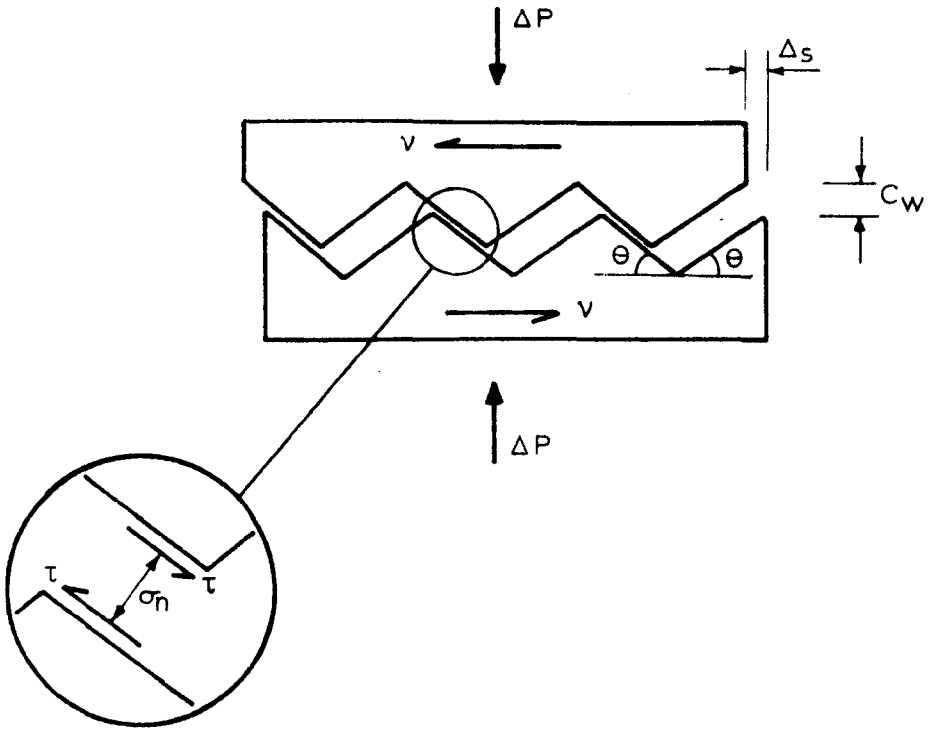

FIGURE 2.24. AGGREGATE INTERLOCK SHEAR STIFFNESS MODEL [37].

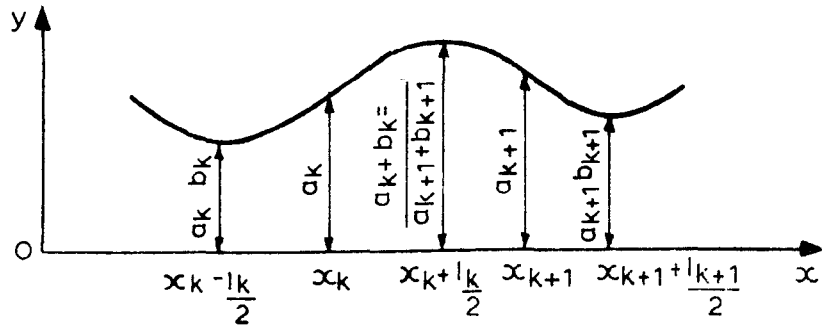

a) Profile of crack (Global roughness), y = f(x).

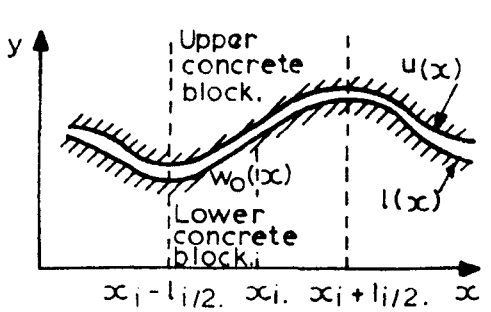

b) Before shear slip.

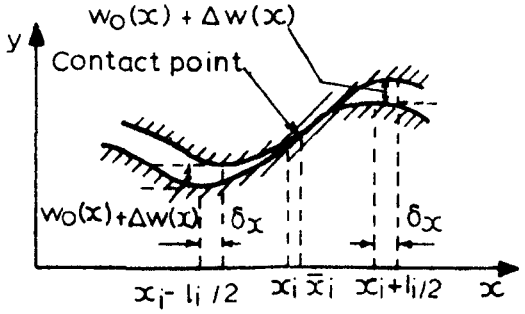

c) After shear slip.

FIGURE 2.25. MODEL FOR AGGREGATE INTER LOCK. [54].

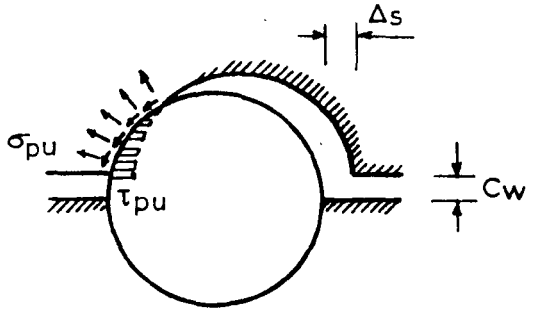

a) Contact stresses on a particle.

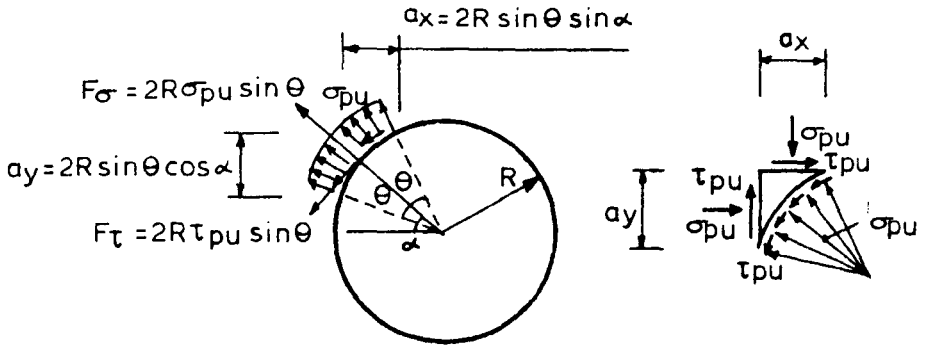

b) Equilibrium conditions.

FIGURE 2.26. MODEL FOR AGGREGATE INTERLOCK. [42].

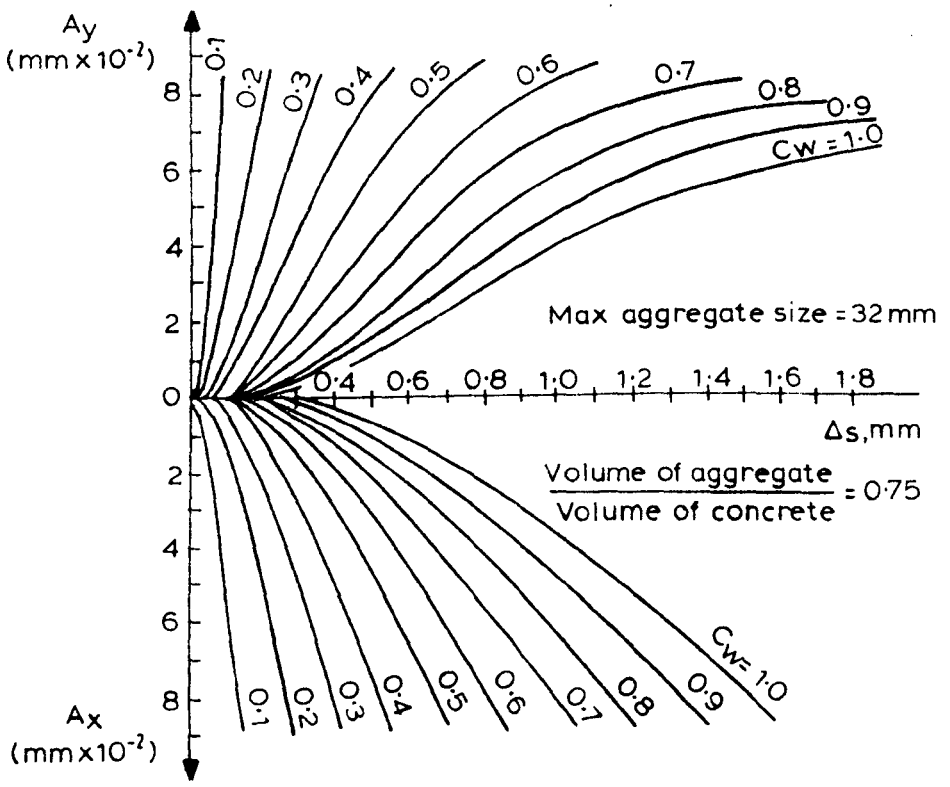

FIGURE 2.27. TOTAL PROJECTED CONTACT AREAS A_y AND A_x FOR 1 mm² CRACK.

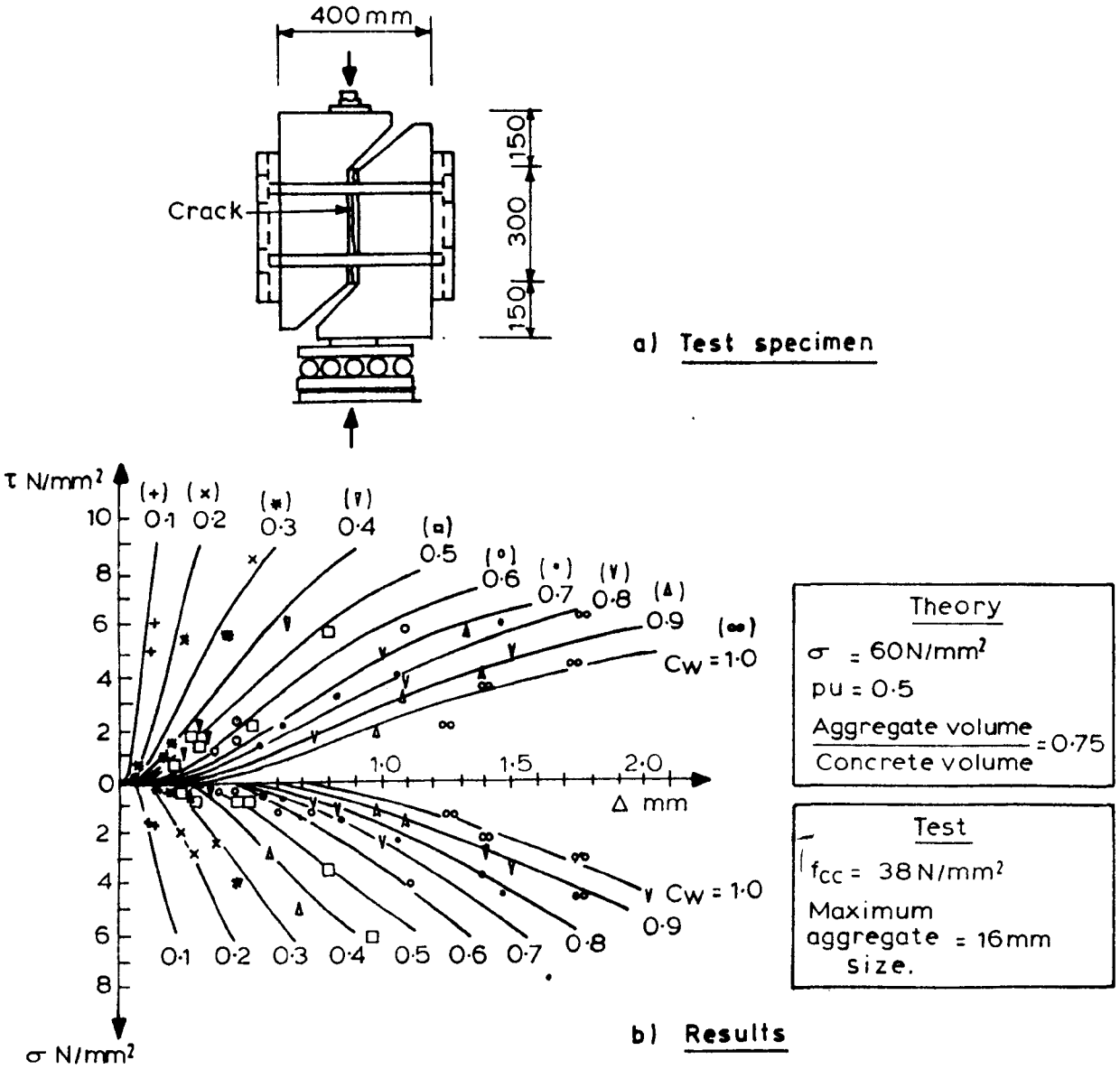

FIGURE 2.28. COMPARISON OF THEORETICAL AND TEST RESULTS. [42].

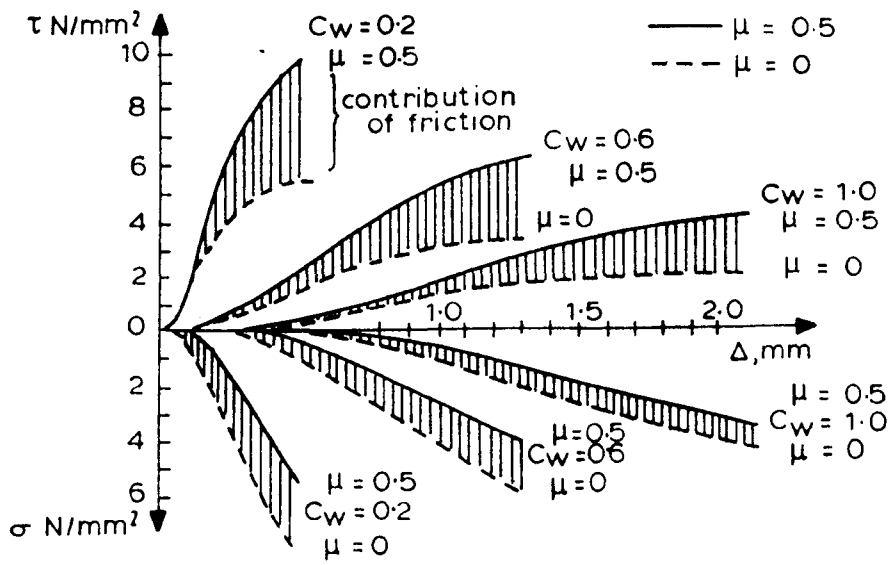

FIGURE 2.29. THE ROLE OF FRICTION BETWEEN AGGREGATE AND MATRIX IN THE TRANSFER OF STRESSES ACROSS A CRACK.

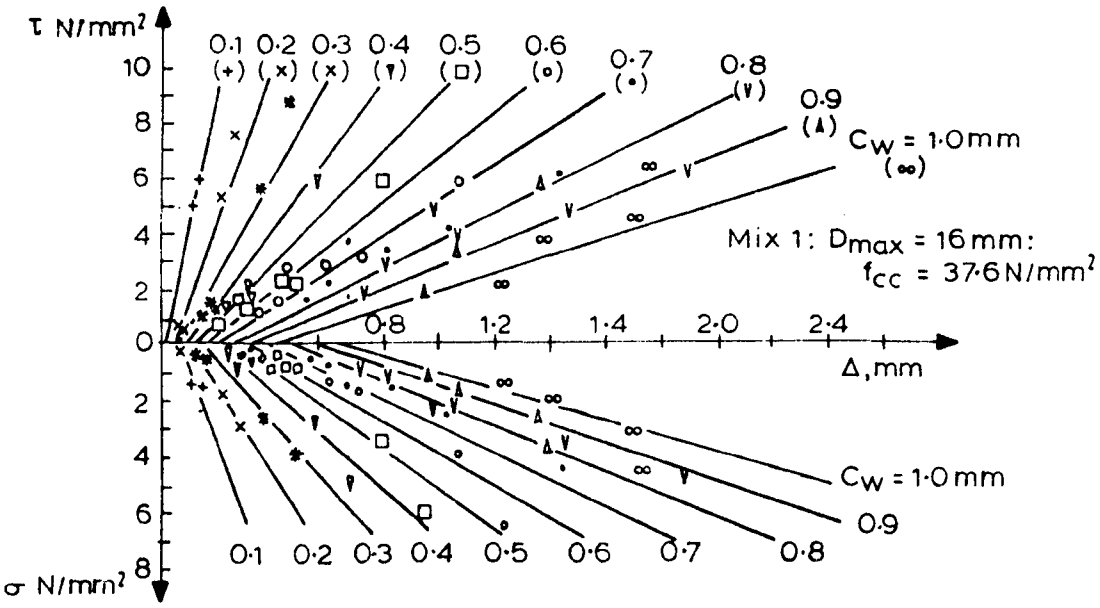

FIGURE 2.30. COMPARISON OF EQUATIONS 2.21 AND 2.22 WITH EXPERIMENTAL RESULTS. [42].

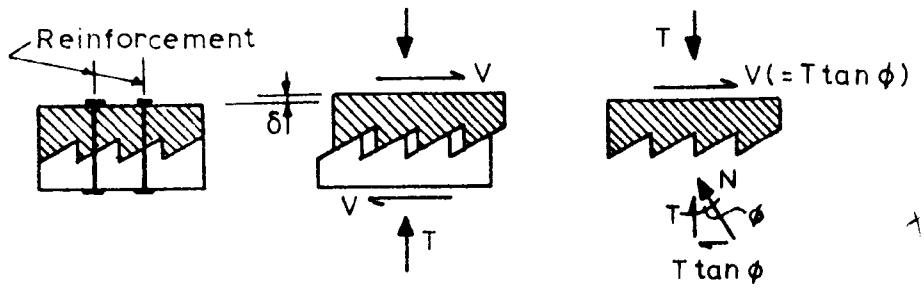

FIGURE 2.31. SHEAR FRICTION MODEL. [55].

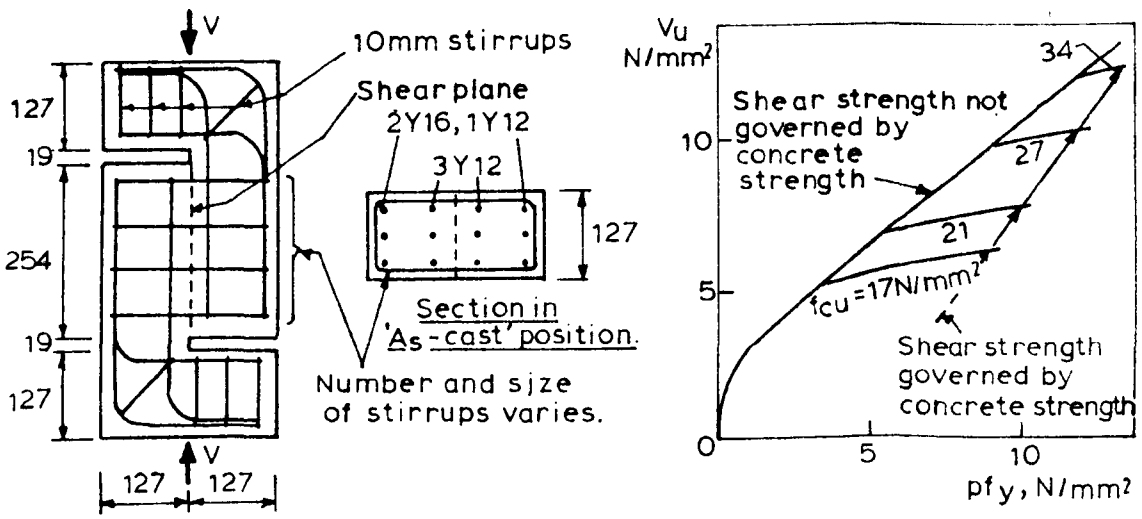

a) Test specimen. b) Test Results.

FIGURE 2.32. PUSH-OFF TEST OF MATLOCK. [55].

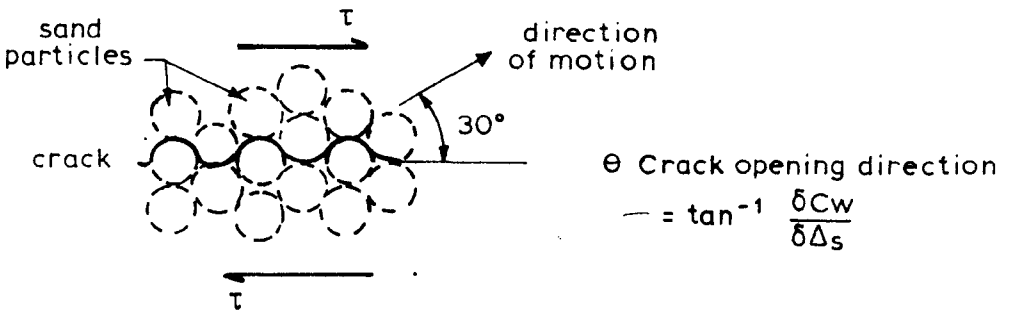

FIGURE 2.33. DIRECTION OF CRACK OPENING. [59]

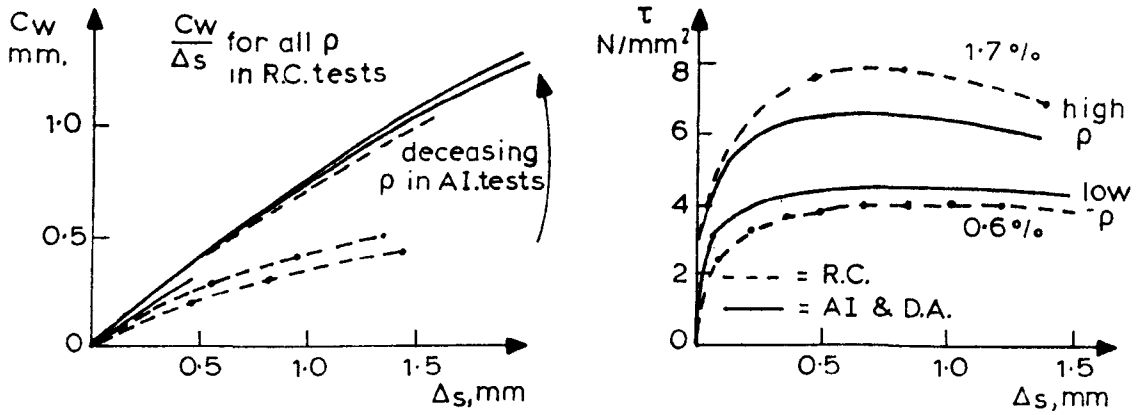

a) Crack opening direction. b) Shear stiffness.

FIGURE 2.34. COMPARISON OF R.C. TEST RESULTS WITH RESULTS PREDICTED FROM A.I. AND D.A. TESTS. [42.]

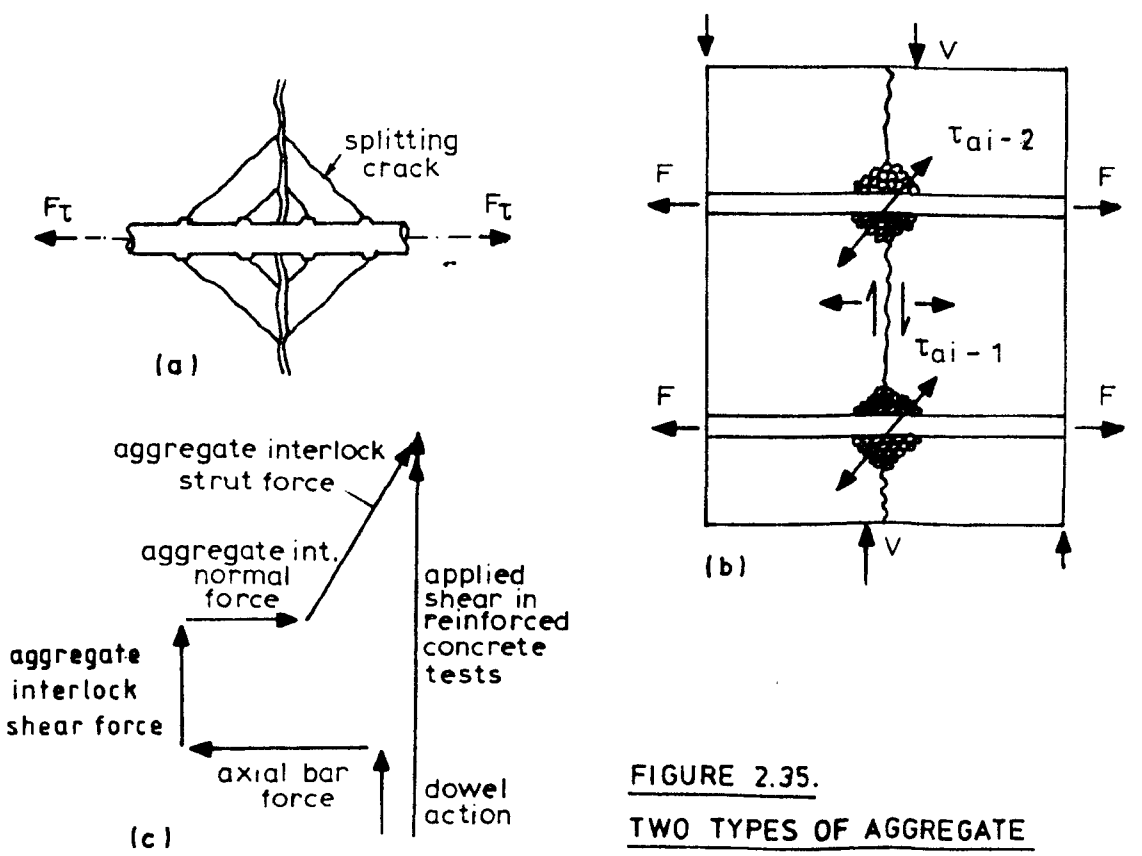

FIGURE 2.35. TWO TYPES OF AGGREGATE INTERLOCK IN R.C. SPECIMENS. [42].

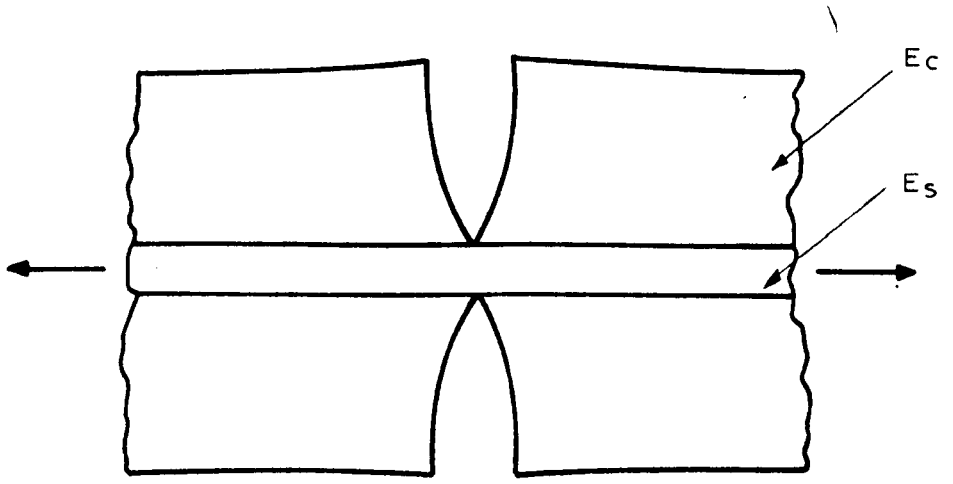

a) Without bondslip

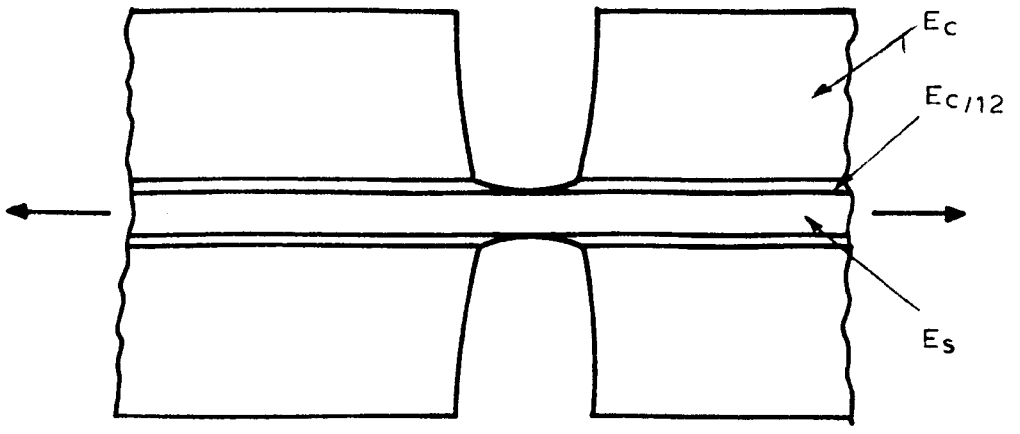

b) With bondslip

FIGURE 2.36. MODELLING OF CRACK PROFILE. [16].

CHAPTER THREE

TESTS ON AGGREGATE INTERLOCK SPECIMENS

3.1 Introduction

The experimental programme was planned so that the separate effects of aggregate interlock and of dowel action could be studied using similar specimens and a comparable loading configuration. Reinforced concrete specimens were then tested to study the combined effect of aggregate interlock and dowel action under a similar loading configuration.

In the aggregate interlock test series, attention was focussed upon the relationship between the shear stiffness of the cracked specimen, the rate of crack widening with shear slip and the normal stiffness restraining the crack from widening. When the project was planned, there was very little published information in this area. A number of investigations (41, 50, 53) into the shear stiffness of cracked concrete had been carried out, but the influence of the stiffness normal to the plane of cracking upon the shear stiffness did not appear to have been studied fully.

The test rig was designed so that shear forces and forces normal to the plane of cracking could be independently applied and so that the displacements parallel and normal to the crack were not restrained by the test rig. In test 2C a compressive force normal to the plane of cracking was progressively applied during shear loading. This was in order to maintain a constant crack width and hence enable a direct comparison with the test results of Paulay and Loeber (50). For all the other aggregate interlock tests, the crack width was

permitted to increase during shear loading.

It had been observed from existing research (51, 53) that neither the shape nor the maximum size of the aggregate used had any significant effect upon the shear stiffness of a cracked concrete specimen, except at very high levels of shear slip or crack width. In this investigation the tests were therefore limited to using just one type and maximum size of aggregate.

3.2 Manufacture of aggregate interlock specimens

3.2.1 General details

The specimens used for testing consisted of rectangular concrete prisms with dimensions as shown in Figure 3.1. It was necessary to ensure the initiation of a central tensile crack in the specimen and this was achieved by reducing the cross section at the centre. A 1 mm wide slot was formed in each specimen by placing a greased steel insert into the mould. The same insert was used for the reinforced concrete specimens and is seen in Figure 5.2. After the concrete had hardened, this insert was removed. Stiff steel plates were glued to the ends of each specimen using a Ciba-Giegy XD800 epoxy resin. The gluing procedure is described in section 3.5.1.

There were two sizes of specimens tested in the aggregate interlock series of tests. The short specimens were used so that the effects of a high normal stiffness could be studied without using excessively large reinforcing bars. A central crack was formed by applying a direct tensile load to the ends of the specimen. When using the longer specimens, it proved difficult to achieve a very small initial crack, i.e. 0.125 mm or less. The release of energy when cracking occurred tended to 'spring' the crack open. If there was a small

shear dislocation due to misalignment of the axial load or to a dislodgement of broken aggregate particles within the crack, it was then difficult to regain the desired small crack width, even if all the external force was removed. This proved to be less of a problem with the stiffer, shorter specimens.

In the early aggregate interlock tests difficulty was found in initiating a central, tensile crack. Instead the specimens would fail prematurely in tension close to the ends. This was initially resolved for specimens 4A(i) and 4A(ii) by forming a deeper crack initiating slot, projecting 20 mm beneath the surface. This left an area of 260 x 60 mm of interlocking concrete. However, for subsequent tests, the method of producing uniform axial tension in the specimen was improved and the depth of the central slot was reduced to 15 mm, resulting in a crack face of 270 x 70 mm.

3.2.2 Reinforcement

Dowel action effects were removed from the aggregate interlock tests by placing the reinforcement into two 25 mm diameter ducts, cast into each specimen. When the specimens had gained strength, stiff steel plates were bonded to each end using an epoxy adhesive. The reinforcement was then clamped onto these end plates by tightening anchoring nuts onto threads machined onto the ends of each bar. Thus the only contact between each bar and the concrete specimen was via these end plates. The dowel stiffness resulting from flexure of the reinforcement over its entire length was negligible. A view of the crack face subsequent to shear loading is shown in Figure 3.2. The location of the crack initiator and the reinforcement ducts are clearly visible.

A typical stress strain curve for a Y12 bar is shown on Figure 3.3. When a 25 mm diameter bar was used, the usual high yield steel was not available. Instead EN8 steel was used. It is seen from Figure 3.3 that, for stresses below 300 N/mm^2, there was no significant difference in the stiffnesses. This stress level is more than double the maximum stress attained by the reinforcement in aggregate interlock tests because of the absence of bond between the reinforcement and the concrete.

3.2.3 Concrete

Two concrete mixes were used. Target strengths and mix designs are given in Table 3.1 and the measured cube strengths in Table 3.2. The concrete was designed to be tested after 21 days and rapid hardening Portland cement was used for both mixes. The fine aggregate was a land-based sand conforming to B.S. 882, Zone 3 requirements. The coarse aggregate was a rounded gravel of maximum size 10 mm.

The concrete was placed in the mould in three layers and was compacted at each stage using a vibrating table. This procedure was employed to minimise the segregation of the concrete and the collection of water beneath the void formers. According to Cambell-Allen and Lau (61) the formation of local areas of weakness can be minimised by using this method.

Each concrete specimen was cured under wet hessian at room temperature for 24 hours and then stored in a thermostatically controlled water tank for 14 days. The end plates were then bonded to the specimen, which was subsequently left in air for a further 7 days before testing. Three 100 mm cubes and two 100 x 100 x 600 mm modulus of rupture beams were cast and tested with each specimen.

The modulus of elasticity was also measured for a range of concretes with different compressive strengths (Figure 3.4a). These results follow the same trends as those of Oehlers (62), using the same aggregates and mix design method.

In Figure 3.4b the stress-strain relationship for the high strength concrete is plotted up until the onset of compressive failure. This curve lies quite close to the curve predicted by Desayi (63).

Figure 3.4c shows the relationship between the compressive strengths of the concrete specimens and the tensile strength obtained by applying third-point loading to the modulus of rupture beams. There is only a slight relationship between the two parameters and a considerable degree of scatter. The scatter is due to the fact that the tensile strength of concrete is determined more by the random occurrence of micro-cracks or points of weakness in the specimen than by the adhesion between the cement paste and the aggregate.

3.3 Description of the test rig and instrumentation

3.3.1 Axial tensile loading

The test rig for applying independent shear and tensile forces to the test specimens is shown in Figure 3.5. Axial tension was applied to the specimen by applying a compressive force between the two loading plates on the left. This force was transferred to steel end plates, resin bonded to the concrete specimen, by stiff compression struts and flexible tension plates. Before the specimen cracked the axial load was carried jointly by the concrete specimen and the reinforcement. Once cracking was initiated, all the axial load was taken by the two reinforcing bars.

The axial force applied to the specimen was measured using a Mayes load cell with a maximum output of 12 tons. The output was 50 mV, which was measured on a digital display voltmeter. To ensure that there were no bending effects caused by misalignment of the jack the flexible tension plates were each fitted with three electrical resistance strain gauges and were calibrated before the test. Any bending forces in the specimen were removed by the use of three turnbuckle adjusting screws, located parallel to the tension jack, between the two loading plates. The pitches of the two threads on each turnbuckle screw had a difference of 0.5 mm. This meant that one complete revolution of a turnbuckle altered the distance between the loading plates by 0.5 mm. This allowed a fine control of the axial force on the specimen which made it possible to achieve a uniform initial surface crack width and to control precisely the axial loading on the specimen during shear testing.

The axial load initially applied to the cracked specimen could also be measured using the pair of electrical resistance strain gauges affixed to each reinforcing bar. This value was verified against the force measured in the load cell and in the flexible loading plates. All the strain gauges used were TML type PL10 gauges. These were polyester backed, temperature compensated gauges which were read manually using a Peekel 5 channel bridge, with an additional 10 channel switch box to include the strain gauges on the flexible loading plates.

Once shear displacement across the crack started to cause overriding of the opposing crack faces, the additional normal compressive forces within the specimen could only be determined from observing the increase in the axial forces in the reinforcement. The widening of the crack resulted in a decrease in the axial force applied by the test rig.

In some tests this force was permitted to diminish whilst in other tests the applied axial force was restored to its initial value after each increment of shear loading (see section 3.5.3). In either case the externally measured axial load no longer corresponded to the internally measured axial load once overriding had commenced. Hence it is essential to instrument the reinforcement to determine what forces are being exerted upon the crack face.

3.3.2 Shear loading

Shear loading was applied across the central crack by applying bearing forces adjacent to the crack on the upper and lower surfaces. Two additional forces were applied at the ends of the specimen, via a distribution beam (Figure 3.6a), to maintain equilibrium. All the forces were applied through knife edge bearing pads to permit unrestrained shear deformation of the specimen and so that the points of application of the forces were accurately known. Similarly, the overall force applied to the distribution beams was transmitted through spherical bearings to avoid any eccentricity. This force was applied by supporting the specimen and test rig in a reaction frame (just visible in Figure 3.5) and placing a manual hydraulic 20 tonne jack beneath the lower spherical bearing. A 25 tonne load cell, connected to a digital voltmeter, was used to determine the magnitude of the load.

In two tests a second load cell was also placed between the upper spherical bearing and the reaction frame to determine the effects of the self weight of the specimen and the test rig upon the shear load transmitted across the crack. In Figure 3.6a the forces on the specimen when the lower load cell indicated a force of 5 tonnes are given. The vertical shear force diagram is plotted in Figure 3.6b.

3.3.3 Independence of tensile and shear loading

One of the difficulties in designing any test rig to apply a number of concurrent loads is to ensure that the separate loads and deflections are independent of each other and the loads are transmitted solely to the specimen and not to other parts of the test rig. The use of flexible plates (Figure 3.6a), to transfer tension to the specimen ends, ensures that this part of the test rig has a low shear stiffness and hence the specimen is free to deform in shear. However, it was also necessary to place needle roller bearings beneath two of the shear loading pads so that the shear distribution beams did not restrain the crack from widening or contribute to the axial stiffness of the specimen.

3.3.4 Measurement of concrete strain and displacements

Strains at the surface of the concrete and displacements across the crack were measured using Demec gauges. Initially twenty one measurements were taken on each side of the specimen, (Figure 3.7a) using gauge lengths of 50 mm and 150 mm. However, the results of the first few tests indicated that the shear slip across the crack was uniform along the length of the crack. This result was corroborated by the results of a finite element analysis (Appendix A1). The number of measurements taken on each side of the specimen was then reduced to ten (Figure 3.7b) and only 100 mm gauge lengths were used. A revised layout for the contact points was required for the shorter specimens (Figure 3.7c).

Referring to Figure 3.7b, the direct strains in the uncracked part of the specimen were obtained from Demec points 1,2 3,4 etc. for strains normal to the plane of cracking and from Demec points 5,9 8, 12 etc. for strains parallel to the plane of cracking.

The surface crack width was defined as the separation of the two crack faces, measured in a direction perpendicular to the mean plane of cracking. When the specimens were being cracked the stress field was uniaxial and hence this definition is appropriate. However in a biaxial stress field the direction in which the crack should be measured may not be obvious. The crack width Demec measurements were adjusted to compensate for any strain in the uncracked concrete over the gauge length e.g. for 2,3

$$C_w = e_{2,3} - \{(e_{1,2} + e_{3,4})/2\} \qquad (3.1)$$

where $e_{2,3}$ is the change in length between points 2 and 3.

It was observed that the effect of strain in the uncracked concrete was very small in comparison to the crack width and hence this adjustment was probably unnecessary. The tangent effect of shear slip across the crack upon the crack width measurement was so small that it was ignored.

The shear slip of the crack was obtained from Demec points 6, 11 and 7, 10 and was given by

$$\Delta_s = (|e_{6,11}| + |e_{7,10}|)/2 \qquad (3.2)$$

The use of crossed pairs of Demec points in this manner meant that the effects of strain in the concrete or crack widening upon the measurement of shear slip were automatically cancelled out.

3.4 Crack roughness

When the aggregate interlock series of tests was planned, it was

thought that the global roughness of the crack, i.e. roughness of order of magnitude of the coarse aggregate particles, would be an important parameter affecting the behaviour of specimens with a crack width greater than 0.25 mm. A variable profile gauge was fabricated (Figure 3.8) with which a cross section of one crack face could be recorded with an accuracy of ± 1 mm. A typical example is shown in Figure 3.9.

3.5 Testing procedure

Each test was conducted in two stages. First a tensile central crack was initiated. This was followed by incremental shear loading across the crack.

3.5.1 Crack initiation

There were a number of problems encountered when trying to obtain a central crack in the specimens by applying direct tension. In the first few attempts bond failure occurred between the resin-steel interface or between the resin-concrete interface, at one end of the specimen. This type of failure was prevented by meticulously preparing the two surfaces before glueing them together. Both surfaces were roughened using a percussion needle gun. The concrete surface was then blown with clean air to remove all dust and loose particles. The steel surface was given a "vapour blast" treatment, consisting of a high pressure jet of water and fine glass beads. This produced a clean, bright finish which then started to oxidise within minutes of drying. This oxidation was prevented by washing the wet surface with acetone, to remove all traces of water. The prepared concrete and steel surfaces were then immediately resin bonded together, whilst care was taken not to touch either surface or allow any contamination by grease.

This procedure eliminated bond failure between the end plates and the concrete. However it was found that the end plates were still becoming detached, before a central tensile crack could form. The failure was now occurring just within the concrete adjacent to the end plate. This second problem was initially solved by increasing the depth of the slot at the centre of the specimen, as described in section 3.2.1, to increase the stress concentration.

However, failures of concrete adjacent to the end plates continued to occur. This was eventually traced to the inadequate flexural rigidity of the 20 mm thick steel end plates. A linear elastic finite element analysis of the specimen was carried out (Appendix A1) and this revealed stress concentrations in the concrete adjacent to the end plate, due to flexure of these plates, of the same order of magnitude as the stress concentration caused by the crack initiating slot. The flexural stiffness of both end plates was increased by an order of magnitude by welding channel section steel to the back of the plates. Subsequently there were no further failures of the end plates and for all tests, with the exception of 4A(i) and 4A(ii), a 15 mm deep crack initiating slot was successfully used.

Once a satisfactory crack had been formed using a hydraulic jack, the load in the jack was transferred to the three turnbuckle screws. By a careful adjustment of these screws the crack was preset to the desired width. It was usually possible to obtain this to within $\pm$ 0.01 mm.

In some tests, in which a small initial crack width was required, it was found that even with no load in the turnbuckle screws, there was insufficient tensile force in the reinforcement to close the crack up.

It was presumed that, either because a small unintentional shear slip had occurred or because a piece of aggregate had become dislodged, the crack had jammed open. Two procedures were used to prevent this happening:

1. An initial prestress of 20 N/mm^2 was applied to the reinforcement, by tightening up the anchoring nuts on each end, before cracking the specimen.

2. The crack was formed and set to the required value with the specimen positioned so that the axes of the reinforcing bars were vertical. This was to ensure that the self weight of the specimen did not cause any unintentional shear slip as soon as the crack was formed. Once the required value for the crack width had been obtained, the specimen and the tensile loading part of the test rig was rotated through 90°, so that shear loading could then be applied.

3.5.2 Shear across the crack

Incremental shear loading was applied across the crack by manually increasing the jacking force beneath the lower load distribution beam (Figure 3.5). All the test data was manually recorded between each increment. Each test was terminated when an increment of shear load caused an excessive shear displacement and it was judged that the specimen was near failure. No attempt was made to follow the descending portion of the load deflection curve using displacement control. It has been observed by Perdikaris, White and Gergely (64) that, at high shear loads in orthogonally cracked slabs, failure occurred by the formation of additional diagonal shear cracks. Hence the post-ultimate shear stiffness of the original

cracks has little importance because it is not the mechanism for shear failure.

3.5.3 Normal restraint stiffness

One of the principal parameters influencing the aggregate interlock stiffness is the stiffness normal to the crack, which restrains it from widening. This stiffness is usually considered to be the anchorage stiffness of the reinforcement normal to the crack, i.e. the compressive stiffness of the uncracked concrete is ignored. The anchorage stiffness of the reinforcement will depend upon the number and size of the bars and also upon the bond, if any, with the concrete.

However, it is important to realise that the tensile stiffness of the test rig will also contribute to the normal restraint stiffness unless measures are taken to prevent this. If the cracked specimen and the test rig are considered as two springs in parallel (Figure 3.10), both will resist a tensile force of F_t when cracking has occurred. Subsequent shear slip will cause overriding, and hence cause an internal compressive force, δF_c, between the crack faces. There will be a resultant increase in the crack width, δC_w. Hence from equilibrium

$$F_t + k_1 \delta C_w = \delta F_c + F_t - k_2 \delta C_w$$

$$\frac{dF_c}{dC_w} = k_1 + k_2 \qquad (3.3)$$

Alternatively, if the external force in the test rig is restored to its initial value once the shear slip has occurred,

$$\frac{dF_c}{dC_w} = k_1 \qquad (3.4)$$

For the first few tests the stiffness of the test rig was permitted to contribute to the normal restraint stiffness. For all later tests, the externally applied tensile force was restored to its initial value after the application of an increment of shear load and before any readings were taken. This was easily achieved using the turnbuckle adjusting screws to reset the strains initially measured on the flexible tensile straps.

In all the aggregate interlock tests there was a disparity between the increase in the crack width, measured with a Demec gauge, and the total increase in the length of the reinforcement, measured with strain gauges. The increase in crack width was typically only 30% to 50% of the increase in the length of the reinforcement (Figure 3.11a). It was at first not clear why this was so. Hence a dial gauge caliper was fabricated to measure, externally, the extension of the reinforcing bars. This measurement was found to correlate reasonably well with the internal measurement from electrical resistance strain gauges (Figure 3.11b). The disparity was therefore attributed to bedding in between the reinforcement, the anchoring nuts on each end and the end plates. The prestress of 20 N/mm^2 placed on the reinforcement before crack initiation helped to reduce the disparity but did not remove it. However, as the change in forces in both the reinforcement and the tension straps were measured, the normal restraint stiffness was known. It is the absolute value of this stiffness and the dependence of the shear stiffness upon it which is required for comparison with the reinforced concrete test results. As this stiffness was known, the bedding in effects of the reinforcing bars did not affect the validity of the aggregate interlock test results.

3.6 Test results

The aggregate interlock test series was subdivided into three groups.

The specimens in group 1 had an initial crack width within the range 0.063 mm to 0.25 mm. This is the range in which Laible et al. (53) predicted that shear would be resisted by bearing or crushing of the "local roughness" of the crack face, as described in section 2.5.2.1.

The specimens in group 2 had an initial crack width within the range 0.5 mm to 0.75 mm. This was the range in which Laible et al. predicted that shear would be resisted by sliding of the "global" roughness of the crack.

Group 4 consisted of the two aggregate interlock specimens where the area of the crack face was reduced to 260 mm x 60 mm, to facilitate tensile cracking. The test results should be considered together with group 2, but the normal restraint stiffness per unit crack area and the shear force per unit crack area are proportionately higher, for otherwise similar specimens and loadings.

3.6.1 Test series 1 - small initial crack widths

The parameters varied in this series were

- the initial crack width
- the normal restraint stiffness
- the concrete strength

The properties of each test specimen are given in Table 3.2. A complete set of the individual results for each test is provided in reference 65. A comparison between all of these test results is

presented in Figures 3.12 to 3.17. From these results the following observations can be made:

3.6.1.1 Repeatability

Tests 1A(i) and 1A(ii) used nominally identical specimens to find out if the aggregate interlock effect could be repeated. However, the normal restraint stiffness of the two specimens differed because of differing "bedding in" stiffness of the restraint bars, as discussed in section 3.5.3. A third specimen, 1A(iii), was tested and had the same normal restraint stiffness as specimen 1A(i). In Figure 3.12 the test results of 1A(i), 1A(ii) and 1A(iii) are compared.

The shear stress, τ_s, is taken as an average stress over the area of the crack face. All the aggregate interlock specimens had a crack face area of 18900 mm^2, with the exception of specimens 4A(i) and 4A(ii). These had a crack face area of 15600 mm^2, due to the deeper crack initiating slot. The normal stress, σ_c, is also defined as the compressive force, normal to the crack face, divided by the crack face area. The crack width, C_w, and the shear slip, Δ_s are defined in section 3.3.4. It can be seen from Figure 3.12a that the shear stiffness of specimens 1A(i) and 1A(iii) are similar. Specimen 1A(ii), which had a higher normal restraint stiffness (Figure 3.12c), had a slightly higher shear stiffness.

There was some unintentional scatter in the strength of the concrete for these specimens. From 3.12b it is seen that a higher strength of concrete tended to increase the ratio of crack widening to shear slip.

3.6.1.2 Initial crack width

In Figure 3.13 it is seen that for two specimens having similar normal restraint stiffness but different initial crack widths, a smaller initial crack width results in a greater shear stiffness. Both specimens exhibited a considerable crack widening, which is inconsistent with the "local roughness" theory of Laible et al. (53). The initial crack width was not observed to influence significantly the ratio of crack widening to shear slip in Figure 3.13b. However, when the results of test 1B and 1G are compared (Figure 3.20b) it was observed that the specimen with the smaller initial crack width did have a greater ratio of crack widening, to shear slip. This may be related to the different normal restraint stiffness obtained in each pair of tests.

3.6.1.3 Normal restraint stiffness

The effect of varying the normal restraint stiffness on two similar specimens with very small initial crack widths is seen in Figure 3.14 and 3.15. Increasing the normal restraint stiffness results in increasing the shear stiffness and decreasing the ratio of crack widening to shear slip. Again there is a disparity between the observed test results and the "local roughness" theory.

3.6.1.4 Concrete strength

From Figure 3.16 it can be seen that increasing the strength of the concrete from 30.0 N/mm^2 to 52.1 N/mm^2 had little effect on the behaviour of the specimens. The slightly higher shear stiffness of specimen 1D could be due to the small difference in the normal restraint stiffness, which was obtained (Figure 3.16c).

3.6.2 Test series 2 and 4 - large initial crack widths

All the specimens in these series had initial crack widths of 0.5 mm or greater. With the exception of specimen 2D, all the specimens were 450 mm long. The overall conclusion from comparing these test results with those of test series 1 is that there seems to be very little difference in the mode of behaviour.

3.6.2.1 Repeatability

A comparison of the results in tests 2F(i), 2F(ii) and 2D is shown in Figure 3.17. Specimen 2F(i) was the first one to be successfully tested and there was a significant shear slip observable in Figure 3.17(a) and (b) before the application of shear loading. This behaviour did not recur in any of the subsequent tests and was attributed to an error in the instrumentation or method of loading. Test 2F(ii) was a repeat test to substantiate this view.

Specimen 2D had similar properties to specimen 2F(ii) except that it was 250 mm long instead of 450 mm long. A comparison of the two sets of results shows very little difference in behaviour and indicates that the aggregate interlock is not dependent upon the specimen length if the axial stiffness is similar. The effect of using a shorter specimen was primarily to increase the normal restraint stiffness without altering the reinforcement ratio.

3.6.2.2 Normal restraint stiffness

The effect of increasing the normal restraint stiffness is seen on Figure 3.18. There is a resulting increase in the shear stiffness and a decrease in the ratio of crack widening to shear slip. These trends are similar to those observed in Test Series 1.

In test 2C the crack width was restored to its initial value, after each increment of shear load, by releasing some of the tensile force in the test rig. When a shear stress of 3.5 N/mm^2 was attained, there was no remaining force in the test rig to maintain the crack width and hence crack widening was subsequently allowed to occur. It is not clear why the shear stiffness suddenly changed after a shear stress of 1 N/mm^2 was applied (Figure 3.17a).

3.6.2.3 Initial crack width

The effect of varying the initial crack width for specimens with similar normal restraint stiffnesses is shown in Figures 3.19 and 3.20. A higher initial crack width resulted in a reduced shear stiffness. However, there was also a tendency for an increase in the crack width to result in a lower ratio of crack widening to shear slip. In Figure 3.20 the results of tests 1B and 1G have also been included and substantiate this trend.

Table 3.1

Concrete mix designs

Target Strength (N/mm^2)	Cement content (kg/m^3)	Water Content (kg/m^3)	Fine aggregate (kg/m^3)	Coarse Aggregate (kg/m^3)
35	300	180	701	1194
55	436	205	615	1094

Table 3.2

Details of aggregate interlock specimens

Specimen mark	Target concrete strength (N/mm^2)	Actual[1] concrete strength (N/mm^2)	Specimen size	Reinforcement type (mm)	Initial crack width (mm)
1A(i)	35	41.6	short	Y12	0.25
1A(ii)	35	36.2	short	Y12	0.25
1A(iii)	35	30.0	short	Y12	0.25
1B	35	40.5	short	Y16	0.25
1C	35	30.1	short	Y12	0.125
1D	55	52.1	short	Y12	0.25
1F	35	36.5	short	Y12	0.063
1G	35	35.7	short	Y16	0.063
1H	35	32.5	short	Y25(2)	0.125
1I	35	33.9	short	Y25(2)	0.25
2C	35	29.1	long	Y16	0.5
2D	35	35.4	short	Y12	0.5
2E	35	31.3	long	Y16	0.75
2F(i)	35	34.0	long	Y12	0.5
2F(ii)	35	34.1	long	Y12	0.5
2G	35	35.2	long	Y16	0.5
2K	35	34.4	long	Y8	0.5
4A(i)	35	37.4	long	Y16	0.5
4A(ii)	35	36.3	long	Y16	0.5

Note: (1) This is a mean of three cube tests

(2) EN8 reinforcing steel used

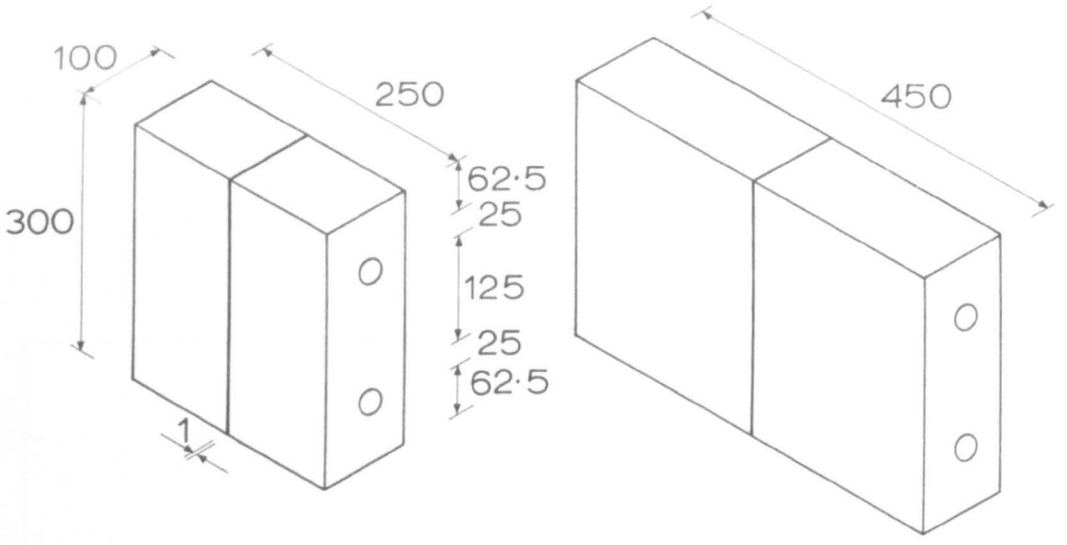

a) Short test specimen b) Long test specimen.

Note:
For specimens 4A(i) and 4A(ii) the central slot was 20mm deep.
For all other specimens the central slot was 15mm deep.

FIGURE 3.1. AGGREGATE INTERLOCK TEST SPECIMENS.

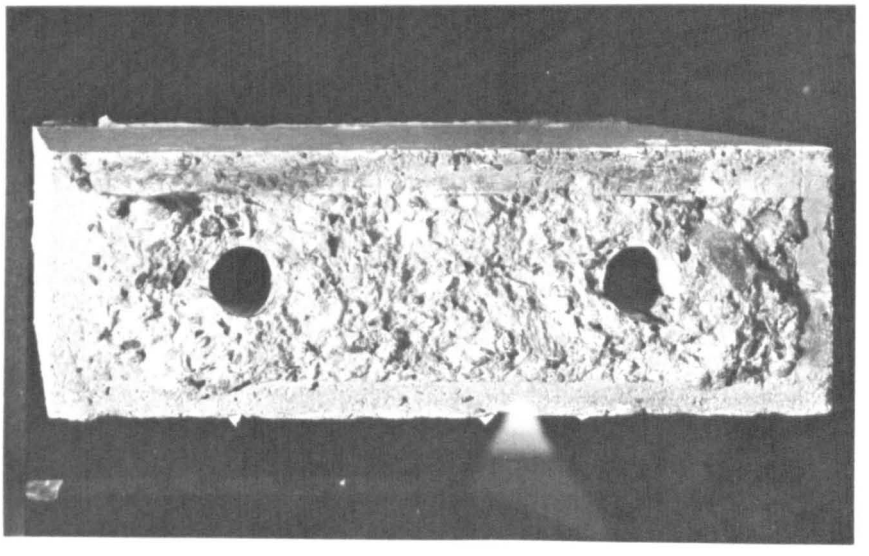

FIGURE 3.2. CRACK FACE OF SPECIMEN 2F(i).

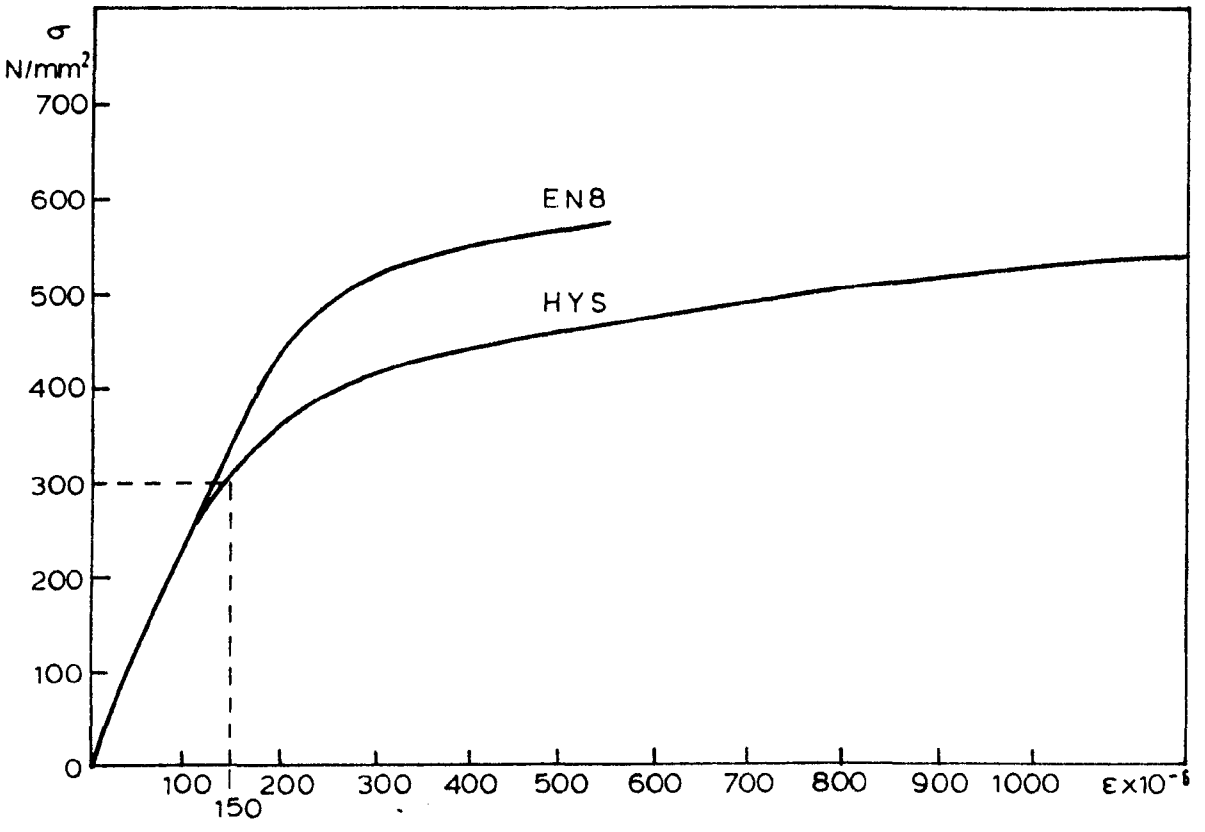

FIGURE 3.3. STRESS-STRAIN CURVE FOR STEEL REINFORCEMENT (ϕ = 12mm)

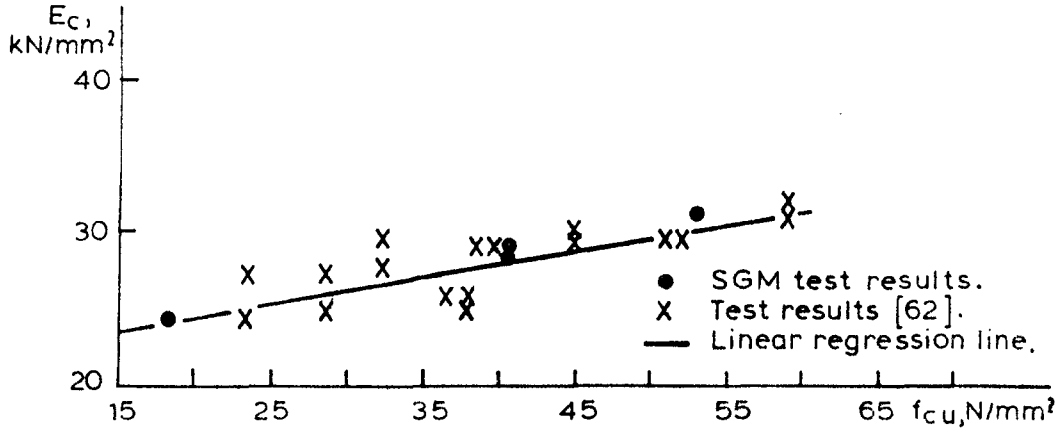

a) Variation in the elastic modulus of concrete with the compressive cube strength.

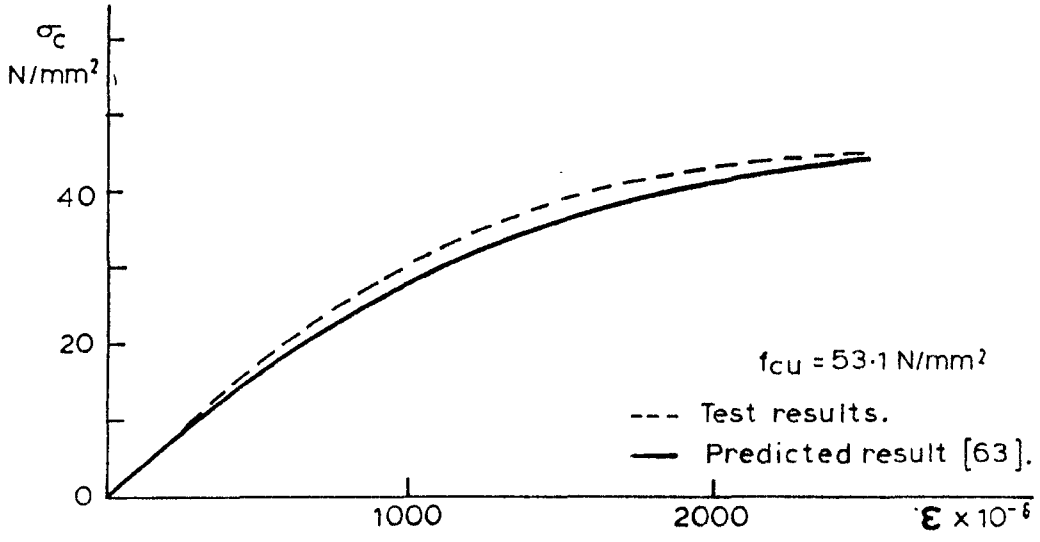

b) Typical stress-strain relation for concrete.

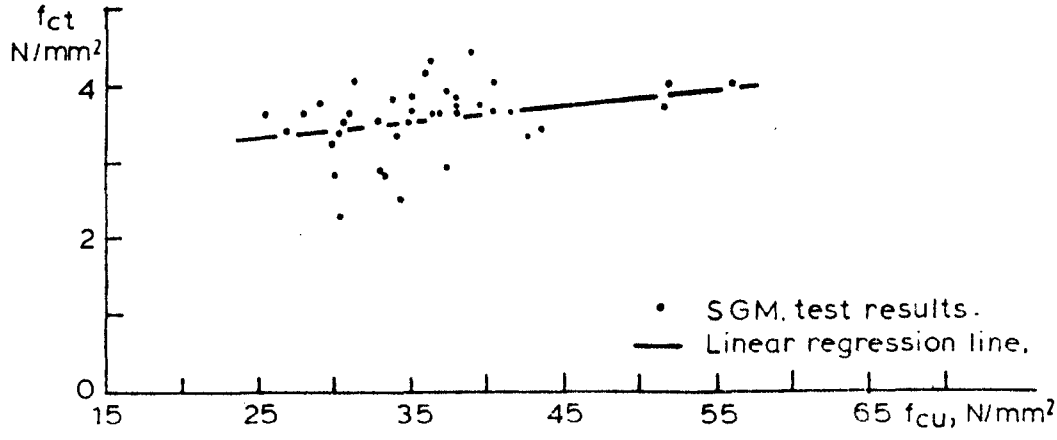

c) Variation in the tensile modulus of rupture of concrete with the compressive cube strength.

FIGURE 3.4. MATERIAL PROPERTIES OF CONCRETE.

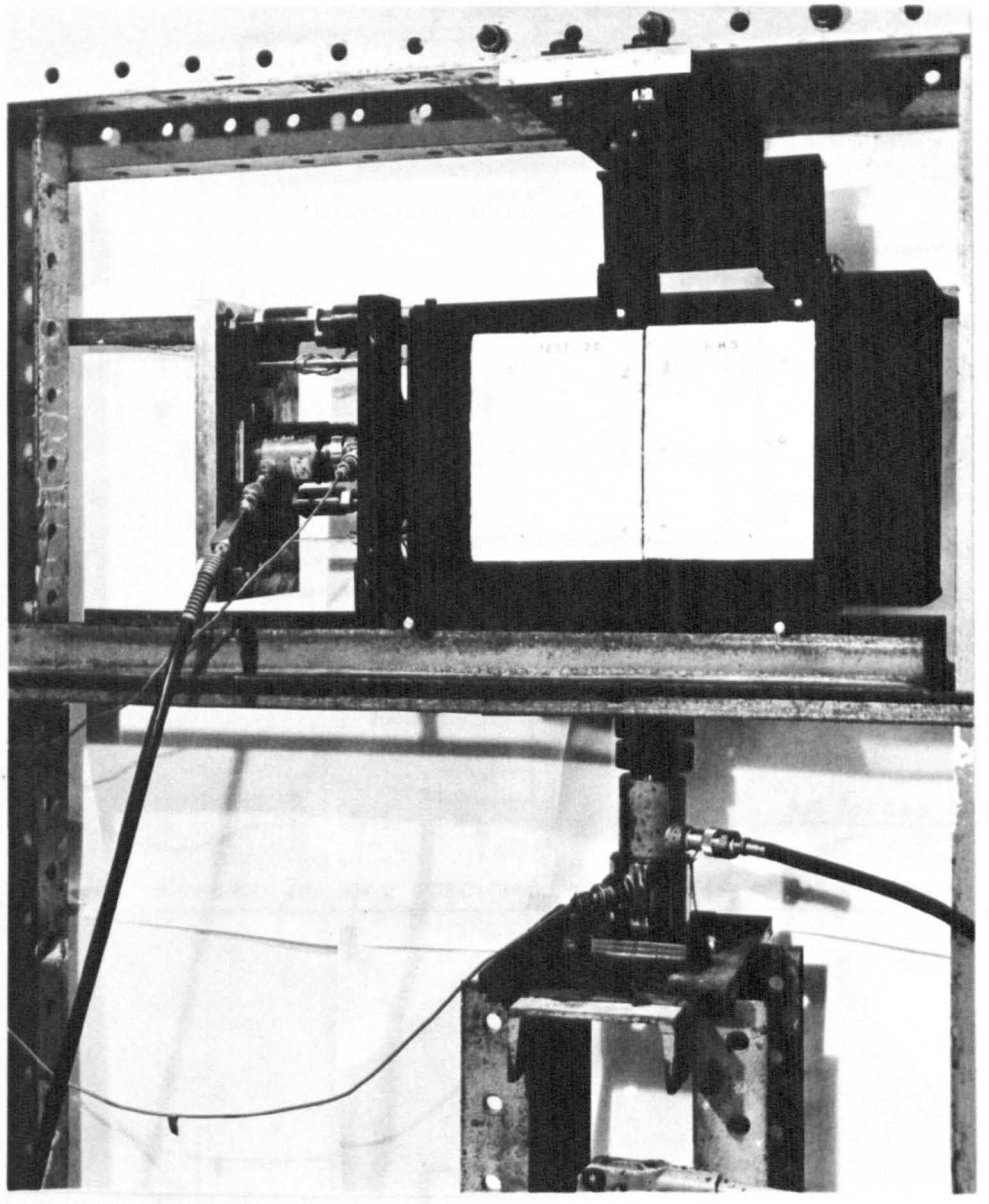

FIGURE 3.5. VIEW OF TEST RIG WITH A LONG SPECIMEN.

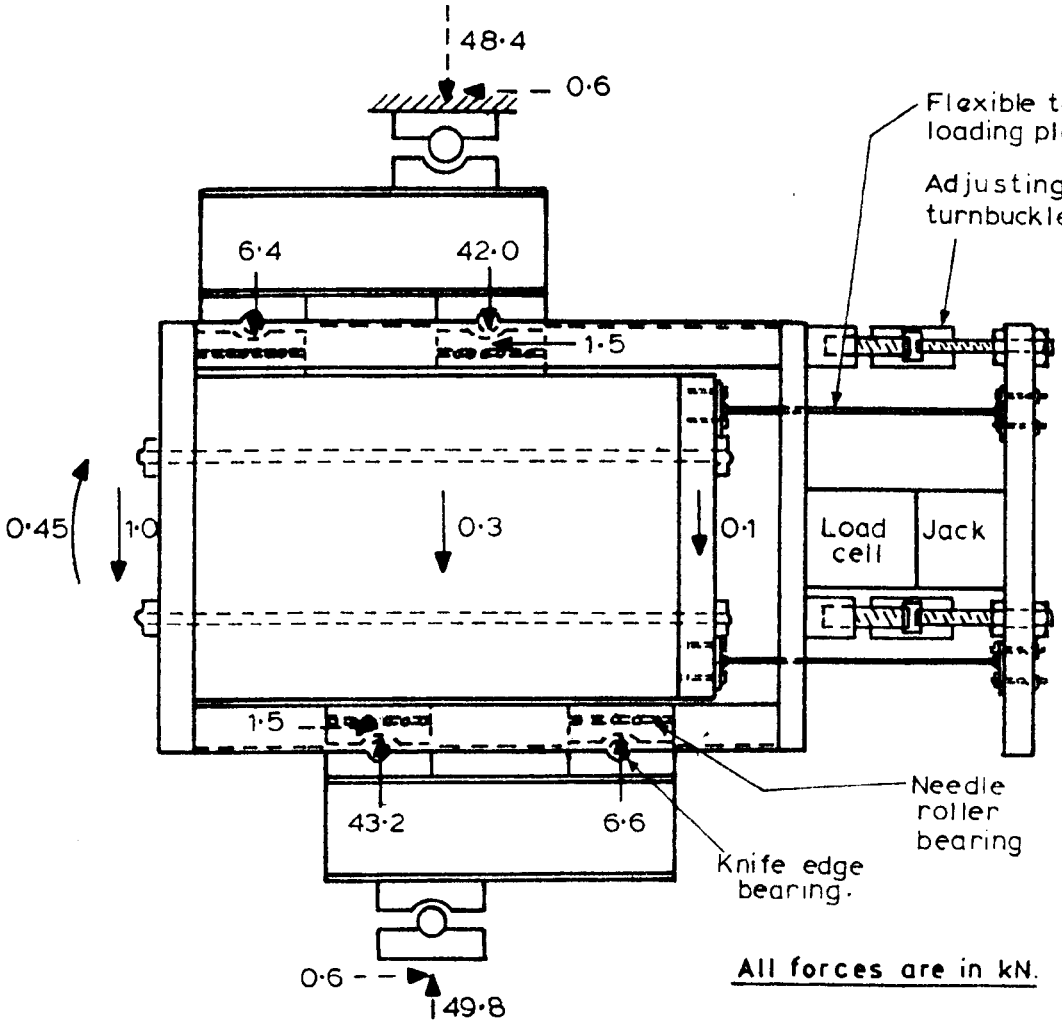

a) Forces on long specimen when lower shear load cell = 5 T.

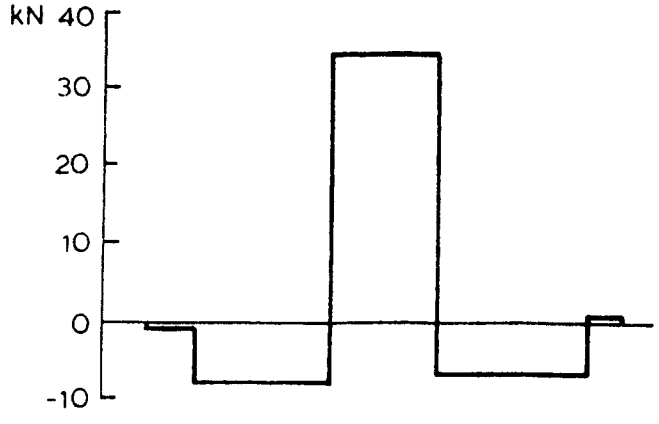

b) Vertical shear force diagram.

FIGURE 3.6.

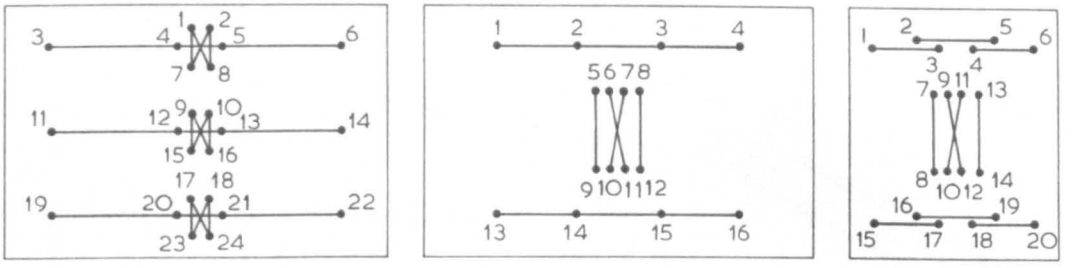

a) Initial layout

b) Revised layout long specimen

c) Revised layout short specimen

FIGURE 3.7. LAYOUT OF DEMEC POINTS.

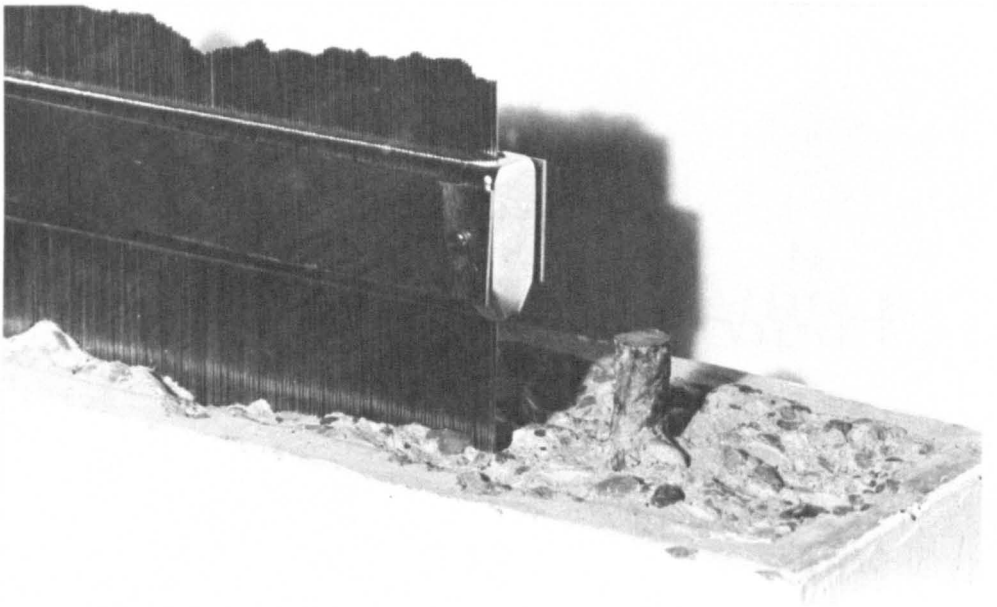

FIGURE 3.8. CRACK PROFILE GAUGE.

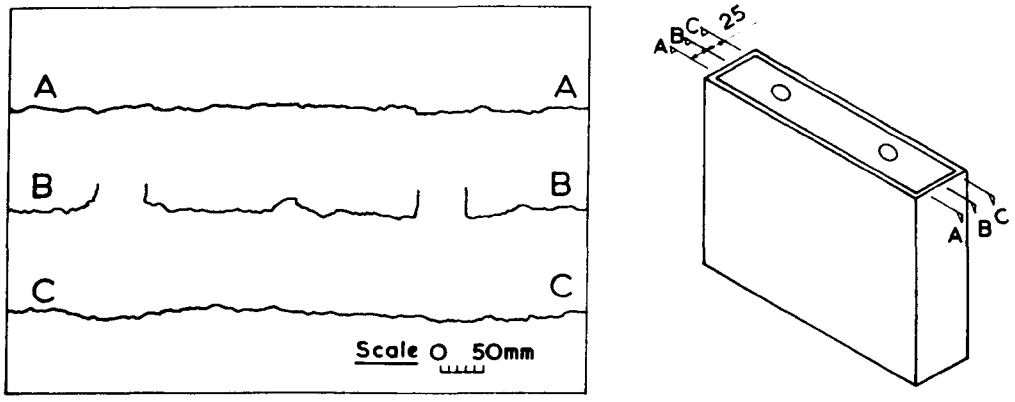

FIGURE 3.9. GLOBAL CRACK PROFILE OF SPECIMEN 2G

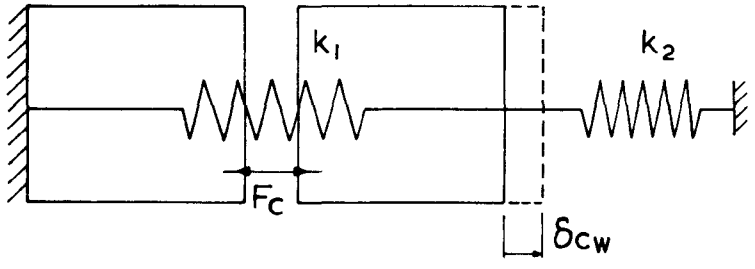

FIGURE 3.10. INTERACTION OF THE STIFFNESSES OF THE SPECIMEN AND THE TEST RIG.

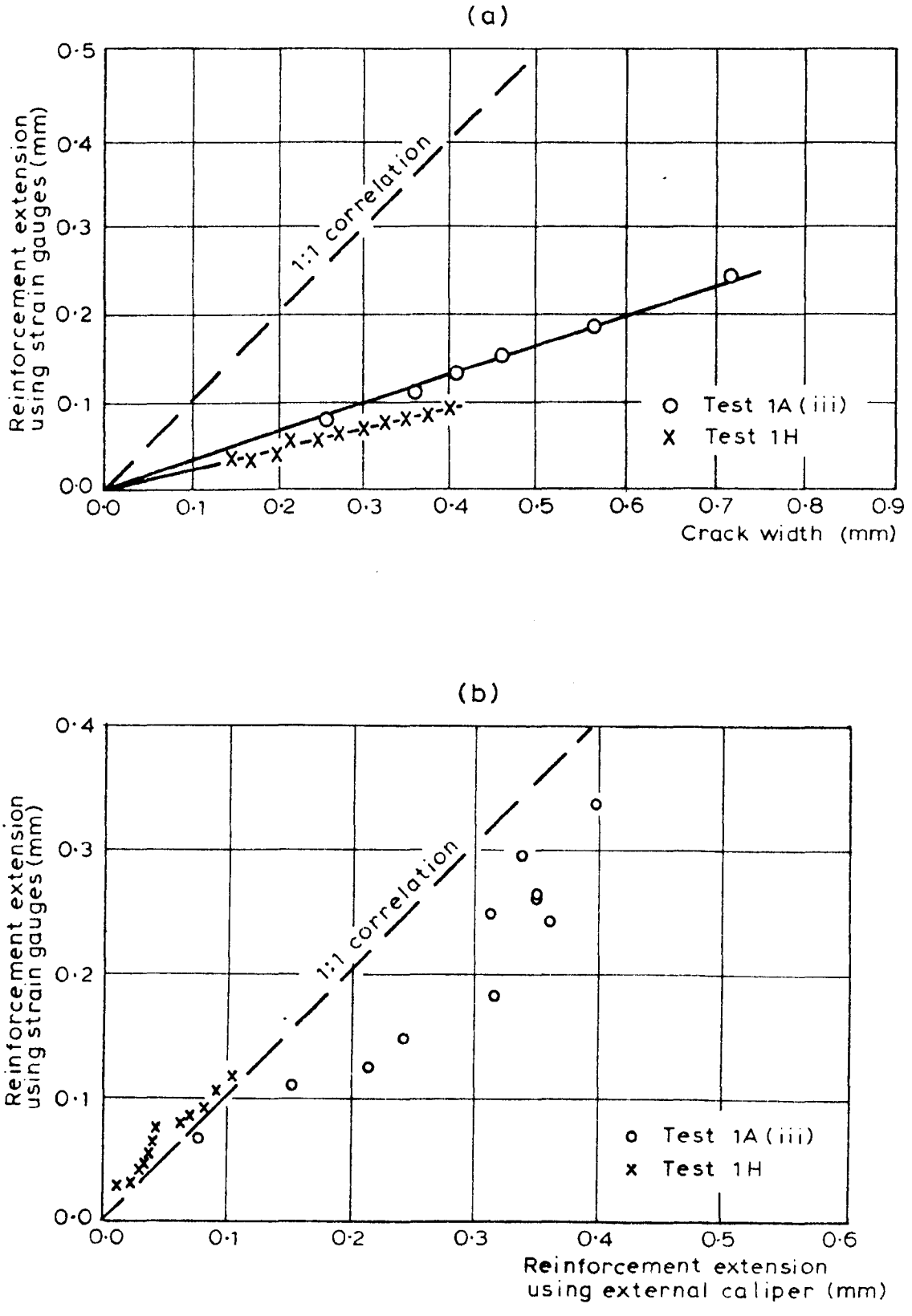

FIGURE 3.11. COMPATIBILITY OF TEST MEASUREMENTS.

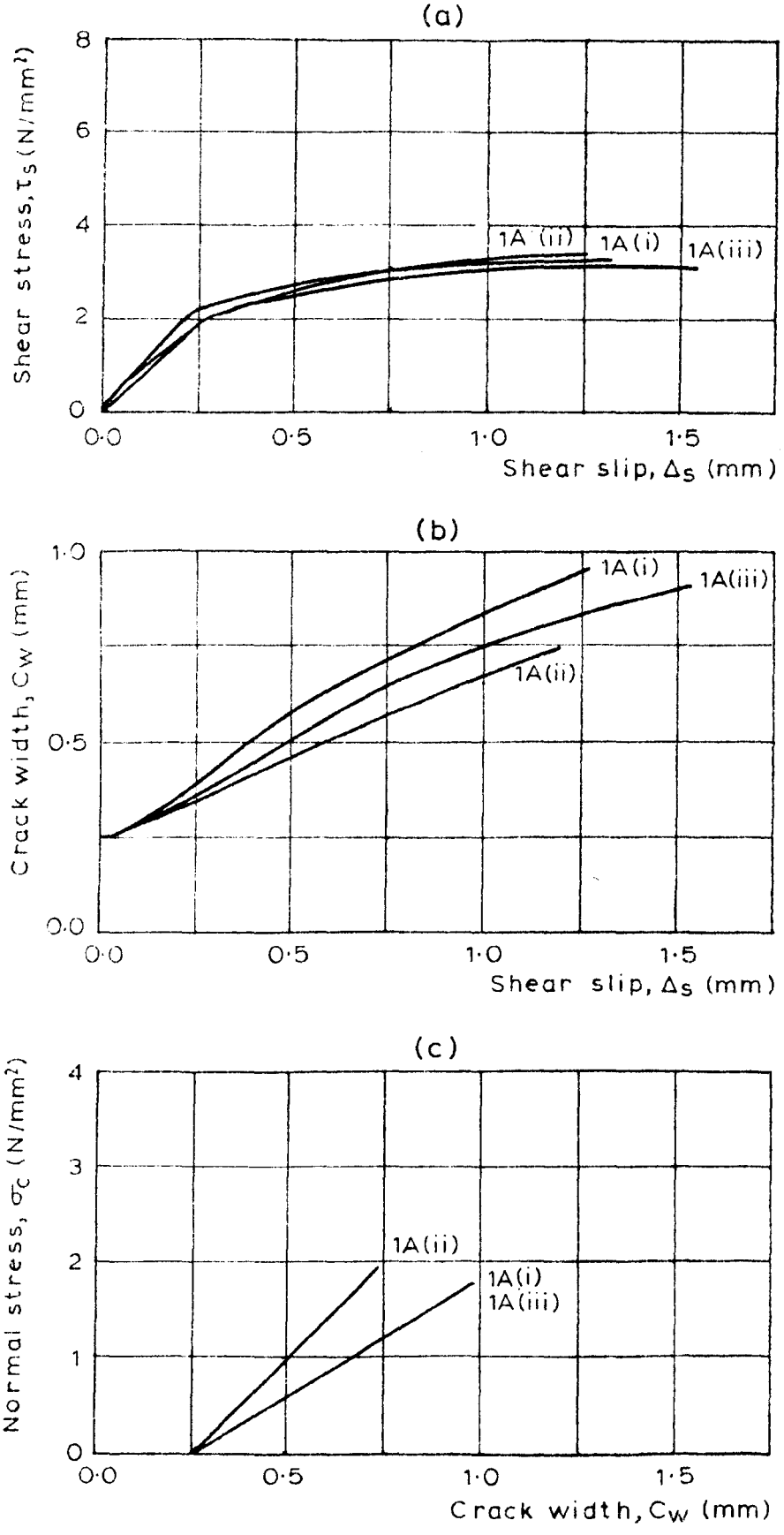

C_{wi} = 0·25mm

f_{cu} { 1A(i) = 41·6N/mm²
1A(ii) = 36·2N/mm²
1A(iii) = 30·0N/mm²

FIGURE 3.12. SIMILAR AGGREGATE INTERLOCK SPECIMENS.

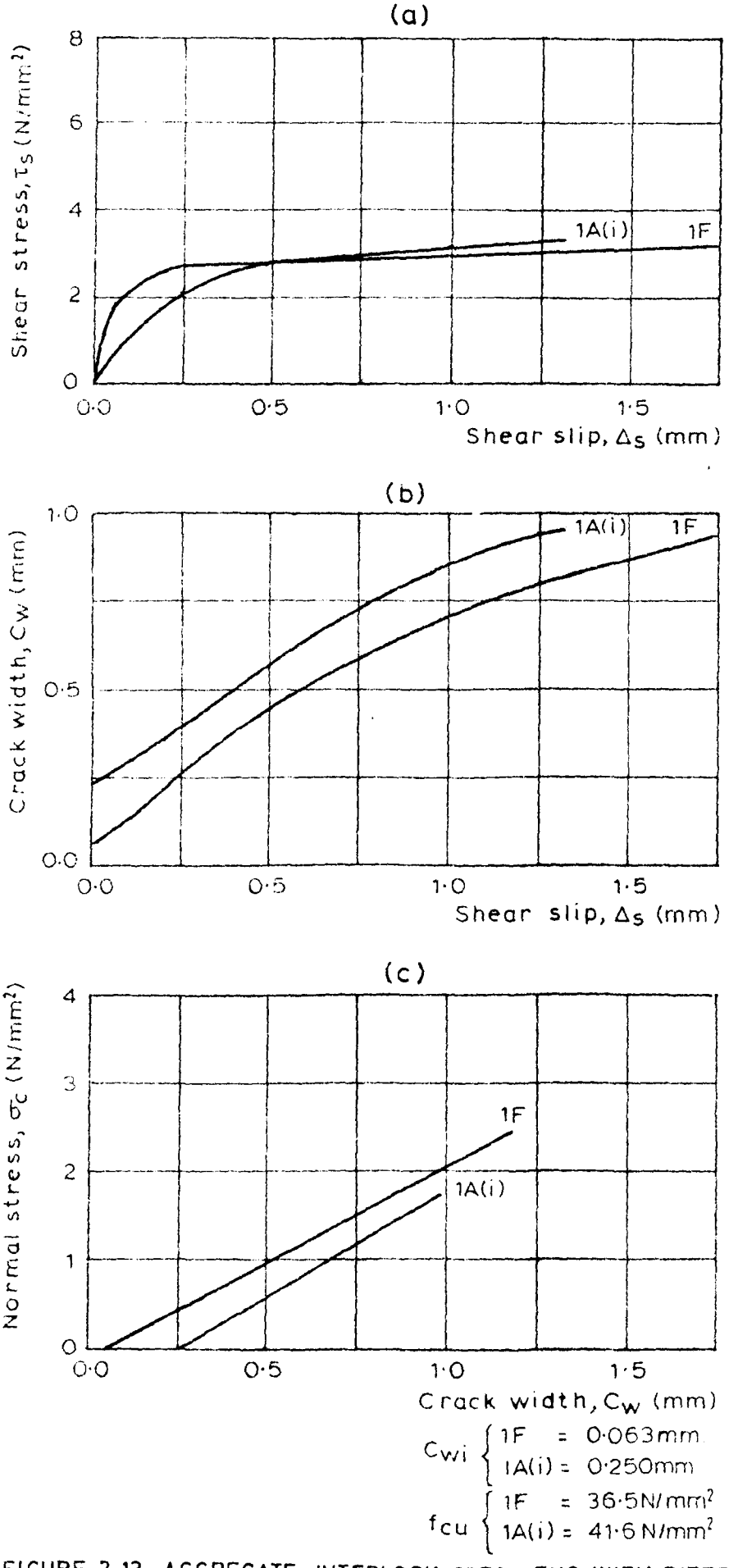

FIGURE 3.13. AGGREGATE INTERLOCK SPECIMENS WITH DIFFERENT INITIAL CRACK WIDTHS.

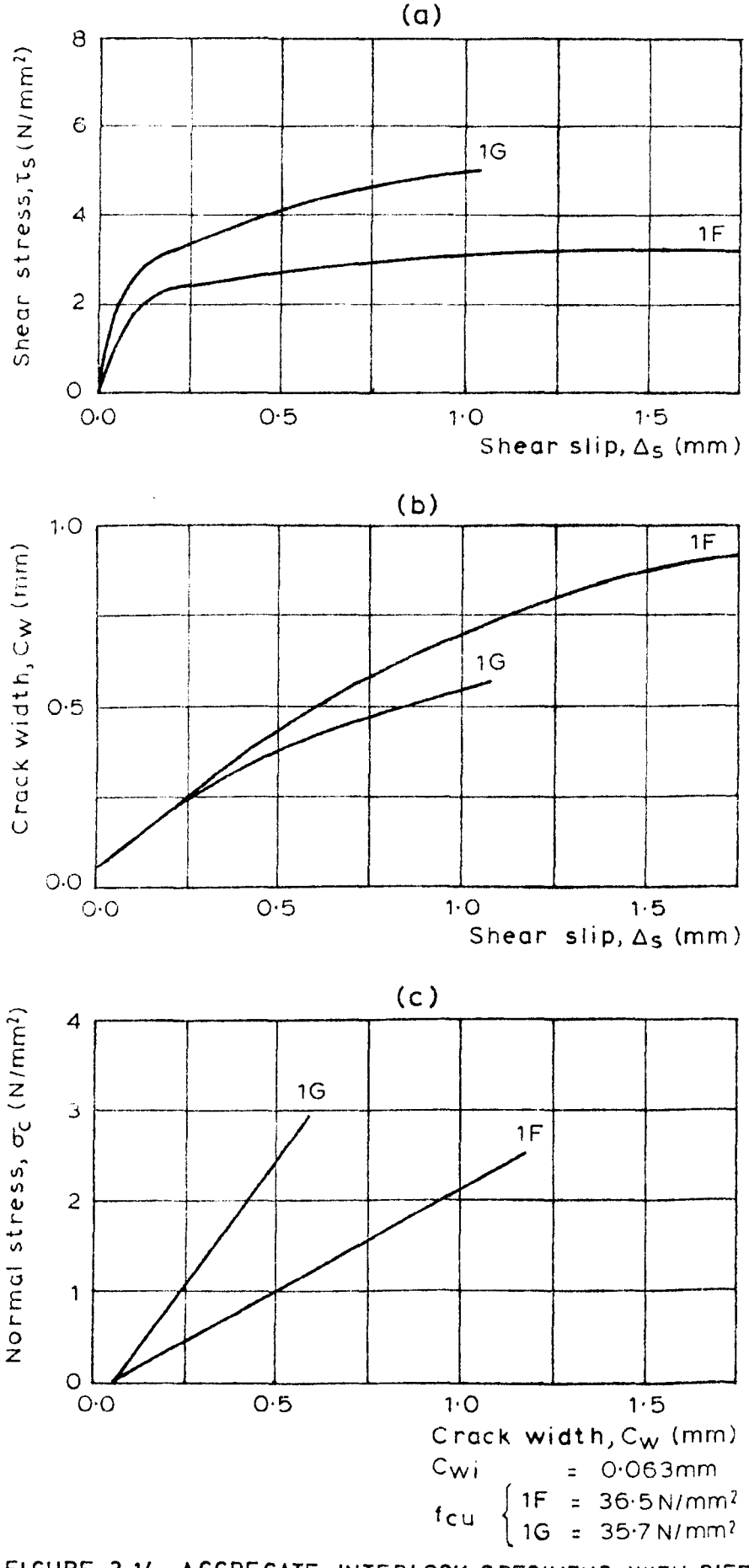

FIGURE 3.14. AGGREGATE INTERLOCK SPECIMENS WITH DIFFERENT NORMAL RESTRAINT STIFFNESSES.

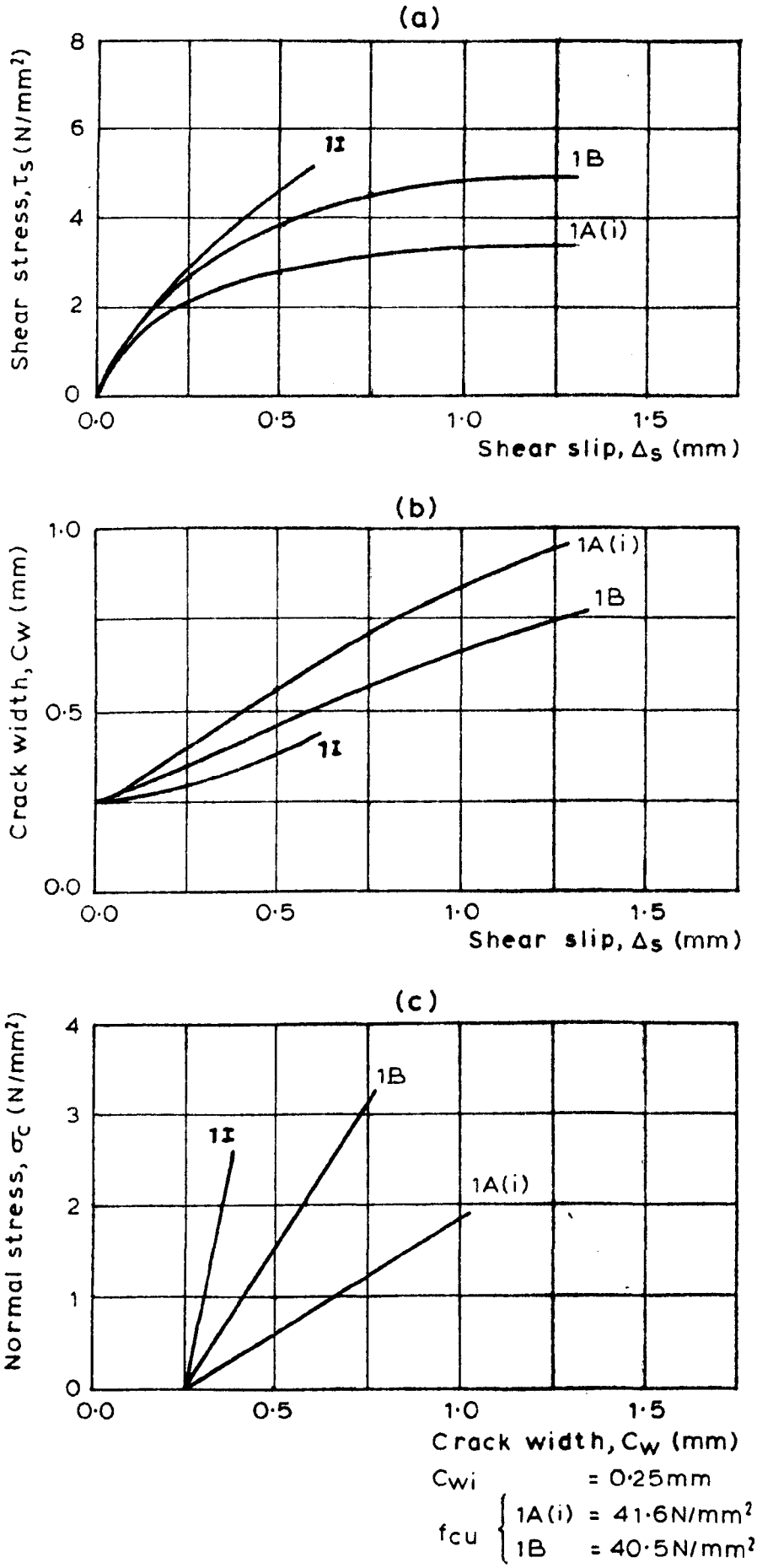

FIGURE 3.15. AGGREGATE INTERLOCK SPECIMENS WITH DIFFERENT NORMAL RESTRAINT STIFFNESSES.

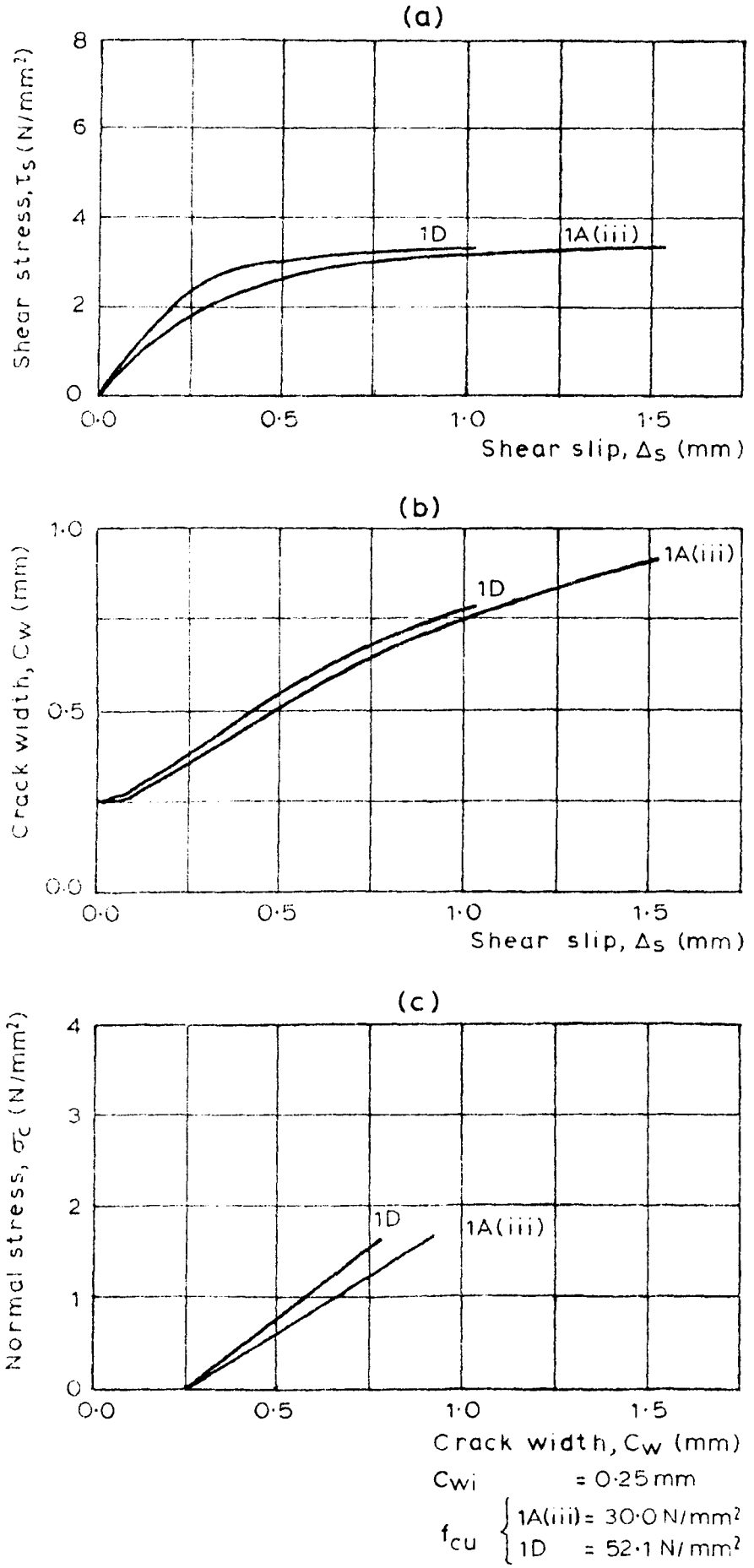

FIGURE 3.16. AGGREGATE INTERLOCK SPECIMENS WITH DIFFERENT CONCRETE STRENGTHS.

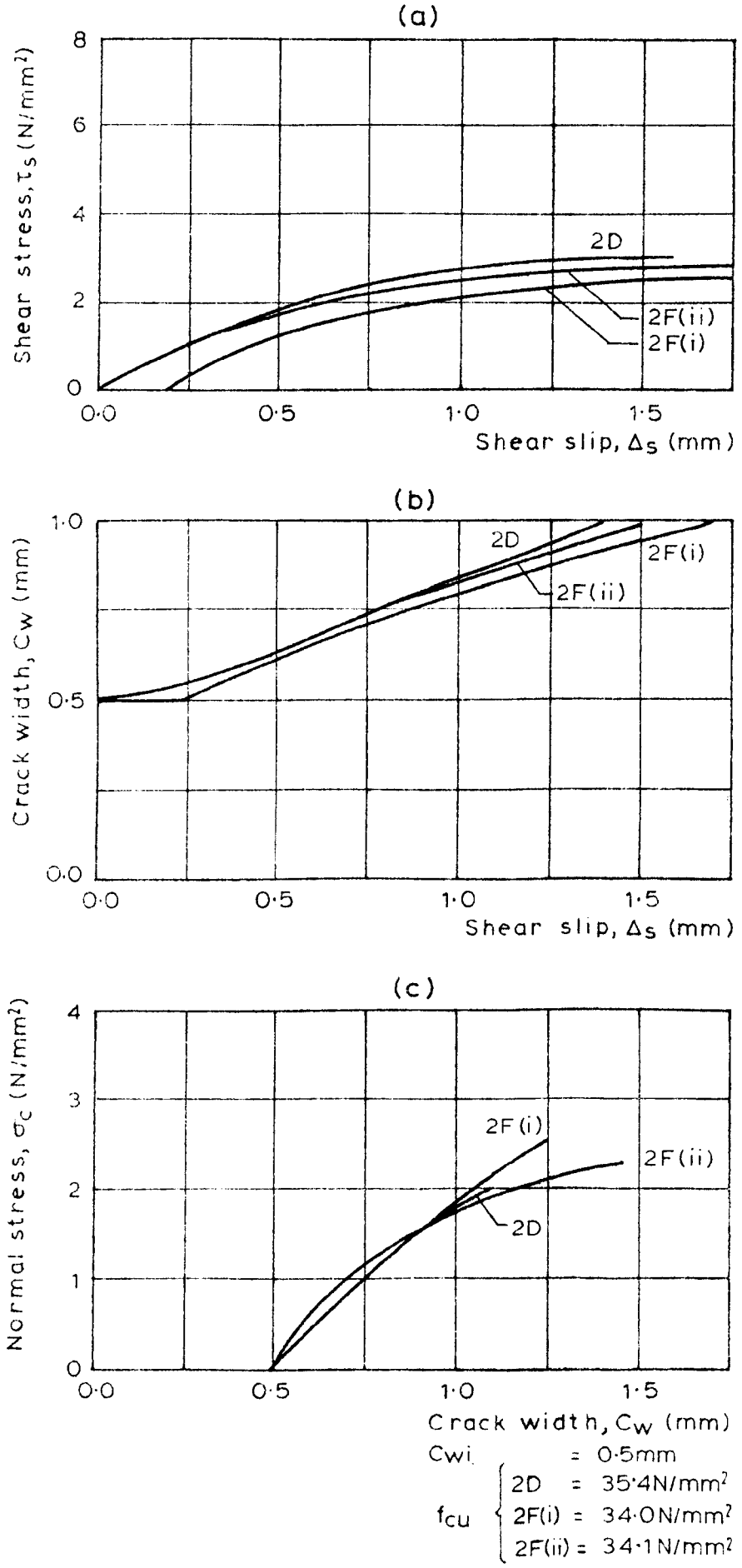

FIGURE 3.17. SIMILAR AGGREGATE INTERLOCK SPECIMENS.

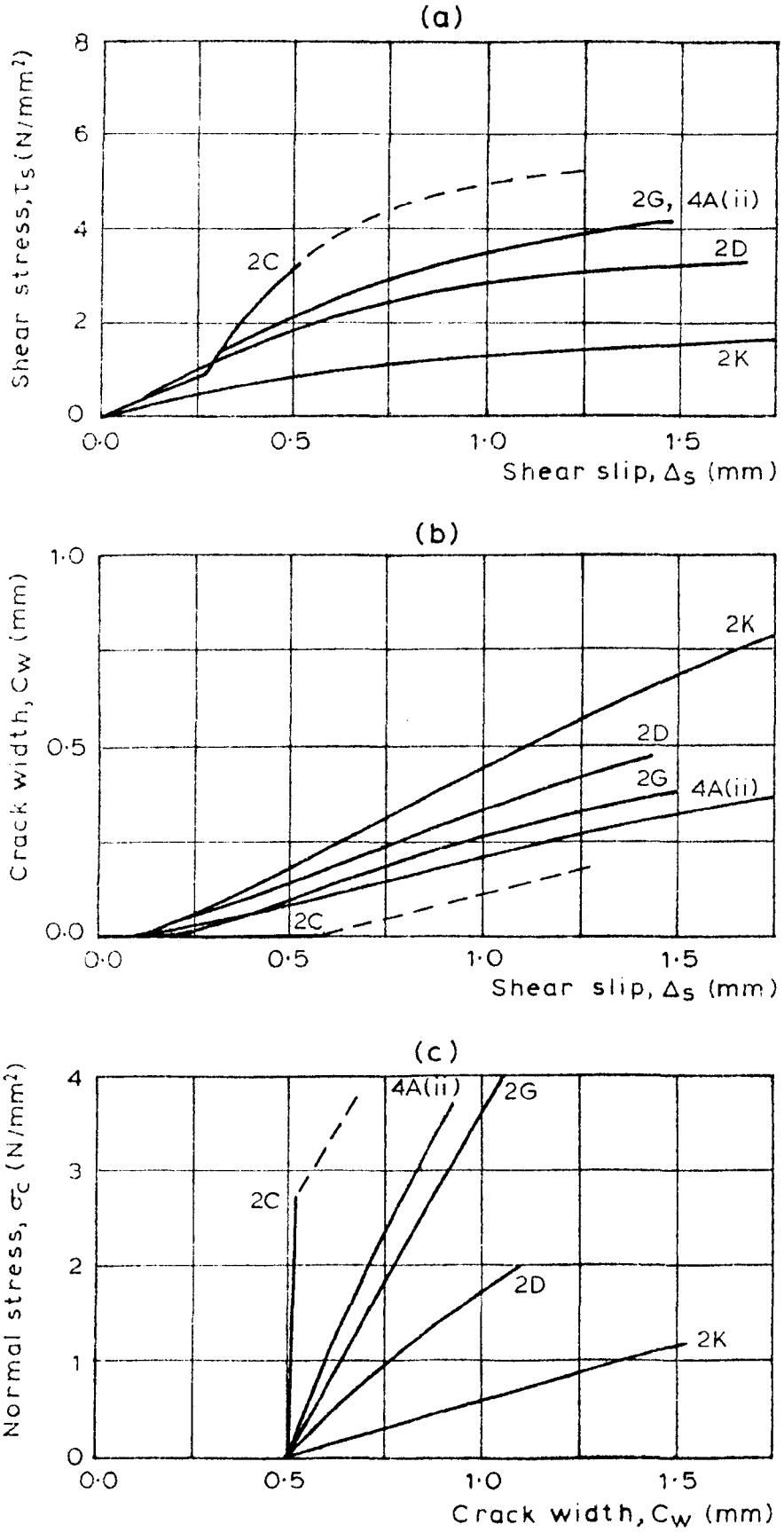

C_{wi} = 0·5mm

f_{cu}
- 2C = 29·1 N/mm²
- 2D = 35·4 N/mm²
- 2G = 35·2 N/mm²
- 2K = 34·4 N/mm²
- 4A(ii) = 36·3 N/mm²

FIGURE 3.18.
AGGREGATE INTERLOCK SPECIMENS WITH DIFFERENT NORMAL RESTRAINT STIFFNESSES.

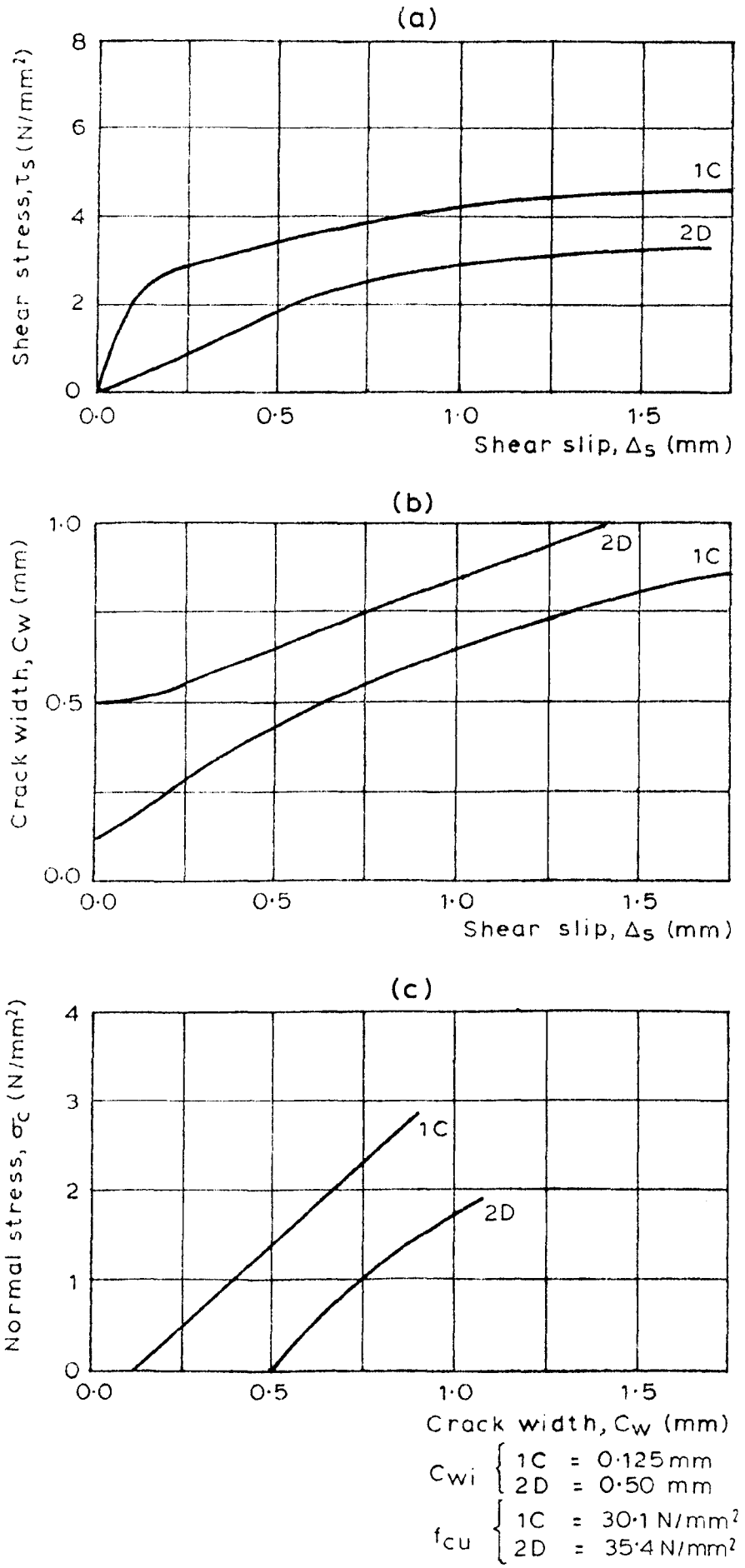

FIGURE 3.19. AGGREGATE INTERLOCK SPECIMENS WITH DIFFERENT INITIAL CRACK WIDTHS.

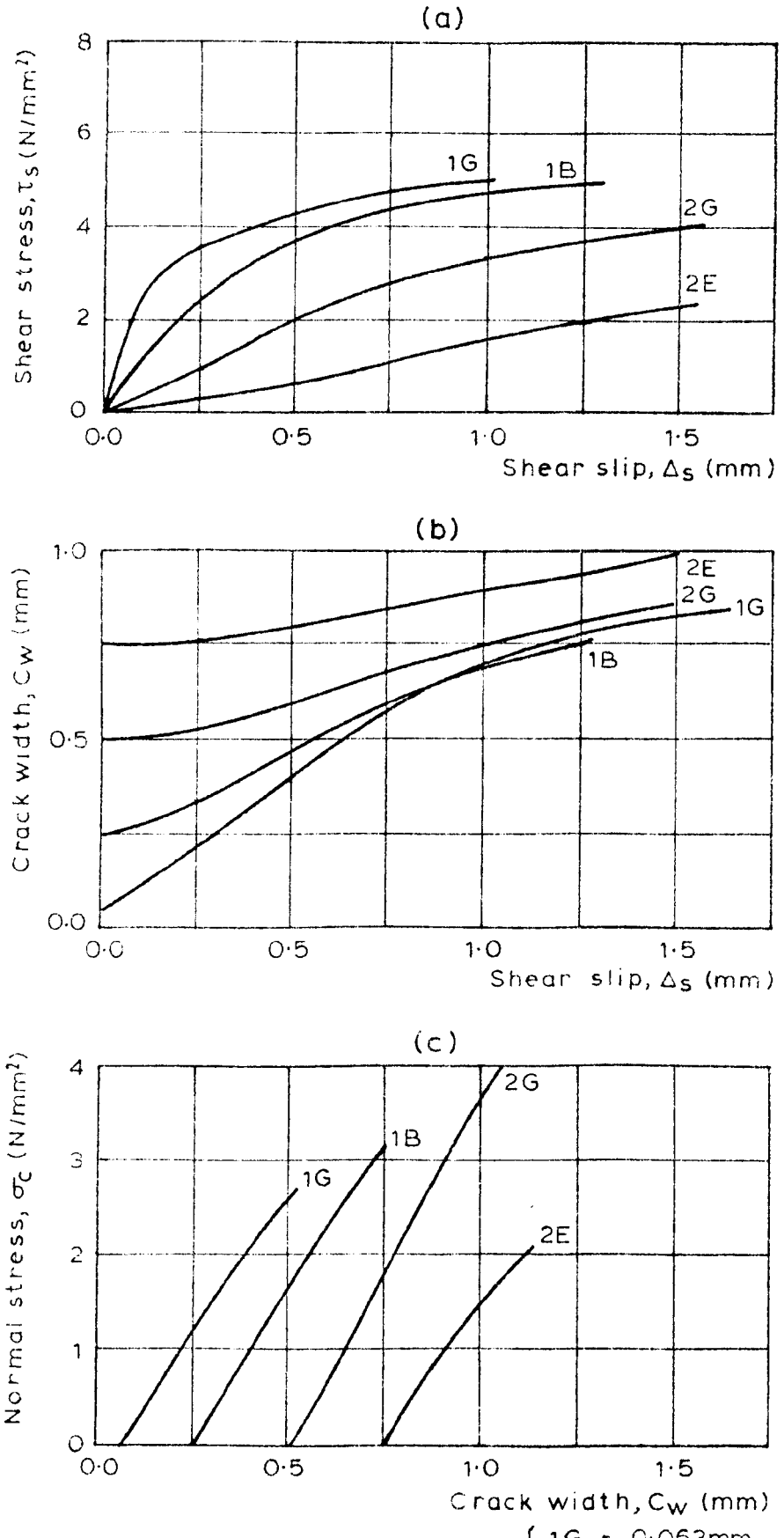

C_{wi}
- 1G = 0·063mm
- 1B = 0·250mm
- 2G = 0·500mm
- 2E = 0·750mm

f_{cu}
- 1G = 35·7N/mm²
- 1B = 40·5N/mm²
- 2G = 35·2N/mm²
- 2E = 31·3N/mm²

FIGURE 3.20.
AGGREGATE INTERLOCK SPECIMENS WITH DIFFERENT INITIAL CRACK WIDTH

CHAPTER FOUR

TESTS ON DOWEL ACTION SPECIMENS

4.1 Introduction

The dowel action tests in test series 3 were carried out using similar specimens and loading arrangements to those used in the aggregate interlock tests. Thus a direct comparison could be drawn between the relative shear stiffnesses.

Specimens 3D and 3E were loaded in axial tension before shear forces were applied. The axial strain in the reinforcement at the centre of the specimen was measured during the tensile loading and was used to study the axial stiffness of reinforcement embedded in concrete. Similar readings taken during the reinforced concrete tests, once cracking had occurred, were also used in this study.

4.2 Manufacture of dowel action specimens

4.2.1 General details

Figure 4.1 shows the overall dimensions of all the series 3 specimens. The reinforcement was embedded within the concrete instead of being placed within ducts as before. The central crack was constructed with smooth, low friction crack faces, to prevent any interlocking effects. This was achieved by casting each specimen in two stages. The first half was cast against a flat steel plate positioned across the centre of the mould. After 24 hours this plate was removed and the exposed face was covered with two layers of thin polythene sheeting. The remainder of the specimen was then cast against this sheeting. Hence any shear forces applied across the crack should be resisted by dowel action of the reinforcement alone.

4.2.2 Concrete

The same mix designs used in test series 1, 2 and 4 were used. These are detailed in Table 3.1. As each specimen contained two different concrete mixes of different ages, test cubes were made from each mix. The cube strengths of each mix together with the mean cube strength for each specimen are given in Table 4.1.

The concrete was placed into the mould in three separate layers with careful compaction of each layer, using a vibrating table. This method was developed by Cambell-Allen and Lau (61) and was used to ensure homogenity of concrete strength throughout the specimen by reducing segregation of the aggregate around the reinforcement or water gain beneath the reinforcement. The mould was designed so that specimens were cast in the orientation shown in Figure 5.2. If any soft regions did form beneath the bars, in spite of the casting techniques used, these would be located to one side of the bars when the specimen was set up for shear testing.

4.2.3 Reinforcement

Each reinforcing bar was fitted with strain gauges at the location of the crack to measure the axial force being transmitted normal to the crack. The standard method of fixing strain gauges to the surface of the reinforcement and covering them with a waterproof protective coating (Figure 4.2a) was considered to be unacceptable. Previous research (47) had shown that most of the transfer of dowel forces occurs within a distance of two bar diameters on each side of the crack. Hence the presence of a relatively large soft spot within this region would be expected to have a considerable effect upon the dowel stiffness.

A method was developed in which narrow strain gauges were embedded in epoxy resin within slots milled into the reinforcement (Figure 4.2b). Initially only one strain gauge was used, located within a deep slot at the centroid of the bar. However it proved to be too difficult to position this gauge so that it was insensitive to flexure of the bar. The use of two gauges close to the surface of the bar was then adopted. From these gauges both the axial and the flexural strains could be obtained.

Initially the resin used to encapsulate the strain gauges was an AE 10 cold cured adhesive produced by Welwyn Strain Measurement Ltd. The bar was tested in axial tension and the strain gauge readings were calibrated against a mechanical extensometer with a gauge length of 50 mm clamped onto the bar. The results (Figure 4.3) showed that for strains above 1250 $\mu\varepsilon$ slip occurred between the epoxy resin and the reinforcement. The strain measured by the electrical strain gauges was then significantly lower than the strain measured mechanically.

This test was then repeated using a heat-cured epoxy resin, AE 15. (The temperature used to cure the epoxy resin was about 50°C). The results show clearly a close correlation between the electrically and mechanically measured strains up to 5000 $\mu\varepsilon$, when the steel was well into the plastic range.

Each reinforcing bar was calibrated in axial tension and in flexure before being cast into a specimen. In the axial calibration the mean strain obtained from the two embedded gauges was noted for incrementally increasing loads resulting in stresses of up to 400 N/mm^2. In the flexural calibration each bar was clamped adjacent to the strain gauges. A cantilever load was then applied in increments up to a maximum of

20 Nm for the 16 mm and 12 mm bars and 10 Nm for the 8 mm bars. In both types of calibration the maximum load was applied and removed repeatedly until the strain gauge readings had stabilized before the calibration readings were taken.

The 8 mm diameter reinforcing bars were too small for the slotted technique for fixing strain gauges to be used. Instead the gauges were bonded conventionally to the surface of the reinforcement. The protective coating to these gauges was reduced to a minimum, but it was found that a thin covering of butyl rubber was indispensible to ensure waterproofing. Although the presence of these strain gauges will undoubtably influence the dowel action stiffness, they were included so that the dowel stiffness of similarly instrumented bars in the reinforced concrete specimens could be evaluated.

The effects of the two slots upon the section properties of the reinforcement are given in Table 4.2. It was necessary to ensure that the plane of the slots was positioned parallel to the plane of intended shear loading when casting the specimens. If this was not done flexure of the modified reinforcing bar would induce high shear stress concentrations in the small area of steel remaining at the centre of the bar.

4.3 Testing procedure

The testing procedure was similar to that used for aggregate interlock tests. In tests 3A to 3C and also test 3F there was no axial tension applied to the specimens. Hence there was no need to bond the steel end plates to the specimens with epoxy resin. Instead a dental paste was used to bed in the ends of each specimen. The dental paste had a compressive strength greater than that of the specimens.

In tests 3D and 3E the effect of concurrent axial and shear forces upon the shear stiffness of the specimen was studied and the end plates were bonded to each specimen with epoxy resin as described in section 3.5.1.

In all the tests in series 3 the crack faces were examined subsequent to shear testing to discover the nature and extent of the damage caused during the test. This was achieved by cutting through the specimens with an industrial masonry saw. The cut was made parallel to the central crack at a distance of 25 to 50 mm to one side. The intervening concrete was easily removed to permit inspection of the crack face.

4.4 Test results

The effect of the following parameters upon dowel action was studied:

- reinforcement diameter
- concrete strength
- axial tension in the reinforcement

One test was repeated to indicate the degree of scatter expected in the results. The details of each test are given in Table 4.1.

4.4.1 Strain gauge readings

During the tests 3A to 3C no consistent pattern was observed from the readings of the strain gauges in the reinforcement. The axial strain, obtained from the mean of the two readings showed a poor correlation with the surface measured crack width and on some occasions changed sign during the test. There was no discernible pattern either in the

flexural strains, obtained from the difference in the strain gauge readings from each bar. A full set of these results is recorded in reference 65 but has not been included here.

The lack of any consistent trends in the reinforcement strains may be attributed to several effects:

(1) The midpoint of the reinforcing bars, where the strain gauges are located, lies at the theoretical point of contraflexure and hence no flexural strains are expected. However if the gauges are slightly misaligned flexural strains will occur. Even if the gauges are correctly positioned, the point of contraflexure may not be at the mid point of the bar if the initial non-homogenity of the concrete causes any asymmetry. The point of contraflexure may also move when the concrete is damaged during shear testing.

(2) If the two strain gauges are not located exactly symmetrically about the neutral axis of the reinforcement any bending due to (1) will result in the measurement of an apparent axial strain, which does not in fact occur.

However the use of reinforcement with strain gauges in tests 3A to 3C was useful in that the instrumentation technique was developed for later use. It also ensured that the reinforcement had the same physical properties as the reinforcement used in the reinforced concrete tests and hence the component of shear stiffness due to dowel action was directly comparable.

In tests 3D and 3E an axial load was incrementally applied to the

specimen before any shear loading was applied. There was a close correlation between the axial force measured externally, using the load cell and the axial force indicated by the strain gauges in the reinforcement (Figure 4.4). The effect of subsequent shear loading upon the internally measured axial force is discussed in section 4.4.5.

Individual test results can be obtained from reference 65. A comparative study of these results revealed the following trends.

4.4.2 Repeatability

In Figure 4.5 the test results of two nominally identical specimens are shown. Very little scatter between the two sets of results is seen.

The shear slip, Δ_s was measured across the crack, as described in section 3.3.4. The shear stress was defined as the shear load applied across the crack divided by the area of the crack face. As there was no crack initiating slot in the dowel action specimens, the crack face used was the full 300 mm x 100 mm. This definition is consistent with that used in other research work (29) and allows a direct comparison. However, it should be realised that the crack area in the reinforced concrete specimens and the aggregate interlock specimens was 270 mm x 70 m. Hence a given shear force will result in the calculation of a proportionally higher shear stress than would be obtained for dowel action specimens.

4.4.3 Reinforcement diameter

It was observed (Figure 4.6) that increasing the diameter of the bars used resulted in a larger shear stiffness and ultimate shear

stress. There was also an increasing tendency for the smooth crack to widen, although this was not of the same magnitude as seen in the aggregate interlock tests.

The specimens were cut open to reveal the crack face, subsequent to shear testing. It was seen (Figure 4.7) that for the specimens with 16 mm or 12 mm diameter bars, a splitting crack had propagated from the bars. In specimen 3F, where 8 mm diameter bars were used, no splitting crack was apparent. In all the dowel action specimens there was some spalling of the concrete beneath the bars on the face where bearing stresses were expected. This spalling was more severe in the specimens with larger diameter bars and may explain the greater tendency for widening of the crack (Figure 4.6b).

The results of Oehler's (66) tests on dowel forces in shear studs are consistent with the trends observed here i.e. splitting cracks are more likely to occur when the ratio of the bar diameter to the width of the specimen is high. In the dowel action test 3F, where 8 mm bars were used, the soft protective covering to the strain gauges will also reduce the bearing stress concentrations and hence make splitting of the concrete less probable. However, in the reinforced concrete test 5J, where 8 mm reinforcement without strain gauges was used, splitting cracks were not observed, which is consistent with the trends observed in reference 66.

4.4.4 Concrete strength

It was found (Figure 4.8a) that an increase in the concrete strength from 38 N/mm^2 to 54 N/mm^2 had very little discernible effect upon the shear stiffness or ultimate shear strength. In both tests splitting cracks were observed beneath each bar when the specimens were cut open,

subsequent to shear testing. It is presumed that once a splitting crack has formed, the dowel stiffness will depend upon the restraint to propagation of this crack provided by the surrounding structure. In neither specimen was lateral reinforcement provided to prevent propagation of the splitting cracks and hence the similar results, once cracking had occurred, are not surprising. The slightly greater tendency for crack widening in test 3B (Figure 4.8b) may be attributed to the greater resistance of the spalled concrete to crushing, as further shear slip occurs.

4.4.5 Axial tension in reinforcement

In tests 3D and 3E the reinforcement was initially loaded incrementally in tension. Throughout the consecutive shear loading this tensile force was held constant, using the three turnbuckle adjusting screws, as described in section 3.5.3.

Although Figure 4.4 shows a close correlation between the axial force applied to the dowel bars and the force indicated by the internal strain gauges, it was uncertain whether the subsequent shear forces on these bars would influence the accuracy of the axial shear measurement. Once shear loading and crack widening start to occur there is no longer any reason to expect the externally applied axial load to be equal to the axial forces in the reinforcing bars. However if the relationship between the axial stress in the reinforcement and the surface crack width is plotted (Figure 4.9), it is seen that the curves follow quite closely that predicted by Martin (24) until high axial stresses are reached. Furthermore the correlation does not appear to be affected by the presence of shear forces. It was deduced from this that the reliability of the internal strain gauges in measuring axial loads was not adversely affected by a superimposed shear load.

The effect of an axial tensile force was to reduce the shear stiffness and the ultimate shear load (Figure 4.10a). There was also an increased tendency for crack widening (Figure 4.10b) when the axial load was increased. An examination of the crack face, after shear loading, revealed that there was more localised crushing and spalling around dowel bars under axial tension (Figure 4.11). The splitting failure crack , evident in similar dowel action tests without axial tension, was not seen.

It was reasoned that axial tension in the reinforcement caused internal cracking and hence a reduction in the stiffness of the concrete adjacent to each reinforcement rib. This softening of the concrete would therefore reduce the support provided to each dowel bar and hence result in an overall reduction of the shear stiffness. If the stiffness in the concrete supporting each bar is reduced in this way, there will also be a reduction in the tensile splitting stresses below each bar, at the crack face and hence splitting is less likely to occur.

The shear loading itself will also further damage the concrete adjacent to the reinforcement. This is likely to reduce the effectiveness of the tensile anchorage of the bar within the concrete and probably explains why the crack became wider as shear loading was applied, even though there was no overriding of the crack faces expected (Figure 4.10b).

Table 4.1 Details of dowel action test specimens

Specimen Mark	Target concrete strength (N/mm^2)	Actual concrete strength			Reinforcement type (mm)	Axial stress in reinforcement (N/mm^2)
		Side A	Side B	Mean		
3A(i)	35	39.8	35.3	37.6	Y12	0
3A(ii)	35	38.2	38.8	38.5	Y12	0
3B	55	56.0	52.1	54.0	Y12	0
3C	35	28.1	27.0	27.6	Y16	0
3D	35	38.0	36.4	37.2	Y12	175
3E	35	36.4	43.3	39.8	Y12	344
3F	35	33.3	31.1	32.2	Y8	0

Table 4.2 Section properties of reinforcement

Reinforcement type	A_s (mm^2)	Reduction	I_{xx} (mm^2)	Reduction
16 mm, unmodified	201	-	3217	-
16 mm, slotted	193	4%	2918	9%
12 mm, unmodified	113	-	1018	-
12 mm, slotted	105	7%	879	14%

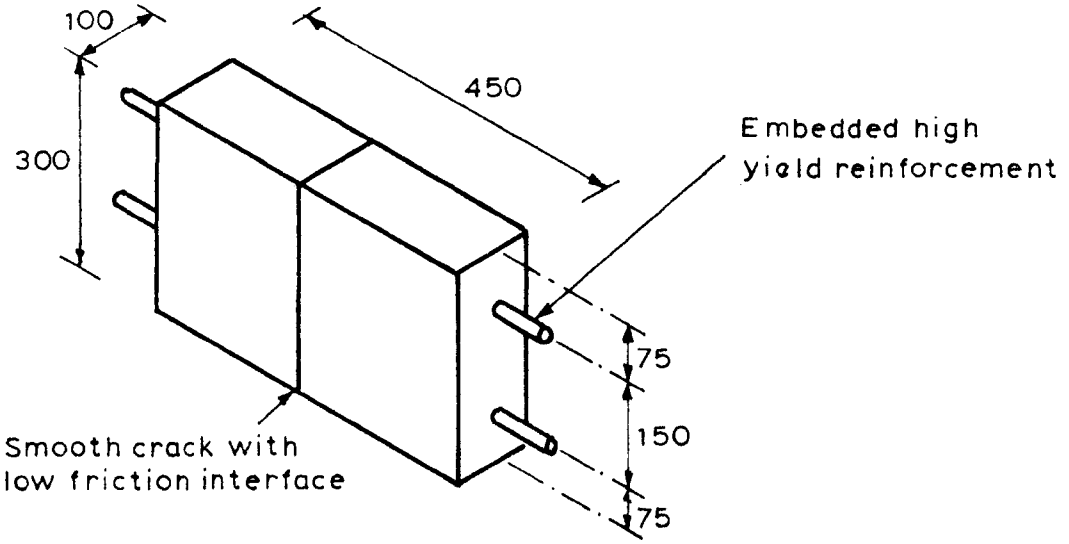

FIGURE 4.1. DOWEL ACTION TEST SPECIMEN.

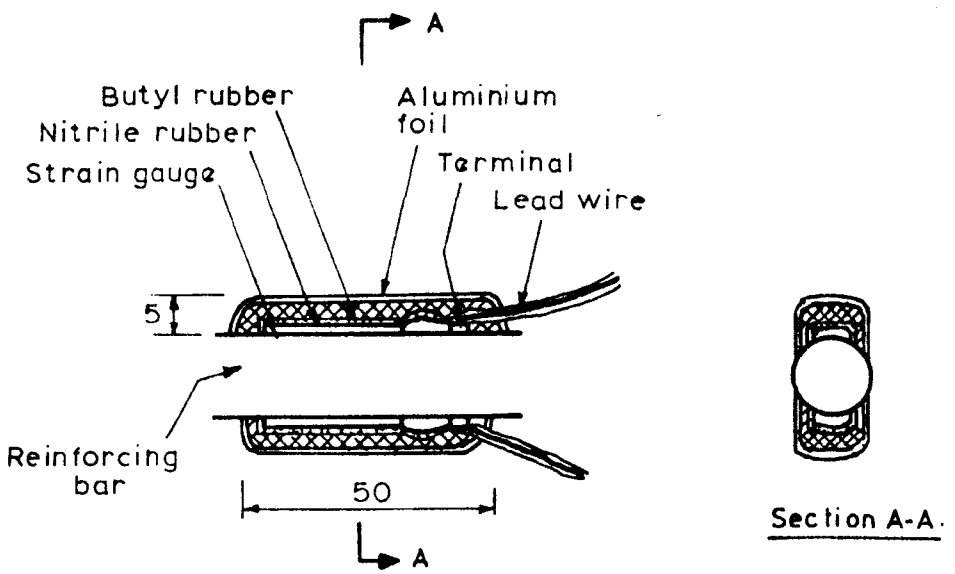

a) Standard strain gauge fixing and protection.

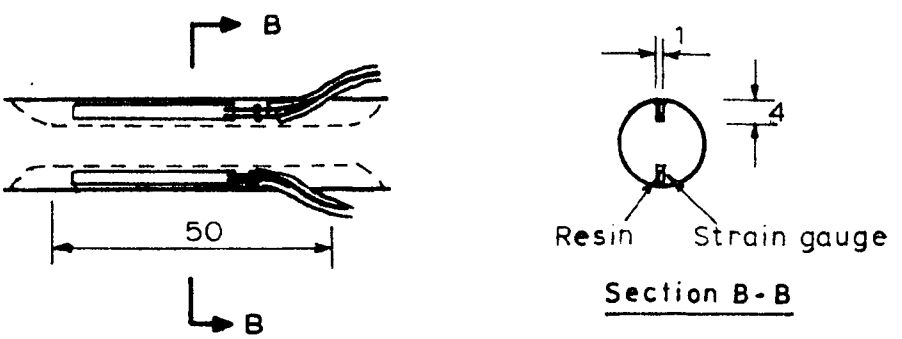

b) Strain gauges encapsulated with slots.

FIGURE 4.2. STRAIN GAUGE DETAILS.

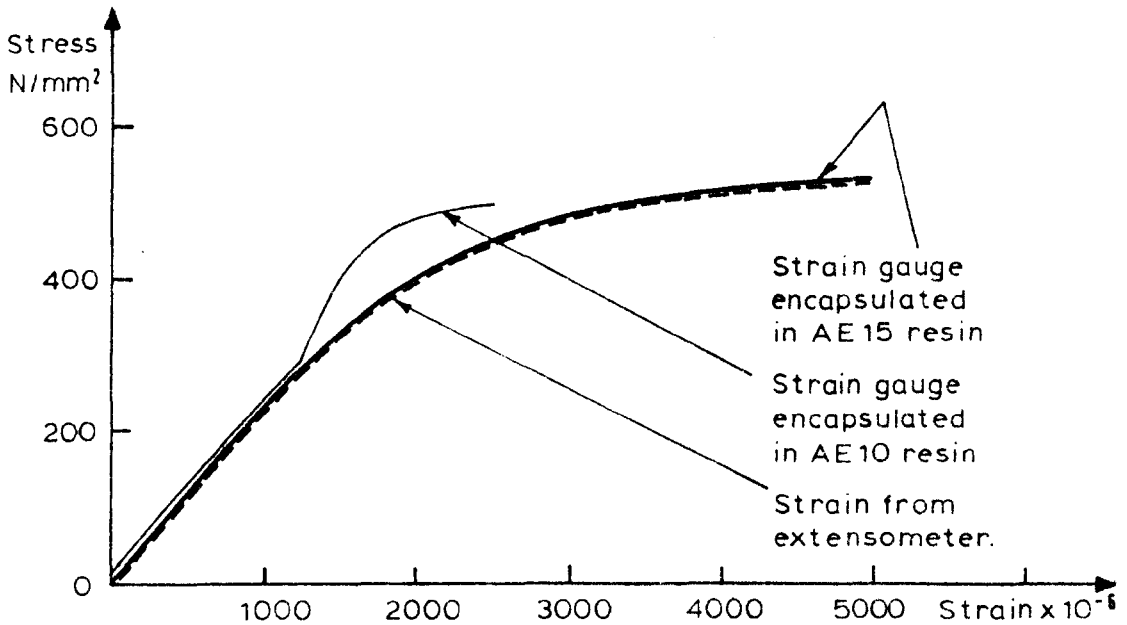

FIGURE 4.3. CALIBRATION OF STRAIN GAUGES LOCATED WITHIN SLOTS IN REINFORCEMENT.

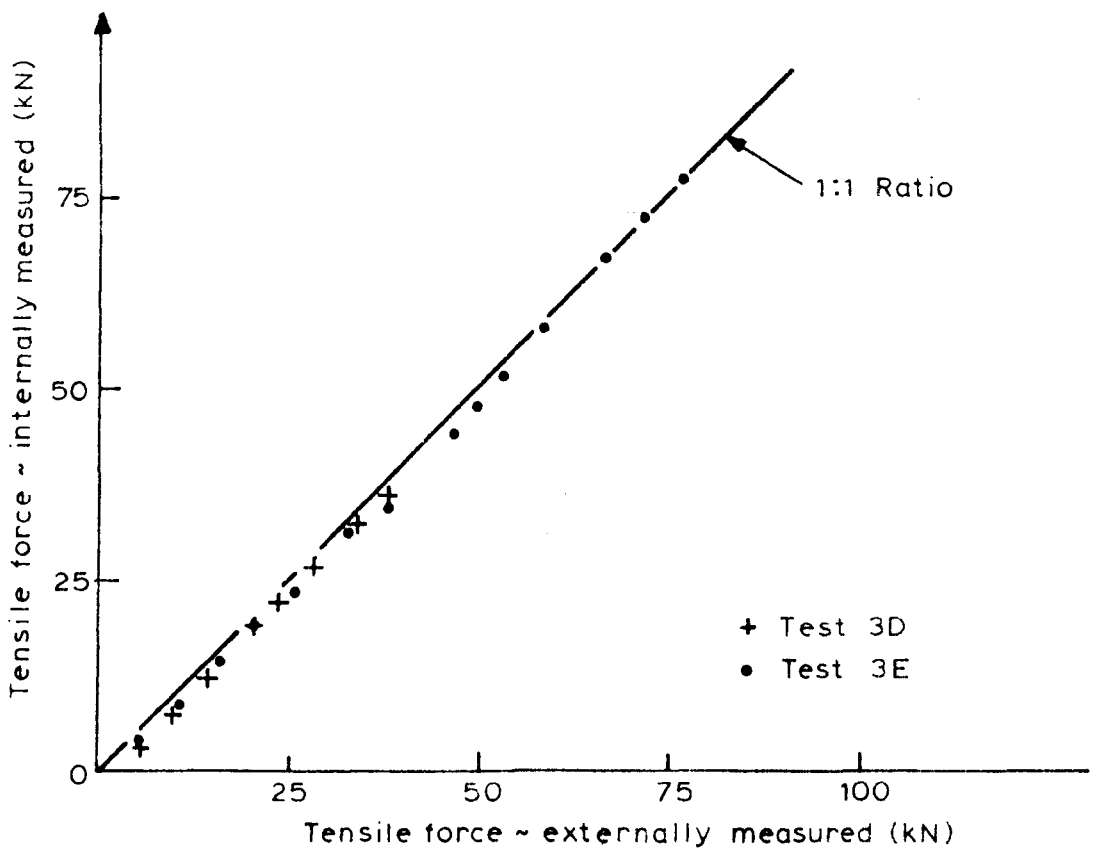

FIGURE 4.4. COMPARISON BETWEEN THE AXIAL FORCE MEASURED EXTERNALLY AND USING INTERNAL STRAIN GAUGES.

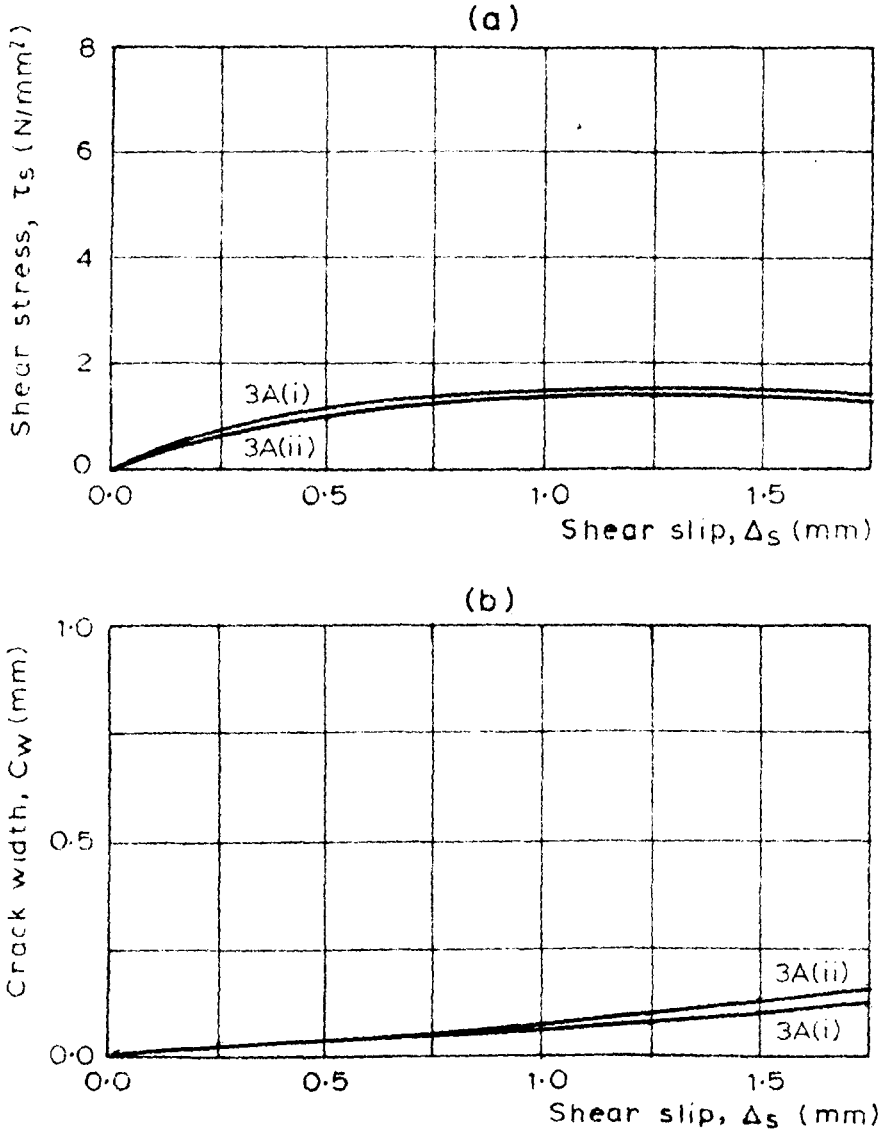

3A (i) ~ f_{cu} = 37·6N/mm²
3A (ii) ~ f_{cu} = 38·5N/mm²
} ϕ = 12mm

FIGURE 4.5. TEST RESULTS OF NOMINALLY IDENTICAL DOWEL ACTION SPECIMENS.

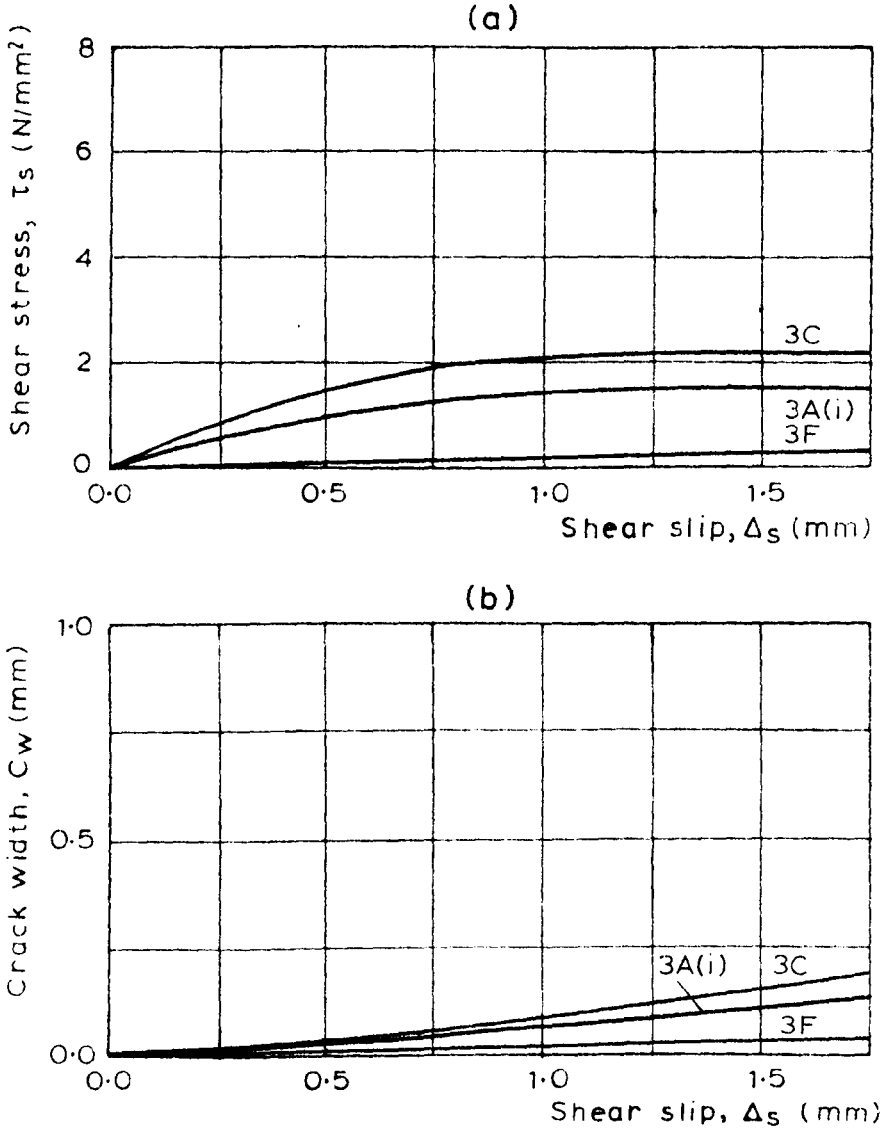

3C ~f_{cu} = 27·6N/mm², ϕ = 16mm
3A(j)~f_{cu} = 37·6N/mm², ϕ = 12mm
3F ~f_{cu} = 32·2N/mm², ϕ = 8mm

FIGURE 4.6. TEST RESULTS OF DOWEL ACTION SPECIMENS WITH DIFFERENT REINFORCEMENT DIAMETERS.

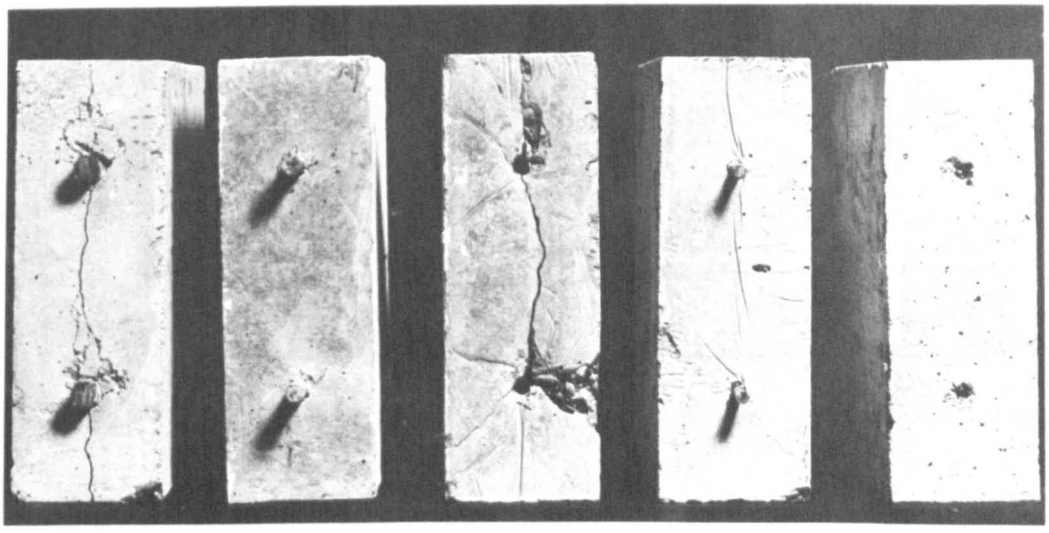

Specimen 3C
ϕ = 16mm.

Both faces of
Specimen 3A(i)
ϕ = 12mm.

Both faces of
Specimen 3F
ϕ = 8mm.

FIGURE 4.7. CRACK FACES OF DOWEL ACTION SPECIMENS AFTER SHEAR TESTING.

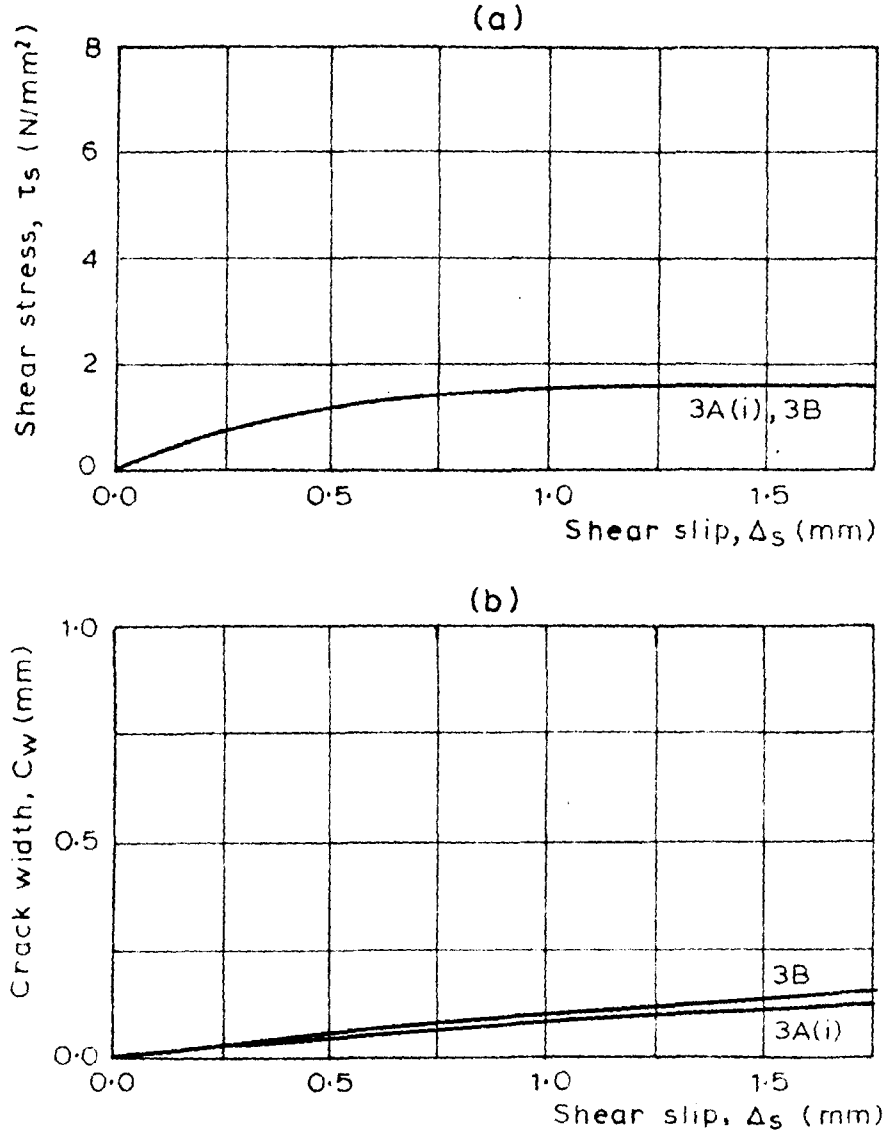

3A(i) ~ f_{cu} = 37·6N/mm² ϕ = 12mm
3B ~ f_{cu} = 54·0N/mm² ϕ = 12mm

FIGURE 4.8. TEST RESULTS OF DOWEL ACTION SPECIMENS WITH DIFFERENT CONCRETE STRENGTHS.

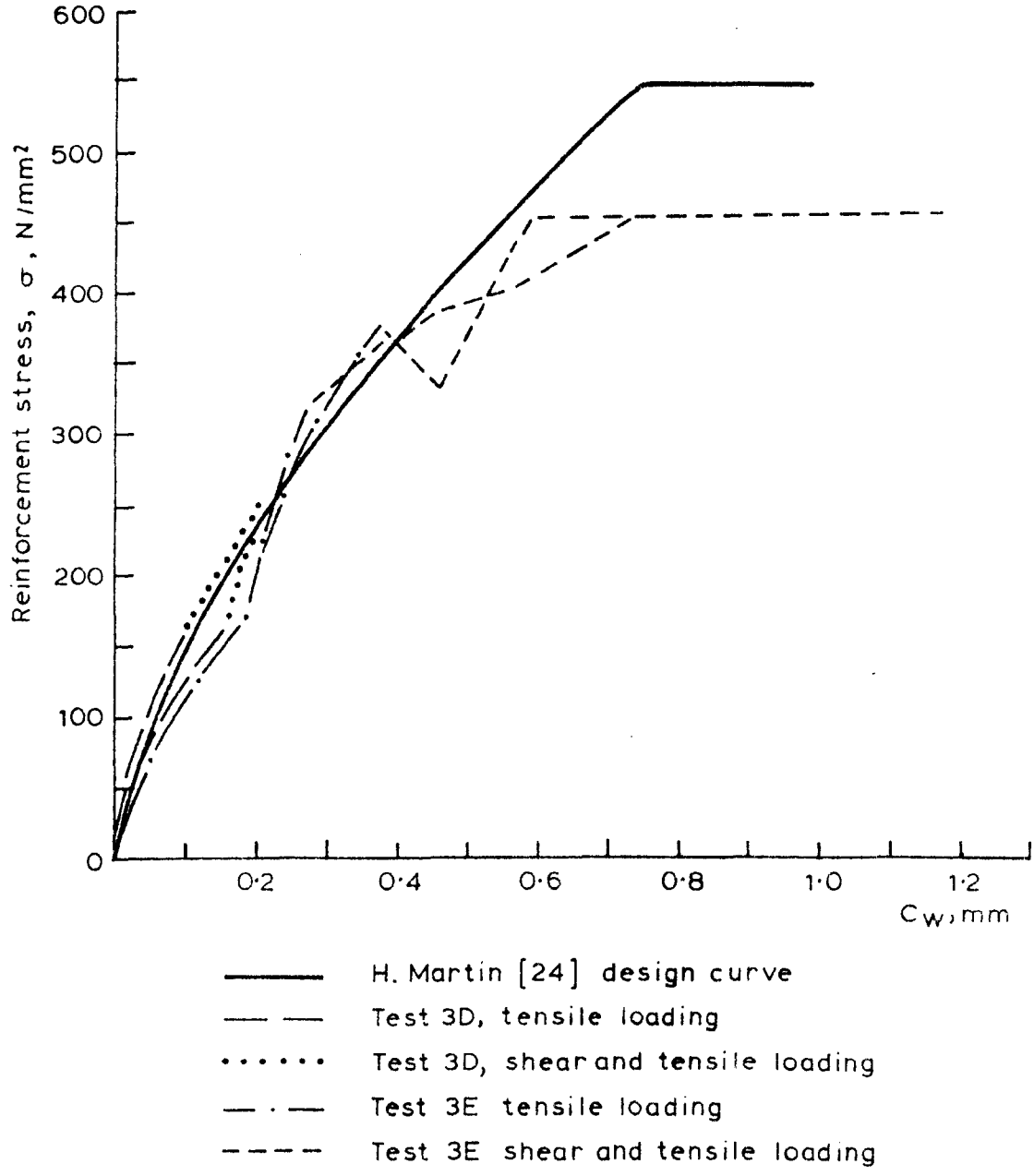

FIGURE 4.9. EFFECT OF SHEAR LOADING UPON STRESSES IN THE REINFORCEMENT.

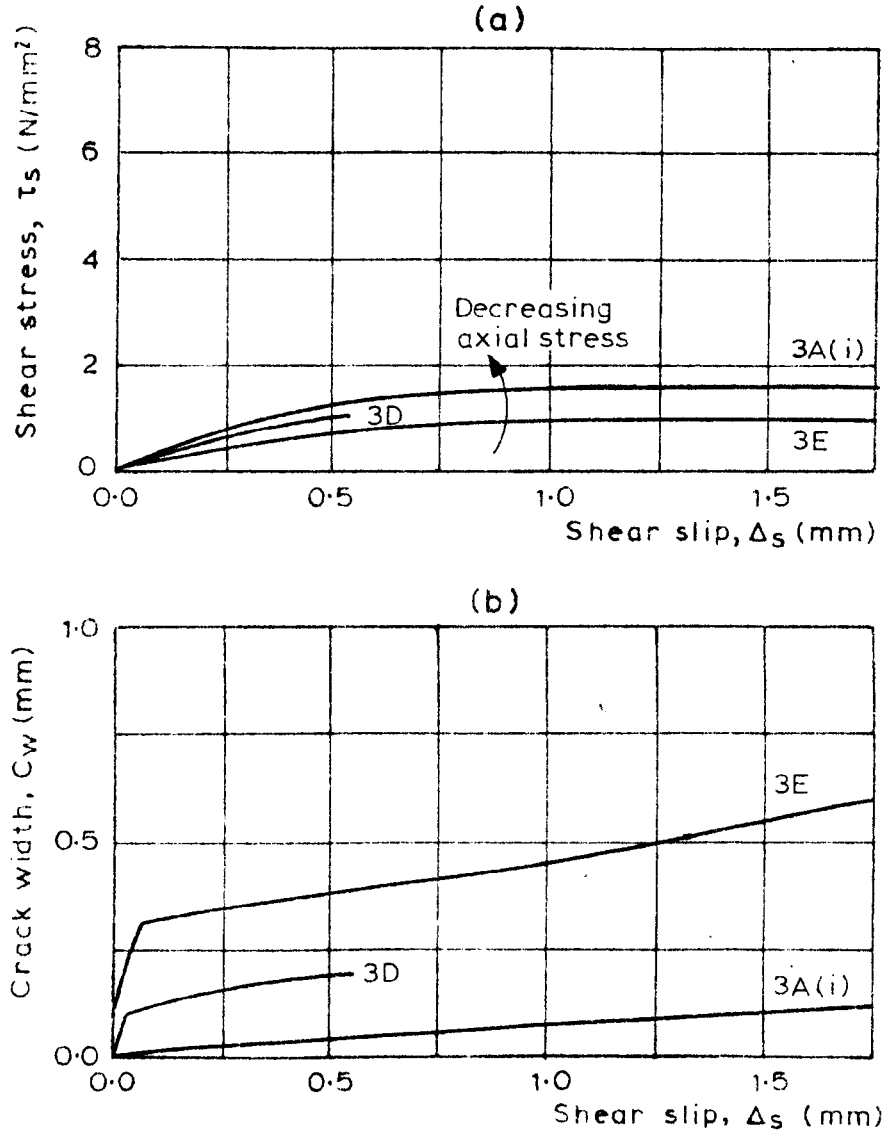

3A(i) ~ ϕ = 12mm, f_{cu} = 37·6 N/mm²; f_{si} = 0 N/mm²
3D ~ ϕ = 12mm, f_{cu} = 37·2 N/mm², f_{si} = 175 N/mm²
3E ~ ϕ = 12mm, f_{cu} = 39·8 N/mm², f_{si} = 344 N/mm²

FIGURE 4.10. TEST RESULTS OF DOWEL ACTION SPECIMENS WITH DIFFERENT INITIAL AXIAL REINFORCEMENT STRESSES.

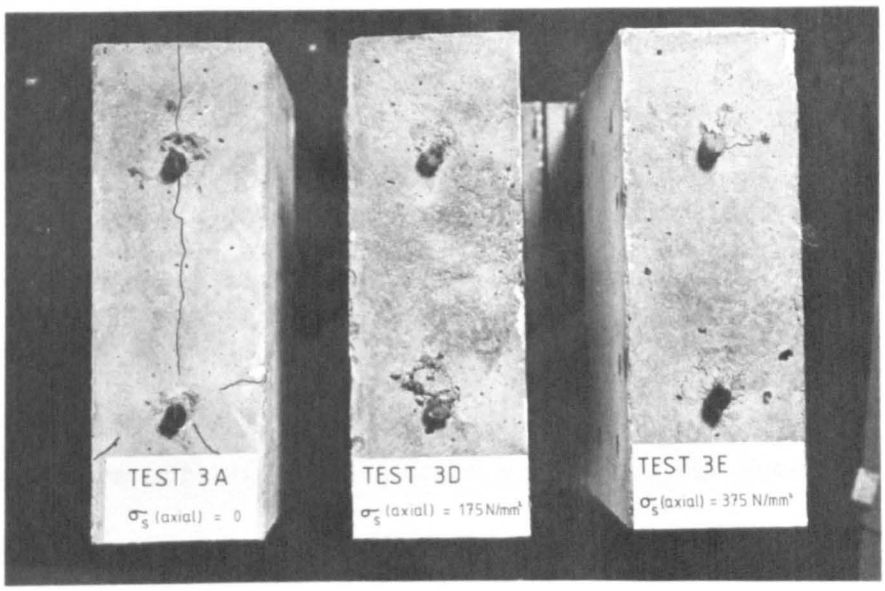

FIGURE 4.11. CRACK FACES OF DOWEL ACTION SPECIMENS WITH DIFFERENT AXIAL LOADS, AFTER SHEAR TESTING.

CHAPTER FIVE

TESTS ON REINFORCED CONCRETE SPECIMENS

5.1 Introduction

Shortly before the reinforced concrete series of specimens were tested, the results of Walraven's (42) experiments on shear in cracked plain and reinforced concrete became available. It was observed from these test results that there was a significant difference between the behaviour of the plain concrete specimens and that of the reinforced concrete specimens.

From tests on unreinforced concrete specimens, the shear stiffness and the ratio of crack widening to shear slip was found to agree closely with the behaviour of the theoretical model, described in section 2.5.2.4. The overall trend was that an increase in the stiffness restraining crack widening resulted in a higher shear stiffness and also a lower rate of crack widening.

From the results of the reinforced concrete tests it was observed that there was a lower bound to the crack opening path, regardless of the amount of reinforcement restraining the crack from widening. For concrete strengths of 20 to 40 N/mm an empirical equation was derived to describe this lower bound

$$\Delta_s = 1.40\ C_w^{1.2} \qquad (5.1)$$

The units of the shear slip, Δ_s and the crack width C_w are in millimetres.

The shear stiffness of the reinforced concrete specimens was found

by the author to be greater than that predicted from the dowel action and aggregate interlock tests. This was attributed to the formation of an internal strut mechanism as described in section 2.6.1.

The present reinforced concrete series of tests was designed to discover whether the shear stiffness could be predicted from the results of the dowel action and aggregate interlock test results alone or whether the trends observed by Walraven (42) could be verified.

One factor which does not appear in Walraven's work is a consideration of the effects of the internal crack width profile. If a crack with uniform surface width is produced in a plane concrete specimen, the crack will have a constant width throughout the depth of the specimen. However, in a reinforced concrete specimen previous research (26, 27) has indicated that the local bond between the concrete and the reinforcing steel results in a crack which diminishes in width beneath the surface of the concrete.

A series of tests were devised in the present investigation to determine how the crack width varies beneath the surface of the concrete in reinforced concrete specimens. Once this profile is known it should be possible to make a more realistic estimate of the contribution of aggregate interlock to the shear stiffness of cracked reinforced concrete.

5.2 Details of tests

The parameters varied in test series 5, studying the shear stiffness of reinforced concrete, were:

a) the initial surface crack width

b) the reinforcement ratio - at constant bar number

c) the reinforcement ratio - at constant bar diameter

d) the reinforcement type

e) the local anchorage

Specimens 5A to 5I were designed to examine the effects of 0.125, 0.25 and 0.5 mm initial surface cracks on specimens reinforced with two 16, 12 or 8 mm diameter reinforcing bars (see Table 5.1). The reinforcement used was G.K.N. Torbar, a high yield bar with a double helix rib pattern.

It was thought that the reinforcement diameter might influence the behaviour of the specimens. Specimen 5K was reinforced with four 8 mm diameter bars, so that the reinforcement ratio was increased above that of specimen 5F without altering the bar diameter.

It became apparent, as the reinforced concrete tests were being completed, that there was a difference in behaviour between the results of Walraven's (42) tests and the results of the present series. The lower bound to the crack opening path, described by Walraven, was not observed in these tests. An increase in the normal restraint stiffness tended to cause a reduction in the rate of crack widening in all cases.

To study whether the difference in behaviour was due to the different rib pattern on the deformed reinforcement, test 5L was planned. This was similar to test 5E, but B.S.C. "Unisteel 410" was used instead of G.K.N. "Torbar" (Figure 5.1). This was the closest available steel

to that used by Walraven.

Tests 5J and 5M were both designed to investigate the effects of local anchorage upon the behaviour of cracked reinforced concrete. Specimen 5J was similar to specimen 5F except that strain gauges were not fixed to the reinforcement. This was to examine if the protective covering over the surface mounted strain gauges on 8 mm diameter bars had a significant effect on the test results.

The specimen in test 5M was reinforced with smooth EN8 steel bars. These had been greased to examine how the loss of adhesion and anchorage would affect the behaviour of the specimen. The extensional stiffness of EN8 steel is very similar to that of high yield reinforcing steel, as can be seen from Figure 3.3

The specimens used in test series 6 were similar to those used in test series 5. The testing procedure however was different and was designed to examine the internal crack width variations. Details of the specimens are given in Table 5.2.

5.3 Manufacture of specimens

5.3.1 Concrete

The concrete mix designs were the same as those used in aggregate interlock and dowel action tests. The high strength concrete mix was not used in any of the reinforced concrete specimens. Placing and curing of the concrete was carried out as before. The specimen mould is seen in Figure 5.2.

5.3.2 Reinforcement

The specimens reinforced with 12 mm or 16 mm bars were fitted with strain gauges encapsulated within slots in the bars as described in 4.2.3. This technique was used to minimise the disturbance of the bond properties of the bars. When 8 mm reinforcing bars were used, there was insufficient space to use this technique and hence strain gauges conventionally bonded to the surface of the bars were used. These gauges were then covered with the minimum amount of protective covering necessary to ensure waterproofing. This was to minimise the disturbance done to dowel action and anchorage of the bars by the soft protective coating.

Every reinforcing bar was calibrated, within its elastic range by applying an incremental axial force as described in section 4.2.3. However, it was expected that some of the bars would be stressed beyond the elastic limit during the latter stages of shear testing. In order to find the stress-strain curve beyond the elastic limit, two bars of each diameter were tested to failure. The accuracy of the strains obtained from strain gauges were corroborated using an extensometer, clamped onto the bar. Hence a mean stress-strain curve from the three bars was obtained for each bar size (Figure 5.3).

It was observed that the 16 mm and 8 mm diameter bars had virtually identical physical properties. However, although the 12 mm diameter bars had a similar initial stiffness and ultimate strength, the stiffness at stresses above 400 N/mm^2 was lower. This resulted in a 0.2% proof stress of 435 N/mm^2 instead of 485 N/mm^2 and was probably due to the steel coming from a different production batch.

A trilinear curve was used to approximate the stress-strain relationship for the reinforcement e.g. for Y16 bars

for $\varepsilon_s < 2350 \times 10^{-6}$

$$\sigma_s = 196 \times 10^3 \times \varepsilon_s \text{ N/mm}^2 \quad (5.2)$$

for $2350 \times 10^{-6} < \varepsilon_s < 11000 \times 10^{-6}$

$$\sigma_s = 461 + (\varepsilon_s - 2350 \times 10^{-6}) \times 10.3 \times 10^3 \text{ N/mm}^2 \quad (5.3)$$

for $11000 \times 10^{-6} < \varepsilon_s$

$$\sigma_s = 550 \text{ N N/mm}^2 \quad (5.4)$$

With the embedded bars the exact location of the crack could not be predetermined. Hence if the strain gauge location was not at the point of contraflexure, a degree of flexure of the bars was expected in addition to axial strains. The following procedure was adopted for 16mm diameter bars to determine the overall tensile force normal to the plane of cracking.

When the strain on all the strain gauges was less than 2350×10^{-6}, the axial strain in each bar was taken as the mean of the two strain gauge readings (Figure 5.4a). The steel stresses were then obtained from Figure 5.3.

When one of the strain gauge readings exceeded 2350×10^{-6} (Figure 5.4b) the position at which a strain of 2350×10^{-6} occurred was found. The centroids of the circle segments above and below this level were

then located and the strains ε_1 and ε_2 at these positions were found. The respective stresses σ_1 and σ_2 were then found from Figure 5.3. The overall force in the bar was then evaluated as

$$F_{axial} = \sigma_1 A_1 + \sigma_2 A_2 \qquad (5.5)$$

When it was necessary to adopt this method to determine the compressive stress, σ_c, in the concrete normal to the plane of cracking, this stress was plotted as a broken line in the test results, e.g. Figure 5.9c.

In the event of one of the strain gauge readings exceeding 11000 x 10^{-6}, that gauge was no longer considered to be reliable and no attempt was made to evaluate the total axial force in the reinforcement. A similar procedure was adopted to evaluate the axial forces in the 12mm and 8mm reinforcement using the appropriate stress-strain curve and bar geometry.

5.4 Testing procedure

5.4.1 Shear tests

The method of obtaining an initial tensile crack at the centre of the specimen was the same as was used for aggregate interlock specimens (section 3.5.1). Once the crack had formed there was a much smaller release of strain energy in the reinforced concrete than in the unbonded aggregate interlock bars. Hence the obtaining of small initial cracks was an easier operation.

The shear load was applied incrementally, as before. In all the reinforced concrete tests the axial tension applied to the specimen was restored to its initial value after each increment of shear loading.

Hence the test rig did not contribute to the axial stiffness of the specimen. The shear test was terminated once large slips across the crack face started to occur for very little additional shear load. This was usually when the overall shear slip was in excess of 1.5mm. Test 5A was terminated after a shear slip of only 0.5mm because the shear load had reached the design capacity of the test rig and could not be safely increased.

After each shear test had been completed, the specimen was cut open, as in the dowel action tests, to examine the damage done to each crack face. When Walraven (42) opened up reinforced concrete shear specimens, after testing, there was a region of localised damage to the concrete adjacent to each reinforcing bar. The method the author used to examine the crack face was to bend the specimen laterally until the reinforcement had yielded sufficiently to permit inspection. In test 5J, this method was duplicated to see if the large axial strains, caused by opening the specimen in this manner produced further damage to the crack face, after the shear test had ended.

5.4.2 Crack width tests

For the crack width tests a reinforced concrete specimen was manufactured and set up in the tensile part of the test rig using the same procedure as in the shear tests. The specimen was then cracked in tension and the crack width preset to the required value using a Demec gauge. The sides and bottom of the crack were sealed by pressing a mastic around the crack initiating slot. The crack was then filled by pouring a very low viscosity resin into the crack initiating slot from above. The resin used was CXL 600, manufactured by Colebrand. Capillary forces were sufficient to draw this resin into the smallest crack visible to the naked eye (i.e. < 0.01mm).

One particular problem with this technique was that air tended to become trapped within some parts of the crack. This was solved by making several air vents in the seal around the edge of the crack, which permitted the air to escape. When resin began to emerge from these vents, they were sealed off with additional mastic.

The resin was allowed to harden for 24 hours. The tensile force was then removed and any changes in the surface crack width were noted. The specimen was then cut open as shown in Figure 5.5 using a masonry saw. The thickness of the crack was measured using a hand-held crack width microscope with a magnification of 25X. Each reading was estimated to the nearest 0.02mm.

Details of the four specimens used to examine crack width variation are given in Table 5.2. For each specimen, making five cuts (Figure 5.5) provided six views of the internal crack. Four of these were where the crack intersected the reinforcement and two were in the centre of the specimen, where it did not. The thickness of the cut made by the masonry saw was approximately 3mm. This meant that the cracks on each side of the cut were similar, but not identical. In some cases the specimen fractured whilst it was being cut. This left a rough surface and the crack could not be examined with any degree of accuracy over this region. If this method is to be developed further, a more effective method of cutting and polishing the sawn face needs to be found.

5.5 Test results

Before any strain gauged reinforcing bars had been used in shear tests it was uncertain how effectively the internal gauges in the reinforced specimens would measure the axial force transmitted normal to the crack

during tensile loading and during the subsequent additional shear loading. The strain gauges in the bars for the dowel action specimens had indicated an axial force which correlated quite closely with the externally applied axial force, (Figure 4.4). However in the dowel action tests the crack was preformed and hence it was known that the position of the strain gauges coincided exactly with the crack. In the reinforced concrete specimens the path of the crack could not be predetermined and it was possible that it might pass to one side of the strain gauges, and that the gauges might not indicate accurately the tensile force transferred across the crack. However there was a close correlation observed between the axial tensile force indicated by the internal strain gauges in the reinforcement and the externally applied force (Figure 5.6). This result was independent of whether surface bonded strain gauges or internal encapsulated strain gauges were used.

A complete record of the results of the individual reinforced concrete tests is given in reference 65. Trends observed from these results are described below. There is an element of scatter in these results which may be inherent in the testing of a non-homogeneous material or may be due to variations in other parameters not controlled in these tests. Because of the degree of scatter, more reinforced concrete tests are needed to establish beyond doubt these trends.

5.5.1 Normal restraint stiffness

It was discovered from tests 5A to 5I that the magnitude of the stiffness normal to the crack, restraining crack widening, could not be directly controlled. In the aggregate interlock tests this stiffness was provided directly by the axial stiffness of the unbonded bars and this did not vary during shear testing and the consequent crack widening.

In the reinforced concrete tests the normal restraint stiffness was affected by a number of factors. It was observed that, for the same reinforcement ratio, an increase in the crack width tended to result in a reduced normal restraint stiffness, either initially or as the test progressed. This could be attributed to two causes:

a) a larger initial crack width was achieved by increasing the external tension applied to the specimen. This can cause local bond damage between the reinforcement and the concrete and hence reduce the axial stiffness of the embedded reinforcement.

b) the increased axial tension in the reinforcement brings it nearer to its limit of proportionality. As soon as this limit is passed in either of the reinforcing bars, the axial stiffness will reduce.

In Figure 5.7 the axial stress in each reinforcing bar at the centre of the specimen is plotted against the crack width for specimens 5A to 5I. The crack width increases as shear slip and overriding occurs. It is seen that there is a non-linear relationship between the crack width and the axial stress. As the reinforcement stresses are all below the 0.2% proof stress (Figure 5.3), this non-linearity must be due to break down of the local bond.

In Figure 5.7 these results are also compared with the result predicted by Martin (24) for a concrete strength of 35 N/mm^2. Most of the results lie quite close to the predicted curve, with the exception of test 5D. In this test the concrete strength attained was only 26 N/mm^2. The reduced axial stiffness of the embedded reinforcement was attributed to a weaker local bond action because of the reduced concrete strength.

The differences between the anchorage stiffnesses of embedded bars in the same specimen can only be attributed to experimental scatter. However, the overall trend is clear. As the initial crack width increased there is an increasing breakdown of the local bond between the reinforcement and the concrete. Hence the anchorage stiffness of the embedded bars, which is restraining the crack from widening, diminishes.

5.5.2 Initial crack width

Figures 5.8 to 5.10 show a comparison of the test results where the initial crack width varies for three different reinforcement ratios. In test 5G the tensile load required to achieve a crack width of 0.5mm was beyond the capacity of the test rig. A 0.35mm initial crack was the maximum which could be safely obtained.

All three figures show that increasing the initial crack width results in a reduction in the shear stiffness and in the ultimate shear capacity.

It is also seen from Figures 5.8b to 5.10b that the specimens with larger initial crack widths have a lower rate of crack widening at low values of shear slip and a higher rate of crack widening towards the end of the shear test.

The way in which the ratio of crack widening to shear slip depends upon the initial crack width and the overall shear slip may be explained in the following manner. Those specimens with a larger initial crack width will have a lower contact area between the opposing crack faces. Hence the applied shear load is liable to cause more crushing than overriding of the contact points and therefore the crack

width will not increase so rapidly during the early part of the test as with specimens with smaller initial crack widths. However, as the crack width increases it was observed that axial stiffness of the reinforcement of those specimens with a larger initial crack width decreased more rapidly (e.g. Figure 5.9 (c)). As it is the axial forces in the reinforcement which restrain the crack from widening, a reduction in the axial stiffness will result in an increase in the ratio of crack widening to shear slip (e.g. Figure 5.9 (b)).

5.5.3 Reinforcement ratio

From Figures 5.11 to 5.13 the effects of variations in the reinforcement diameter, for specimens with the same initial crack width can be seen. The three Figures (a) show that an increase in the reinforcement ratio results in a larger shear stiffness. There does not however appear to be a strong correlation between the reinforcement ratio and the ratio of crack widening to shear slip seen in the three Figures (b).

It is also apparent from the three Figures (c) that there is some scatter in the anchorage properties of the reinforcing bars. Comparison of the results of tests 5A and 5B shows that although the diameters of the reinforcement are different, both specimens have the same initial axial stiffness. This situation occurs again in tests 5H and 5I and highlights the importance of measuring axial reinforcement strains internally in each test instead of deducing these strains indirectly from the results of previous pull-out tests. In the latter stages of the shear tests, the difference in axial reinforcement stiffness, for specimens using different bar diameters, becomes more pronounced and a corresponding difference in the direction of crack opening was observed (e.g. Figure 5.11b).

In test 5K the specimen was reinforced with four 8mm bars to increase reinforcement ratio above that of specimen 5F without altering the reinforcement diameter, and hence the anchorage properties. Comparison of the results of these tests (Figure 5.14) shows that an increase in the overall axial stiffness of the reinforcement resulted in a higher shear stiffness, but did not affect the ratio of crack widening to shear slip.

5.5.4 Reinforcement type

The specimen in test 5L was reinforced with two 12mm bars of B.S.C. Unisteel 410. This had a quite different rib pattern to the GKN Torbar used in the rest of the tests (Figure 5.1), which was thought to be more likely to initiate "Goto" type internal cracking (22) and hence to cause internal damage to the concrete adjacent to the bar and the crack face, as observed by Walraven (42). The axial stiffness of unbonded Unisteel 410 was found to be lightly lower than that of Torbar (Figure 5.15), but this was not expected to influence the test results significantly.

The Unisteel 410 reinforcement had better bond properties than Torbar reinforcement (Fig. 5.16c) and hence a higher anchorage stiffness was obtained. In spite of this, there was a considerably greater widening of the crack in test 5L (Figure 5.16b). There was very little difference observed in the shear stiffness of the two specimens (Figure 5.16a).

5.5.5 Local bond

In test 5M, the reinforcement consisted of smooth, greased EN8 steel bars. If the results of this test are compared with those of test 5E (Figure 5.17) the effects of the absence of local bond to the

reinforcement can be seen. As would be expected, the anchorage stiffness of the debonded reinforcement is considerably lower than that of the ribbed reinforcement in test 5E. The shear stiffness of the specimen in test 5M is therefore correspondingly lower. However one point of particular interest is that there is very little difference between the tests in the ratio of crack widening to shear slip (Figure 5.17b). In both tests the lower bound to crack widening, predicted by Walraven (42), was not observed.

5.5.6 Crack face damage

In Figure 5.18a the crack faces of specimens 5B, 5E and 5H are shown after shear testing. From this it can be seen that whilst there were general signs of crushing of the aggregate and mortar over the entire crack face, there was no evidence of a localised cone of damage adjacent to the reinforcement, as reported by Walraven (42). The different axial strains produced in the reinforcement of each specimen before shear testing did not cause any noticeable difference in the damage to each crack face.

Figure 5.18b shows the crack face of specimen 5L after testing. Even though the reinforcement type is similar to that used in Ref. 42 there is no sign of any significant damage to the concrete adjacent to the reinforcement.

In test 5J the crack face was exposed, subsequent to shear testing, by causing the reinforcement to yield (section 5.4.1) in the same manner used in Ref. 42. It can be seen from Figure 5.18c that the strains in the reinforcement were so large that necking occurred and the reinforcement fractured. There was, however, still no sign of localised damage to the concrete adjacent to the reinforcement.

There was insufficient time to try using this method of exposing the crack together with using Unisteel 410 reinforcement, as used by Walraven. However, these results have shown that a conical region of damage around the reinforcement is not typical for all reinforced concrete and warrants further study.

5.5.7 Profile of crack width

It was observed that there was less than 1% reduction in the width of the surface cracks in test series 6 when the injection resin had hardened and the tensile load was removed. The method of cutting open each specimen (Figure 5.5) provided six views of a crack travelling from the tip of the crack initiating slot down to the surface of the reinforcement or the centre of the specimen. Measurements of the internal crack widths, with an accuracy of 0.02mm, are plotted in Figures 5.19 to 5.22. Each reading is the mean of the crack width measurement taken on both sides of the saw cut.

Several problems occurred during the internal crack measuring procedure. In some cases the resin did not fully penetrate the crack, due to air entrapment, and so it was not possible to measure the complete crack. Alternatively the specimens fractured during the cutting process and the resulting surface roughness made it impossible to make accurate measurements. Occasionally the crack would fork and the individual cracks would be too small to measure. For these reasons there are not always six lines plotted in each of the Figures 5.19 to 5.22. The least successful test was 6D, where it was only possible to measure two views of the crack.

However, these results and the photographs of specimens 6A to 6D (Figures 5.23 to 5.26) show clearly that the crack width remained

almost uniform throughout the section, regardless of the distance to the reinforcement.

Close examination of the imprint of the bar left in the concrete in test 5L revealed that the surface of the indentation caused by each rib was polished. This occurred only on the sides which were nearer to the crack face i.e. the bearing faces (Figure 5.27).

It was inferred from these observations that some sliding between the concrete and the reinforcement was occurring in spite of the fact that deformed, high bond reinforcement was used.

In tests on the bond mechanism of deformed reinforcement, Lutz and Gergely (21) reported that if the angle between the longitudinal axis of the bar and the face of the rib (i.e. the slope of the rib face measured along the axis of the bar) was less than 40°, sliding between the concrete and the bar was liable to occur.

The profile of the ribs of both types of reinforcing bar used in this investigation were examined using a Leitz projection microscope to determine if their geometry was consistent with sliding. In Figure 5.28a the outline of both types of rib are seen. However in neither case are the ribs orientated normal to the axis of the bar (Figure 5.1). If these rib profiles are projected onto a plane parallel with the axis of the bar, it is seen (Figure 5.28b) that the mean slope of the rib faces is about 28° for both rib types. Hence the results of Ref. 21 would indicate that sliding between the reinforcement and the concrete is likely to occur.

Table 5.1 Details of reinforced concrete shear specimens

Specimen mark	Target concrete strength (N/mm^2)	Actual concrete strength (N/mm^2)	Reinforcement details	Initial crack width (mm)	Initial axial reinforcement stress (N/mm^2)
5A	35	30.9	2-Y16	0.125	164
5B	35	38.9	2-Y12	0.125	139
5C	35	30.4	2-Y8	0.125	165
5D	35	25.5	2-Y16	0.25	228
5E	35	33.2	2-Y12	0.25	212
5F	35	34.5	2-Y8	0.25	277
5G	35	37.3	2-Y16	0.35	311
5H	35	37.0	2-Y12	0.5	386
5I	35	32.9	2-Y8	0.5	385
5J	35	33.4	2-Y8(1)	0.25	-
5K	35	45.4	4-Y8	0.25	236
5L	35	40.5	2-Y12(2)	0.25	276
5M	35	30.6	2-Y12(3)	0.25	-

Notes

(1) Test 5J was a repeat of test 5F but without fitting strain gauges to the bar

(2) Y12 bars of Unisteel 410 with parallel ribbing

(3) Smooth debonded bars with no ribs

Table 5.2 Details of reinforced concrete crack width specimens

Specimen mark	Concrete strength (N/mm^2)	Reinforcement details	Surface crack width (mm)
6A	36.2	2-Y12	0.5
6B	38.2	2-Y12	0.5
6C	31.5	2-Y12	0.25
6D	32.7	2-Y12	0.125

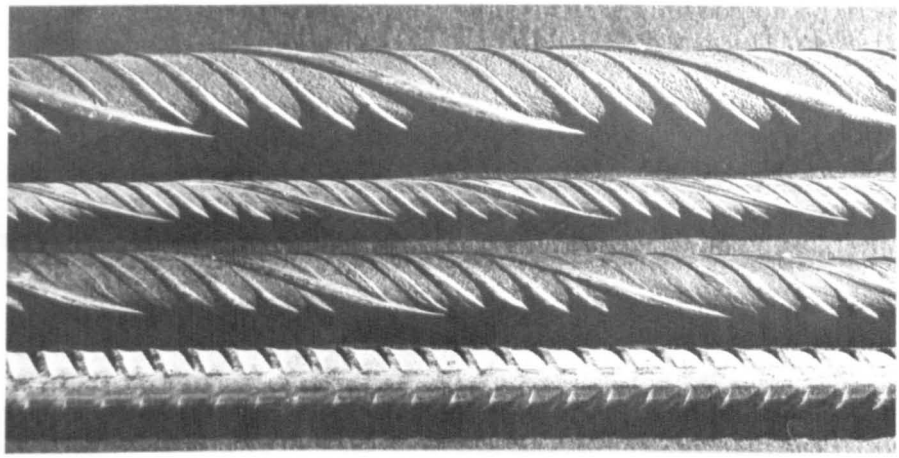

1 - 16mm ϕ Torbar
2 - 8mm ϕ Torbar
3 - 12mm ϕ Torbar
4 - 12mm ϕ Unisteel

FIGURE 5.1. TYPES OF REINFORCEMENT.

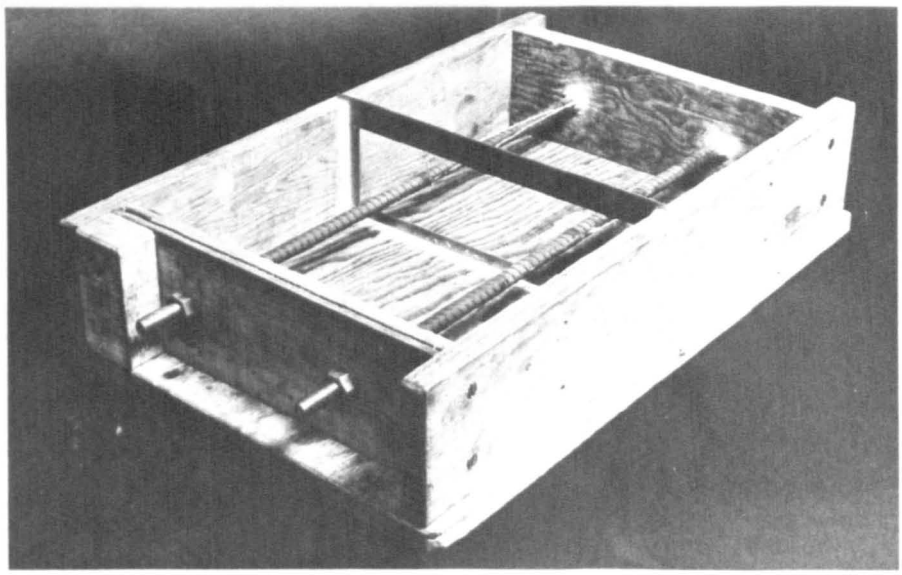

FIGURE 5.2. SPECIMEN MOULD (FOR SPECIMEN 5L)

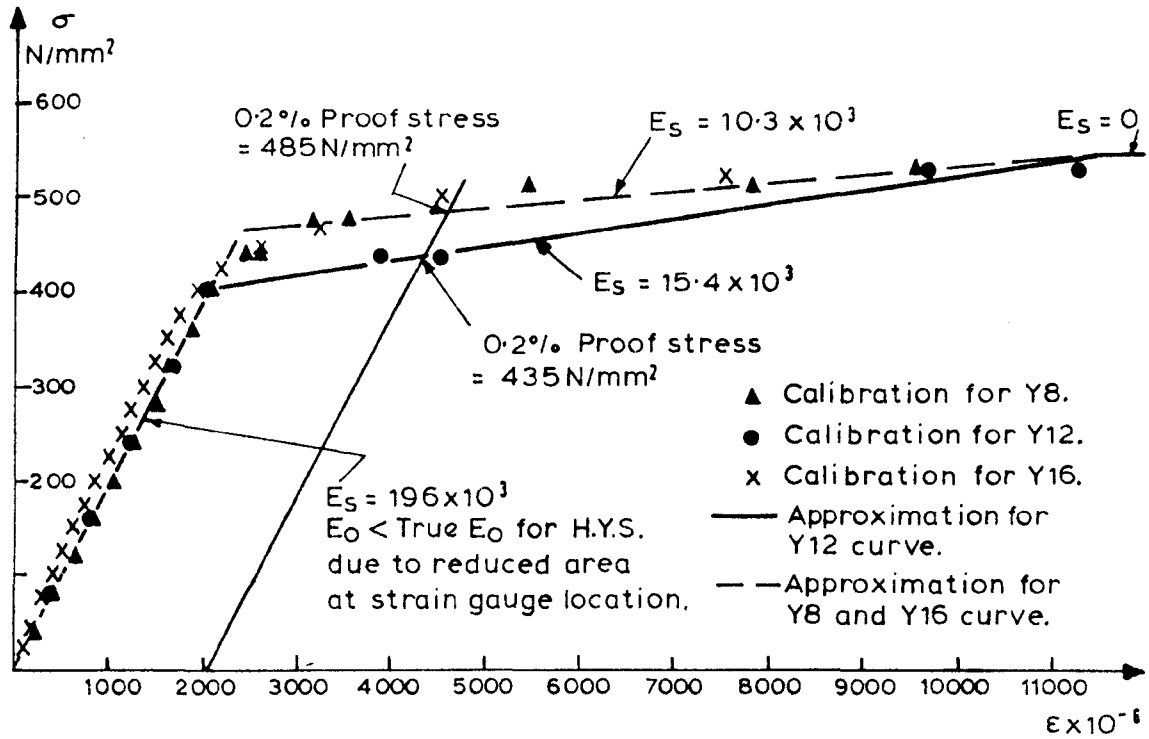

FIGURE 5.3. TENSILE STRESS - STRAIN CURVE FOR REINFORCEMENT.

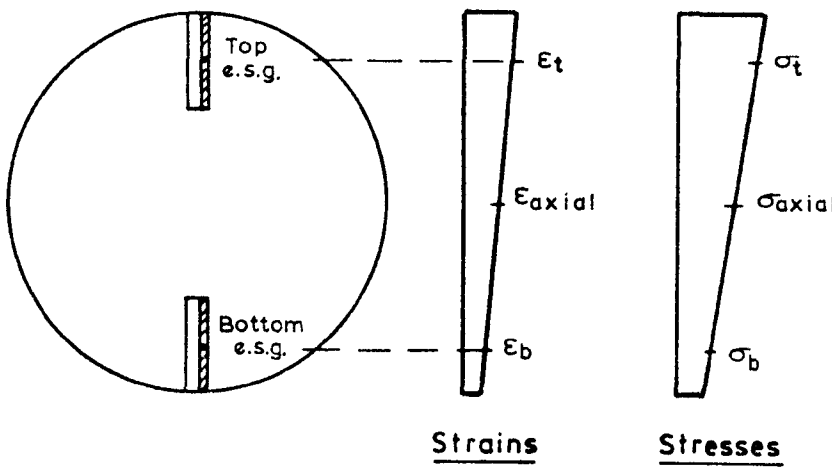

a) For all $\varepsilon < 2350 \times 10^{-6}$

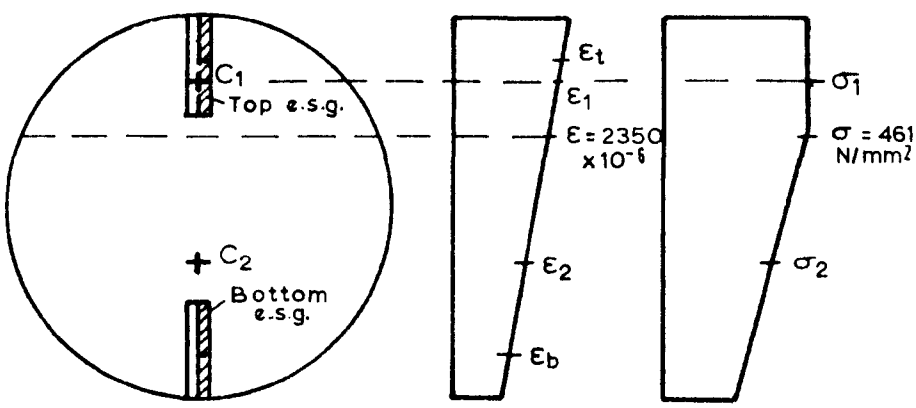

b) For all $\varepsilon_t > 2350 \times 10^{-6}$

FIGURE 5.4. DERIVATION OF AXIAL STRESSES FOR 16mm BAR.

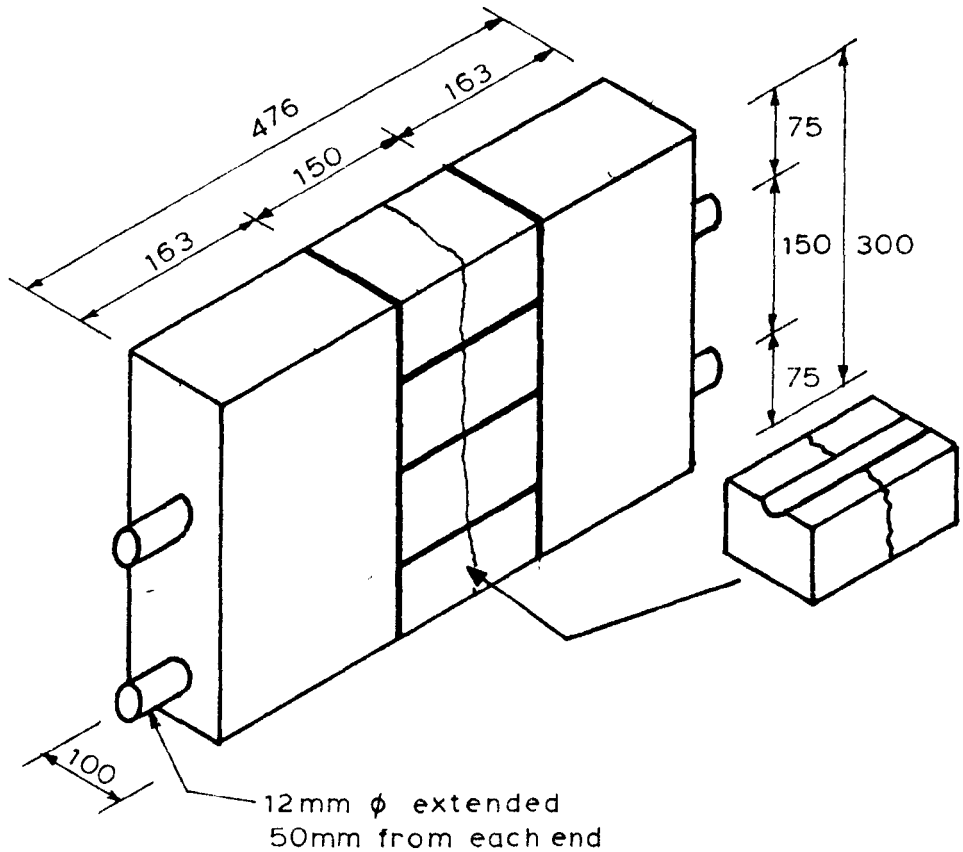

FIGURE 5.5. METHOD OF CUTTING SPECIMEN TO ALLOW INTERNAL CRACK INSPECTION.

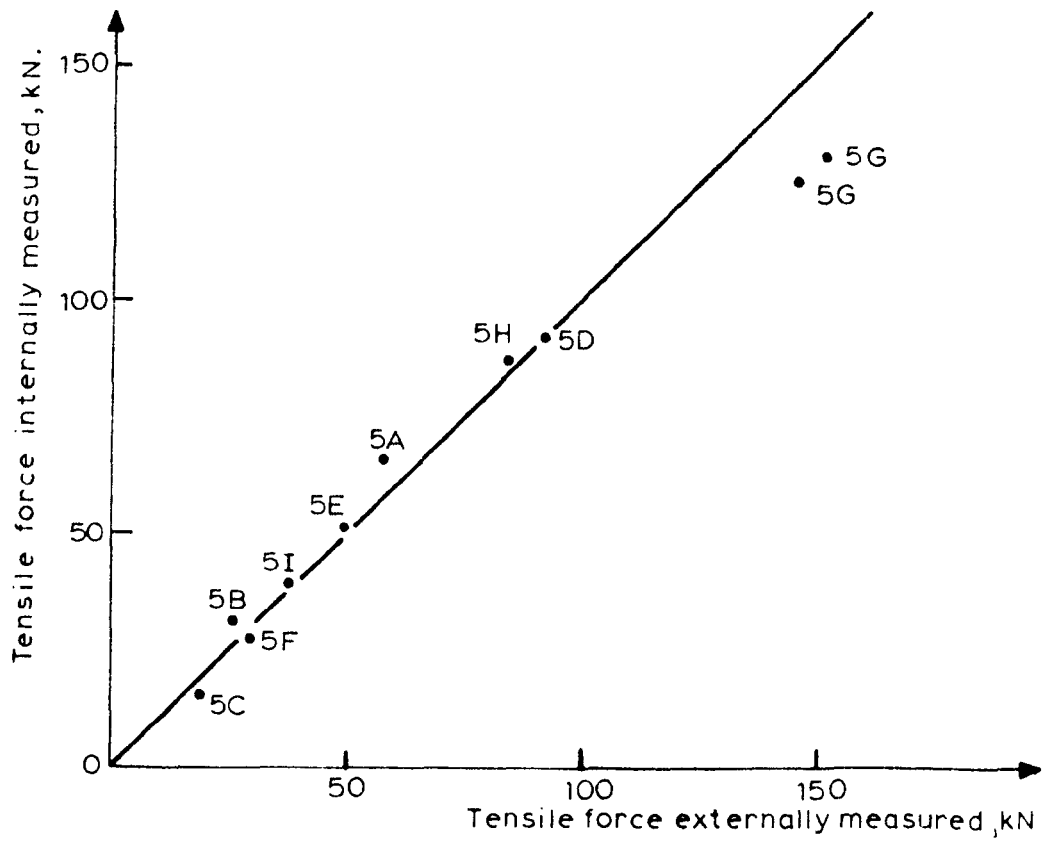

FIGURE 5.6. TENSILE FORCES IN THE REINFORCMENT.

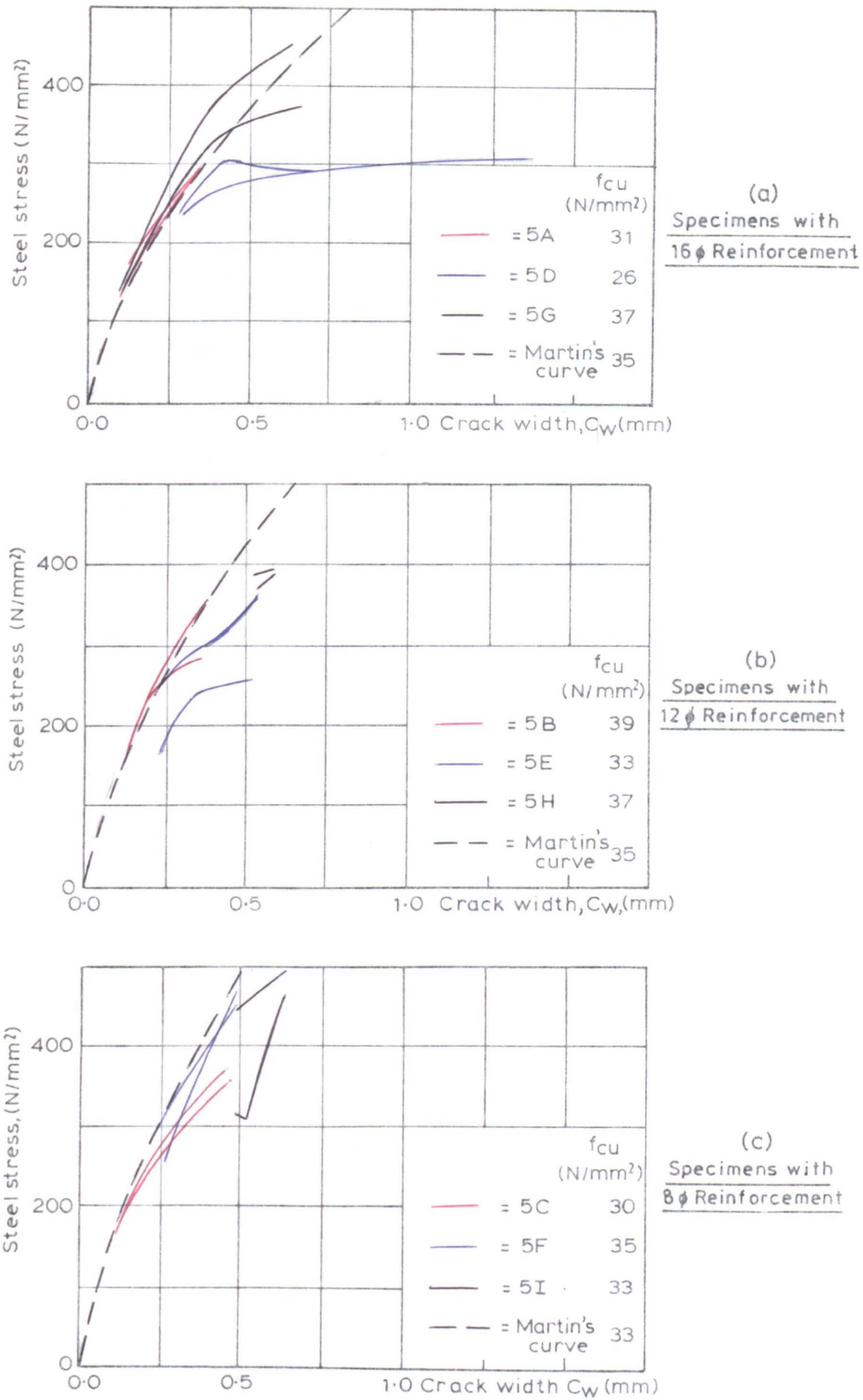

FIGURE 5.7. ANCHORAGE STIFFNESS OF EMBEDDED REINFORCEMENT.

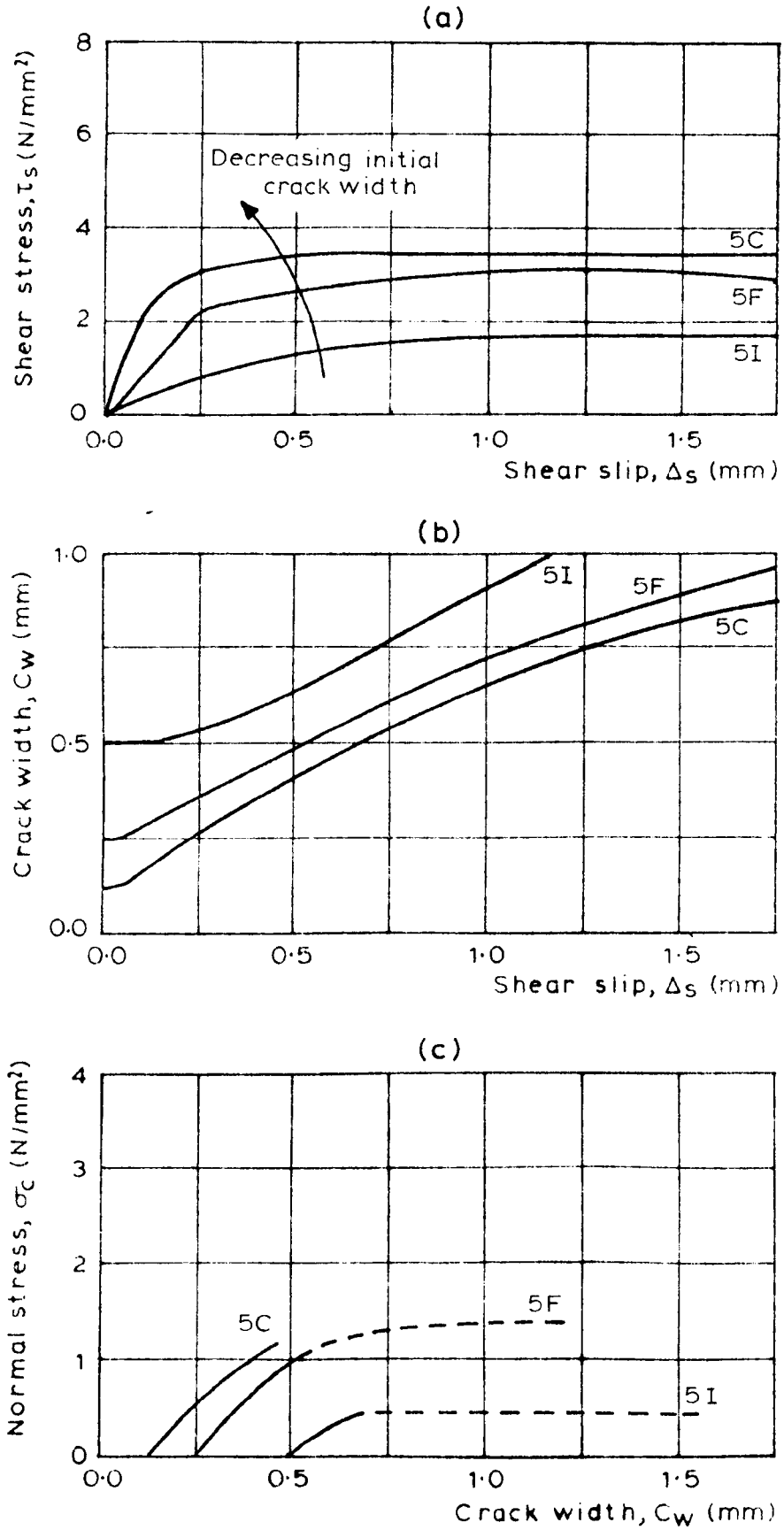

FIGURE 5.8. TEST RESULTS FOR SPECIMENS WITH 8mm REINFORCEMENT AND DIFFERENT INITIAL CRACK WIDTHS.

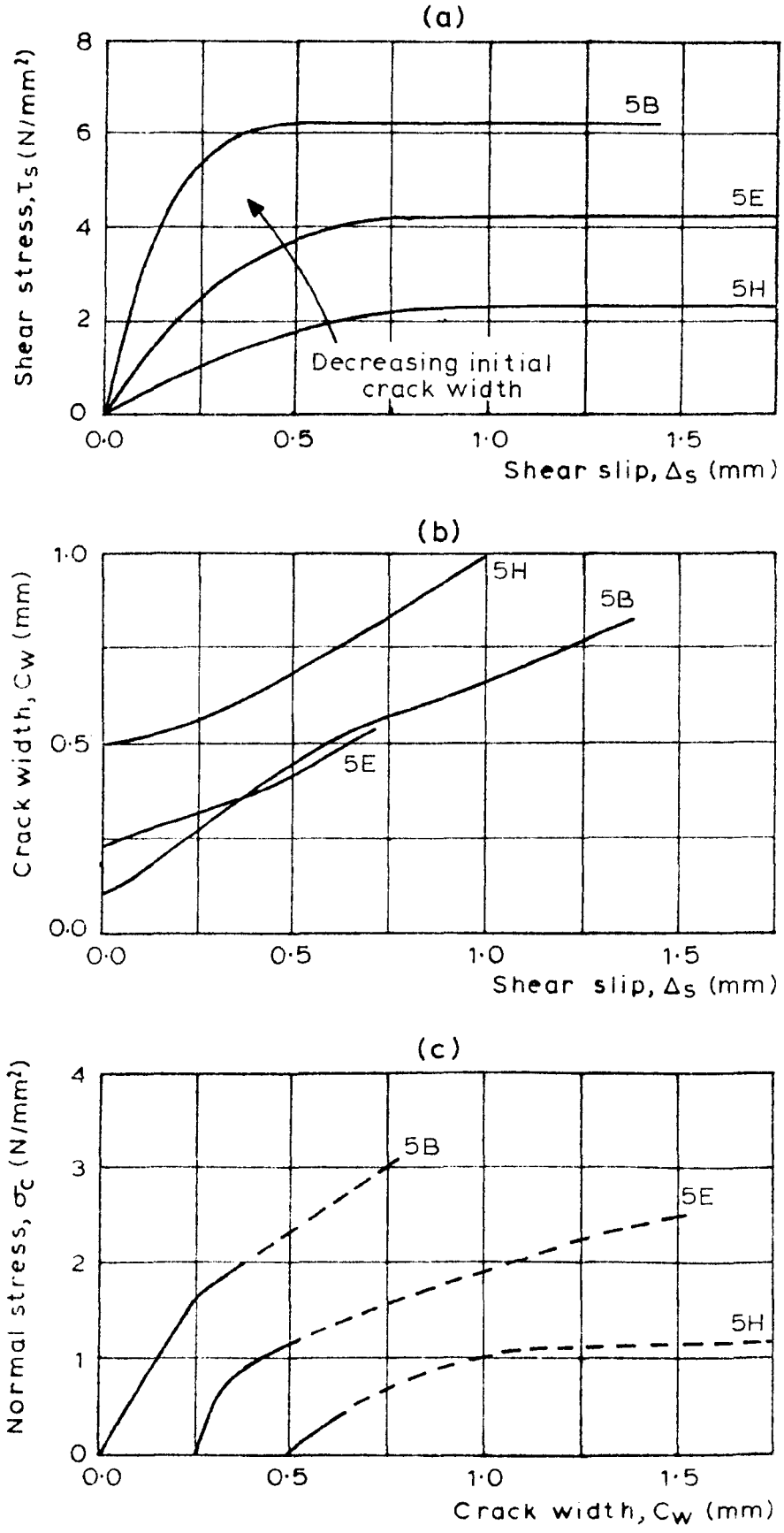

FIGURE 5.9. TEST RESULTS FOR SPECIMENS WITH 12mm REINFORCEMENT AND DIFFERENT INITIAL CRACK WIDTHS.

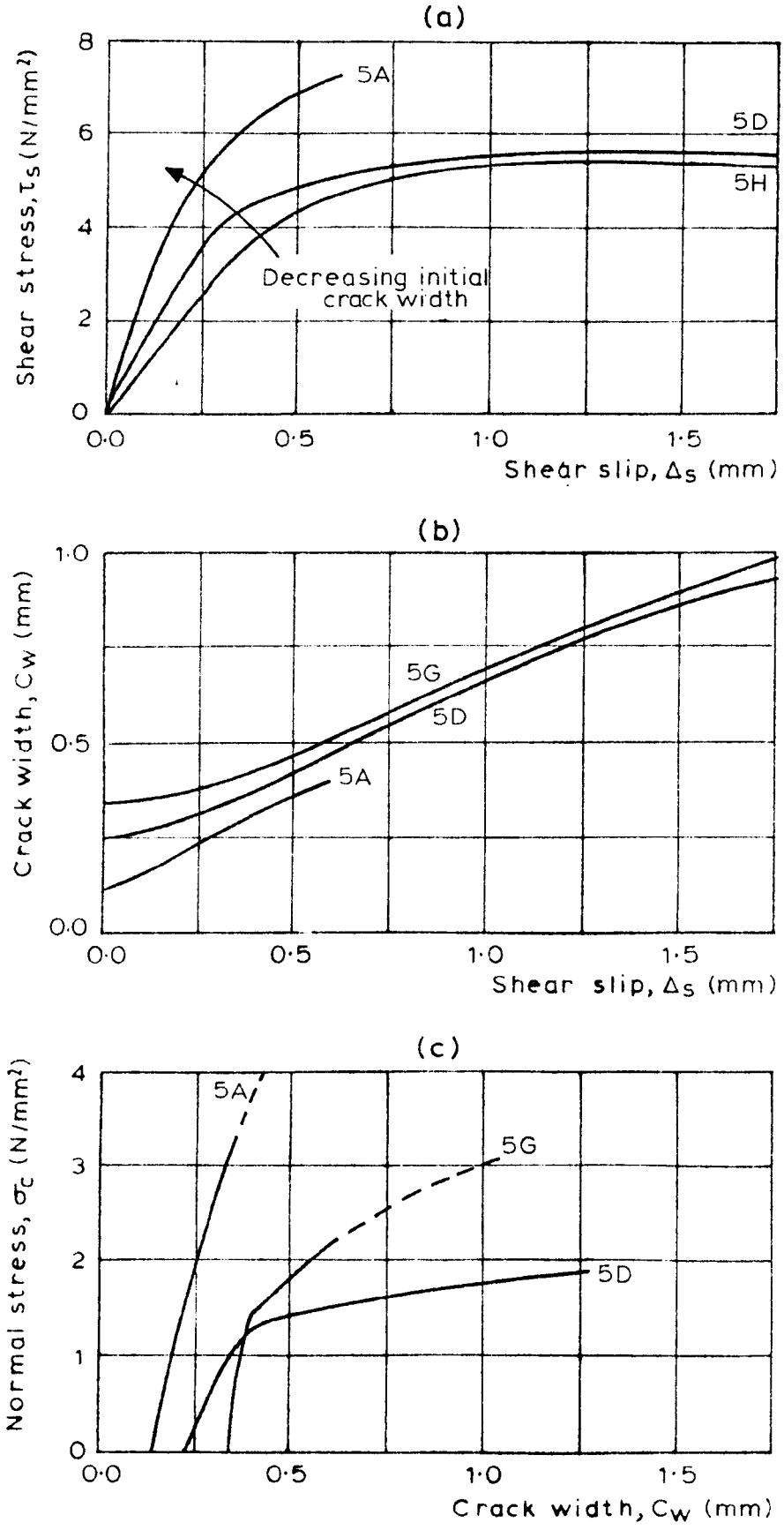

FIGURE 5.10. TEST RESULTS FOR SPECIMENS WITH 16mm REINFORCEMENT AND DIFFERENT INITIAL CRACK WIDTHS.

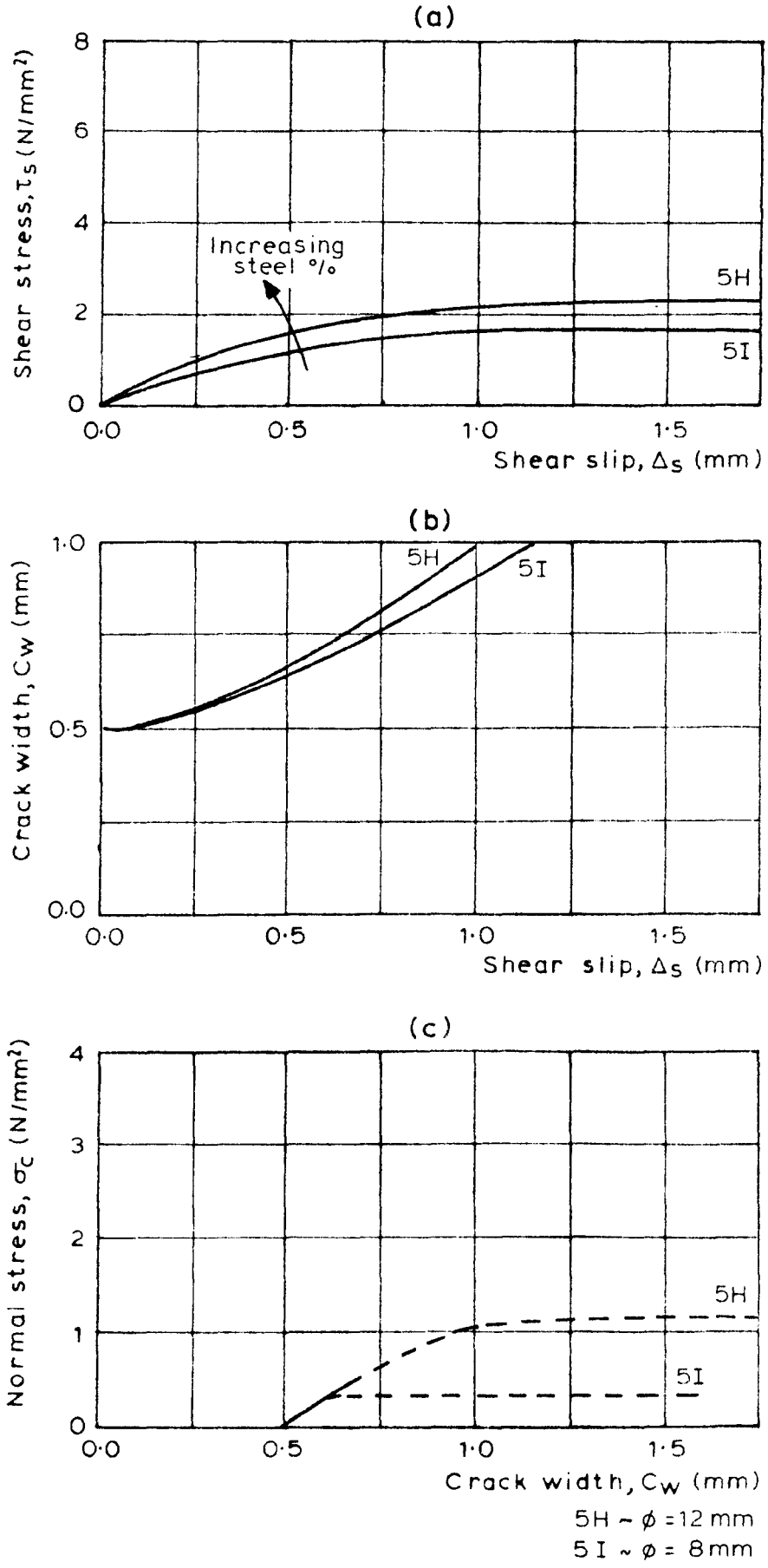

FIGURE 5.11. TEST RESULTS FOR SPECIMENS WITH 0·5mm INITIAL CRACK WIDTH AND DIFFERENT REINFORCEMENT.

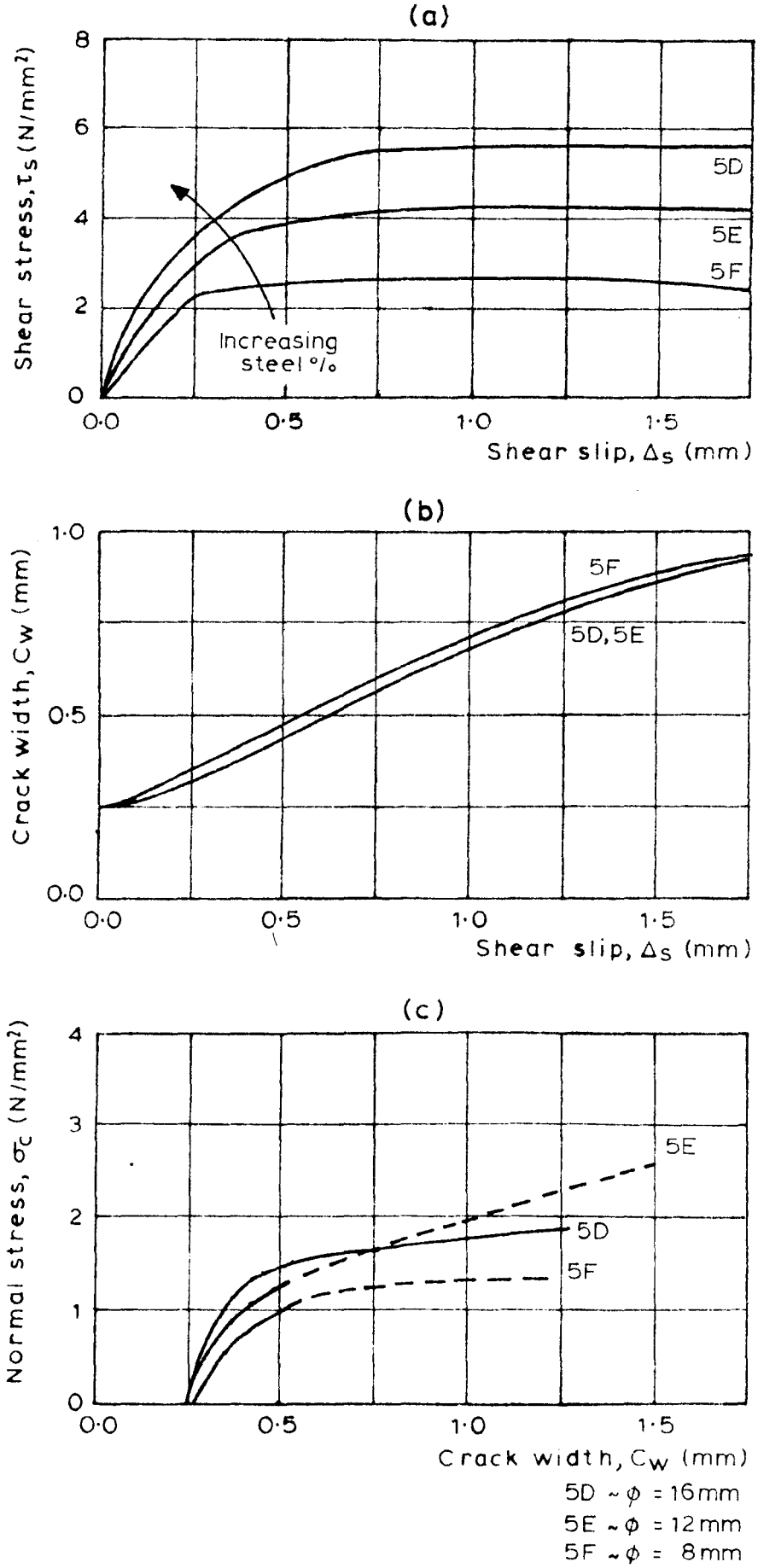

FIGURE 5.12. TEST RESULTS FOR SPECIMENS WITH 0·25mm INITIAL CRACK WIDTH AND DIFFERENT REINFORCEMENT.

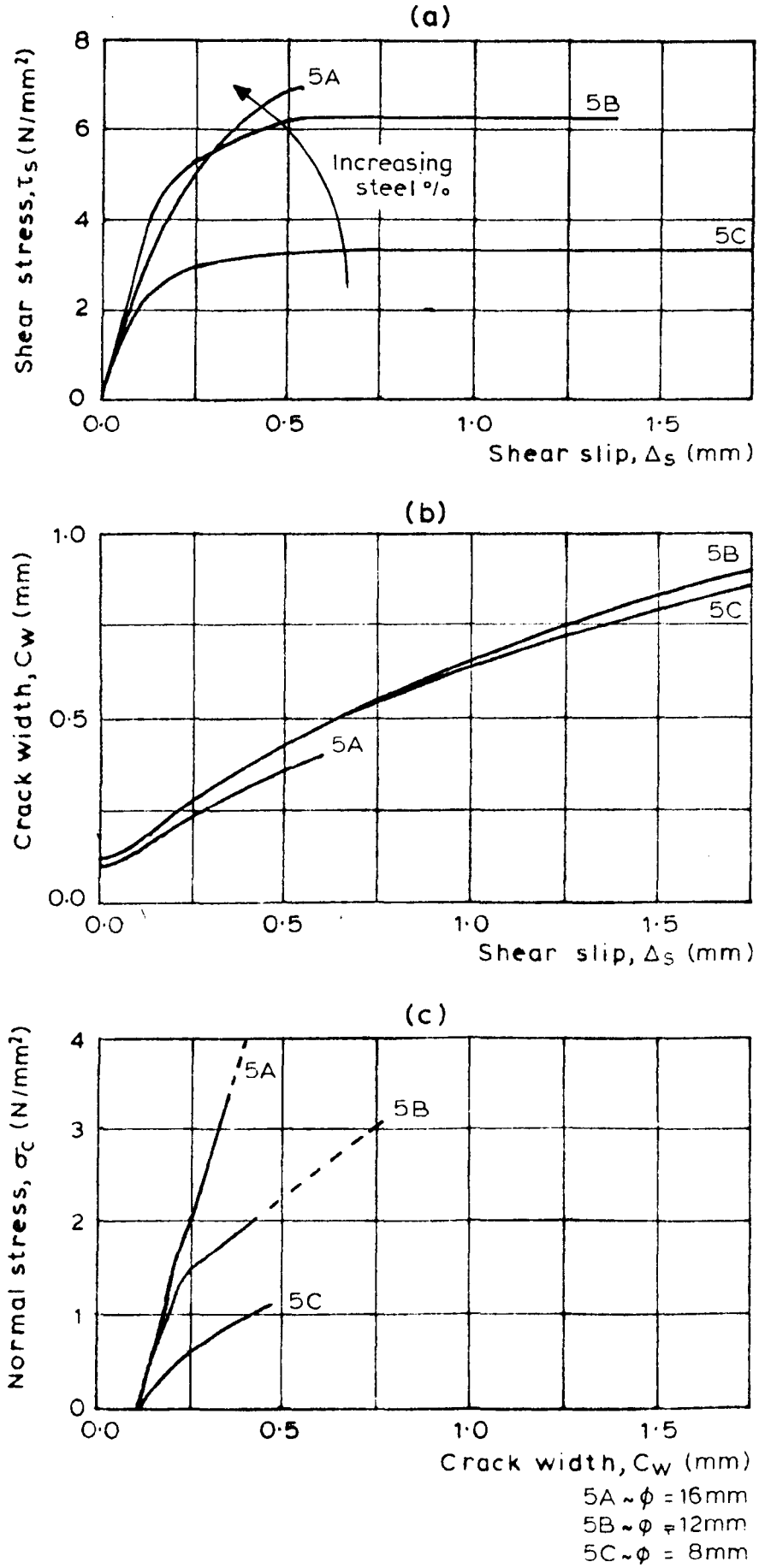

FIGURE 5.13. TEST RESULTS FOR SPECIMENS WITH 0·125 mm INITIAL CRACK WIDTH AND DIFFERENT REINFORCEMENT.

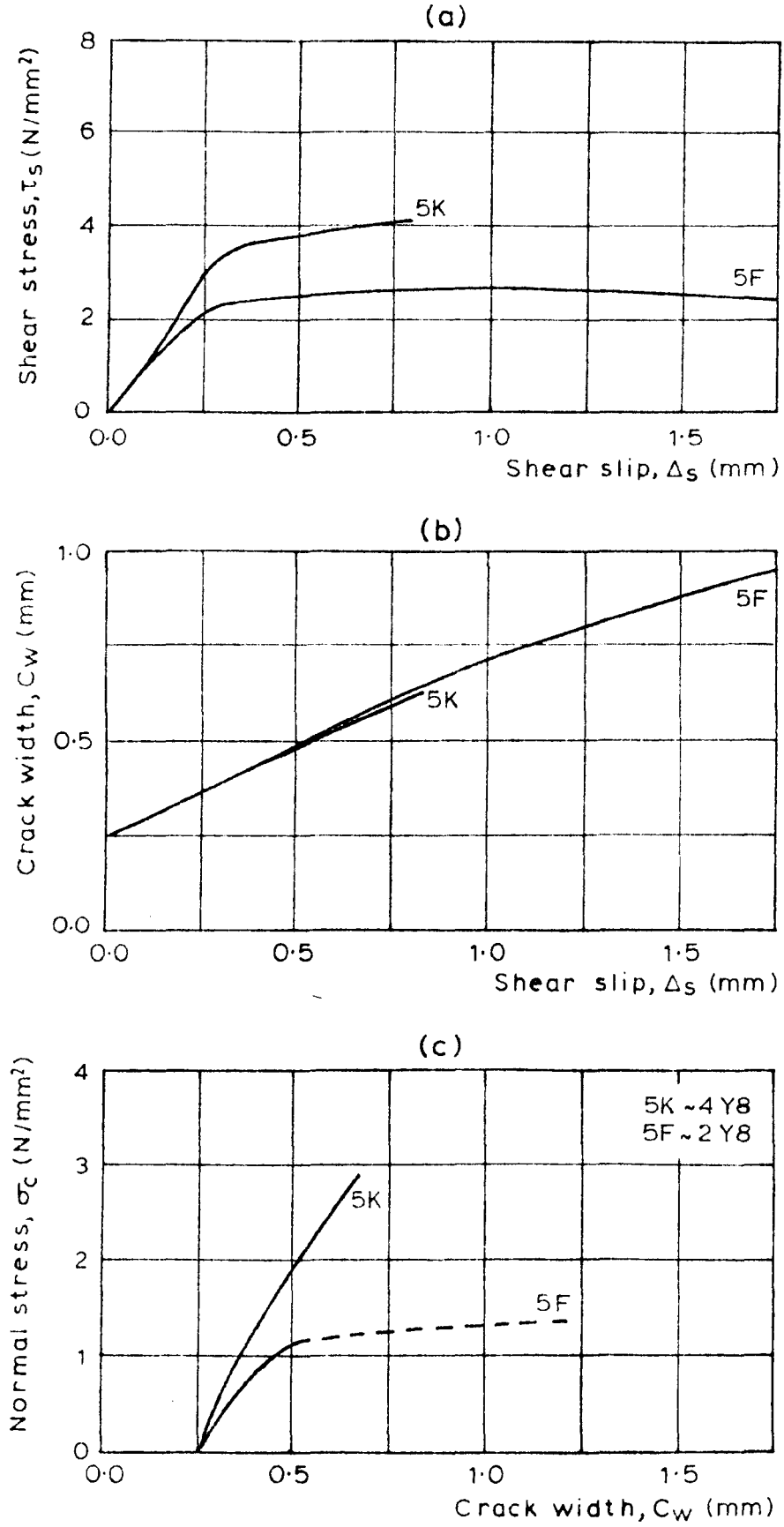

FIGURE 5.14. TEST RESULTS FOR SPECIMENS WITH DIFFERENT REINFORCEMENT RATIOS BUT SAME BAR DIAMETER.

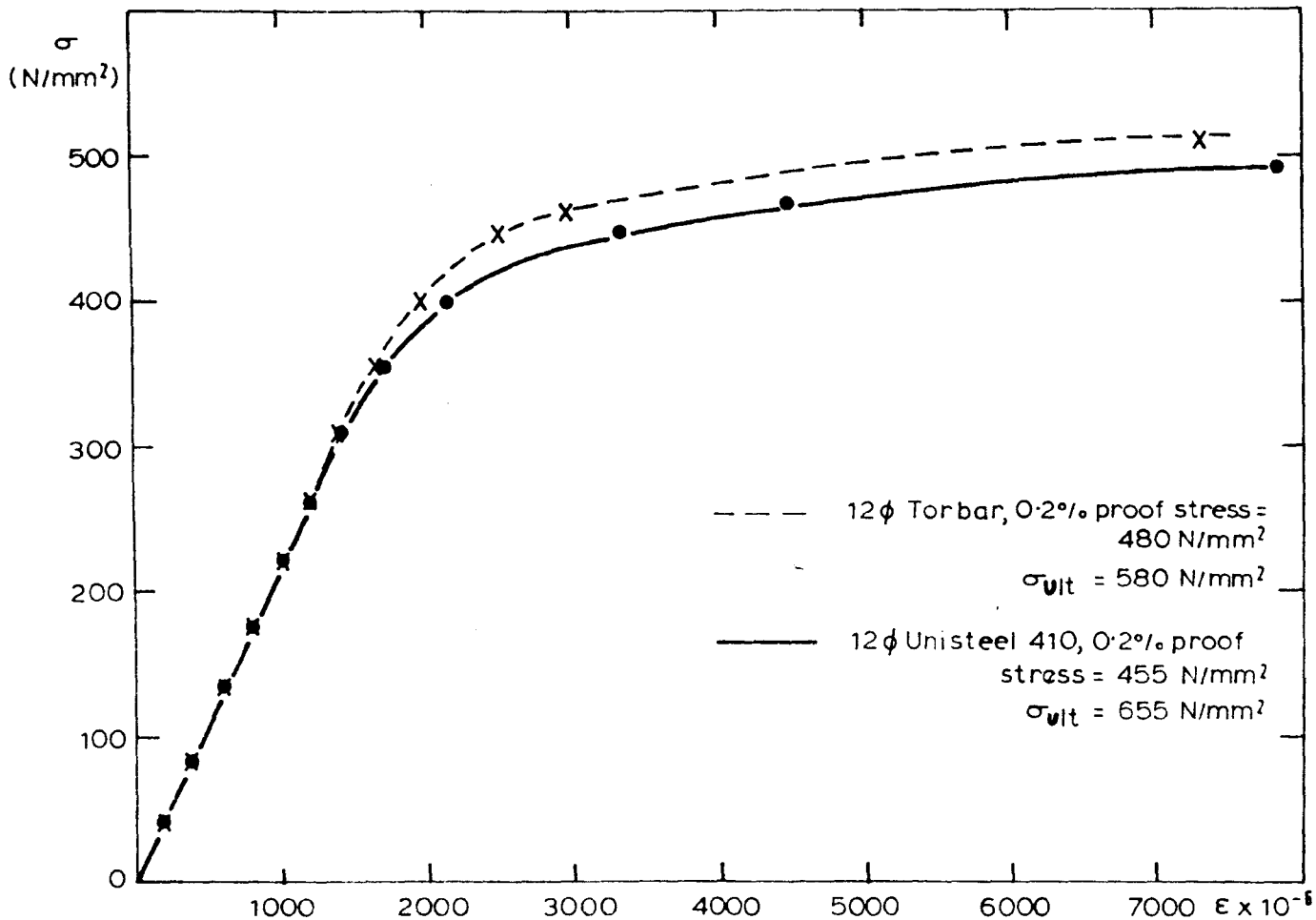

FIGURE 5.15. TENSILE STRESS-STRAIN RELATIONSHIP FOR REINFORCMENT.

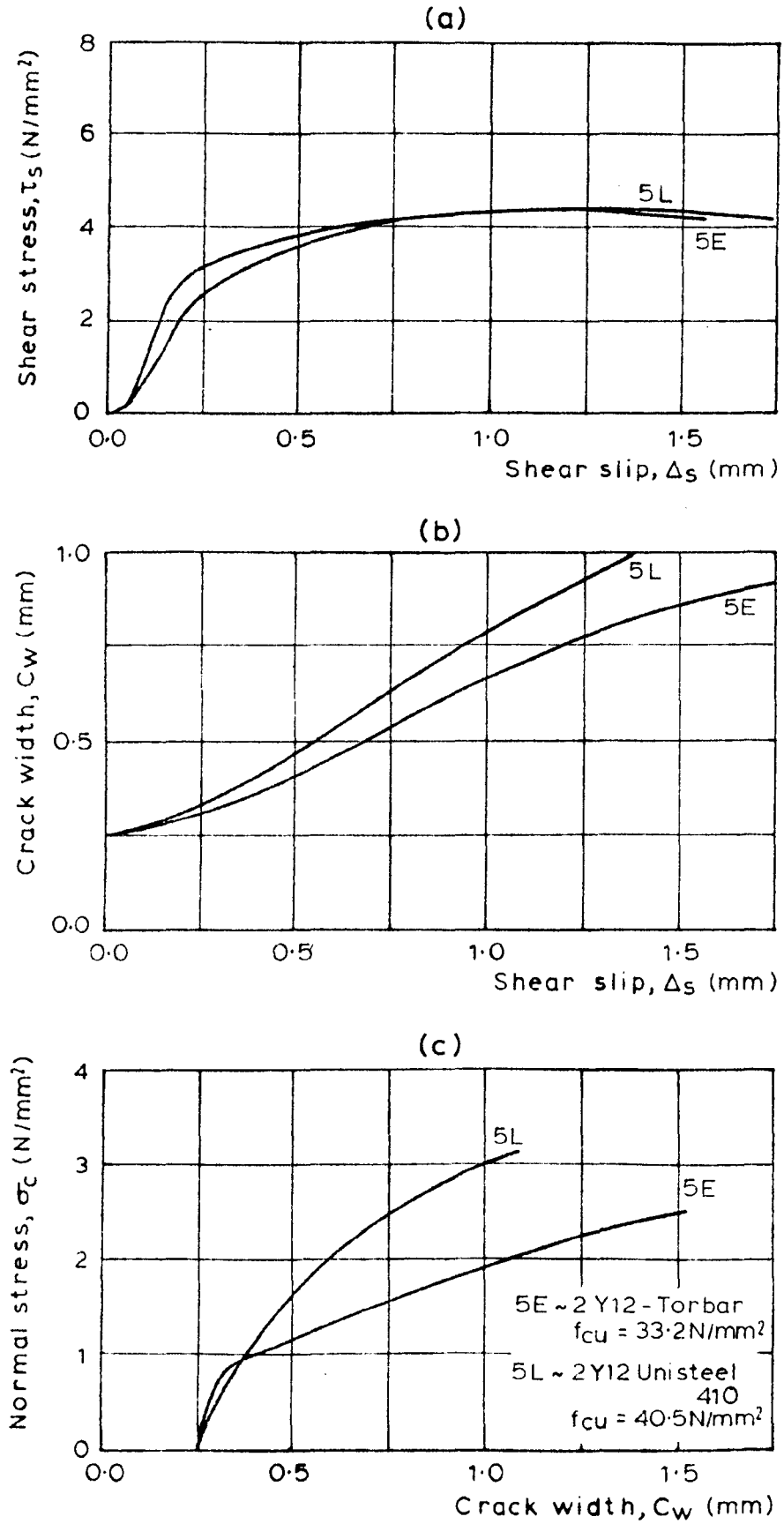

FIGURE 5.16. TEST RESULTS FOR SIMULAR SPECIMENS WITH DIFFERENT REINFORCEMENT TYPES.

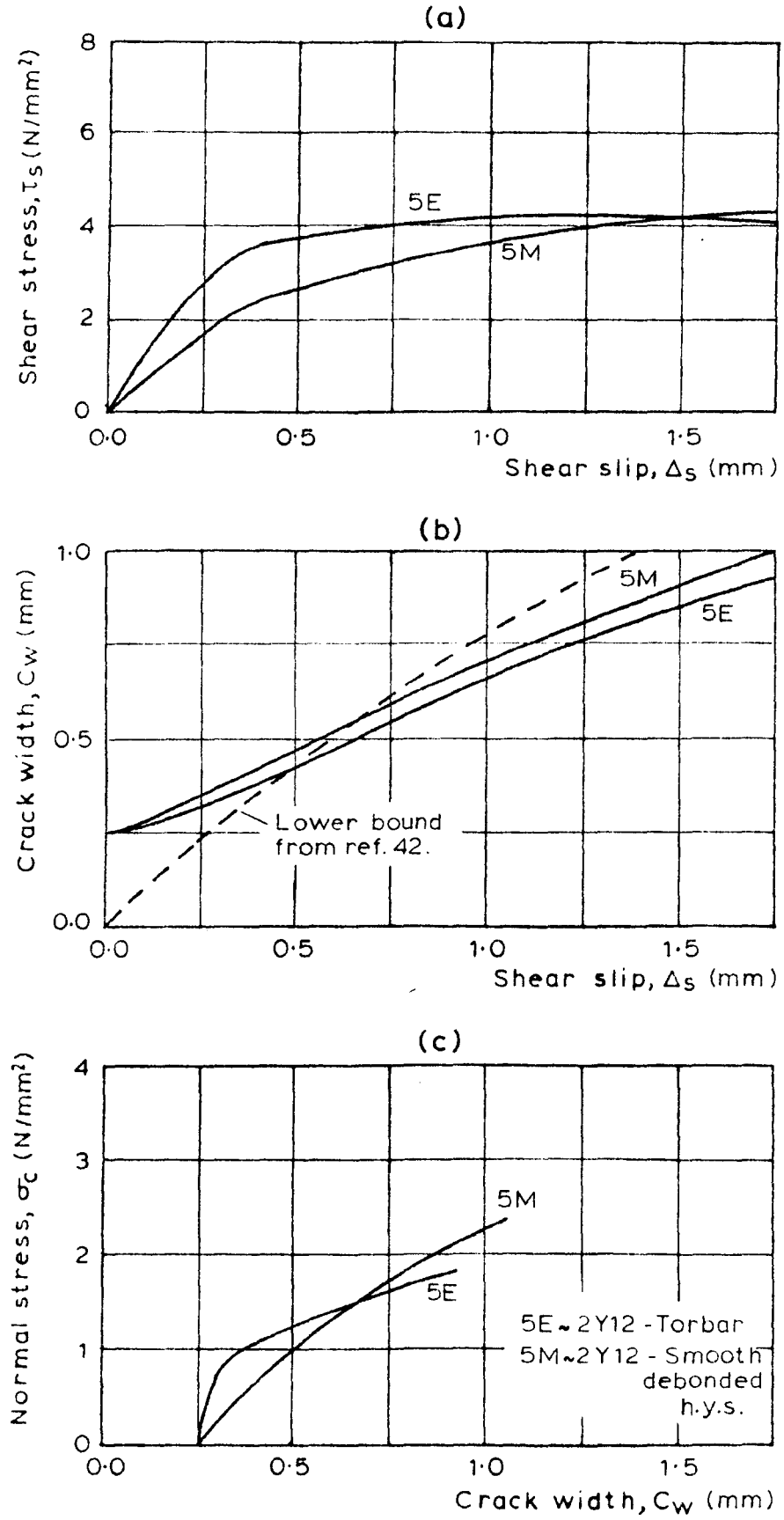

FIGURE 5.17. TEST RESULTS FOR SPECIMENS WITH DIFFERENT LOCAL BOND ACTION.

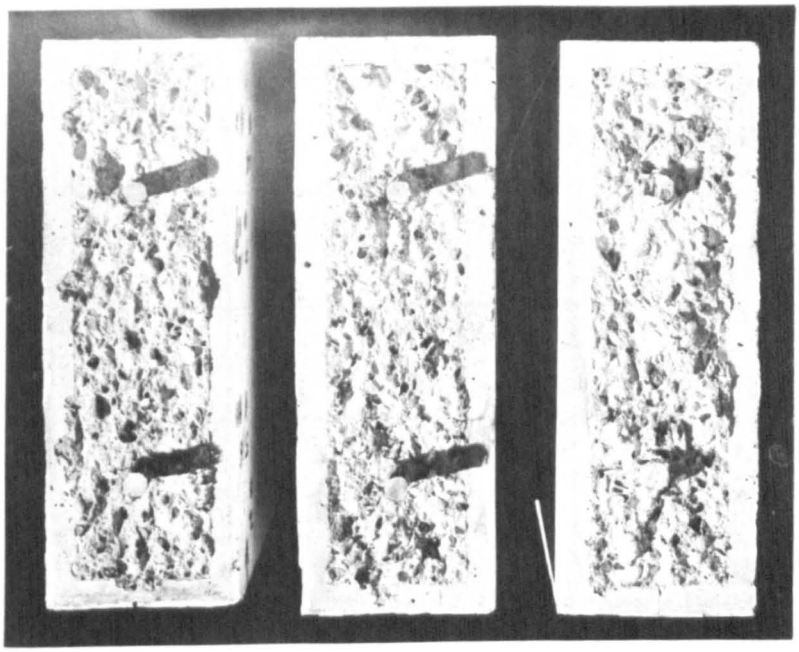

a) 5B 5E 5H

b) 5L

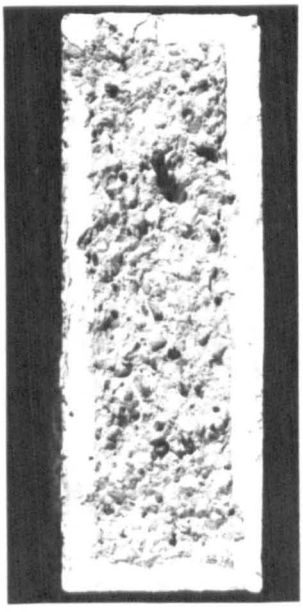

c) 5J

FIGURE 5.18. CRACK FACES OF REINFORCED CONCRETE SPECIMENS AFTER SHEAR TESTING

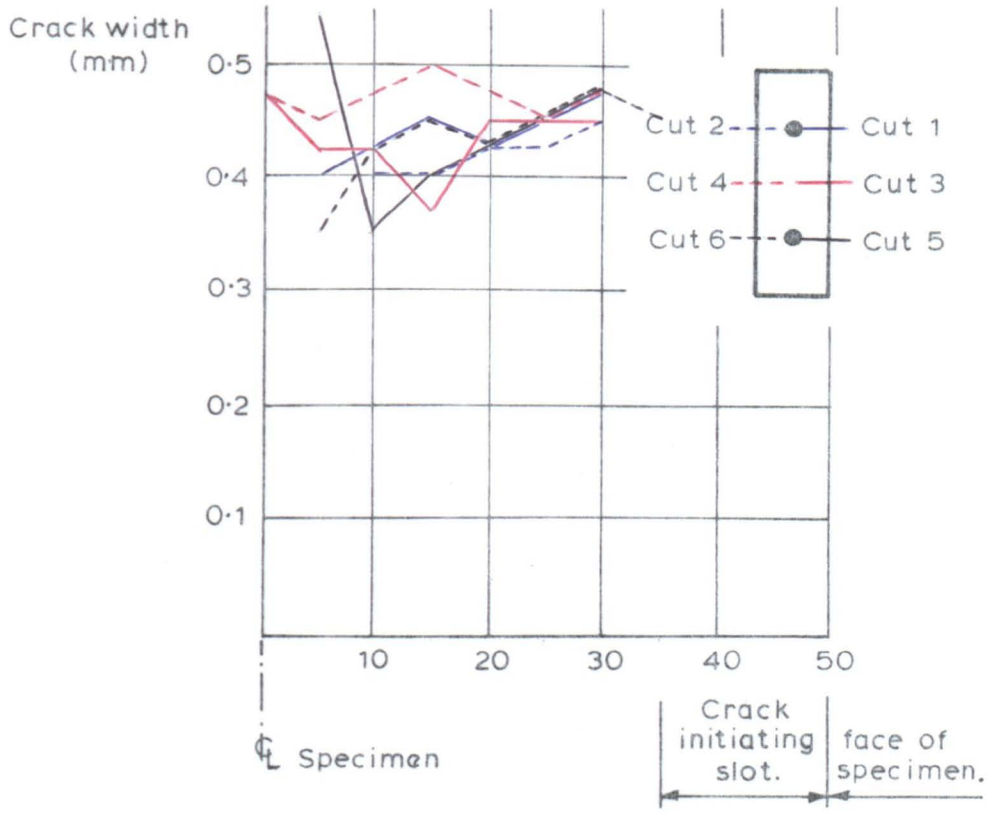

FIGURE 5.19. INTERNAL CRACK WIDTH MEASUREMENTS FOR SPECIMEN 6A

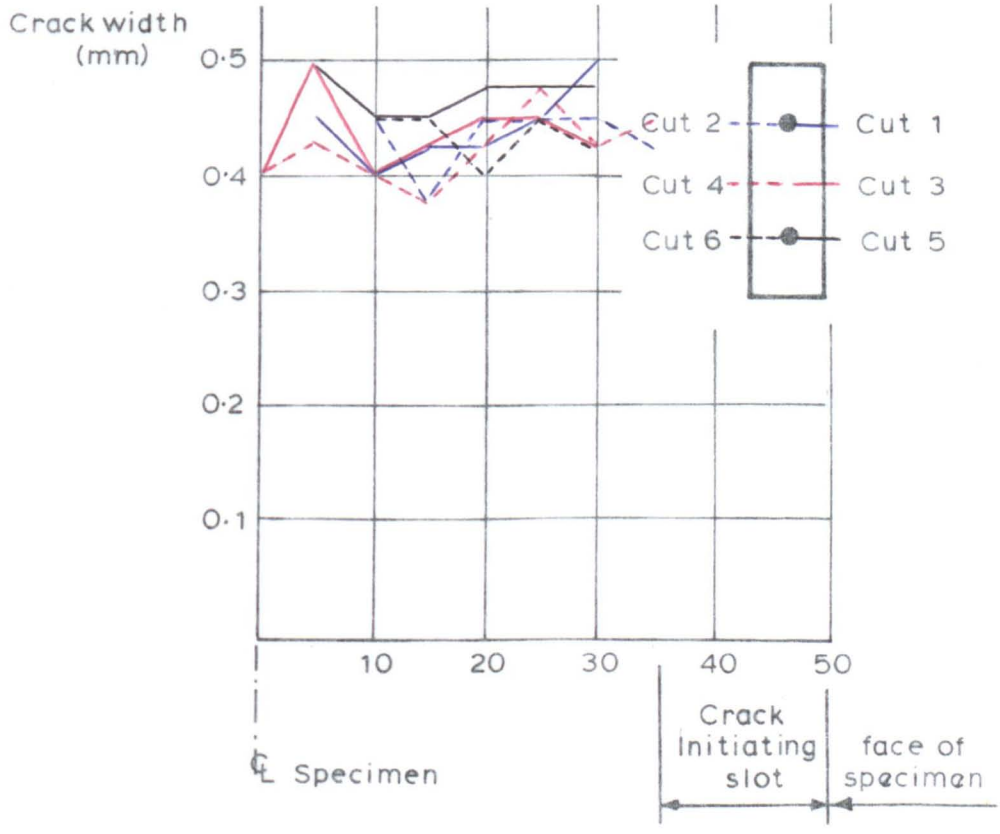

FIGURE 5.20. INTERNAL CRACK WIDTH MEASUREMENTS FOR SPECIMEN 6B

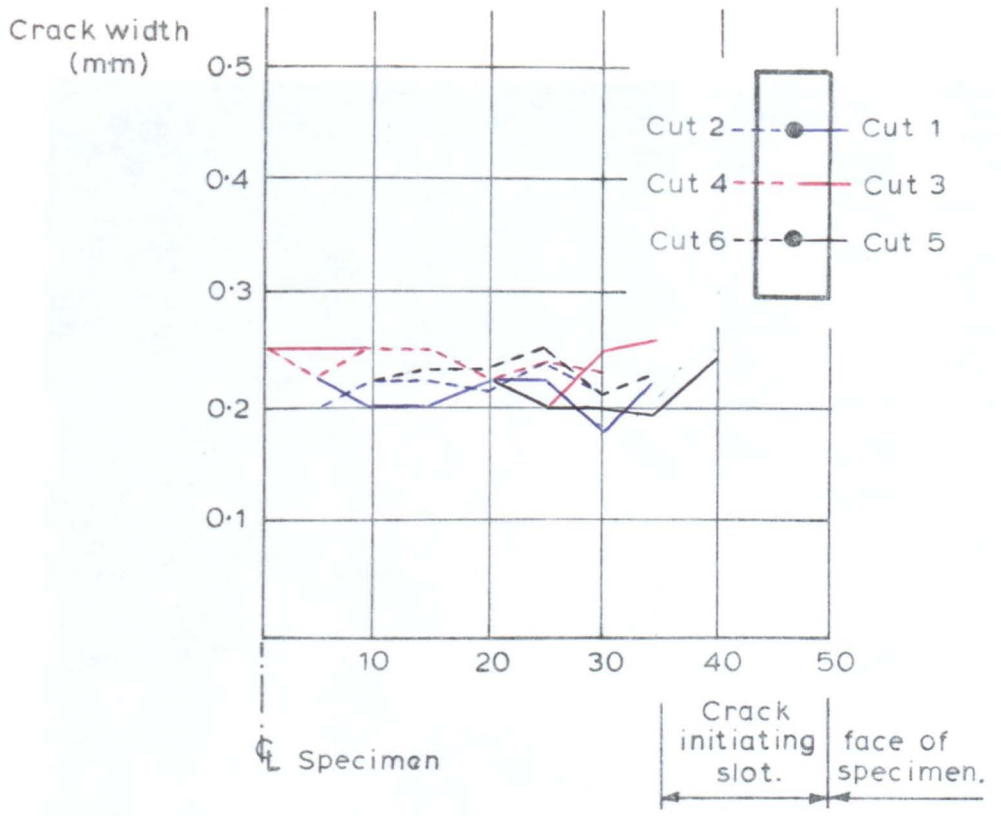

FIGURE 5.21. INTERNAL CRACK WIDTH MEASUREMENTS FOR SPECIMEN 6C

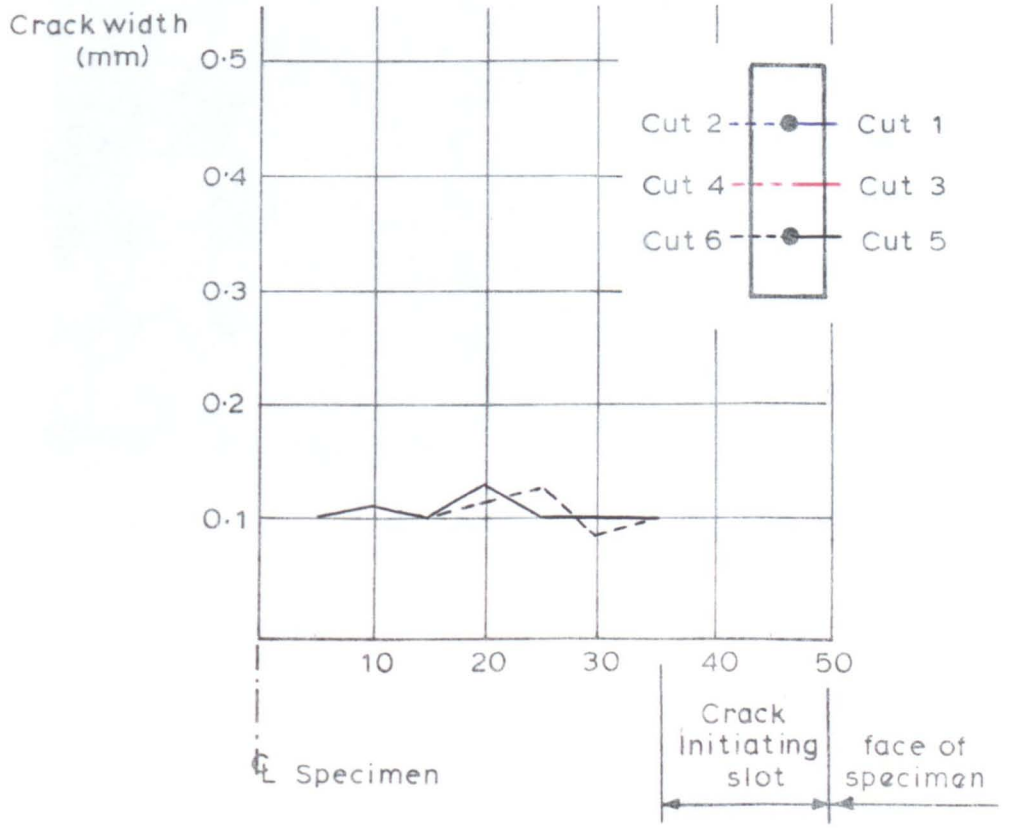

FIGURE 5.22. INTERNAL CRACK WIDTH MEASUREMENTS FOR SPECIMEN 6D

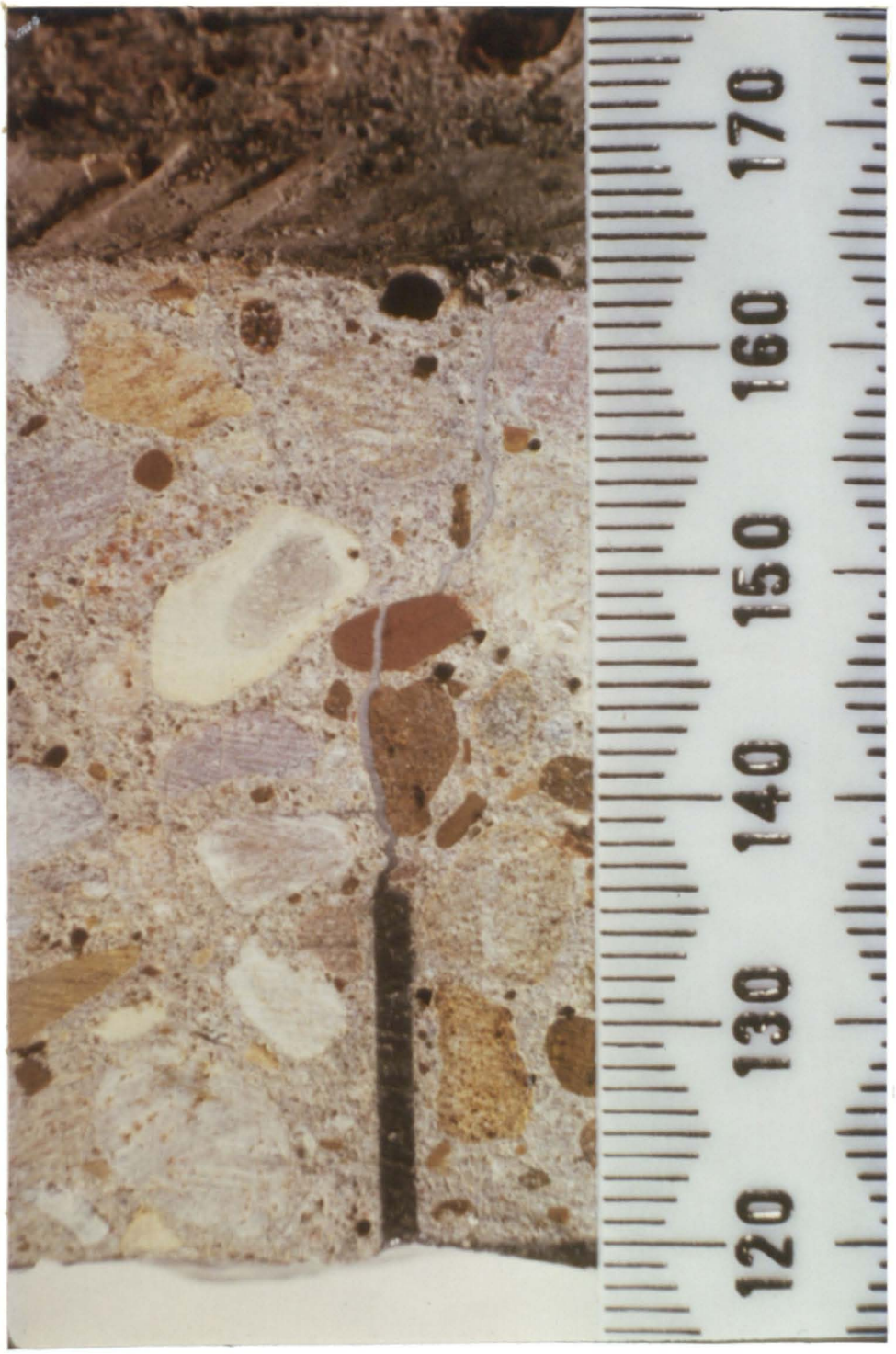

FIGURE 5.23. SPECIMEN 6A - INTERNAL CRACK, SURFACE WIDTH = 0·5mm.

FIGURE 5.24. SPECIMEN 6B - INTERNAL CRACK, SURFACE WIDTH = 0·5mm.

FIGURE 5.25. SPECIMEN 6C - INTERNAL CRACK, SURFACE WIDTH = 0·25mm.

FIGURE 5.26. SPECIMEN 6D - INTERNAL CRACK, SURFACE WIDTH = 0·125mm.

FIGURE 5.27. IMPRINT IN CONCRETE LEFT BY REINFORCING BAR IN TEST 5L.

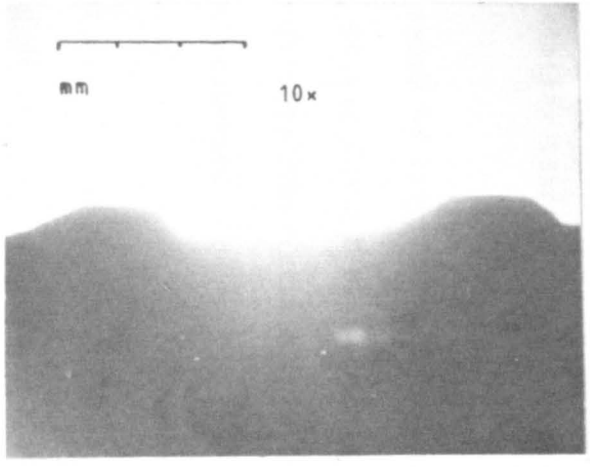

a) Outline of ribs Unisteel 410.

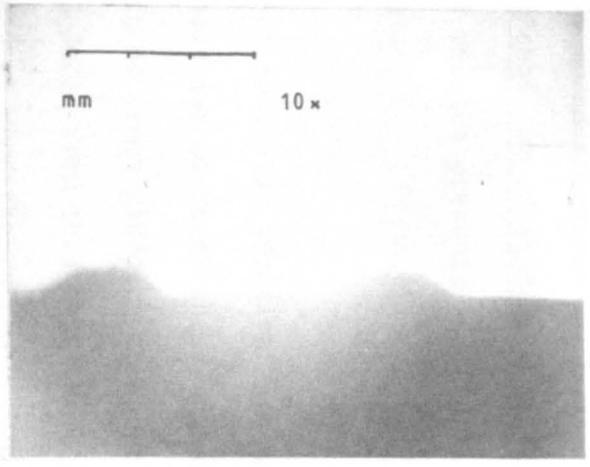

Torbar.

b) Projection of ribs onto axis of bar.

SCALE 10 x

FIGURE 5.28. GEOMETRY OF REINFORCEMENT RIBS.

CHAPTER SIX

DISCUSSION OF TEST RESULTS

6.1 Aggregate interlock

6.1.1 Behaviour of aggregate interlock specimens

From the results presented in Chapter 3 the following trends were observed:-

Testing of nominally identical specimens resulted in similar shear stiffnesses and ultimate shear strengths (Figures 3.12 and 3.17). The ratio of crack widening to shear slip did not vary significantly. It was deduced from this that the aggregate interlock mechanism is not dependent upon the random path of propagation of a tensile crack. The different contact angle, contact area and protrusion height for each aggregate particle crossing the crack plane must "average out" to give an overall property of the crack face which does not vary between similar tests.

For the range of initial crack widths investigated, i.e. 0.063 mm to 0.75 mm, it was found that the shear stiffness across the crack and the ultimate shear stress both decreased as the initial crack width was increased.

In almost all the tests the shear stiffness was greatest at the beginning of the test and diminished as the shear loading was increased.

In all aggregate interlock tests there was an increase in the crack width as shear slip occurred, regardless of the initial crack width. For shear slips of less than 0.25 mm, the ratio of crack widening to

shear slip decreased with increasing initial crack width. However for shear slips in excess of 0.25 mm, the ratio of crack widening to shear slip was independent of the initial crack width. (Figures 3.13b, 3.19b, 3.20b).

An increase in the axial stiffness restraining the crack from widening resulted in a reduction in the ratio of crack widening to shear slip. It also resulted in a higher shear stiffness and ultimate shear stress (Figures 3.14, 3.15, 3.18). These trends were independent of the initial crack width.

For the range of concrete cube strengths 30 N/mm^2 to 50 N/mm^2, the concrete strength had only a marginal effect upon the shear stiffness and the ultimate shear stress of the specimens and upon the ratio of crack widening to shear slip (Figure 3.16). However the effect of the different concrete strengths may have been masked to some extent by the difference in the axial stiffnesses of the specimens.

6.1.2 Comparison of aggregate interlock test results with previous research and theory

One of the advantages of using a system of direct tensile loading is that the initial crack width and internal forces at the beginning of a shear test can be carefully controlled.

The method of crack initiation often used in other research (42, 57) was to apply an indirect tensile splitting load to the centre of the specimen (Figure 6.1a). This load was then incrementally increased and released until the crack remained open at the required width (Figure 6.1b). At this point there are two possible explanations as

to why the crack remained open when tensile load was removed. There may have been a small misalignment of the crack faces or a dislodgement of an aggregate particle, resulting in a lack of fit when the faces are brought back together. This will cause a tensile force in the reinforcement and a compressive force in the concrete, the magnitude of which will be determined by the amount of reinforcement crossing the crack and the anchorage properties of the reinforcement (Figure 6.1c). Alternatively, in the reinforced concrete specimens there may have been some plastic strain in the reinforcement resulting in a residual non-zero crack width.

The results of the aggregate interlock tests showed that the shear stiffness was greater when compressive forces normal to the plane of cracking were present. If such compressive forces of unknown magnitude are present at the beginning of shear testing, due to the method of obtaining the initial crack, the results are bound to be difficult to interpret or to correlate with theoretical models. Hence care must be taken when comparing apparently similar tests that the initial conditions really are the same.

6.1.2.1 Local/global roughness theory

A model proposed by Laible et al (53) and discussed in Chapter 2 can be summarised as follows:-

For specimens with initial cracks less than 0.25 mm wide the aggregate interlock mechanism is said to be principally one of bearing and crushing of the crack faces against each other. From this it was deduced that there would be little tendency for the crack to widen. Consequently, the shear stiffness across the crack was predicted to be sensitive to changes in the initial crack width (i.e. the contact area) but insensitive to changes in the axial

stiffness normal to the plane of cracking.

For specimens with an initial crack width greater than 0.25 mm the aggregate interlock mechanism is said to be a sliding action of the crack faces over each other. From this it was deduced that the crack would widen as the protruding aggregate particles were forced to override each other. Consequently, a change in the axial stiffness of the specimen normal to the plane of cracking would be expected to affect the shear stiffness. It was also deduced that as the resistance to shear is provided by friction, which is independent of the contact area, the shear stiffness would not be sensitive to changes in the initial crack width.

The aggregate interlock test results described in Chapter 3 do not support this theory of local/global roughness. There is little evidence of any major difference in behaviour between specimens with initial crack widths greater or less than 0.25 mm which would suggest that a different type of action was occurring.

The crack width tended to increase during shear testing regardless of the initial crack width (Figures 3.13, 3.19, 3.20). In fact during the early part of the tests there is a greater tendency for the crack to widen for specimens with smaller initial crack widths, not less as suggested in reference 53.

The shear stiffness of specimens with small initial crack widths was found to be sensitive to changes in the axial stiffness normal to the plane of cracking (Figure 3.14). Specimen 1G has a higher axial stiffness (Figure 3.14c) and this results in a higher shear stiffness (Figure 3.14a) than with specimen 1F. From these results it was

deduced that shear resistance, for specimens with initial crack widths of less than 0.25 mm, is not provided solely by a bearing/crushing action.

Similarly, for specimens with an initial crack width greater than 0.25 mm, the shear stiffness is still sensitive to changes in the initial crack width (Figure 3.20). The specimens 2G and 2E in Figure 3.20c both have similar axial stiffnesses and have initial crack widths of 0.5 and 0.75 mm respectively. However a lower shear stiffness was obtained from specimen 2E than from specimen 2G (Figure 3.20a). Laible argued that when the mechanism for aggregate interlock was frictional, the shear stiffness should be independent of the initial crack width.

However, these results do not necessarily imply that the mechanism is not a frictional one. The shear stiffness would only be independent of the initial crack width if the mean angle of contact between the crack faces did not vary. If the particles protruding from each crack face are rounded it is clear that the average contact angle must decrease as the crack width increases. This could explain the reduction in shear stiffness and also the lower ratio of crack widening to shear slip for those specimens with larger initial crack widths. A more sophisticated friction model than that proposed by Laible (53) is required to predict the aggregate interlock mechanism.

It is possible that some of the differences between the test results reported in reference 53 and those presented in Chapter 3 were caused by using different methods to obtain the initial crack width. It is not clear whether external compressive forces subsequent to

tensile cracking were required in reference 53 to obtain the small initial crack widths. Nor is it clear how the larger crack widths were maintained before the commencement of shear testing.

It is the opinion of the writer that both crushing and sliding occur during aggregate interlock throughout the range of crack widths examined. It seems unlikely that any crushing of the concrete would be limited to the specimens with small crack widths. With a larger crack width the effective area of contact is reduced and hence the bearing compressive stresses are greater. It is necessary therefore to find a model which will simulate the aggregate interlock action and include all the parameters discussed.

6.1.2.2 Aggregate interlock tests at constant crack width

In the investigations of aggregate interlock where widening of the crack during shear testing is prevented by applying an external restraint (10, 49, 50), it is expected that the applied shear forces will be resisted mainly by a bearing action and crushing of the concrete rather than by a frictional sliding action. The results from these studies were consistent with this theory. In all the tests an increase in the permitted separation of the crack faces resulted in a reduced shear stiffness. Likewise, in all the tests, an increase of the strength of the concrete resulted in a greater shear stiffness.

It was seen in Chapter 2 that the results of Houde's (10) tests correlated quite closely to those of Paulay and Loeber (50). In Figure 6.2a the results of test 2C, where the crack width was held constant, are compared with the results of similar tests by both Houde and Paulay and Loeber. The shear stiffness obtained from

test 2C was similar to that found by Houde but rather less than observed by Paulay and Loeber. It is possible that this lower result was due to the testing procedure adopted by Houde and also by the writer. In these tests the crack was permitted to widen during each increment of shear loading. At the end of the increment of shear loading the crack was restored to its initial width by applying a compressive force normal to the plane of cracking. In Paulay and Loeber's test the crack was continuously restrained from widening during shear loading. From the difference in these results it can be inferred that the crushing aggregate interlock mechanism is a history dependent one. Hence it would be inconsistent to compare the results of these tests where the crack width is totally restrained from widening with the results of other tests where there is only a partial restraint.

In Figure 6.2b the applied stress, σ_c, normal to the plane of cracking which is required to maintain a constant crack width C_w is plotted against the applied shear stress τ. This curve shows the tendency for overriding of the crack faces to occur. The results of test 2C lie within the region found for most of the tests from reference 50, but at high levels of shear stress a lower direct compressive stress is required in test 2C. From just a single test result it is not possible to determine whether this is due to differences in the strengths of the cement matrix and aggregate used or to experimental scatter.

It could be deduced from Figure 6.2b that there is an effective coefficient of friction, μ, between 1.0 and 2.0, but this seems an inappropriate concept to apply when the crack width is restrained from widening.

6.1.2.3 Shear friction model for predicting the ultimate shear stress

Mattock (57) used the shear friction analogy to predict the ultimate shear stress of cracked reinforced concrete specimens. It was found that the ultimate shear stress, τ_{ult} resisted by a cracked specimen was proportional to the maximum compressive stress attainable normal to the plane of cracking. Hence for specimens with reinforcement normal to the plane of cracking,

$$\tau_{ult} = \rho f_y \tan \phi \qquad (6.1)$$

where ρ = the reinforcement ratio

f_y = the yield stress of the reinforcement

$\tan \phi$ = the apparent coefficient of friction

It was noted in reference 57 that the value of τ_{ult} was given by equation 6.1 only if $\rho f_y < 4.0$ N/mm^2. The ultimate shear stress was also observed to be independent of the concrete strength and failure occurred by sliding of the crack faces over each other.

However, if $\rho f_y > 4.0$ N/mm^2, equation 6.1 no longer predicted τ_{ult} and a change in the concrete strength did influence τ_{ult}. In this case failure occurred by crushing of the concrete, 'locking up' of the crack, and finally the formation of additional shear cracks at 45° to the original crack. Hence if the shear friction model is to be used to predict τ_{ult} it must be restricted to the case where failure occurs through tensile yielding of the reinforcement.

In the aggregate interlock tests described in Chapter 3, ultimate

shear failure was not caused by yielding of the reinforcement nor by additional diagonal shear cracking of the specimens. The reinforcement normal to the plane of cracking was not bonded to the concrete and hence the axial strains measured were never high enough to cause yielding.

The axial tension in the reinforcement causes a compressive stress, σ_c, in the concrete normal to the plane of cracking. If this compressive stress at the onset of shear failure is plotted against the ultimate shear stress, τ_{ult}, a curve similar to that given by equation 6.1 can be fitted to the results (Figure 6.3). Some of the scatter may be due to the judgement required in determining exactly when the onset of shear failure had occurred.

However although these results appear to fit the shear friction model, in spite of the reinforcement not yielding, a closer inspection of the behaviour reveals that the simple shear friction model proposed in reference 57 is not valid for aggregate interlock tests. The shear friction equation 6.1 proposes a linear relationship between the ultimate shear stress and the direct compressive stress normal to the plane of cracking. This is not observed from the results of the aggregate interlock tests. After the onset of shear failure (Figure 3.13a) a further increment of shear slip results in an increase in the normal compressive stress σ_c (Figure 3.13c) without the corresponding increase in the shear stress τ_s, which would be predicted by equation 6.1.

Because the reinforcement does not yield in the aggregate interlock tests the shear friction model does not provide a way of determining the normal compressive stress at the onset of shear failure. Hence

the results shown in Figure 6.3 can only be obtained retrospectively. However if a relationship between the shear slip, the crack width and the normal compressive stress can be found, it may be more appropriate to use a shear friction model to predict the shear stiffness of aggregate interlock action rather than the ultimate shear stress.

6.1.2.4 Shear friction model to determine the shear stiffness

Birkeland and Birkeland (49) proposed the shear friction model or 'saw tooth' theory for the behaviour of precast concrete connections or of cracked monolithic reinforced concrete. The rough surface is modelled as a series of rigid frictionless ramps having a slope of $\tan^{-1} \phi$. A value of 60° for ϕ is required so that the model will fit experimental results for cracked reinforced concrete specimens. However it can be seen from the aggregate interlock test results (e.g. Figure 3.13b) that the ratio of crack widening to shear slip is closer to tan 30°. This model is also unrealistic because the sawtooth ramps are assumed to be frictionless. Mattock's (50) solution to this problem was to assume an initial cohesion between the crack faces and to reduce the contact angle (equation 2.24) to 39°.

It is more reasonable to assume that the saw teeth are not frictionless. Hence from vertical and horizontal equilibrium (Figure 6.4b),

$$V = P \frac{(\mu \cos\Theta + \sin\Theta)}{(\cos\Theta - \mu \sin\Theta)}$$

This can be simplified to

$$V = P \tan(\Theta + \phi) \quad .$$

where $\tan \phi = \mu$

Let K_n be the axial stiffness normal to the plane of cracking

i.e. $K_n = \frac{P}{C_w}$

$$P = K_n \Delta_s \tan \Theta$$

Hence the shear stiffness, K_s, is given by

$$K_s = \frac{V}{\Delta_s} = K_n \tan\Theta \tan(\Theta + \phi) \qquad (6.2)$$

The stiffness K_n is provided by the reinforcement crossing the crack and its value can be measured or estimated. A value of 0.8 for $\tan \phi$ was proposed by Kriz and Raths (67) on the basis of friction tests between precast concrete surfaces. However, it is difficult to assess Θ, the mean contact angle between the crack faces. It may vary between similar specimens with different initial crack widths. It may also vary as the crack width changes during the testing of a specimen (e.g. Figure 3.14b) clearly no single value for Θ is going to be valid for all combinations of crack width and shear slip. A model is needed in which Θ does not remain constant throughout the tests.

6.1.2.5 Shear friction with varying contact angle

A model which attempted to include the effects of a varying contact

angle was developed by Fardis and Buyuktozturk (54) and is reviewed in Chapter 2. This model assumes that shear resistance by aggregate interlock only occurs when the large aggregate particles protruding from each crack face make contact. It is assumed that these particles are perfectly rigid and hence only sliding and overriding of the crack faces occurs. The crack path is modelled as a series of parabolic curves of different pitch and amplitude (Figure 2.25).

It was then claimed that because the shape of any crack was entirely random it was not possible to evaluate the parabolic functions and hence determine the way in which the crack would act. This argument is not consistent with the results of repeat aggregate interlock tests in the present study. It was observed (Figure 3.17) that two cracked specimens with similar physical properties gave very similar responses to shear loading, even though the crack path must be quite different in each specimen.

It was then considered by the writer that if two specimens having different crack face shapes had the same overall shear stiffness and the same ratio of crack widening to shear slip, it might be possible to formulate an averaged crack shape which would produce this response. However, further inspection of the test results showed that this cannot be done. Specimens having the same initial crack width but different axial stiffnesses normal to the plane of cracking exhibit quite different ratios of crack widening to shear slip when a shear loading was applied (Figures 3.14 and 3.15). From this it was inferred that the original assumption, that the crack faces were perfectly rigid, could not be true. If it were true then any two specimens with the same initial crack width should show the same rate of increase of this crack width regardless of the restraint to

crack widening.

It is apparent from Figures 3.14 and 3.15 that a combination of crushing and overriding is taking place. The amount of overriding which occurs is dependent upon the initial crack width, the axial stiffness normal to the plane of cracking and the amount of shear slip which has occurred. A viable model for aggregate interlock must attempt to evaluate the degree of crushing and overriding of the crack faces which will occur and hence find the shear stiffness.

6.1.2.6 Two phase aggregate interlock model

A model was developed by Walraven (42), simultaneously with the writer's research, which considered concrete as a two phase material. The aggregate was modelled as a family of perfectly rigid spheres and the cement paste was assumed to be rigid plastic. The probability of finding an aggregate particle of a specific size and degree of embedment on the crack plane was then derived. Hence, for a given crack width and shear displacement, the normal and shear forces can be determined, as described in Chapter 2, from a study of the internal equilibrium.

The underlying assumption in this model is that, regardless of the size of the crack width or the degree of shear slip, two aggregate particles never come into contact. The interaction is entirely between the hard aggregate particles and the softer cement matrix. This assumption is directly opposed to that made by Fardis and Buyuktozturk (54) i.e. that the shear resistance was only developed when aggregate particles made contact and that the cement matrix played no part except to influence the coefficient of friction. It is probable that the actual behaviour lies somewhere between these

two extremes. The use of a rigid plastic stress strain relation for cement paste under high strains in reference 42 is also questionable.

In spite of these defects of the two phase model there are a number of clear benefits over the models previously discussed. The model is the first to be developed which will predict the ratio of crack widening to shear slip as a non-linear function, dependent upon the initial crack width and the axial stiffness normal to the plane of cracking. The shear stress can also be derived as a non-linear function of the shear slip, which is dependent upon the cement paste strength and the axial stiffness normal to the plane of cracking.

The theoretical model developed by Walraven leads to a number of complex expressions which are difficult to use. A simple linear expression was therefore derived which is given in equations 2.41 and 2.42. An example of this is plotted in Figure 2.30 for a particular concrete strength and maximum aggregate size.

When the results of the aggregate interlock tests were compared with the results predicted by equations 2.41 and 2.42 a reasonably good fit was observed. In Figure 6.5 the two phase model predicts quite closely the results of test 2C, where the crack width was maintained at a constant value. In Figures 6.6 to 6.8 the two phase model is compared with the results of the three nominally identical tests 1A(i), 1A(ii) and 1A(iii). When the diameter of the reinforcement was increased in test 1B the model still matches the results quite closely (Figure 6.9). These figures are quite typical of the fit provided by the two phase model for all the aggregate interlock test results.

One of the problems resulting from the use of the simplified equations 2.41 and 2.42 is that pairs of lines of constant crack width in Figure 2.30 do not intersect the origin. Consequently there is a region of "free slip" where no shear stress is developed and the crack does not widen. This is apparent in Figures 6.6a to 6.9a where it is seen that the predicted $\tau_s - \Delta_s$ curve does not intersect the origin. The initial crack widening is also predicted to be zero, which does not correspond with the test results.

A further discrepancy resulting from the use of the simplified equations 2.41 and 2.42 is that any pair of constant crack width lines do not intersect each other when they meet the x-axis (Figure 2.30). Hence for zero normal stress there is a shear slip and consequently a shear stress associated with any crack width. This contravenes the equilibrium equations originally derived and is a consequence of simplifying the originally derived curves (Figure 2.28) to straight lines (Figure 2.30).

It is probable that the strength of the cement paste associated with a particular concrete strength has been assumed too high to compensate for the "free slip" zone predicted by the model. If this were the case it would explain why in Figures 6.6 to 6.9 the slope of the $C_w - \Delta_s$ curve is always predicted to be higher than that found experimentally.

Some of these problems with the two phase model could be solved by using a more complex expression than equations 2.41 and 2.42, such as a bilinear equation. Other problems may only be solved by changing the basic model to include aggregate to aggregate contact. However, the model as it stands provides a reasonably close fit to

the aggregate interlock test results and hence it was decided not to spend further effort into refining it. Walraven (42) found that the basic model would not predict the results of reinforced concrete tests using embedded reinforcement. It was therefore decided to spend the remaining time concentrating upon dowel action and reinforced concrete behaviour.

6.2 Dowel action

6.2.1 Behaviour of dowel action specimens

From the results of the dowel action tests presented in Chapter 4 the following trends and observations can be observed:-

The tangential shear stiffness of each specimen reduces in magnitude as an increasing shear stress is applied. At the ultimate shear stress the tangential shear stiffness is zero (Figure 4.5),

The scatter between the results of similar tests was low (Figure 4.5),

A higher shear stiffness and ultimate shear stress was measured if the diameter of the reinforcement was increased (Figure 4.6),

The behaviour of dowel action specimens did not vary greatly if the concrete strength was altered,

A tensile axial stress in the reinforcement caused a reduction in the shear stiffness and in the ultimate shear stress obtained. A tensile axial stress also causes a tendency for the crack to widen as shear loading is applied (Figure 4.8).

As all the dowel action specimens were made with smooth preformed cracks, the crack widening during shear loading of 3D and 3E was unexpected. However, it was reasoned that the shear loading probably caused damage to the concrete around each reinforcing bar. This would reduce the effective anchorage of the bar and would explain why crack widening occurred even though there was no overriding of the crack faces. Alternatively this crack widening effect may be due to the increased spalling of concrete associated with tensile forces in the dowel bars (Figure 4.11).

6.2.2 Theoretical modelling of dowel action

6.2.2.1 Beam on elastic foundation theory

The beam supported on elastic foundation (b.e.f.) theory has been used by several research workers (38, 39, 40) as a model to describe the behaviour of dowel bars and is discussed in section 2.3.1. The model is compared here with the experimental results presented in Chapter 4 (Figure 6.25) by making the following assumptions:-

The reinforcing bar has been modelled as a beam of rectangular section with the same width and flexural stiffness as the original circular section.

Tensile adhesion between the bar and the concrete is ignored. The concrete sustaining compressive bearing stresses is assumed to support the bar uniformly across the width of the bar.

A typical value for the foundation modulus for medium strength (30 N/mm^2) concrete, G_f, was found by White and Gergely (48) to be 750 N/mm^3. This value has been used in the evaluation of the dowel action stiffness from equation 2.23.

For the high strength concrete used in test 3B it has been assumed that $G_f \propto \sqrt{f_{cu}}$.

It was found that the initial shear stiffness of the specimens with 12 mm and 16 mm reinforcement was quite closely predicted by the b.e.f. model (Figure 6.12), but that the shear stiffness of the specimen reinforced with 8 mm bars was much lower than predicted. This lower result was attributed to the effects of the soft protective covering over the surface strain gauges. This covering was not necessary on the larger diameter bars using strain gauges embedded within slots instead of being bonded to the surface of the reinforcement.

It is possible that a better fit to the initial stiffnesses of specimens 3D and 3E could be obtained by reducing the foundation modulus, G_f, to allow for the localised damage of the concrete resulting from axial tension in the reinforcement. However, there is insufficient information from only two tests to give a reasonable estimate of what reduction is necessary and whether it would be generally applicable.

6.2.2.2 Non-elastic dowel action

Figure 6.12 also shows that the shear stiffness from the test results diminishes for higher values of shear slip. This non-linear response may be attributed to one of two causes or to a combination of both.

1. The high localised bearing stresses predicted by the b.e.f. model can result in crushing or lateral splitting of the concrete beneath the bar.

2. The shear and flexural loading on the reinforcement can cause plastic strains in the reinforcement and hence a reduction of the dowel stiffness.

The strain gauges in the dowel bars did not indicate that yielding was occurring. However these were placed at the nominal point of contraflexure to measure axial strains. Furthermore any non-elastic behaviour of the concrete will tend to cause a redistribution of the bearing stresses so that if a plastic hinge forms its location will be remote from the crack (Figure 2.19).

Walraven (42) formulated a semi-empirical expression (equation 2.12) to predict the behaviour of dowel action specimens, as described in Chapter 2. This expression,

$$F_d = 10(C_w + 0.2)^{-1} \Delta_s^{0.36} \phi^{1.75} f_{cu}^{0.38}$$

is based upon a curve fit of the dowel action test results of Paulay et al (29) and White and Gergely (48) and assumes that both shear slip and axial tension in the reinforcement cause a reduction in the foundation modulus because of damage to the concrete. A comparison of the results of the dowel action tests described in Chapter 4 with the shear stress-shear slip response predicted by equation 2.12 is shown in Figure 6.10. The shear stress, τ_s has been obtained from the total dowel force, as described in section 4.4.2.

It can be seen that overall the prediction of the dowel force is rather low. It is not clear exactly why this is so but it is not surprising since the modifications to the beam on elastic foundations theory were empirically derived from just a few test results rather

than resulting from an understanding of the internal micro-mechanisms involved.

Rasmussen (47) suggested that the high bearing stresses in the concrete immediately adjacent to the crack face caused a compressive failure in the concrete and hence a redistribution of the bearing forces away from the crack face (Figure 2.19). Failure eventually occurred with the formation of a plastic hinge on each side of the crack. The plastic moment, M_p can be obtained from an analysis of the section, see Appendix 2, giving,

$$M_p = \frac{1}{6} f_{sy} \phi^3$$

where f_{sy} is the ultimate yield stress of the reinforcing bar and ϕ is the diameter of the bar.

A study of the internal equilibrium required to produce this moment gives the ultimate dowel force as

$$F_{du} = C \phi^2 f_{sy}^{\frac{1}{2}} f_{cu}^{\frac{1}{2}} \qquad (6.2)$$

where C is an experimentally derived constant found to be 1.30 in reference 47.

Dulacska (43) proposed a more complex expression for reinforcement inclined to the plane of cracking. However this simplifies to equation 6.2 when the reinforcement is normal to the plane of cracking. In this study C was found experimentally to be 1.16.

However in neither study was the effect of an axial stress in the

reinforcing bar upon its ultimate dowel force considered. From an analysis of the section (Appendix 2) it is found that an axial stress in the reinforcing bar of αf_{sy} results in a plastic moment capacity given by

$$M_p = \frac{1}{6} \phi^3 f_{sy}(1 - \alpha^2) \tag{6.3}$$

Substituting this into the internal equilibrium equations gives

$$F_{du} = C \phi^2 f_{cu}^{\frac{1}{2}} \{f_{sy}(1 - \alpha^2)\}^{\frac{1}{2}} \tag{6.4}$$

where C is the constant used in equation 6.2.

If the ultimate dowel force from each test result is compared with the value predicted by Eq. 6.4 it is seen (Fig. 6.11) that most of the test results are close to their predicted values. However more test results, particularly from combined axial tension and shear loading, are required to confirm the general validity of equation 6.4.

At this stage an exponential function was thought to be the most appropriate expression to describe the overall shear stiffness due to dowel action. The actual deterioration of the concrete beneath the reinforcement and the resulting redistribution of internal forces is too complex to permit a realistic analytical modelling without considerably more experimental data than is presently available.

Thus the dowel force is given by

$$F_d = F_{du}\left(1 - e^{-\frac{K_i \Delta_s}{F_{du}}}\right) \tag{6.5}$$

where F_{du} is the ultimate dowel force given by equation 6.4.

K_i is the initial dowel shear stiffness given by the b.e.f. model.

From equation 2.10

$$K_i = \frac{F_d}{\Delta_o} = C\ \phi^{1.75}\ G_f^{0.75}\ E_s^{0.25} \qquad (6.6)$$

where the constant, C is equal to 0.166 and is dimensionless.

Equation 6.5 provides a close fit to the test results (Figure 6.12).

6.3 Reinforced concrete

6.3.1 Behaviour of reinforced concrete specimens

From the results of the reinforced concrete tests described in Chapter 5 the following comments and observations can be made.

Although the shear stiffness and ultimate shear strength of the reinforced concrete specimens must include components due to aggregate interlock and dowel action, some important differences in behaviour were noted. These were attributed to the effects of local bond between the reinforcement and the concrete upon the axial stiffness of the specimens normal to the plane of cracking. The local bond caused higher reinforcement stresses and hence a greater axial stiffness restraining crack widening than was provided by an unbonded bar. In some cases this led to plasticity in the reinforcement and thus a non-linear axial stiffness normal to the plane of cracking was observed. However this non-linearity was also observed before yield of the reinforcement and was attributed to a breakdown

of the local bond between the concrete and the reinforcement as the axial stresses in the reinforcement increased.

From a comparison of Figures 3.13 and 5.9 it can be seen that the axial stiffness normal to the plane of cracking (i.e. the gradient of Figures 3.13 and 5.9c) is constant for aggregate interlock specimens but decreases with increasing crack width for reinforced concrete specimens. Hence the shear stiffness and the ultimate shear stress are more sensitive to changes in the initial crack width in the reinforced concrete tests than in the aggregate interlock tests (Figures 3.13a and 5.9a).

The local bond between the concrete and the reinforcement also influences the way in which changes in the reinforcement ratio affect the shear stiffness of the specimens. From Figure 5.13c it is seen that although specimens 5A and 5B were reinforced with Y16 and Y12 bars respectively, the initial axial stiffnesses normal to the plane of cracking are very similar because of the better anchorage properties of the smaller diameter bars. Only when the local bond starts to break down does specimen 5B have a significantly lower axial stiffness and hence a lower shear stiffness (Figure 5.13a). This influence of local bond on the axial stiffness clearly did not occur in the aggregate interlock tests, where the reinforcement was debonded. From Figure 3.12c and 3.13c it is seen that using larger diameter reinforcement increases the axial stiffness directly and causes a consequent increase in the shear stiffness.

A third effect of local bond in the reinforced concrete tests was to make the shear stiffness of the specimens more sensitive to changes in the concrete strength than were the aggregate interlock

specimens. From Figure 5.10c it is seen that the low compressive strength of specimen 5D caused a lower axial stiffness than that of specimen 5G. Consequently the shear stiffnesses of these two specimens were much closer than would otherwise have been expected. In the aggregate interlock tests the compressive strength of the concrete did not significantly affect the axial stiffness normal to the plane of cracking and hence had less influence upon the shear properties of the specimens.

The mechanism of local bond may also influence the shear behaviour of the reinforced concrete specimens in a way that depends upon the type of reinforcing bar used. Walraven (42) reported a greater ratio of crack widening to shear slip in reinforced concrete specimens than would have been expected from the results of the aggregate interlock tests. This was attributed to the effects of internal cracking at each reinforcement rib, caused by high local bond stresses. This internal cracking (Figure 2.8) was observed by Goto (22) using deformed reinforcement with the ribs normal to the axis of the bar.

Kanabar (68) repeated Goto's tests using Torbar and Unisteel 410 (Figure 5.1) reinforcement of the same type as used in this project. Unisteel 410 was the most similar available reinforcement to that used by Goto (22) and by Walraven (42). It was observed that internal cracks were not initiated from every reinforcement rib in the manner found in reference 22 using either type of reinforcement. Illston and Stevens (27) also could not repeat the findings of Goto (22). It is not yet clear why there was this difference in local bond behaviour but it is believed that the small angle measured between the face of each reinforcement rib and the axis of the

reinforcement on both types of bar (Figure 5.28) may have caused sliding of the concrete over the ribs instead of initiating internal cracks. The polished surface of the concrete in contact with each rib (Figure 5.27) on the compression face observed after testing provides support for this theory.

The absence of internal cracking in the reinforced concrete specimens could explain why the ratio of crack widening to shear slip was sometimes below the lower bound observed by Walraven (42) (Figure 5.17b). It can be seen here that there is little difference between the behaviour of specimen 5E, reinforced with Torbar, and that of specimen 5M, reinforced with smooth debonded reinforcement. The small differences observed can be attributed to the different axial stiffnesses of each specimen (Figure 5.17c).

More study of the nature and effects of local bond is required before the high ratio of crack widening to shear slip observed in specimen 5L, reinforced with Unibond 410, (Figure 5.16) can be explained. From Figure 5.16b it is seen that although the axial stiffness of the reinforcement in test 5L was greater than that used in test 5E, the ratio of crack widening to shear slip was greater throughout the test. This is contrary to the trends followed by the other specimens. It would be expected that the higher axial stiffness of the reinforcement in test 5L would restrain the crack from widening at the same rate as in test 5E. Hence there would be more crushing of the crack faces in contact and less overriding. This was not observed.

It was then thought that the difference between the two results in Figure 5.16b might be attributed to the higher concrete strength

achieved in test 5L. This would provide a greater resistance to crushing and hence increase the degree of overriding of the crack faces. However, this hypothesis was not supported by the results of tests 5D and 5K (Figure 6.13). The cube strengths of these specimens range from 25.5 N/mm^2 to 45.4 N/mm^2. Although each specimen has different reinforcement, the effect of the different anchorage properties has resulted in a very similar overall axial stiffness of the reinforcement up to a crack width of 0.4 mm (Figure 6.13c). It is therefore seen from Figure 6.13b that the different concrete strengths do not result in a significant difference in the ratio of crack widening to shear slip. The differences in shear stiffnesses, Figure 6.13a, are probably attributable to the different dowel action stiffnesses.

It is possible that the difference in behaviour between specimens 5L and 5E was due to the effects of different internal cracking produced by the respective rib patterns on the reinforcement, but no evidence of such cracking was found.

6.3.2 Comparison of reinforced concrete test results with aggregate interlock and dowel action test results

In endeavouring to assess the relative components of aggregate interlock and dowel action in the behaviour of a reinforced concrete specimen it is necessary to consider several points:-

In a reinforced concrete specimen there is always crack widening associated with shear slip. This causes axial tension in the reinforcement which will reduce the dowel action shear stiffness.

It has been shown that the axial stiffness of a reinforced

concrete specimen normal to the crack plane is not the same as that of an aggregate interlock specimen with the same reinforcement because of the effects of local bond. Furthermore this stiffness is non-linear in a reinforced concrete specimen. It is therefore necessary to compare specimens having the same axial stiffness, not the same reinforcement ratio, in order to determine the shear stiffness due to aggregate interlock in a reinforced concrete specimen.

When assessing the contribution of aggregate interlock to the shear stiffness of reinforced concrete, it is essential that both specimens have the same crack width profile or if the crack width profiles differ, that this is taken into account. It was seen in section 5.4.6 that the cracks in the reinforced concrete specimens tested in this investigation had a uniform width beneath the surface of the concrete. As there is no local bond in the aggregate interlock tests the cracks in these specimens will also have a uniform width.

The existence of a uniform crack width in a tensile reinforced concrete specimen is not consistent with the findings of Goto (22), Illston and Stevens (27) or Broms (26). However none of these research workers used Torbar or a similar reinforcement with helical ribbing (Figure 5.1).

Goto (22) used an ink injection method to examine internal cracks and hence could not measure the crack width directly. A crack which diminished in width towards the reinforcement was therefore deduced by Goto from the pattern of internal cracking (Figure 2.8). This internal crack pattern was not observed in the present

investigation (Figures 5.23 - 5.26).

Broms (26) and Illston and Stevens (27) did not record what type of reinforcement was tested but it appears to be similar to Unisteel 410 (used in test 5L). Resin injection tests were not carried out using this type of reinforcement by the writer. However, Kanabar (68) did carry out similar tests to Goto (22) using Unisteel 410 and did not observe the type of cracking reported by Goto.

A recent paper by Skorobogatov and Edwards (69) compares the local bond behaviour of Unisteel 410 with the Swedish manufactured Wellbond. Both reinforcements have a similar rib pattern, but a different rib cross-section. The internal bond action was reported to be quite different. It is possible that the reinforcement used by Broms (26) and Illston and Stevens (27) was also acting in a different manner to the Torbar in this investigation which may explain the different crack width profile observed. It is also important to note that both Broms and Illston and Stevens required a high pressure to force the epoxy resin into their cracks in reinforced concrete. The resultant hydraulic force would also tend to widen the crack remote from the reinforcement and may explain the divergent results. If a low viscosity high capillary action resin is used as in this investigation the possibility of this effect does not arise.

It would appear that regardless of whether the local bond stresses cause internal cracking at each rib or crushing or sliding of the concrete against each rib, an adequate bond strength is obtained. Both Torbar and the reinforcement used by Goto (22) et al, with

ribbing normal to the axis of the bar, are widely used in reinforced concrete construction and satisfy the requirements of CP110 for enhanced bond reinforcement. Neither CP110 nor the continental requirements for minimum "related rib area" contain any specification for a minimum angle between the rib face and the axis of the reinforcing bar.

When the results of reinforced concrete tests and aggregate interlock tests, with similar axial stiffnesses normal to the plane of cracking, are compared (Figures 6.14 to 6.16) it is found that the shear stiffnesses and the ratios of crack widening to shear slip are also quite similar. All the curves have been plotted as broken lines when the normal stiffnesses in Figures 6.14c, 6.15c and 6.16c are no longer similar, due to break down of local bond in the reinforced concrete specimens. In Figures 6.14a, 6.15a and 6.16a the contribution of dowel action to the shear stiffness, predicted from equation 6.5, is also drawn.

From these figures it is deduced that, for the reinforcement ratios and diameters examined, the majority of the shear stiffness is provided by the aggregate interlock component. In Figures 6.14a and 6.15a, where the reinforcement in the reinforced concrete specimens has a diameter of 8 mm, equation 6.5 provides an overestimate of the dowel action shear stiffness because the softening effect of the protective rubber coating over the strain gauges has not been taken into account. This softening effect is clearly seen in Figure 6.12f where the shear stiffness of specimen 3F was half that predicted by equation 6.5.

It is less clear why in Figure 6.15a the sum of the dowel action

and aggregate interlock stiffnesses is greater than the stiffness of the reinforced concrete specimen. Equation 6.5 should give a realistic estimate of the dowel action stiffness because the strain gauges are embedded within the 12 mm reinforcing bars and hence should have little influence upon the dowel stiffness. It is seen from Figure 6.16b that the ratio of crack widening to shear slip is higher for the reinforced concrete specimen and hence from the model discussed in section 6.1.2.6 a lower aggregate interlock stiffness is predicted. However as both the reinforced concrete specimen and the aggregate interlock specimen had similar axial stiffnesses normal to the crack plane (Figure 6.16c), it is not clear why the ratios of crack widening to shear slip are not more similar.

From the comparisons of aggregate interlock and dowel action test results with those of the reinforced concrete tests there appears to be no obvious difference in the behaviour that cannot be attributed to the effects of local bond, as discussed. The ratio of crack widening to shear slip and the shear stiffness of a reinforced concrete specimen are similar to that which would have been expected from the dowel action and aggregate interlock test results. More aggregate interlock and reinforced concrete tests with the same axial stiffness normal to the crack plane are needed to confirm this hypothesis. However an initial verification can be made by attempting to predict the results of the reinforced concrete tests from the aggregate interlock equations 2.21 and 2.22 and the dowel action equations 6.4 and 6.5.

6.3.3 Prediction of the behaviour of reinforced concrete specimens

In Figures 6.17a to 6.17ℓ the aggregate interlock and dowel action components of the shear stiffness of each reinforced concrete specimen have been evaluated from equations 2.21, 2.22, 6.4 and 6.5. These components are then summed and compared with the reinforced concrete shear stiffness.

These equations can only be used with confidence if the axial force in the reinforcement is accurately known for any given crack width. This information was obtained from the experimental results. When one of the measured strains exceeded 0.00235 the material at this point was no longer elastic and the method described in section 5.3.2 was used to obtain an estimate of the axial tensile force. Once this had occurred the curves plotted in Figure 6.17 were depicted as broken lines to indicate that less confidence should be placed upon the accuracy.

In Figures 6.17c, 6.17f and 6.17i, where 8 mm reinforcement was used, the dowel action stiffness was over-estimated because of the softening effect of the protective covering to the strain gauges. All the dowel action curves have been evaluated using a constant value of 750 N/mm^3 for the foundation modulus, G_f, used to find the initial stiffness K_1 in equation 6.5.

It is seen that when the initial crack width is 0.25 mm or less the shear stiffness of the reinforced concrete specimens can be quite closely predicted (Figures 6.17a to 6.17f). However for specimens with an initial crack width of 0.5 mm (Figures 6.17g to 6.17i) an overestimate of the shear stiffness is obtained.

This overestimate is particularly noticeable for specimens 5H and 5I where the component of shear from aggregate interlock is calculated to be a greater value than the total shear in the reinforced concrete specimen. This error may come from using the linear equations 2.21 and 2.22 to determine the aggregate interlock stresses. These functions do not intersect the origin (Figure 2.30) and as a result an overestimate of the aggregate interlock component is obtained, particularly for specimens with a large initial crack width and a low axial stiffness normal to the plane of cracking.

In test 5J the 8 mm reinforcement was not fitted with strain gauges. The bondslip curve (Figure 2.9) derived from the work of Martin (24) was used to evaluate the axial stress. This resulted in a more rapid curtailment of the dowel action shear stiffness than in the other tests (Figure 6.17j). It was seen from the dowel action and reinforced concrete tests (Figure 4.9 and 5.7) that for a crack width greater than 0.5 mm the axial reinforcement stress was no longer predicted accurately by Martin's theory. More test results of axially loaded reinforced concrete specimens, with and without coincident shear loading, are needed before the entire range of Figure 2.9 may be used with confidence. However, using Figure 2.9 the predicted shear stiffness for the reinforced concrete specimen 5J was within 13% of the actual shear stiffness, for the whole range of shear slip examined.

Figure 6.17k shows that an overestimate of the shear stiffness is obtained for specimen 5K, reinforced with four 8 mm bars. The high value calculated for the aggregate interlock stiffness cannot yet be explained. However, the use of four closely spaced bars makes splitting of the concrete more probable. This, together with the

presence of a rubber coating over the strain gauges, may be the reason that the dowel action stiffness was lower than expected.

The shear stiffness of specimen 5L, reinforced with two 12 mm Unisteel 410 bars was predicted fairly closely (Figure 6.17ℓ) by the aggregate interlock and dowel action theory. This supports the belief that Torbar and Unisteel 410 both act in a similar manner because of the shape of the rib section and in spite of the different pattern of ribbing.

In Figure 6.18a to 6.18ℓ the crack widening to shear slip from the test results is compared with the behaviour predicted by equation 2.21. This is again plotted as a broken line when less confidence is held in the accuracy of the curve.

It can be seen that the predicted crack width to shear slip relationships follow the trends observed for aggregate interlock specimens. An initial shear slip with no crack widening is predicted, but not observed in the tests. This is again due to equation 2.21 not intersecting the origin. After this initial slip the ratio of crack widening to shear slip is usually a little higher than measured in the tests.

From all these results it was concluded that, for the range of specimens tested, there was no fundamental difference between the action of aggregate interlock in a specimen with embedded reinforcement to that in a specimen with sleeved reinforcement. The high ratio of crack widening to shear slip and the additional shear stiffness observed by Walraven (42) in reinforced concrete specimens when compared with aggregate interlock specimens (section 2.5.2.4) was not

observed in this investigation. It is believed that the "internal strut" effect may be peculiar to a reinforcement type not used in these tests. Although there is some unexplained scatter between the predicted behaviour of reinforced concrete specimens and the measured behaviour, the aggregate interlock and dowel action models discussed give a useful insight into the micro-mechanics of shear transfer in cracked reinforced concrete and provide a reasonable estimation of shear stiffness up to ultimate loading. The specimens whose behaviour was predicted with the least accuracy were those with an initial crack width greater than 0.25 mm, the maximum serviceability crack width permitted by B.S. 5400.

The shear behaviour of the reinforced concrete specimens has been predicted by using the experimentally measured relationship between the crack width and the axial reinforcement stress for each specimen. More research is needed on this relationship so that the axial reinforcement stress for any given crack width can be calculated without the need for internal strain gauges. Once this has been achieved the proposed equations can be used to predict the behaviour of a cracked reinforced concrete structure.

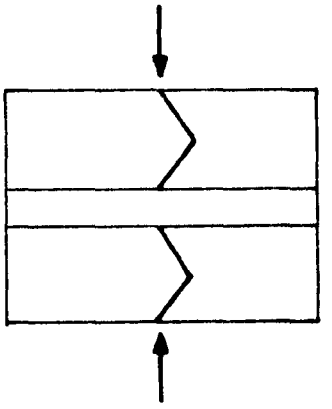

a) Lateral load causes splitting crack.

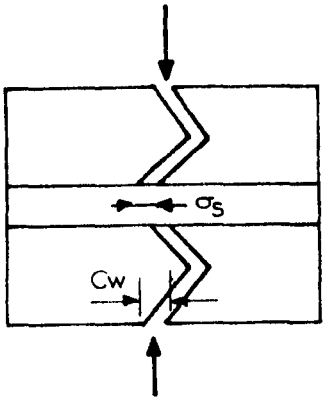

b) Increased lateral load causes opening of crack, Cw
⇒ tensile stress in steel, σ_s

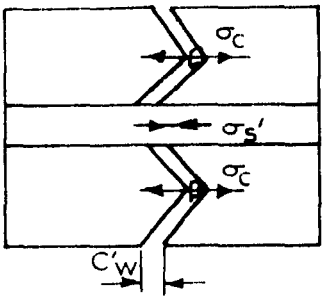

$$\int \sigma_c \, dA_c = - \int \sigma_s \, dA_s$$

$$C'_w < C_w$$

$$\sigma'_s < \sigma_s$$

c) Removal of lateral load, crack remains open because of lack of fit of crack faces ⇒ residual tension in steel σ_s' and compression in concrete.

FIGURE 6.1. SCHEMATIC DIAGRAM OF CRACK FORMATION USING INDIRECT TENSILE FORCES.

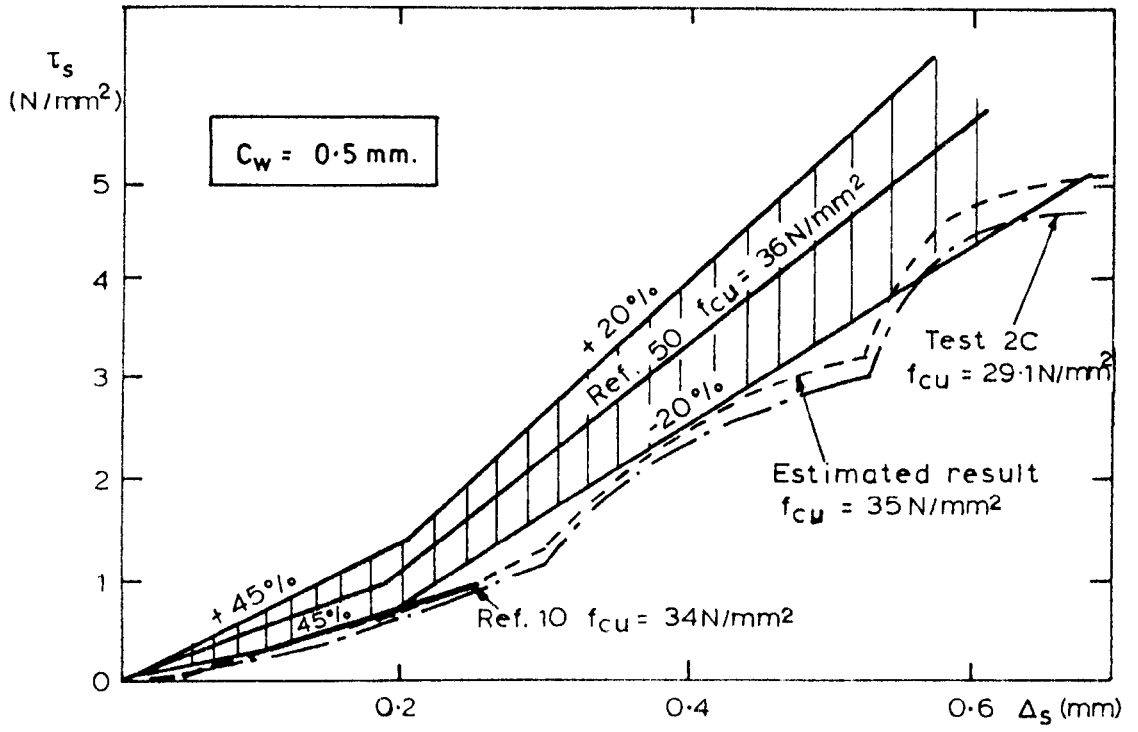

a) Comparison of shear stiffness of specimen 2C with similar shear tests.

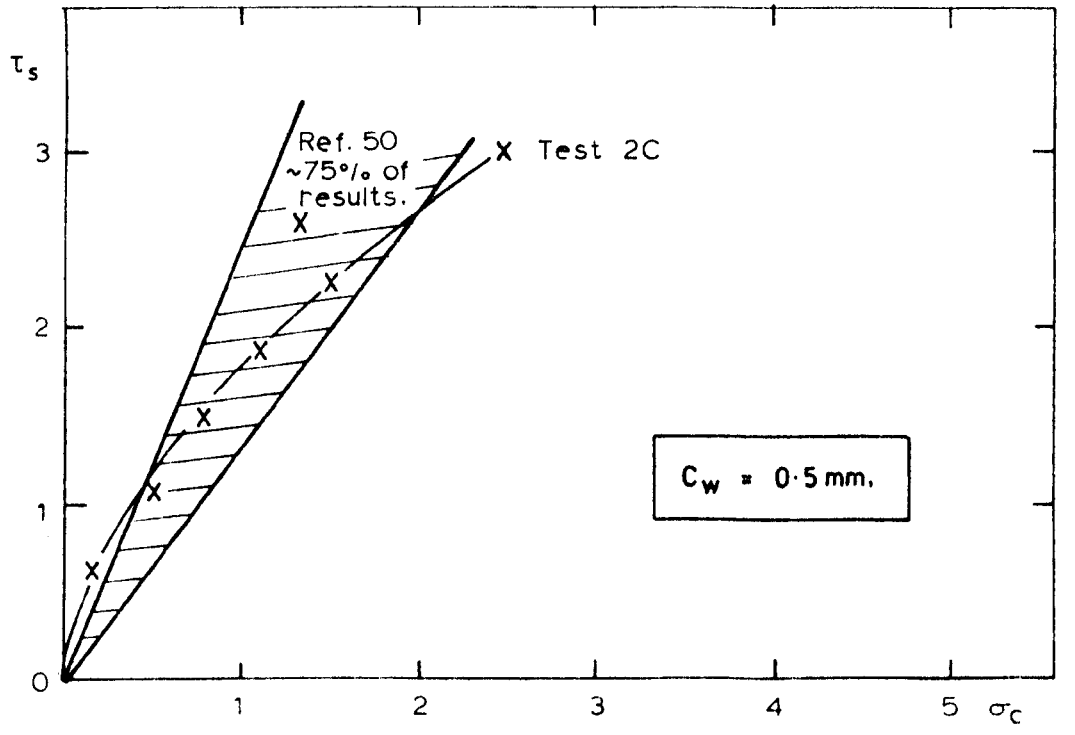

b) Normal stress σ_c, required to maintain crack width.

FIGURE 6.2. AGGREGATE INTERLOCK TEST RESULTS AT CONSTANT CRACK WIDTH.

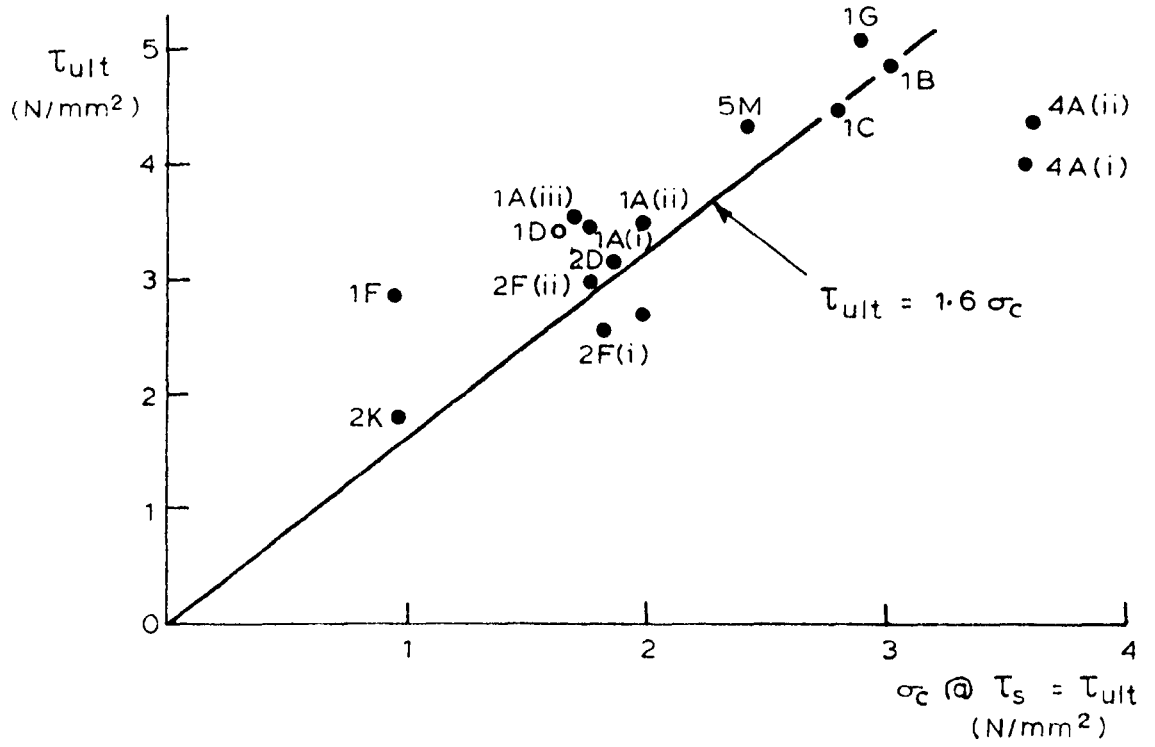

FIGURE 6.3. SHEAR FRICTION MODEL FOR AGGREGATE INTERLOCK ULTIMATE SHEAR STRESS

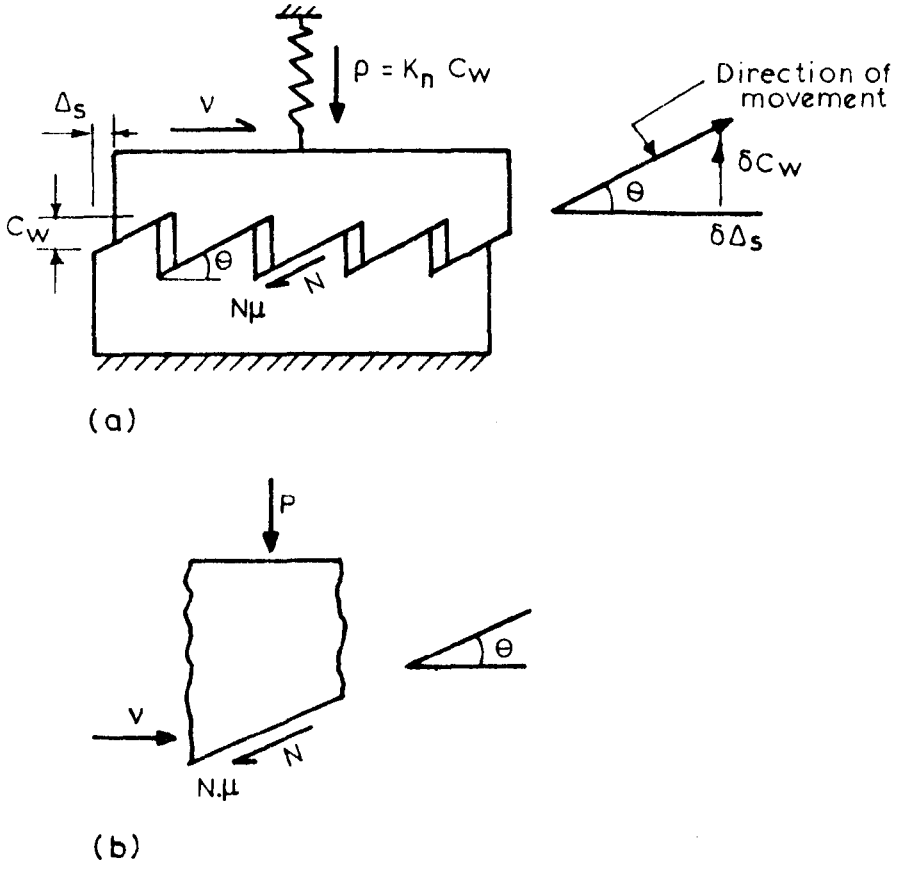

FIGURE 6.4. MODIFIED SAW TOOTH MODEL.

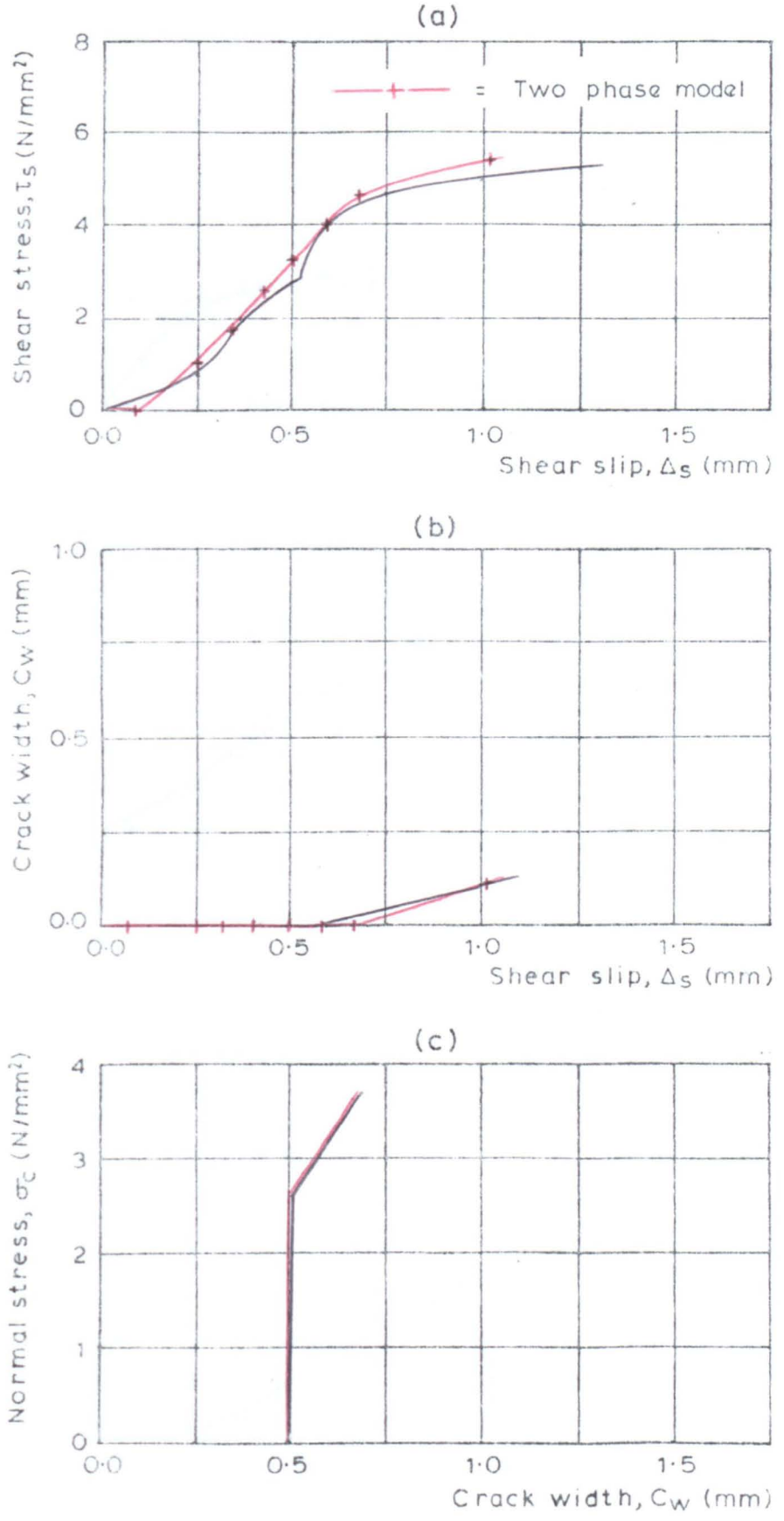

FIGURE 6.5 COMPARISON OF TWO PHASE AGGREGATE INTERLOCK MODEL WITH THE RESULTS OF TEST 2C.

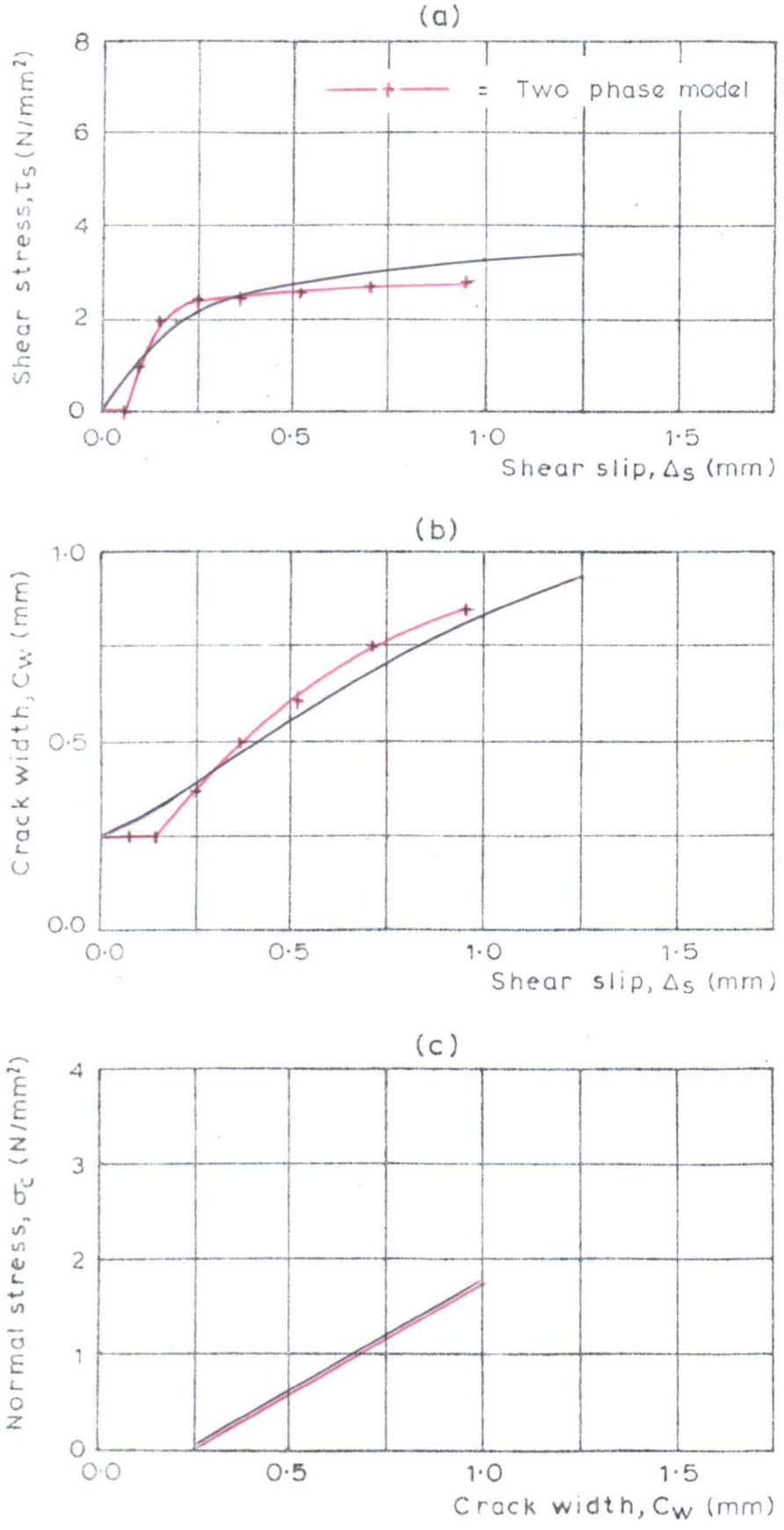

FIGURE 6.6 COMPARISON OF TWO PHASE AGGREGATE INTERLOCK MODEL WITH THE RESULTS OF TEST 1A(i)

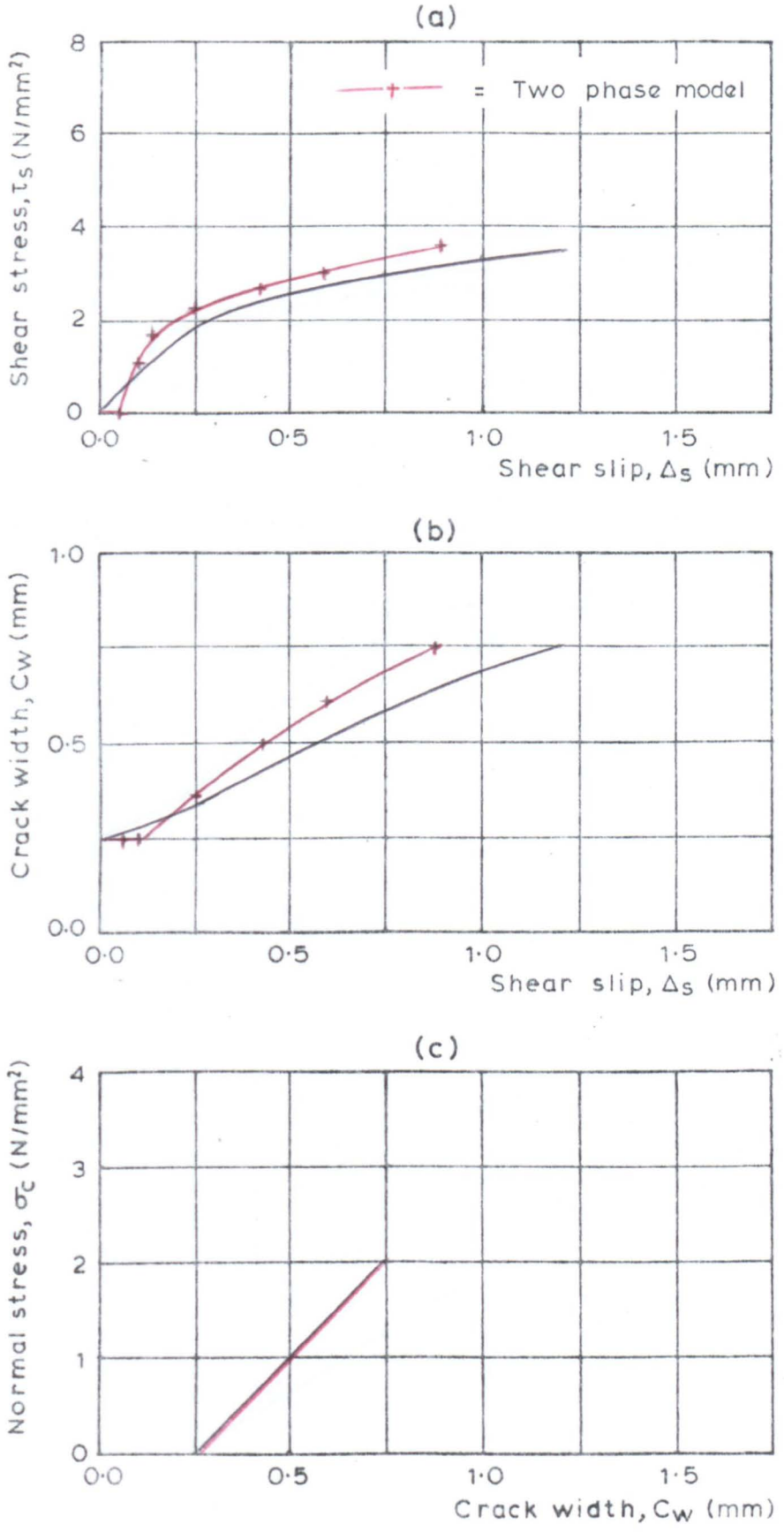

FIGURE 6.7 COMPARISON OF TWO PHASE AGGREGATE INTERLOCK MODEL WITH THE RESULTS OF TEST 1A(ii)

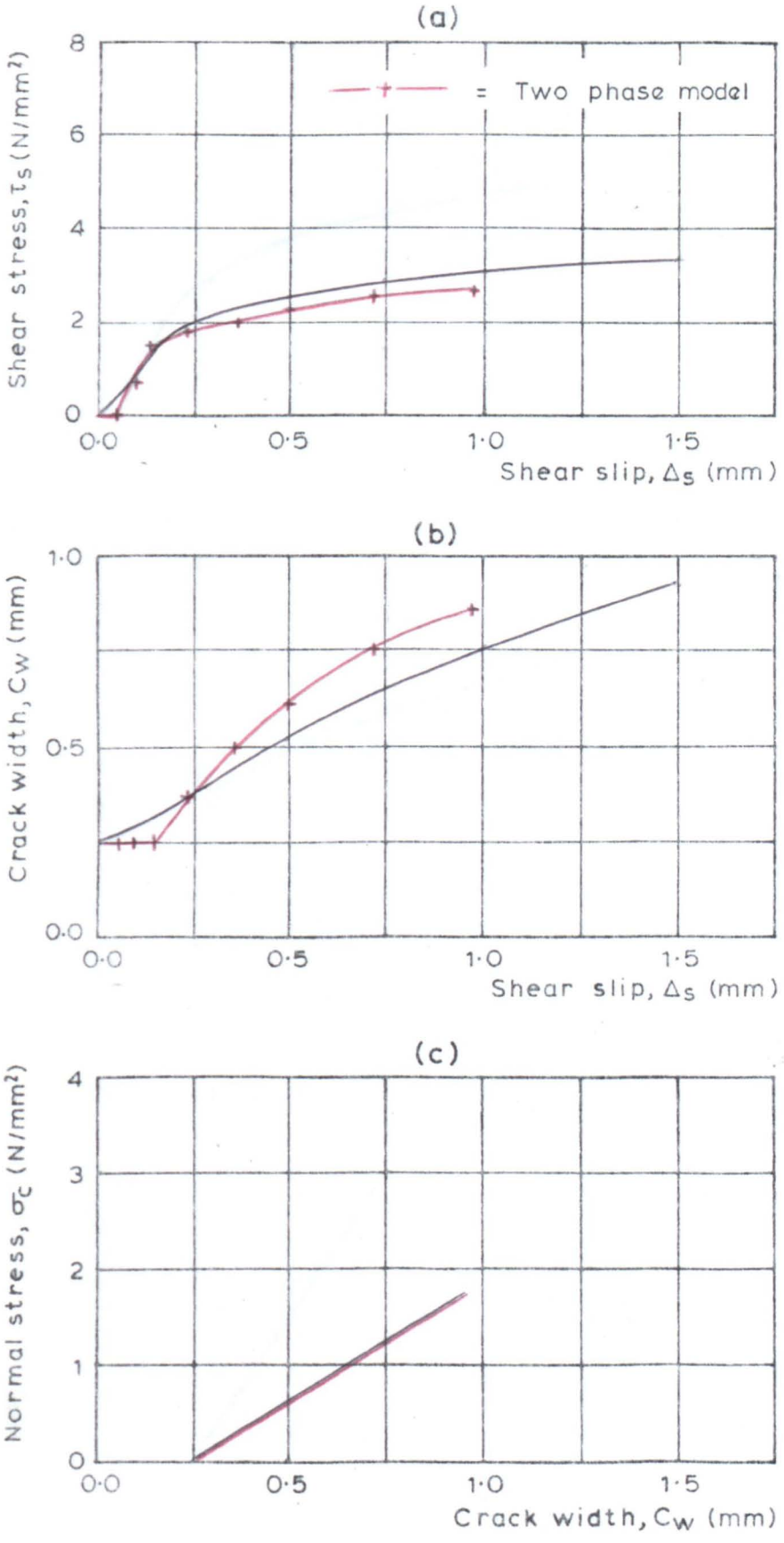

FIGURE 6.8. COMPARISON OF TWO PHASE AGGREGATE INTERLOCK MODEL WITH THE RESULTS OF TEST 1A(iii)

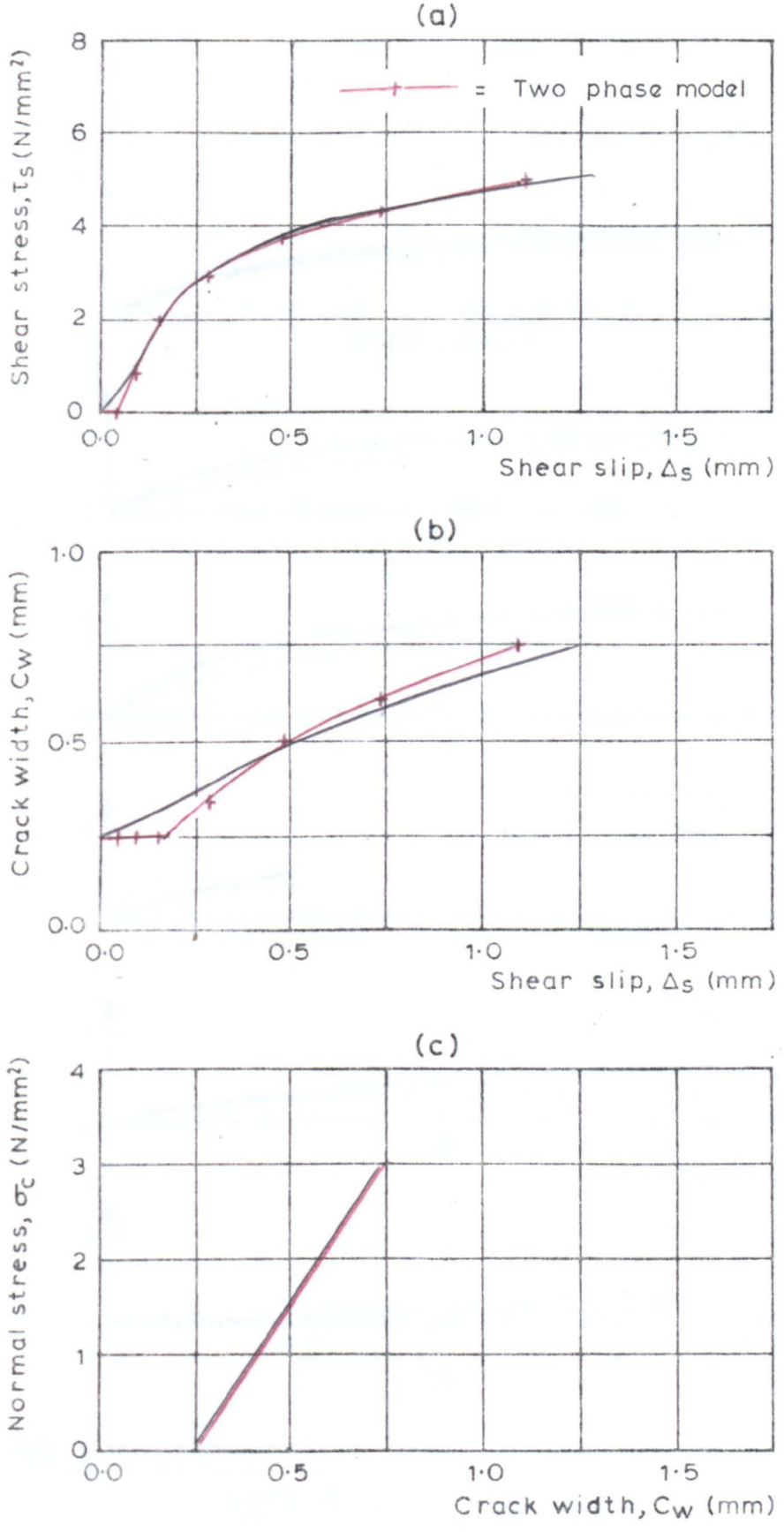

FIGURE 6.9. COMPARISON OF TWO PHASE AGGREGATE INTERLOCK MODEL WITH THE RESULTS OF TEST 1B.

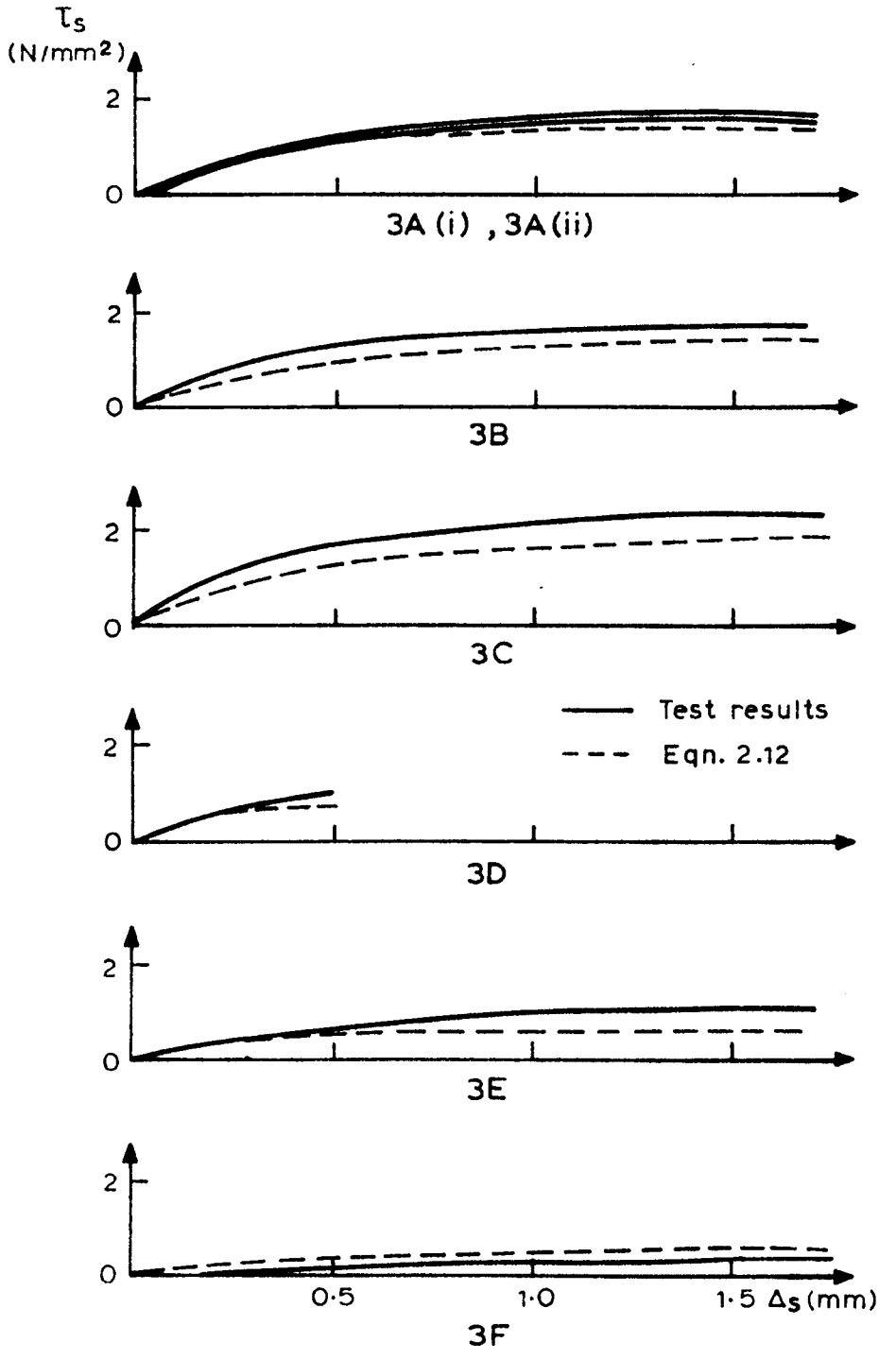

FIGURE 6.10. COMPARISON OF DOWEL ACTION TEST RESULTS WITH WITH RESULTS PREDICTED BY EQUATION 2·12.

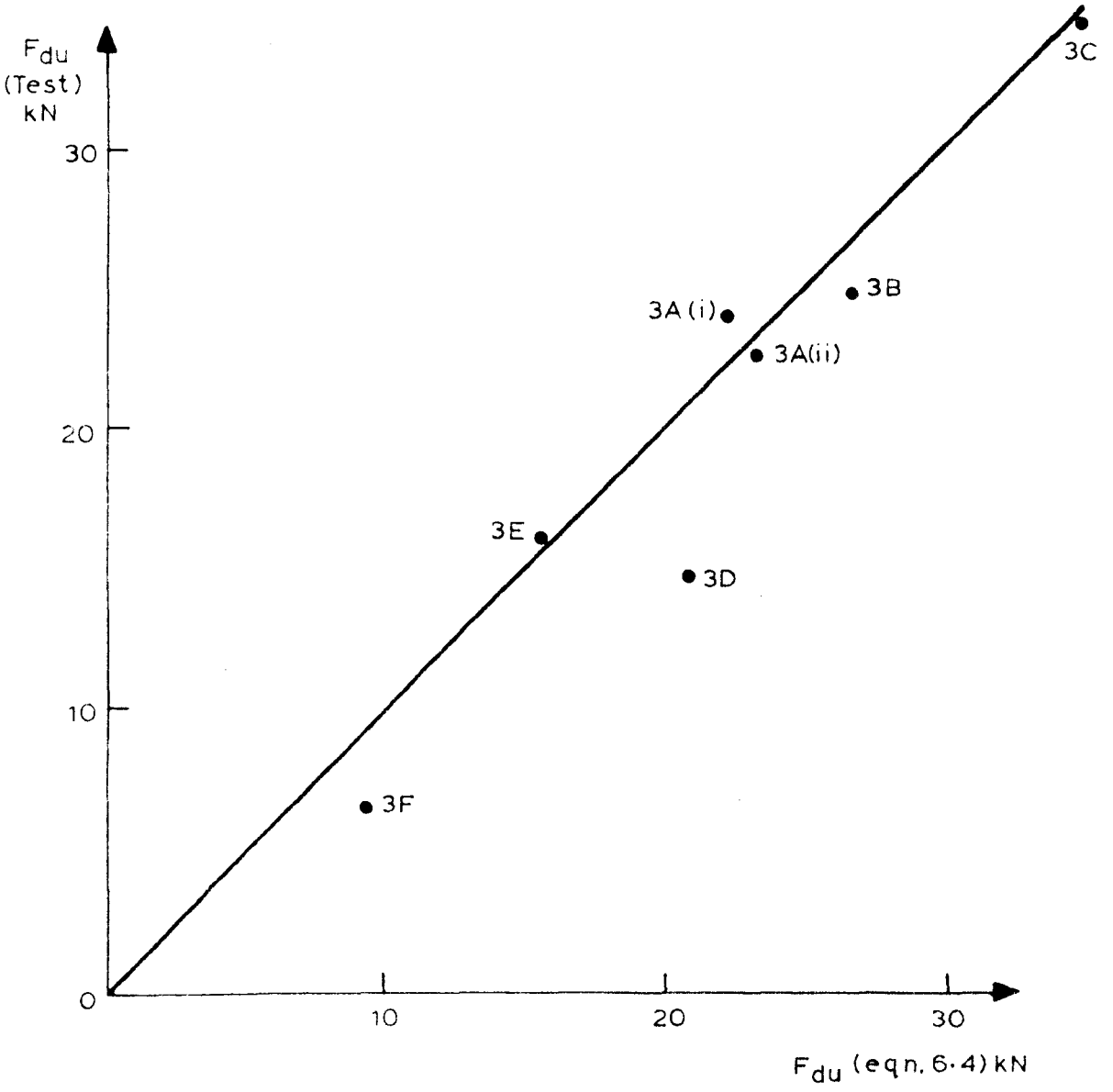

FIGURE 6.11. COMPARISON OF ULTIMATE DOWEL FORCE FROM TEST RESULTS WITH THAT PREDICTED BY EQUATION 6·4.

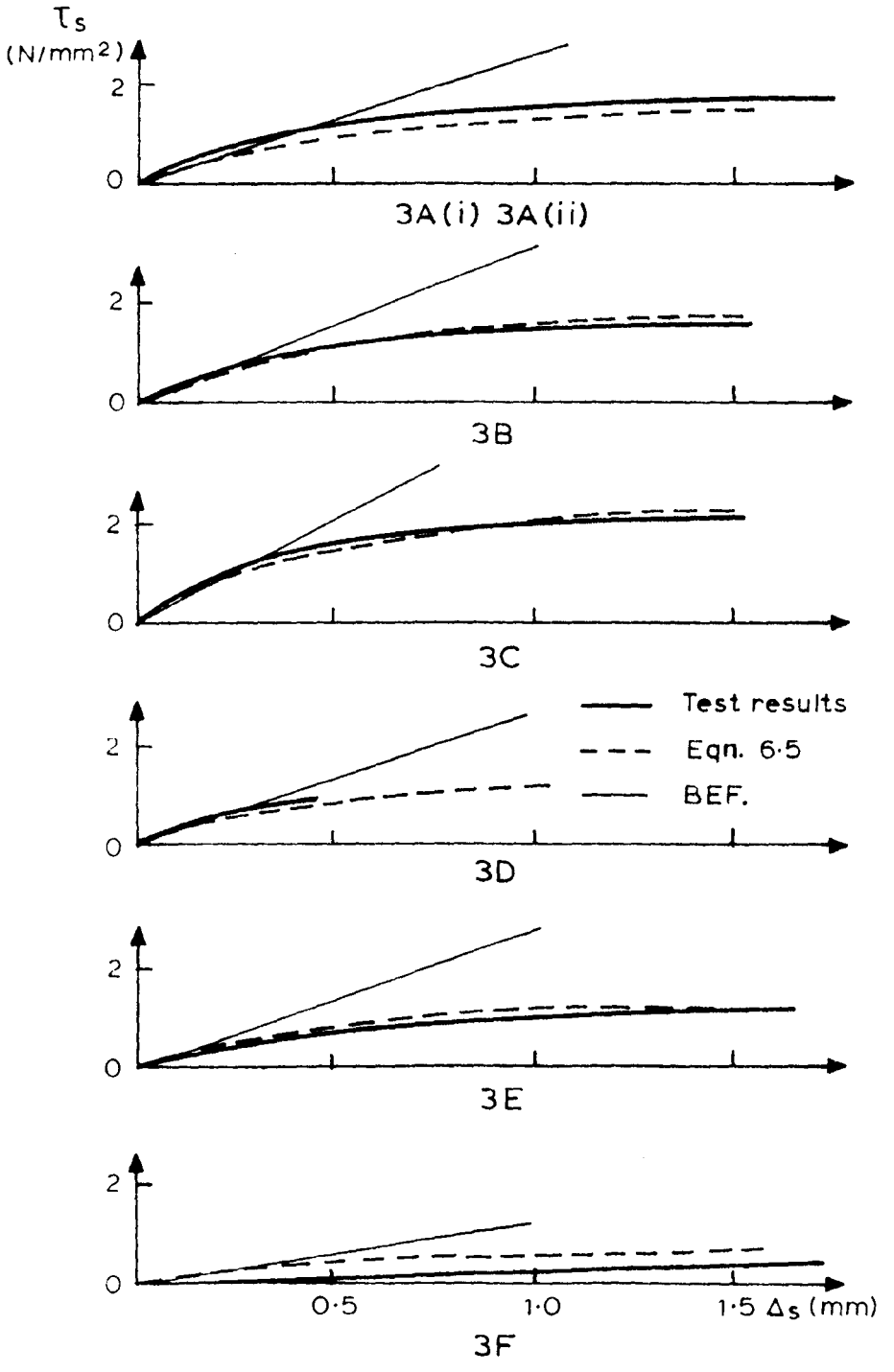

FIGURE 6.12. COMPARISON OF DOWEL ACTION SHEAR STRESS - SHEAR SLIP WITH BEF THEORY AND EQUATION 6.5

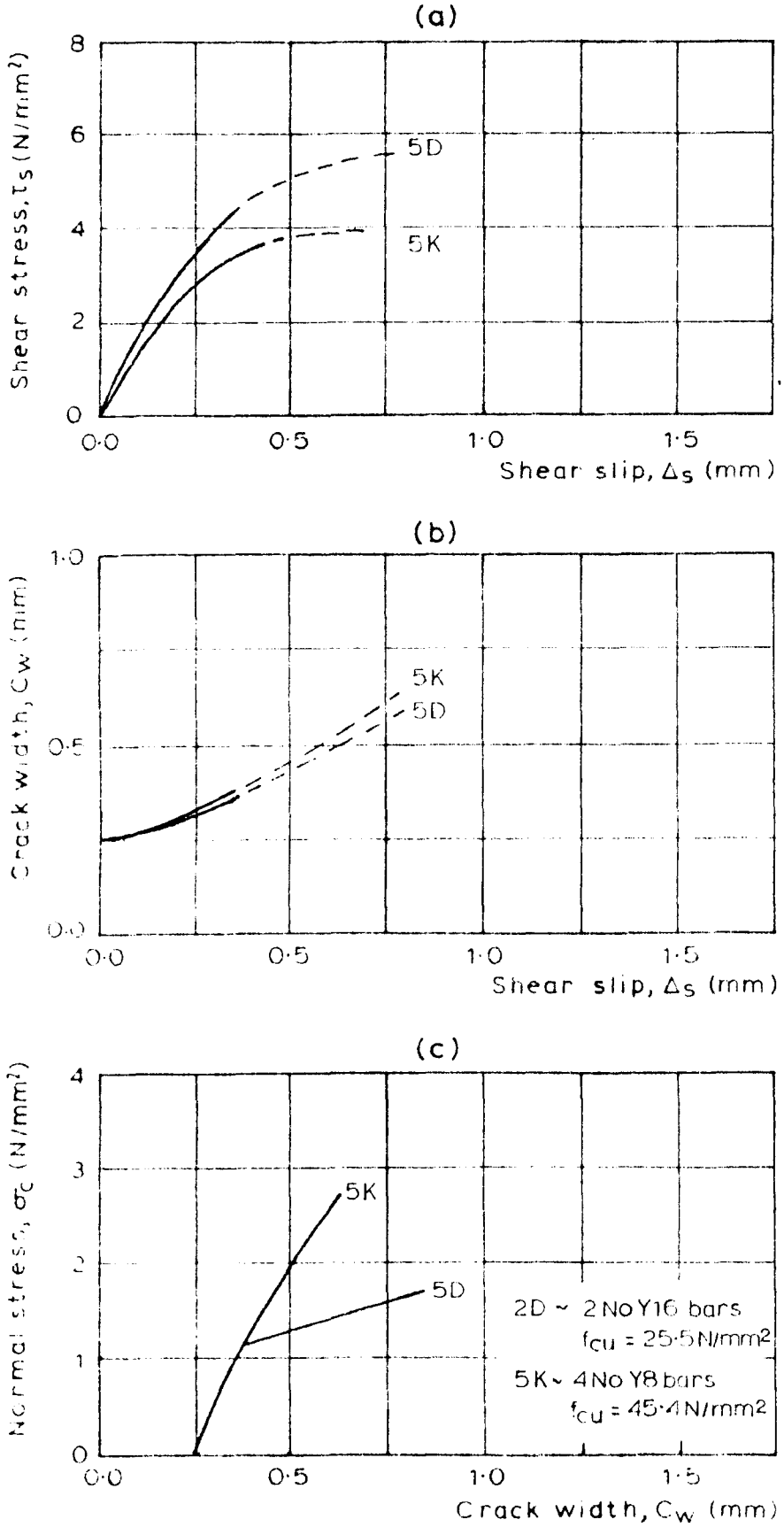

FIGURE 6.13. COMPARISON OF REINFORCED CONCRETE TEST RESULTS WITH THE SAME AXIAL STIFFNESS BUT DIFFERENT CONCRETE STRENGTHS

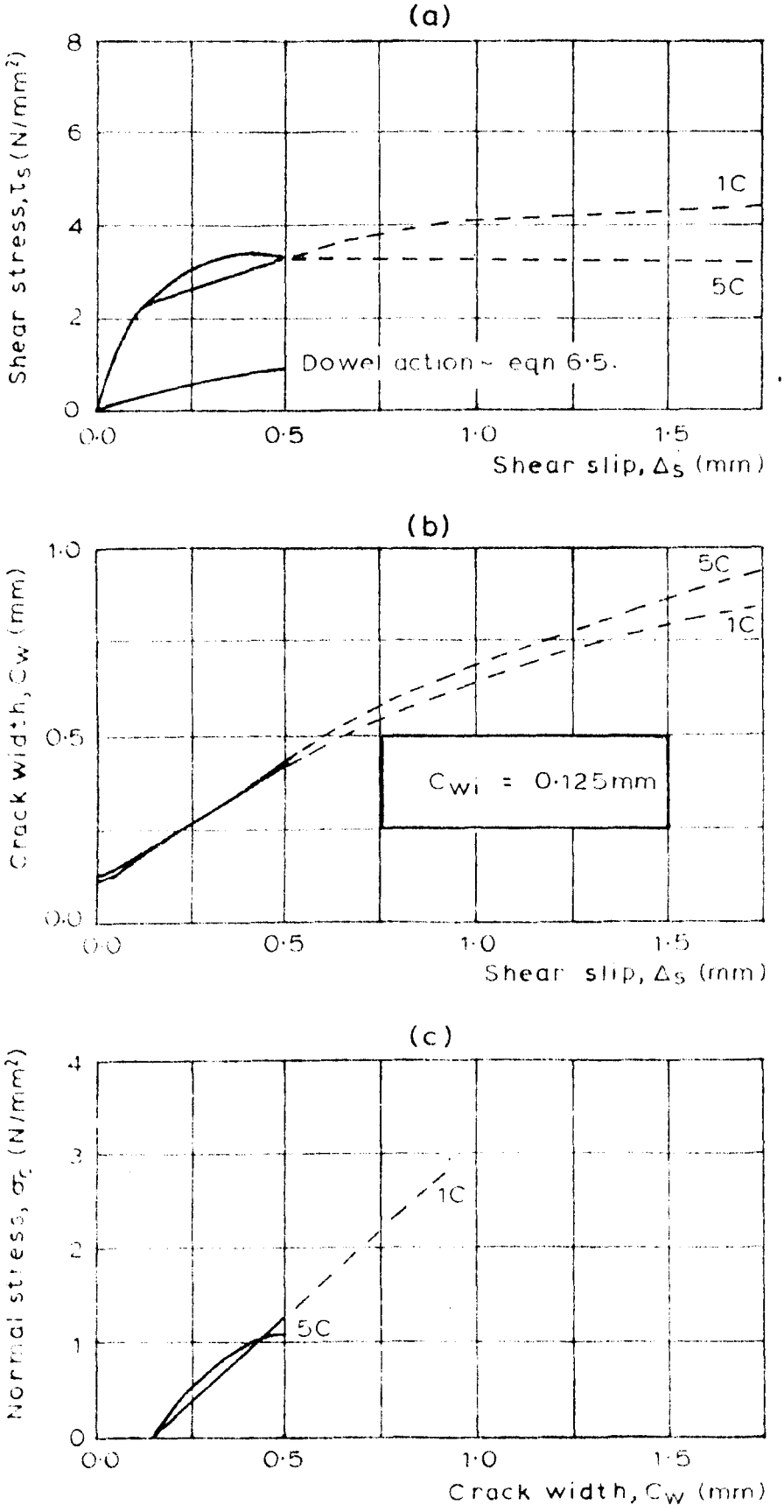

FIGURE 6.14. COMPARISON OF AGGREGATE INTERLOCK AND REINFORCED CONCRETE TEST RESULTS WITH SIMILAR AXIAL STIFFNESSES

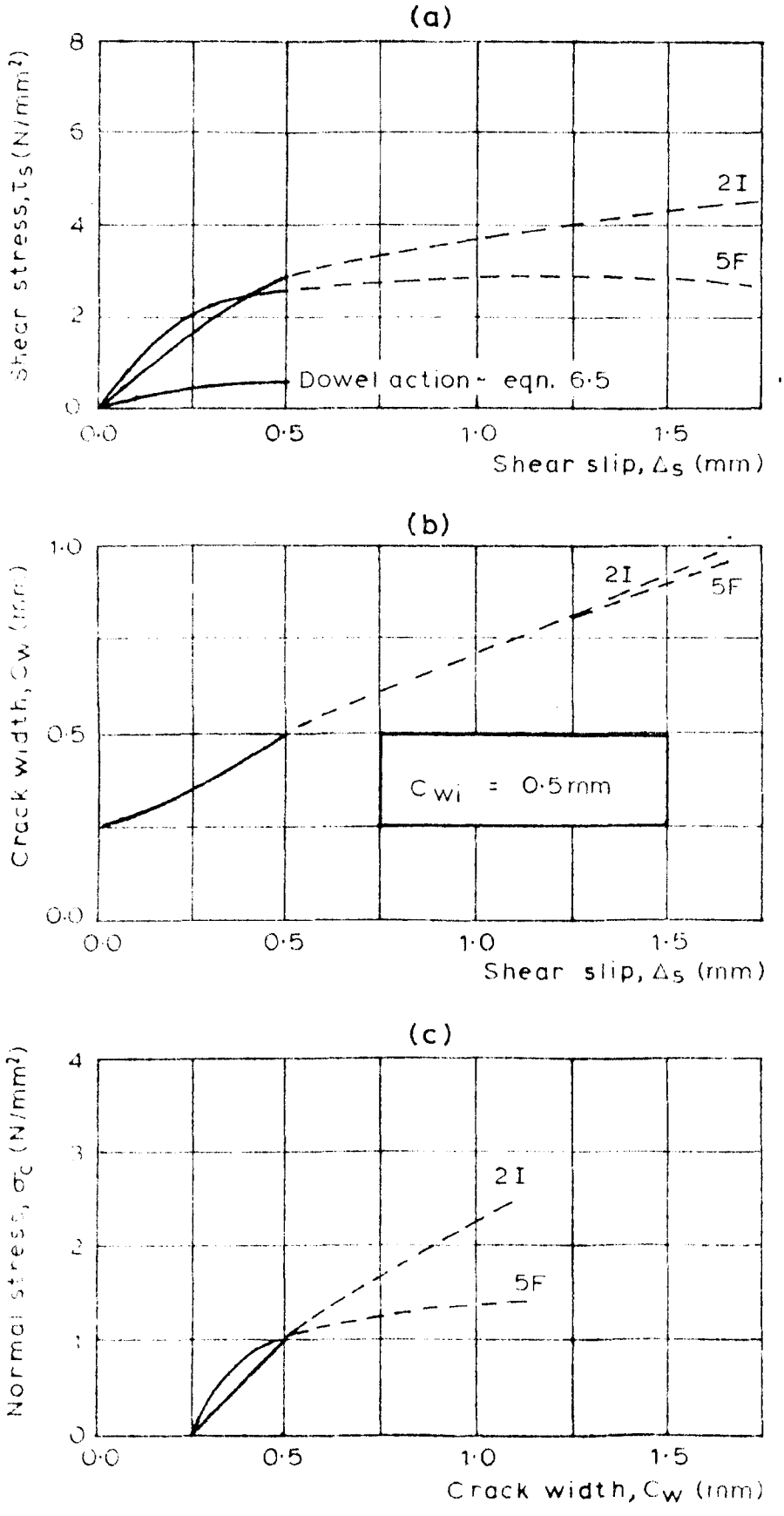

FIGURE 6.15. COMPARISON OF AGGREGATE INTERLOCK AND REINFORCED CONCRETE TEST RESULTS WITH SIMILAR AXIAL STIFFNESSES

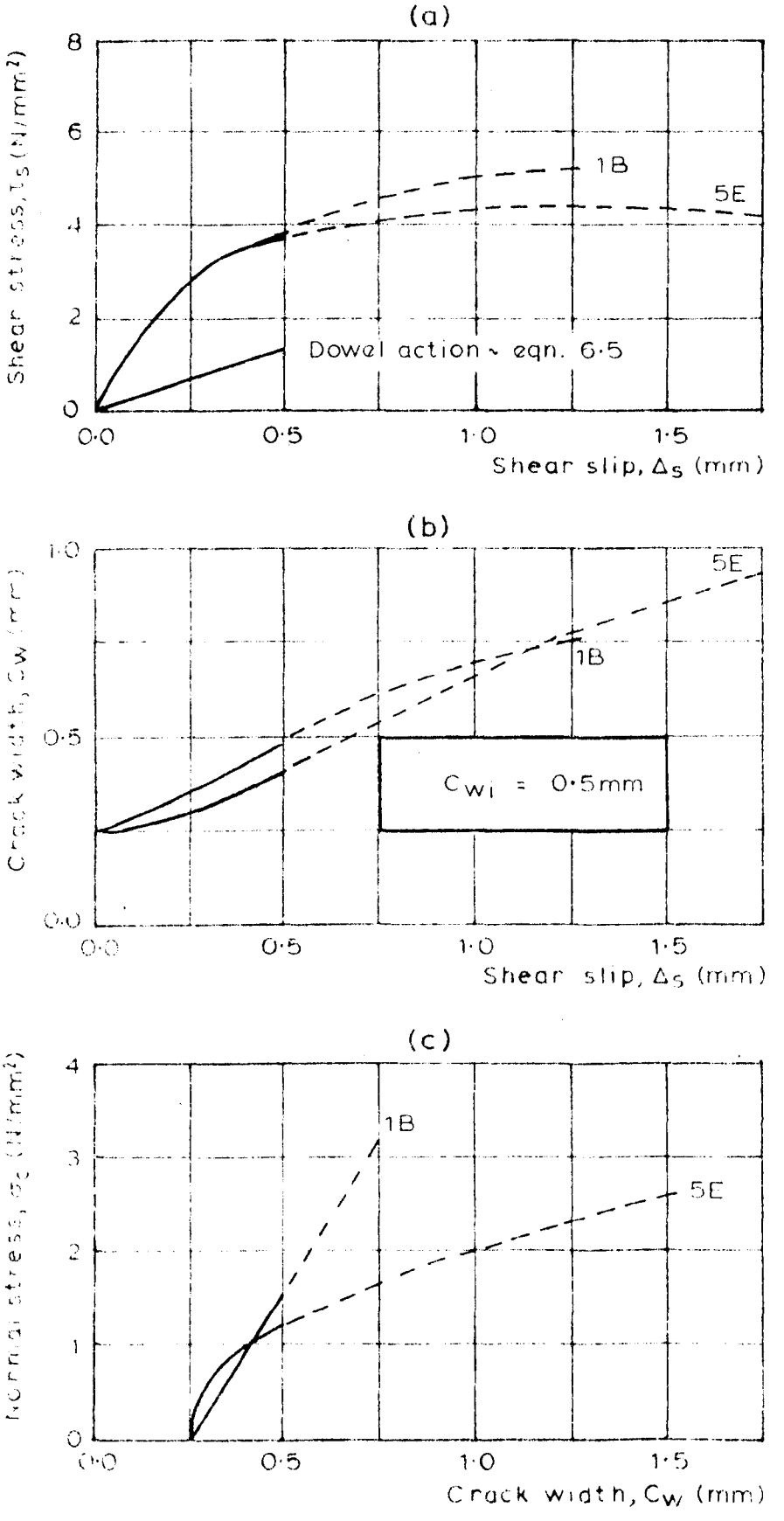

FIGURE 6.16. COMPARISON OF AGGREGATE INTERLOCK AND REINFORCED CONCRETE TEST RESULTS WITH SIMILAR AXIAL STIFFNESSES.

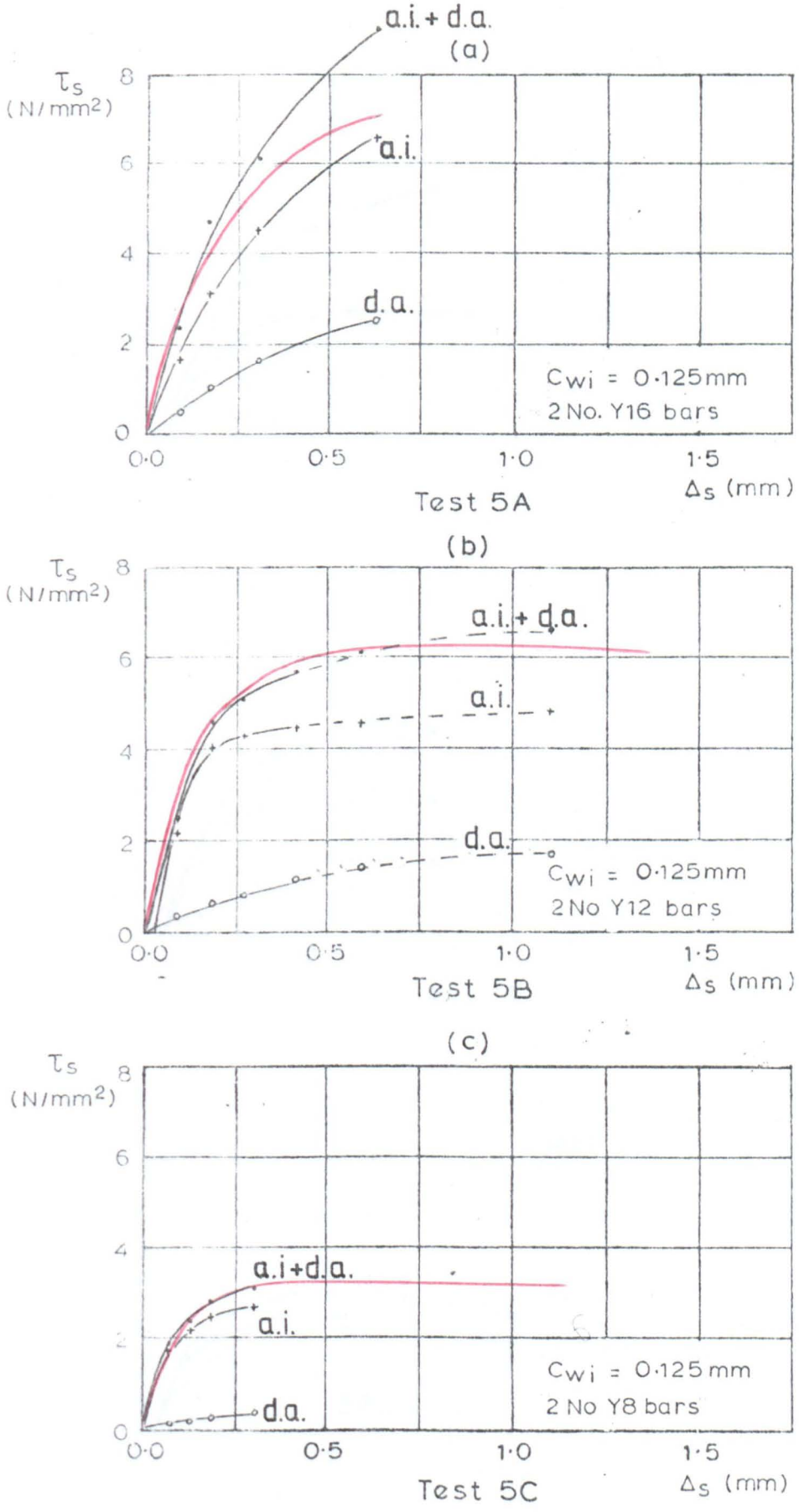

FIGURE 6.17. COMPARISON OF REINFORCED CONCRETE TEST RESULTS WITH PREDICTED AGGREGATE INTERLOCK AND DOWEL ACTION COMPONENTS.

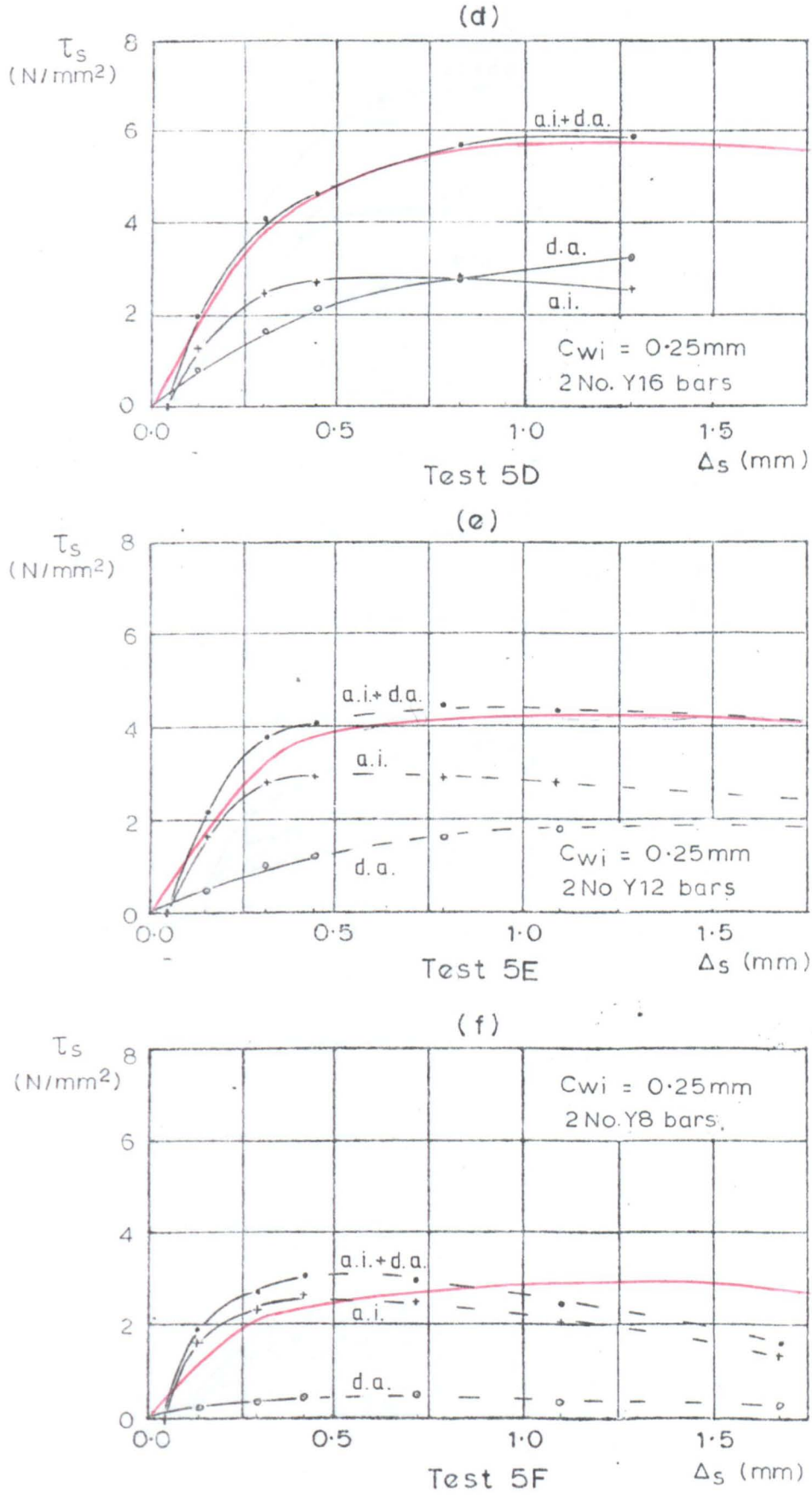

FIGURE 6.17. CONTINUED

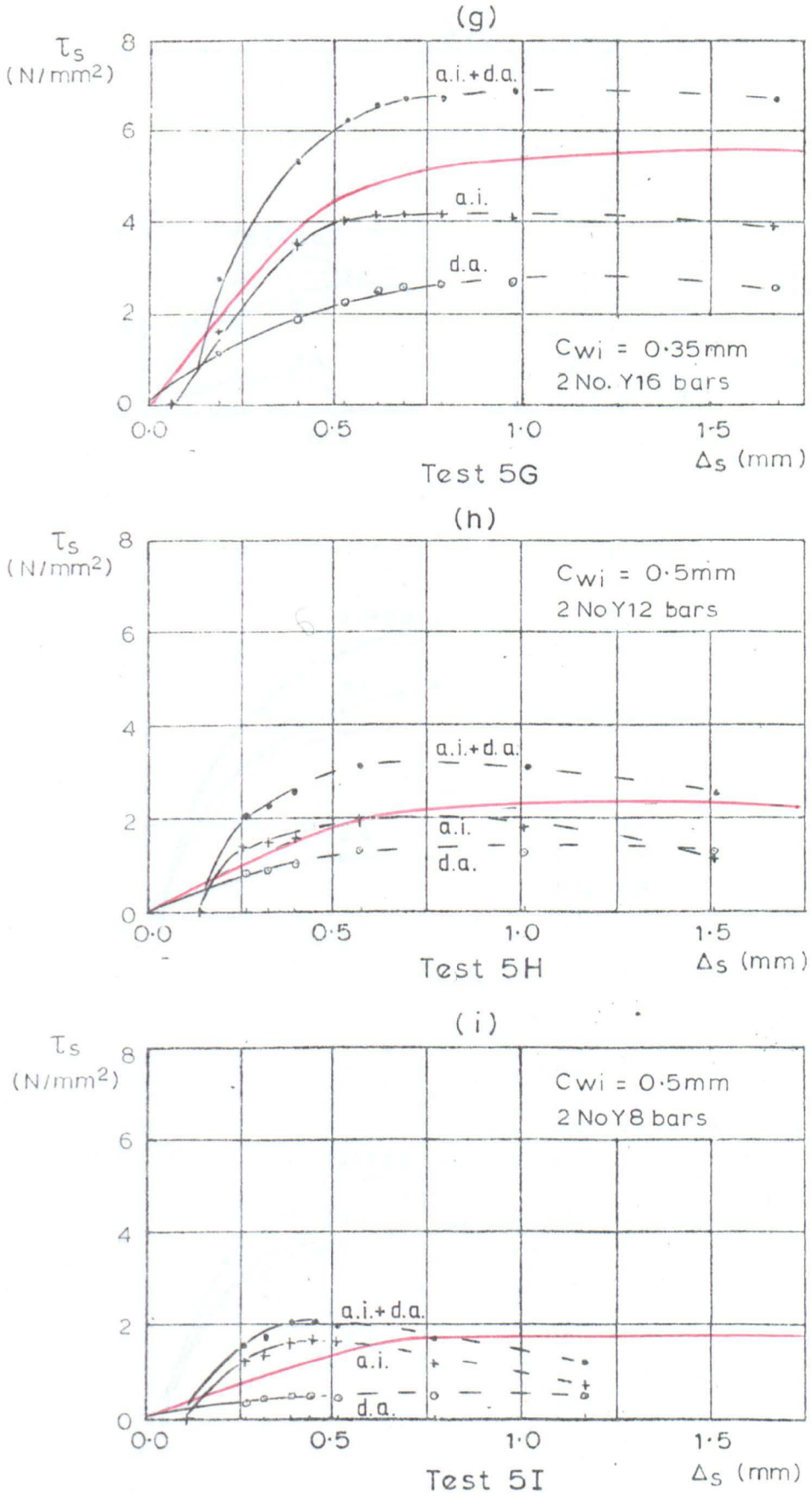

FIGURE 6.17. CONTINUED

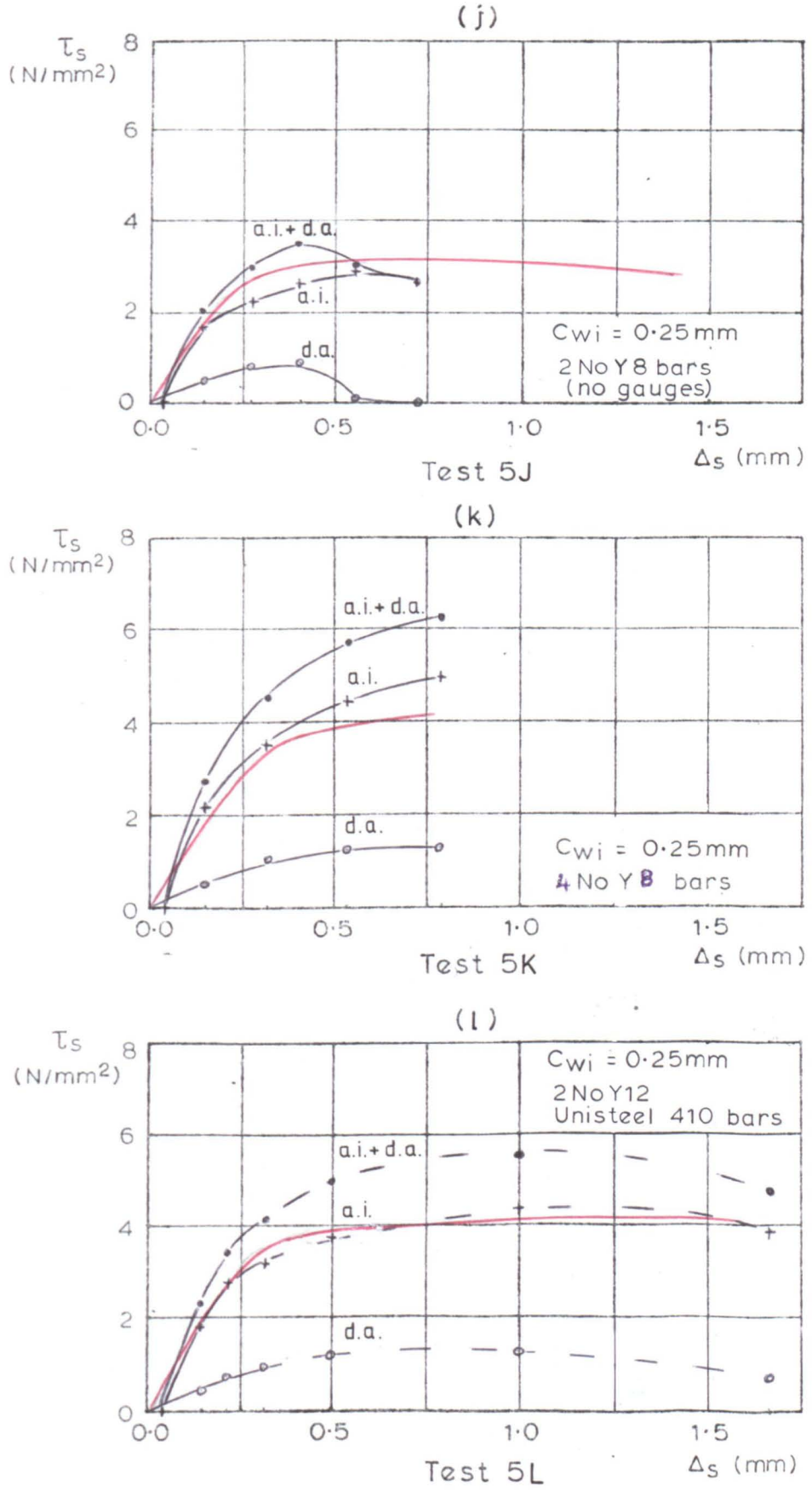

FIGURE 6.17. CONTINUED

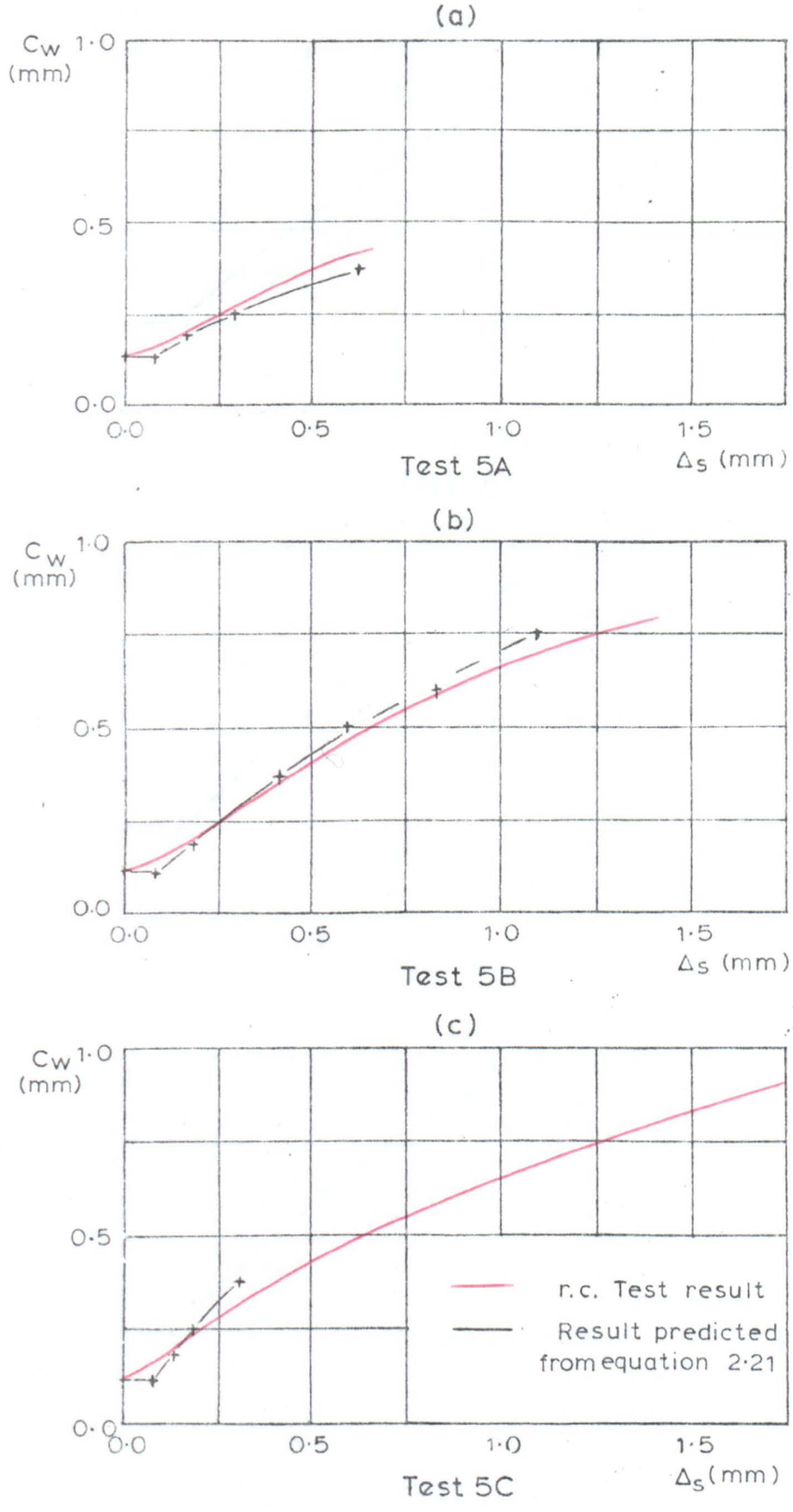

FIGURE 6.18. PREDICTED CRACK WIDTH - SHEAR SLIP RELATIONSHIP FOR REINFORCED CONCRETE SPECIMENS.

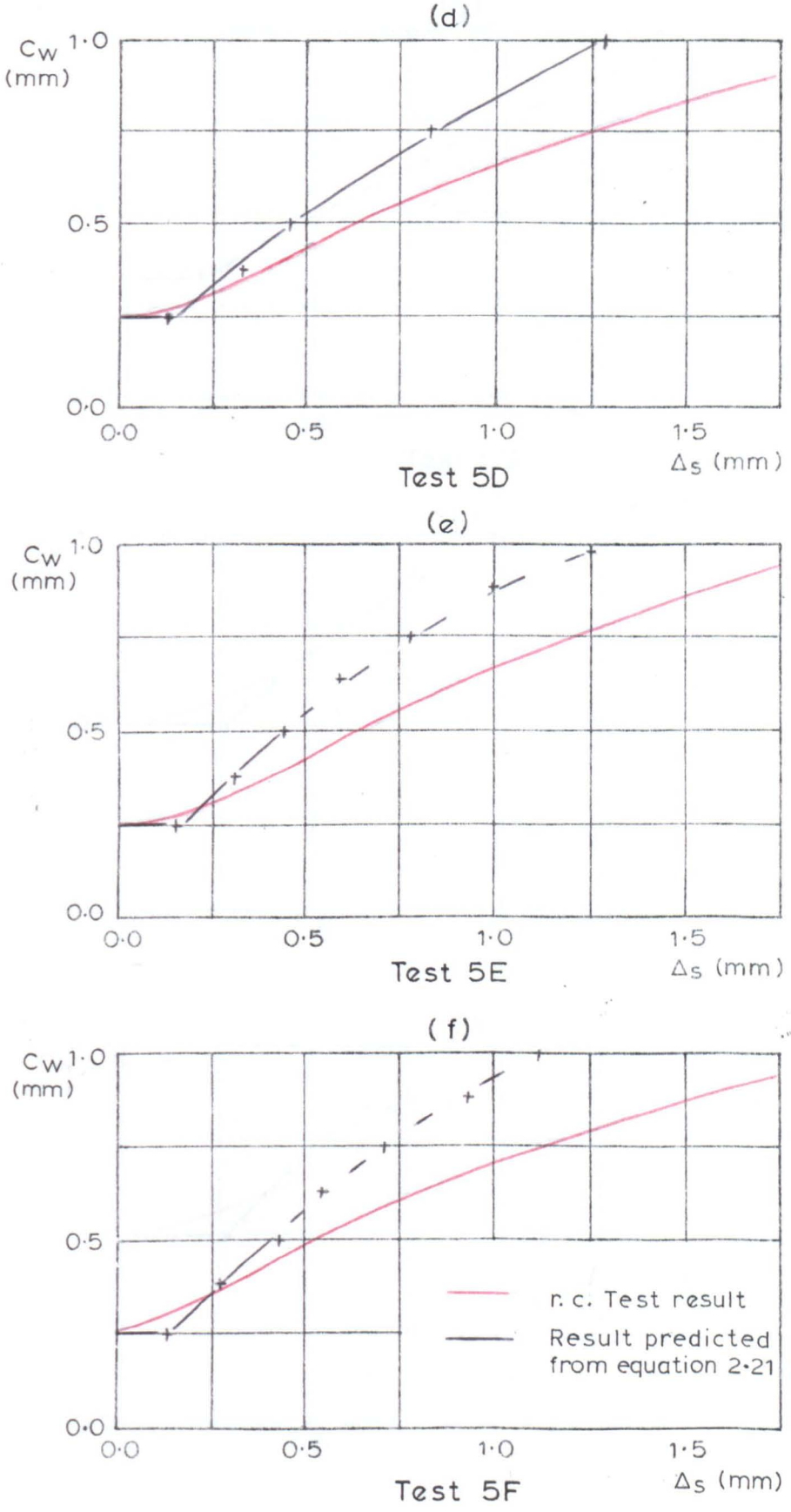

FIGURE 6.18. CONTINUED

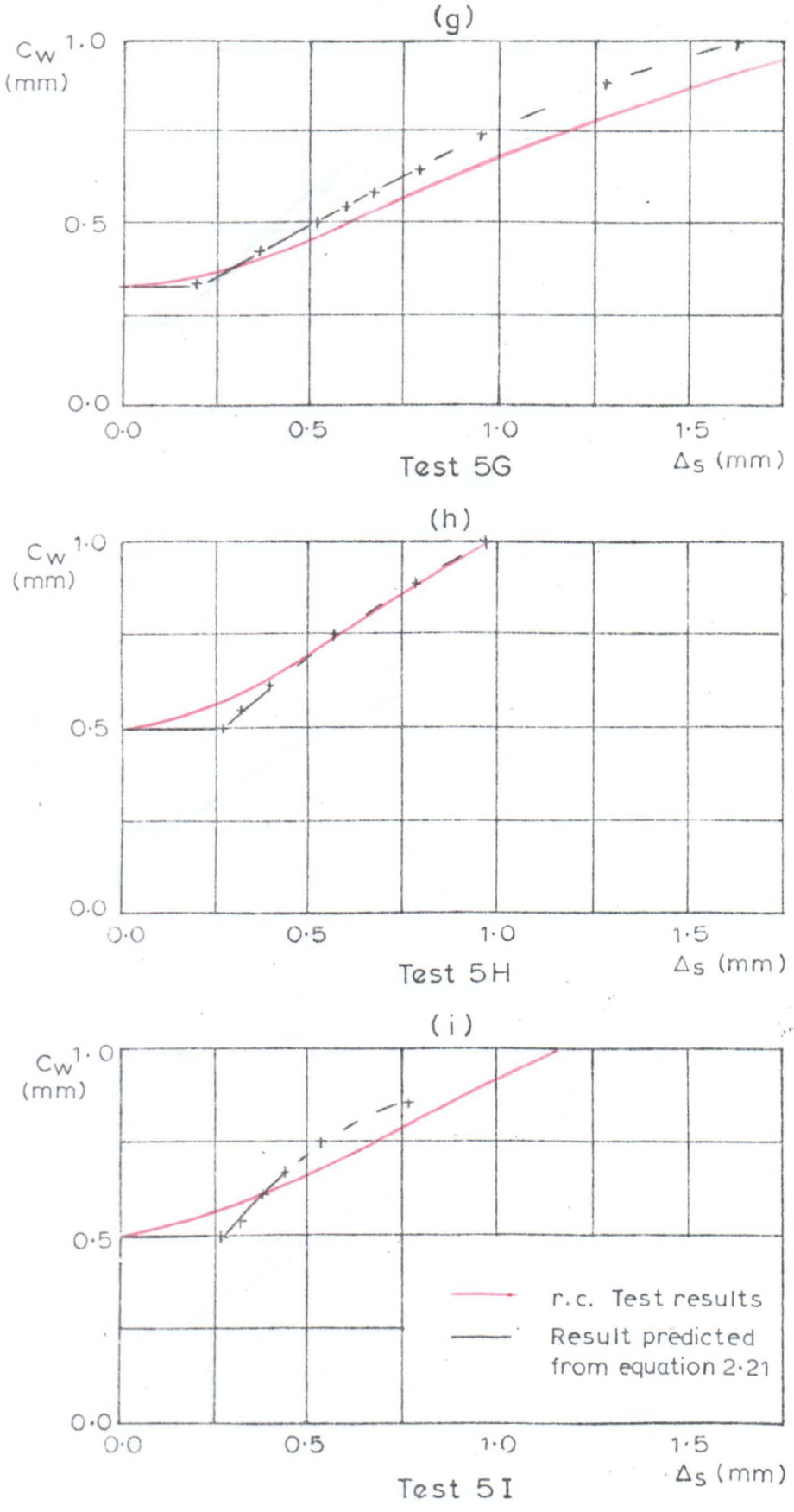

FIGURE 6.18. CONTINUED

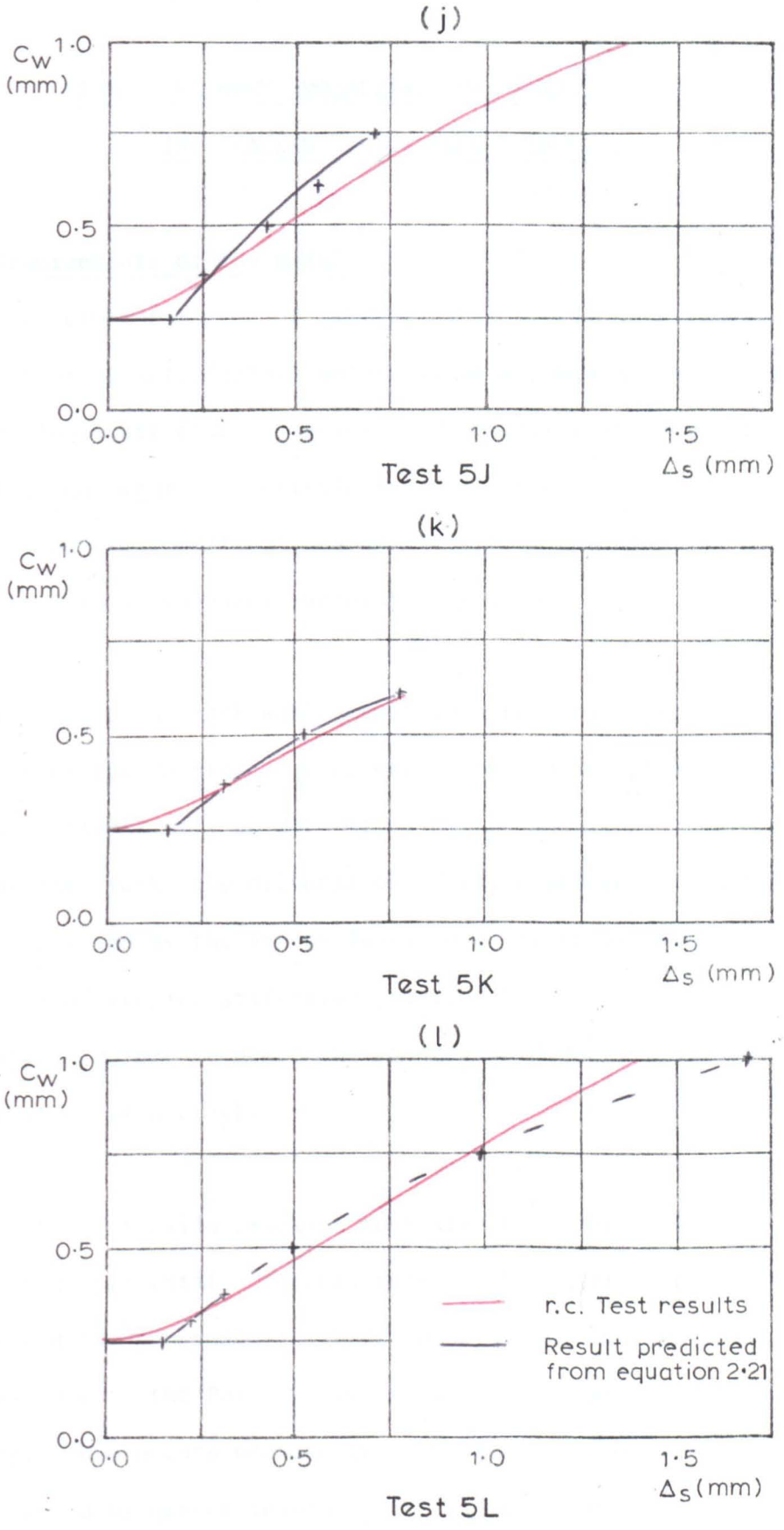

FIGURE 6.18. CONTINUED

CHAPTER SEVEN

FINITE ELEMENT MODELLING OF SHEAR TRANSFER IN CRACKED REINFORCED CONCRETE

7.1 Requirements of the model

The finite element method of analysis is a widely used numerical method enabling satisfactory solutions to be obtained for many otherwise insoluble structural problems. However, if it is to be used to model the behaviour of a brittle material, such as reinforced concrete, there are several modifications which must be made to the standard method to give a reasonably accurate solution.

The formation of a crack will result in a reduction in the tensile stiffness of the reinforced concrete normal to the plane of cracking. The new stiffness will be determined by the amount of reinforcement crossing the crack, the orientation of the reinforcement with respect to the crack and by the stress level in the reinforcement and hence the amount of tension stiffening provided by the concrete. It is necessary therefore to model the changes in direct stiffness due to the formation of a crack.

The effects of tensile cracking must also be modelled by making changes in the other elemental stiffness terms. Shear slip across the crack will reduce the shear stiffness of the cracked element. The indirect stiffness due to the Poisson effect may also be affected by tensile cracking. This occurs because the lateral strain normal to the crack, caused by direct loading parallel to the crack, will tend to result in a change in the crack width instead of inducing a direct stress in the concrete. The Poisson stress resulting from loading

normal to the crack will not be affected by the crack. However, as the direct tensile stiffness of the concrete normal to the crack diminishes with increasing tensile strain, this Poisson effect stiffness also becomes very small.

A further need to modify the elemental stiffness as a result of tensile cracking results from the tendency of the crack to widen as shear slip occurs. This can be modelled by including a new "cross linking" stiffness term relating the direct stress normal to the crack with the shear slip across the crack. However, from observations of the behaviour of the shear test specimens on unloading it was found that this relationship is not reversible. Releasing the externally applied axial tensile force has the effect of increasing the compressive force applied across the crack. This only caused a minimal reversal of the shear slip. It was reasoned that the frictional forces on the crack faces in contact tended to "lock-up" the crack and prevent shear slip when a compressive force normal to the crack was applied.

The finite element programs which were available to the writer were all long and complex general purpose packages which could not be easily modified to model the changes in stiffness caused by tensile cracking. It was decided to write a simpler program which could be easily understood and easily modified to represent the behaviour of cracked reinforced concrete.

7.2 Triangular, constant strain elements

The three-node constant strain finite element was initially studied in order to gain experience in finite element techniques and programming. This two-dimensional element is simple to understand and can be used

to model complex geometrical shapes. The element mesh can easily be graded to give a more accurate solution in regions of high stress concentration. In Appendix A1 a linear, elastic analysis of the test specimen under axial loading is described which predicted high concentrations of stress at the edges of the unstiffened end plates. The premature tensile failure of the end plates was attributed to these stress concentrations and from further analysis a suitable stiffness for the end plate was obtained to prevent this mode of failure.

The major disadvantage of the triangular, constant strain element lies in the inaccuracy of the solution obtained. No variation in strain within the element is modelled and hence a large number of elements are required to produce an acceptably accurate solution, particularly where there is a region of high strain gradient. The solution given by a mesh of triangular elements also tends to be erratic and convergence onto an exact solution by reducing the mesh size is slow. A more efficient solution is obtained by using a smaller number of higher order elements.

7.3 Quadrilateral isoparametric element

The quadrilateral isoparametric element has eight nodal degrees of freedom and can model a linear variation of strain ϵ_x in direction y and strain ϵ_y in direction x. The strain is sampled at four Gauss points within the element and a numerical integration procedure is used to obtain the internal elemental strain energy from the sampled strains and hence to formulate the elemental stiffness matrix. The isoparametric family of elements all use a single interpolation function to define the geometry of the element and to define displacements within the element.

The four node element is the simplest type of isoparametric element (Figure 7.1). It is more accurate than the triangular element but still has several disadvantages. It is difficult to grade a mesh of quadrilateral elements to produce a fine mesh in the region of expected stress concentrations. The strain ε_x cannot vary in direction x, nor can ε_y vary in direction y. Consequently the bending strains are constant within each element and so the solution can still be quite crude. The biggest disadvantage however is that under pure bending the model predicts a shear strain at each of the Gaussian sample points, where none actually occurs in a real specimen. This "parasitic" shear strain energy results in the formulation of an element with too high a flexural stiffness (Figure 7.2).

The flexural stiffness can be reduced to a more realistic value by using a method of reduced integration of the internal element strain energy (70). The direct strain energy is numerically integrated as before using samples from the four Gauss points (Figure 7.1b). The shear strain however is assumed to be uniform throughout the element and is sampled at $\eta, \xi = 0$. Hence a zero shear strain energy is associated with pure bending (Figure 7.2b).

Care must be taken when using these modified quadrilateral elements. Unless the quadrilateral is restricted to a rectangle the element fails the "patch test". This is a test derived by Irons (70) which ensures that the solution of the analysis converges onto the exact solution as a successively finer element mesh is used.

Cook (71) has also shown that the modified rectangular element is not invariant and hence discourages its use in preference to more complex elements. The property of invariance means that the element

strain or strain energy under a given set of loads in local element coordinates is independent of the orientation of the loads and the element to the global coordinates. Invariance is claimed to be a desirable, but not essential attribute of a finite element.

The modified four-node element was considered to be sufficiently accurate for the purposes of this study. As the material properties of cracked reinforced concrete are not known accurately, the value of developing a more elaborate analysis is questionable.

7.4 Modelling of material non-linearity

The finite element method discussed so far has been based upon the assumption that the materials behave in a linear elastic manner. If the materials behave in a non-linear way, this can be modelled by one of several iterative approaches. In this analysis the modified Newton-Raphson method was used which can be summarised as follows.

From the known non-linear functions for the material properties an initial tangent stiffness matrix is derived. Hence a load matrix $\{P\}$ is applied and the resultant displacement matrix $\{d_1\}$ determined (Figure 7.3a). From $\{d_1\}$ an updated secant stiffness matrix is found and hence a new load matrix $\{P_1\}$ which is consistent with $\{d_1\}$. $\{P_1\}$ is then compared with the applied load $\{P\}$. If there is a significant difference, the out of balance load $\{P - P_1\}$ is reapplied to the structure and an additional displacement matrix $\{d_2\}$ is found using the same initial tangent stiffness matrix. A new secant stiffness matrix and load $\{P_2\}$ is then determined from the total deflection $\{d_1 + d_2\}$. The procedure is repeated until the out of balance load matrix is negligible. In this analysis convergence was deemed to have occurred when,

$$(\Sigma\ (P - P_i)^2)^{\frac{1}{2}} \leq \frac{(\Sigma\ P^2)^{\frac{1}{2}}}{1000}$$

where $P - P_i$ is the out of balance force at each node, with the exception of restrained nodes. P is the applied loading at each node.

The use of the initial tangent stiffness matrix to determine the displacements during each iteration results in more iterations to achieve convergence than if this stiffness matrix is updated between each iteration. However it usually results in a more efficient solution procedure because inversion of the stiffness matrix only occurs once.

This non linear method was further refined by applying the load in increments and then updating the tangent stiffness matrix after each convergence, Figure 7.3b. This method provided a load-deflection curve instead of just one final solution. It should be noted that each interim solution in Figure 7.3a is a correct solution for an incorrect load matrix and hence is of no value. Only the solution obtained when convergence has been achieved is relevant to the applied loading.

7.5 Formulation of a stiffness matrix for reinforced concrete

The elemental stiffness matrix $[K^e]$ may be obtained by a minimisation of the potential energy of the deformed element, under any given loading. It can be shown (72) that in the absence of body forces or surface traction that

$$[K^e]\ \{\delta^e\} = \{P^e\} \qquad (7.1)$$

where $\{\delta^e\}$ are the nodal displacements and $[P^e]$ are the nodal forces

on the element. The elemental stiffness matrix $[K^e]$ is given by,

$$[K^e] = t \iint [B]^T [D] [B] \, dx \, dy$$

where t = the uniform thickness of the element

[B] is a matrix relating the internal strains $\{\varepsilon\}$ at any point to the nodal displacements, $\{\delta^e\}$

[D] is the material property matrix

Hence

$$\{\sigma\} = [D] \{\varepsilon\} \tag{7.2}$$

In a two dimensional, plane stress analysis [D] is a 3 x 3 matrix. Thus,

$$\begin{Bmatrix} \sigma_x \\ \sigma_y \\ \tau_{xy} \end{Bmatrix} = \begin{bmatrix} D_{11} & D_{12} & D_{13} \\ D_{21} & D_{22} & D_{23} \\ D_{31} & D_{32} & D_{33} \end{bmatrix} \begin{Bmatrix} \varepsilon_x \\ \varepsilon_y \\ \gamma_{xy} \end{Bmatrix} \tag{7.3}$$

For an uncracked reinforced concrete slab with bars oriented in the x and y directions, the reinforcement may be considered as "smeared" uniformly throughout the element. Hence the [D] matrix in equation 7.2 is the sum of the components $[D^c]$ for concrete and $[D^s]$ for steel,

where,

$$[D^c] = \frac{E_c}{1 - \nu_c^2} \begin{bmatrix} 1 & \nu_c & 0 \\ \nu_c & 1 & 0 \\ 0 & 0 & \frac{1 - \nu_c}{2} \end{bmatrix} \tag{7.4}$$

and

$$[D^s] = \begin{bmatrix} \rho_x E_s & 0 & 0 \\ 0 & \rho_y E_s & 0 \\ 0 & 0 & 0 \end{bmatrix} \qquad (7.5)$$

ρ_x and ρ_y are the reinforcement ratios in the x and y directions.
ν_c is the Poisson ratio for concrete.

7.6 Modelling of tensile cracking

If the mean principal tensile stress in the concrete of an element exceeds the tensile strength of concrete then the element is assumed to have cracked in a direction normal to the principal tensile direction. This crack can be modelled by assuming its effects are distributed throughout the element and hence altering the [D] matrix by attributing modified material properties to the reinforced concrete, which result in the same overall elemental stiffness. The [D] matrix is normally formulated with respect to local axes parallel and perpendicular to the crack and is then transformed into global coordinates. The effect of modelling a crack in this way will be that the overall behaviour of a cracked structure can be predicted quite closely, but the behaviour within a cracked element will not resemble that occurring adjacent to a real crack.

Cracked reinforced concrete still has a residual tensile stiffness normal to the plane of cracking because of the tension stiffening provided by the local bond of the reinforcement. Tension stiffening was observed by Clark and Speirs (21) to decrease at higher strains as the local bond was destroyed and also as new cracks were formed (Figure 7.4).

Gilbert and Warner (73) considered several techniques for incorporating the global effects of tension stiffening into a finite element analysis. One technique was to model the stiffness of the concrete as reducing incrementally as the tensile strain increases (Figure 7.5a). An alternative approach is to use a concrete stiffness which diminishes continuously with increasing tensile strain (Figure 7.5b).

The first approach is simple to adopt and will apply to loading, unloading and reloading of the element. However, the discontinuities in stiffness are not reflected by the response of a real tensile member and may lead to convergence onto a false situation. The alternative method models closer the behaviour of a real structure. However, it will be more difficult to implement and it does not model the possibility of a reduction in strain in the element subsequent to cracking. This may occur if an adjacent element suffers a rapid loss of stiffness even if the external load is monotonically increasing.

A third approach discussed in reference 73 was to assume zero stiffness for the concrete at the onset of cracking. Tension stiffening was then modelled by increasing the stiffness of the reinforcement to represent the additional stiffness (Figure 7.6). All these methods of modelling tension stiffening can be expected to give an approximation to the overall stiffness of the structure. However they cannot be expected to provide close estimates of the localised stresses in the concrete and the reinforcement immediately adjacent to a crack. One major disadvantage of including the tension stiffening effect within the stiffness matrix for the reinforcement becomes apparent when a layered finite element analysis is used to model flexure of a slab. The tension stiffening effect is caused by

local bond with the reinforcement and would be expected to diminish with distance from the reinforcement. However if the tension stiffness is included in the reinforcement stiffness this effect cannot be modelled because all the tension stiffening effect is applied at the level of the reinforcement.

Cope et al. (49) developed a simple but effective method of modelling tensile cracking and subsequent tension stiffening by reducing the tensile stiffness of the concrete, until at a high strain the concrete makes no contribution to the matrix stiffness normal to the crack (Figure 7.7a). A reduction in the tensile strain subsequent to cracking is modelled by adopting a secant stiffness intersecting the cracking strain on the x axis from the position reached on the stress strain curve. This was done in order to model the observation that tensile cracks do not close up completely when all the tensile load has been removed.

It was decided in this study not to attempt to model the initiation of tensile cracking but to assume that it had already occurred and that the position and direction of the cracks were known. The study was further restricted to cracking in a direction normal to the reinforcement, as in the experimental tests.

For a precracked element, a simple stiffness model for tension stiffening is proposed (Figure 7.5b). It is assumed that the stiffness curve for any unloading and reloading will intersect the origin i.e. at zero load the crack closes up completely.

Hence if the crack is normal to the x-axis, the elemental tensile stiffness D_{11} in equation 7.3 is given by,

$$D_{11} = \rho_x E_s + \alpha E_c \text{ where } 0 < \alpha < 1 \qquad (7.6)$$

If the strain is high enough that the stiffness is given by line BC on Figure 7.7b, α becomes negative for the tangent stiffness matrix and is given by a bilinear expression for the secant stiffness matrix.

A similar approach is adopted for cracking normal to the y-axis. The element is considered as having orthotropic material properties, the shear stiffness D_{33} being independent of D_{11}, D_{12}, D_{21} and D_{22}.

It was assumed that the Poisson effects were negligible for cracked elements. Hence ν_c is zero in equation 7.4.

In the analysis carried out it was assumed that the spacing of the cracks was greater than the element size so that only one crack could pass through an element in the x or y direction. It is only possible to use this method if the initiation of new cracks no longer occurs and if the stabilized crack pattern is known in advance.

The value for the shear stiffness D_{33} in equation 7.4 will be provided by the shear stiffness of the uncracked concrete and the shear stiffness across the crack. Hence for all elements,

$$D_{33} = \alpha G_o \qquad (7.7)$$

where for an uncracked element

$$\alpha = 1, \quad G_o = \frac{1 + \nu_c}{2} E_c$$

and for a cracked element,

$$\frac{1}{\alpha G_o} = \frac{1}{G_o} + \frac{1}{G_{crack}}$$

G_{crack} is the effective shear stiffness of the element due to shear slip across the crack and is given by,

$$G_{crack} = \frac{\tau_s}{\gamma_{crack}} = \frac{\tau_s \ell_e}{\Delta_s} \qquad (7.8)$$

for the secant shear stiffness and,

$$G_{crack} = \frac{d \tau_s}{d \gamma_{crack}} = \ell_e \frac{d \tau_s}{d \Delta_s} \qquad (7.9)$$

for the tangent shear stiffness,

where ℓ_e is the element size normal to the direction of cracking.

As D_{33} is a function of the finite element mesh it must be redetermined if the element mesh is altered.

The equations 6.5, 2.41 and 2.42 may be used to determine the shear stiffness, D_{33}, of the crack due to dowel action and aggregate interlock and can be expressed as

$$\sigma_x = f_1(C_w, \Delta_s) \qquad (7.10)$$

$$\tau_{xy} = f_2(C_w, \Delta_s) \qquad (7.11)$$

If the crack displacements are again considered as strains averaged over the whole element,

i.e. $\gamma_{crack} = \frac{\Delta_s}{\ell_e}$, $\varepsilon_{crack} = \frac{C_w}{\ell_e}$

For cracking normal to the x axis, the equations may be rewritten as,

$$\sigma_x = f_3(\varepsilon, \gamma)$$

$$\tau_{xy} = f_4(\varepsilon, \gamma)$$

These expressions are unsuitable for the derivation of secant stiffnesses in matrix form. However, the tangent stiffness, which is needed for the formulation of the overall stiffness matrix can be obtained by partial differentiation. Hence

$$\begin{Bmatrix} d\sigma_x \\ d\tau_{xy} \end{Bmatrix} = \begin{bmatrix} \delta f_3(\varepsilon, \gamma)/\delta\varepsilon & \delta f_3(\varepsilon, \gamma)/\delta\gamma \\ \delta f_4(\varepsilon, \gamma)/\delta\varepsilon & \delta f_4(\varepsilon, \gamma)/\delta\gamma \end{bmatrix} \begin{Bmatrix} d\varepsilon \\ d\gamma \end{Bmatrix} \qquad (7.12)$$

For the initial development of a non-linear analysis these complex expressions for terms in the tangent and secant [D] matrices were avoided. A fourth order polynomial was used to fit the $\tau_s - \Delta_s$ test results in Chapter 5.

Hence,

$$\tau = a\,\gamma_{crack} + b\,\gamma^2_{crack} + c\,\gamma^3_{crack} + d\,\gamma^4_{crack} \qquad (7.13)$$

where γ_{crack} is defined in equation 7.8. The constants were explicitly found for each test result.

The tendency of a crack to widen when shear slip occurs should also be included in the cracked [D] matrix. Bazant (51) attempted this

by using an empirical relationship between C_w and Δ_s and hence between ε_x and γ_{xy}. This expression resulted in a [D] matrix for concrete which was singular. This result is not surprising since if ε_x and γ_{xy} are no longer independent parameters the 3 x 3 [D] matrix may be replaced by a 2 x 2 [D] matrix.

In this study the crack widening associated with shear slip is modelled by including a D_{13} term in the [D] matrix when cracking occurs normal to the x axis. Hence the material properties of the cracked reinforced concrete element are represented by,

$$[D] = \begin{bmatrix} D_{11}^c + D_{11}^s & 0 & D_{13}^c \\ 0 & D_{22}^c + D_{22}^s & \\ 0 & 0 & D_{33}^c \end{bmatrix} \qquad (7.14)$$

where the superscripts refer to the respective components of stiffness due to the steel and due to the cracked concrete, as shown in equations 7.4 and 7.5. The asymmetric [D] matrix in equation 7.14 results in an asymmetric overall structural stiffness matrix.

A general, non linear expression for D_{13}^c may again be derived from equations 2.41 and 2.42. However for the initial analysis D_{13}^c was assumed to be a linear term and was obtained empirically from the test results in Chapter 5.

If an element represented by equation 7.14 is subjected to a shear stress τ^c,

$$\tau^c = D_{33}^c \gamma$$

From equilibrium the composite direct stress σ_x is zero. Hence,

$$0 = (D_{11}^c + D_{11}^s)\ \varepsilon_x + D_{13}^c\ \gamma$$

$$\therefore \quad \varepsilon_x = \frac{-\ D_{13}^c\ \gamma}{(D_{11}^c + D_{11}^s)} \tag{7.15}$$

Therefore the direct stress in the concrete σ_x^c is given by,

$$\sigma_x^c = D_{11}^c\ \varepsilon_x + D_{13}^c\ \gamma$$

$$\therefore \quad \sigma_x^c = \frac{-\ D_{11}^c\ D_{13}^c\ \gamma}{(D_{11}^c + D_{11}^s)} + \frac{D_{13}^c\ \tau^c}{D_{33}^c}$$

Hence,

$$D_{13}^c = \frac{\sigma_x^c}{\tau^c}\ \frac{D_{33}^c(D_{11}^c + D_{11}^s)}{D_{11}^s} \tag{7.16}$$

For simplicity D_{13}^c has been assumed to be a constant term. Hence the ratio of $\frac{\sigma_x^c}{\tau^c}$ and D_{33}^c in equation 7.16 are mean values obtained from the slopes of the experimental results in Chapter 5.

A shear slip will cause the crack width to increase regardless of the direction of shear slip. This means that D_{13}^c must always have an opposite sign to that of the shear strain γ, to produce an expanding lateral strain in equation 7.15. A dilemma then arises when trying to solve a general problem. The stiffness matrix must be formulated first. Loads are then applied to the structure and the nodal displacements are found. From these displacements the strains within each element are determined. However until the sign of the shear

strain is known, the sign of the D_{13}^{c} term is unknown and hence the stiffness matrix cannot be found.

In the analysis carried out in this study the direction of shear deformation was obvious from the direction of the applied loads. However in a more complex analysis a guess of the probable direction of shear deformation in each element must be made before any analysis can be carried out. A check on the sign of the shear strains given by the solution can later be made to confirm the original guess but this does not guarantee a correct solution. An incorrect original guess may result in an incorrect solution which is nevertheless consistent with the guess. More analysis needs to be carried out to determine whether this is an important problem or not.

Equation 7.14 is only valid for monotonically increasing shear loading. This is because the shear stiffness of a cracked element is not elastic and hence equation 7.13, which is used to obtain D_{33}^{c}, will only model the behaviour during increasing shear loading. Therefore it is necessary to check during the analysis that no element is unloading in shear.

However it was then realised that there were more fundamental objections to the use of an asymmetric term D_{13} in the [D] matrix. The use of non-symmetric terms contravenes the Maxwell-Betti reciprocal theorem and implies that the internal strain energy stored in a structure is dependent upon the sequence of loading i.e. the system is non-conservative. This is in fact what happens. It is an energy dissipating action such as friction or crushing which is preventing the crack from tending to shear when a normal compressive force is applied, in the same way in which the crack tends to widen

when a shear force across the crack is applied. If the finite element method is based upon a minimisation of the total potential energy in a system, using the Raleigh/Ritz method, then this is invalid for a non-conservative system. Nevertheless the finite element method has been used with some considerable success upon non-conservative systems such as viscous fluid flow, using the Galerkin method. This has been done (72) by treating viscosity as a reversible property, similar to the shear modulus, G, in a stress problem. Reversal of flow is not permitted. Where convective acceleration terms cause the [D] matrix to be asymmetric, these terms are usually ignored. If they are too large to be ignored a Newton-Raphson iteration, using a symmetric tangent matrix stiffness to converge onto an asymmetric secant equation, can be used.

A similar procedure can be used to solve the problem resulting from the asymmetric [D] matrix in equation 7.14. An approximate tangent $[D]^c$ matrix is given by,

$$[D]^c = \begin{bmatrix} D_{11} & 0 & D_{13/2} \\ 0 & D_{22} & 0 \\ D_{13/2} & 0 & D_{33} \end{bmatrix} \qquad (7.16)$$

or by

$$[D]^c \quad \begin{bmatrix} D_{11} & 0 & 0 \\ 0 & D_{22} & 0 \\ 0 & 0 & D_{33} \end{bmatrix} \qquad (7.17)$$

The resulting structural tangent stiffness matrix may then be used to converge onto a solution displacement matrix, from which internal stress resultants, in equilibrium with the applied loading, are

obtained by using the asymmetric secant [D] matrix.

Although the initial tangent stiffness resulting from equations 7.16 or 7.17 is only approximate, convergence onto a satisfactory solution should be obtained. Even if the tangent stiffness was initially correct, it becomes approximate after the first iteration (Figure 7.3a). Tangent stiffnesses derived from equations 7.16 and 7.17 will both produce convergence onto the same solution but depending upon the relative magnitude of the [D] matrix terms, one will produce a more rapid convergence than the other.

7.7 The behaviour of cracked reinforced concrete structures under shear loading

The aim of this section is to study the behaviour of a real structure which has been cracked in tension and undergone subsequent shear loading and to compare this with the behaviour which is predicted from a theoretical analysis based upon the shear test results described.

The programme of this collaborative research project with the Transport and Road Research Laboratory was linked with the testing of a half scale bridge deck. This bridge deck (Figure 7.8) was of composite construction with an insitu reinforced concrete slab cast onto precast pretensioned beams. It was planned that an abnormal HB load would be applied in a loading sequence which would cause longitudinal cracking right through the slab, adjacent to one of the precast beams. Cracking in this position would be expected to cause significant shear lag when a flexural load is subsequently applied to the beam. It was hoped that the difference in flexural stiffness of the beam, caused by longitudinal cracking, could be predicted using the knowledge of the in-plane shear stiffness of a cracked element.

Measurements of the shear slip occurring across the longitudinal cracks would provide additional confirmation of the validity of the model.

In the event, the bridge tests were not carried out during the duration of the project. It was necessary therefore to search through existing publications to find a set of test results which would prove suitable for comparison with the model developed.

This search proved to be harder than first expected. There were very few published experimental results of tests where tensile cracking was initiated in a structure which was subsequently reloaded to apply shear stress across the cracks and none where there was sufficient test data to permit comparison in detail of the overall structural behaviour with the writer's results.

A recent publication by Jimenez et al. (37) concerning the effects of earthquake loading upon reinforced concrete pressure vessels was discovered in which the specimens did have a suitable loading sequence and instrumentation to allow some comparison with the theoretical model. A test slab (Figure 7.9a) was initially loaded in biaxial tension, causing a series of tensile cracks normal to the direction of loading. The tensile loads were then maintained whilst shear stresses were caused by applying direct loads at the thickened corners of the slab (Figure 7.9b).

An effective shear modulus, $\bar{G}$ was obtained relating the mean shear stress in the slab, $\bar{\tau}$, to an average shear strain value, $\bar{\gamma}$, obtained from the direct strain of the diagonals D1 and D2. The widening and shear slip across the tensile cracks was also recorded during shear loading.

It was observed that for a mean shear stress less than 1 N/mm^2 shear slip across the cracks did occur and the crack widths increased. However, at higher levels of shear stress diagonal shear cracks started to form. Further shear strain was accommodated by a widening of these diagonal cracks and the formation of new diagonal cracks. Very little additional shear slip across the original tensile cracks occurred for shear stresses above 1 N/mm^2.

The shear stiffness across a crack was seen in Chapter 5 (e.g. Figure 5.13a) to be constant at stresses less than 1 N/mm^2. It was therefore decided to use a linear finite element analysis to compare these test results with the initial behaviour of the biaxially cracked slab. The slab was modelled using a mesh of linear, rectangular isoparametric elements (Figure 7.10).

An elastic analysis of the uncracked slab was initially carried out, to determine the effect of deriving the shear modulus, $\bar{G}$, from averaged shear stresses and strains. Concrete properties of $E_o = 25 \times 10^3$ N/mm^2 and $\nu = 0.2$ were used, resulting in $G_o = 10.4 \times 10^3$ N/mm^2. The effect of the reinforcement upon the shear stiffness of the slab was ignored. Compressive and tensile corner loads of 131 kN were applied to give a mean stress of 1 N/mm^2. From the displacements of nodes 12, 19, 82 and 89, an average shear strain of 1.63×10^{-4} was obtained.

Hence,

$$\bar{G} = 0.59\ G_o$$

The reason for this difference between G_o and $\bar{G}$ is that the corner loading does not produce a state of pure shear in the slab. The shear

stresses in the central region of the slab, where the shear strain is measured, are considerably greater than the mean shear stress over the entire slab (Figure 7.11a). The presence of cracks in the slab also alters the distribution of shear stresses (Figure 7.11b) and so it is not possible to use a constant term to obtain a material shear modulus for cracked concrete from $\bar{G}$. Hence the parameter $\bar{G}$ can only be used for a comparison between the shear stiffnesses of different slabs. It must not be considered as an effective material modulus of the cracked slab.

Specimen 0.3(M) in reference 37 was then modelled by reducing the shear stiffnesses of alternate rows and columns of elements to represent shear slip across the biaxial tension cracks. This was the closest approximation to the crack spacing observed in reference 37 (see Figures 7.8 and 7.11).

In specimen 0.3(M) reinforcement ratios of 2.4% and 1.2% were used. The slab was loaded in tension to cause axial stresses in the reinforcement of 248 N/mm^2 (0.6 f_y). These stresses were then maintained at 124 N/mm^2 (0.3 f_y) whilst the corner shear loading was applied.

The test specimens with specifications and load history most similar to those of slab 0.3(M) were specimens 5A and 5B. These had reinforcement ratios of 2.1% and 1.2%. The axial loadings maintained during shear loading were also quite similar (reinforcement stresses of 164 N/mm^2 and 139 N/mm^2). Hence the behaviour of the cracked slab 0.3(M) was modelled by reducing the shear modulus of the cracked elements appropriate to the test results 5A and 5B. From Figure 5.13a and equations 7.7 and 7.8, a shear modulus of 0.18 G_o was derived for elements with a crack in either direction. A shear modulus of 0.10 G_o

was derived for elements cracked in both directions.

The predicted average shear stiffness of the slab was much higher than the result obtained from test 0.3(M), (Figure 7.12). There are two factors which may contribute towards this discrepancy. The specimen slab 0.3(M) was first loaded in tension so that the axial stresses in the reinforcement in each direction reached 0.6 f_y, to initiate all the tensile cracks. These stresses were then reduced to 0.3 f_y before shear loading was applied. This load history was not followed by specimens 5A and 5B, where the reinforcement was only stressed to 0.3 f_y before the application of shear loading. The additional tensile loading on specimen 0.3(M) probably caused extra damage to the reinforcement bond and hence resulted in a reduced aggregate interlock shear stiffness. Dowel action may also be impaired. It is also quite probably that the crack widths in test 0.3(M) are higher than those in tests 5A and 5B, due to a lack of fit of the crack faces as the tensile stresses were reduced from 0.6 f_y to 0.3 f_y. This would also cause a reduction of the shear stiffness. We have been unable to obtain further data on these crack widths.

The second factor which could well influence the differences in shear stiffness is related to the presence of reinforcement and cracks in both directions in test 0.3(M) but in only one direction in tests 5A and 5B. The tensile cracks in test 0.3(M) tend to follow the path of the reinforcement (Figure 7.13) and hence the local bond between any of the reinforcement and the concrete is almost certainly negligible. The reduced stiffness normal to each crack will result in a lower shear stiffness due to aggregate interlock than was observed in tests 5A and 5B, where cracks were only present normal to

the reinforcement. The presence of cracks following the line of reinforcement will also reduce the shear stiffness due to dowel action.

It was therefore decided to reanalyse the slab using a shear stiffness for cracked elements derived from aggregate interlock tests, using unbonded reinforcement. Unfortunately it has not been possible to obtain details of the width of the cracks before shear loading on test 0.3(M) and an estimated width of 0.25 mm has been used. From the results of test 1A and 1B a shear modulus of 0.07 G_o has been derived for elements cracked parallel to the y axis (Figure 7.10) and 0.05 G_o for elements cracked parallel to the x axis. Elements with two cracks had a shear modulus of 0.03 G_o attributed to them. These values are probably a little too low because the length of specimens 1A and 1B is 250 mm but the mean crack spacing in test 0.3(M) is 150 mm. The averaged shear stiffness from this analysis is still higher than that obtained from test 0.3(M) (Figure 7.12) but is much closer than before.

It is also possible that the shear stiffness of the uncracked parts of the slab is lower than has been assumed here. Biaxial slab reinforcement provides a restraint to shrinkage and thermal contraction in the concrete. This may result in internal microcracking throughout the slab and hence a reduction in the shear stiffness over and above that caused by the primary tensile cracks. Without more details of test 0.3(M) any further development of this analysis was not considered to be worthwhile.

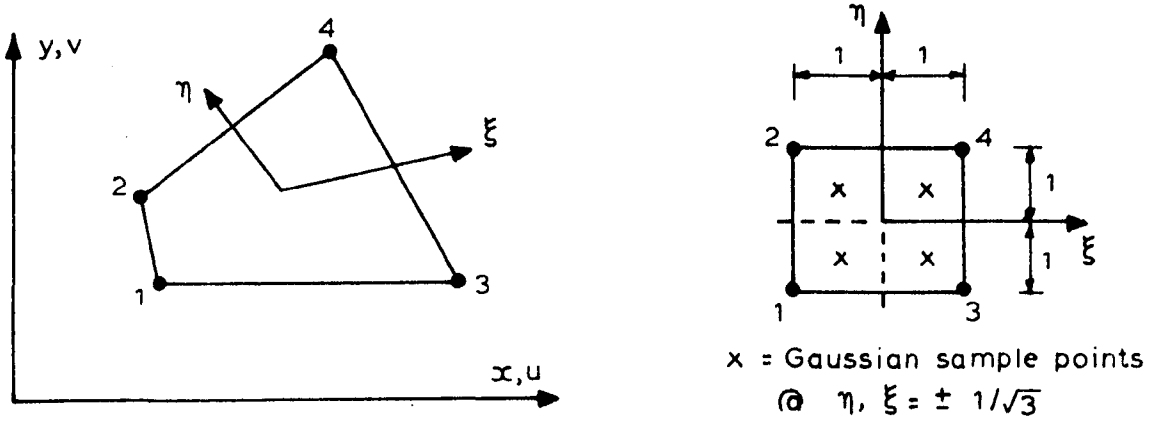

a) Element in global co-ordinates.

b) Mapping onto square.

FIGURE 7.1. PLANE QUADRILATERAL ISOPARAMETRIC ELEMENT

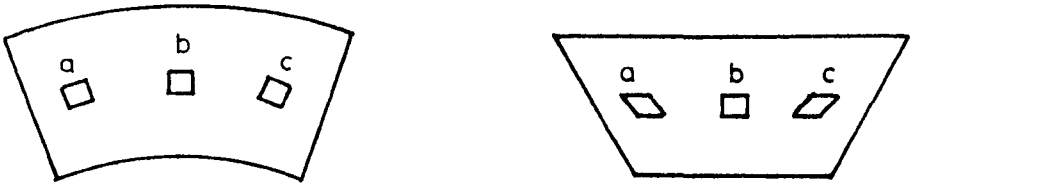

a) True bending
(⇒ no shear strain)

Bending modelled by 4-node element
(⇒ shear strain everywhere except at b.)

FIGURE 7.2. PARASITIC SHEAR IN THE QUADRILATERAL ELEMENT.

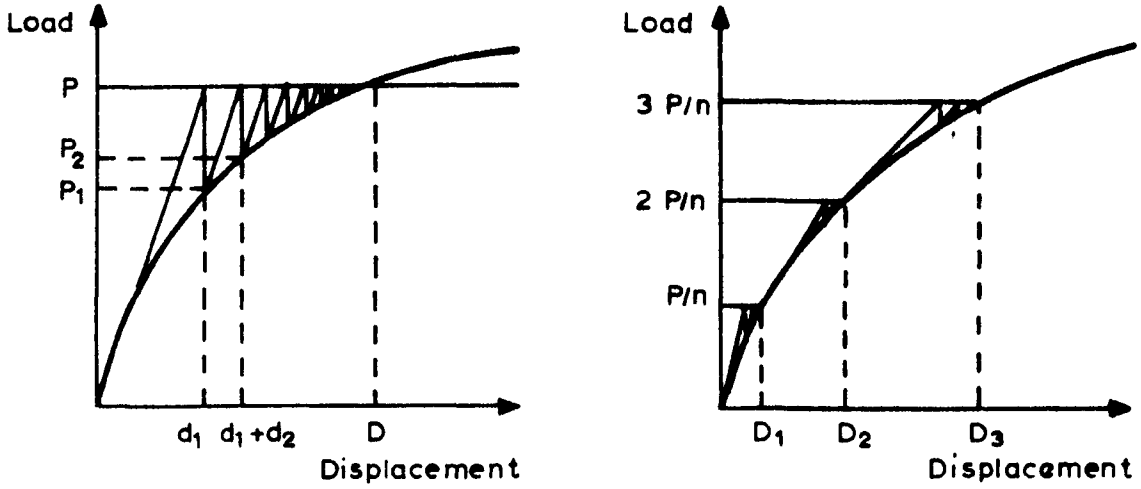

a) Modified Newton Raphson method.

b) Incremental modified Newton Raphson method.

FIGURE 7.3. MODELLING OF MATERIAL NON-LINEARITY.

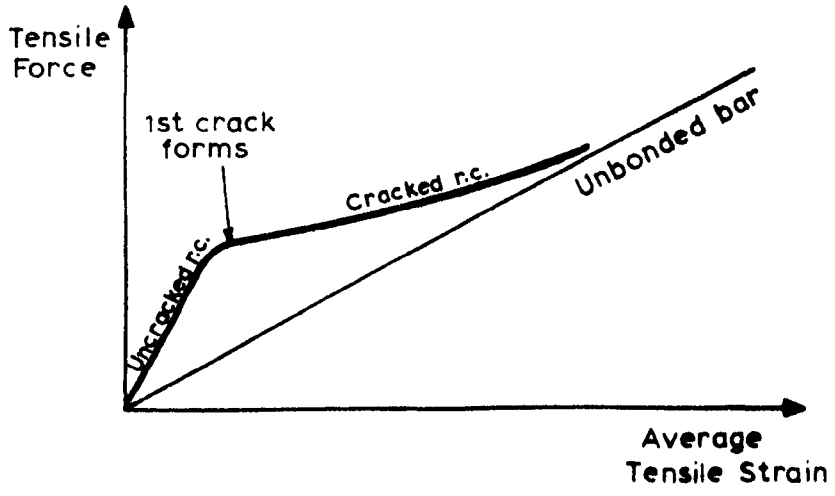

FIGURE 7.4. TENSION STIFFENING OF CRACKED REINFORCED CONCRETE.

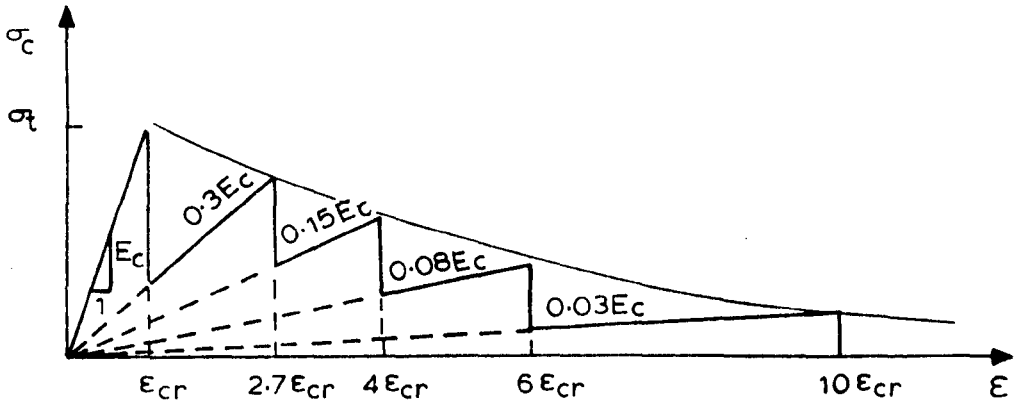

a) Stepped response after cracking.

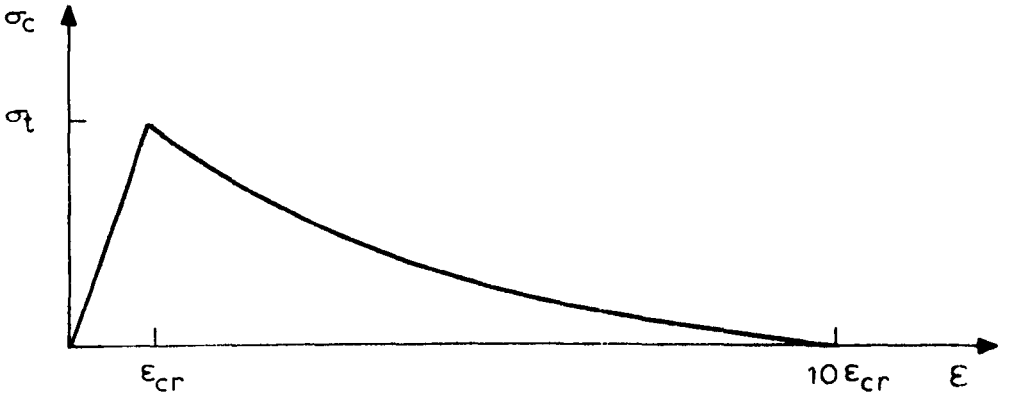

b) Gradually unloading response after cracking.

FIGURE 7.5. ALTERNATIVE STRESS - STRAIN DIAGRAMS FOR CONCRETE IN TENSION.

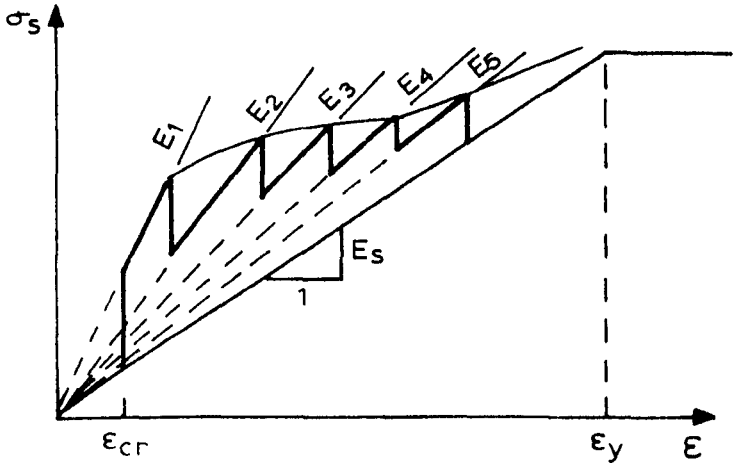

FIGURE 7.6. MODIFIED STRESS- STRAIN DIAGRAM FOR TENSION STEEL AFTER CRACKING.

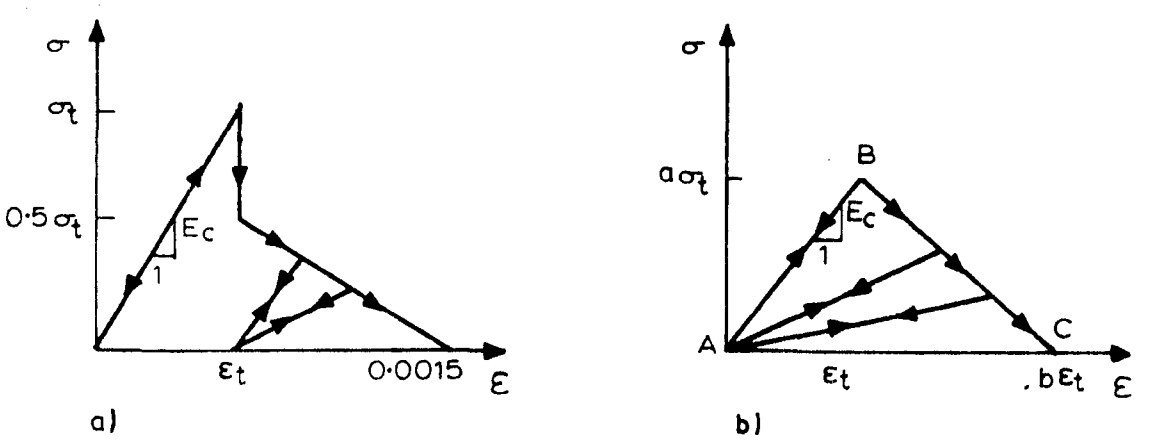

FIGURE 7.7. MODIFIED STRESS - STRAIN CURVES FOR CONCRETE IN DIRECT TENSION.

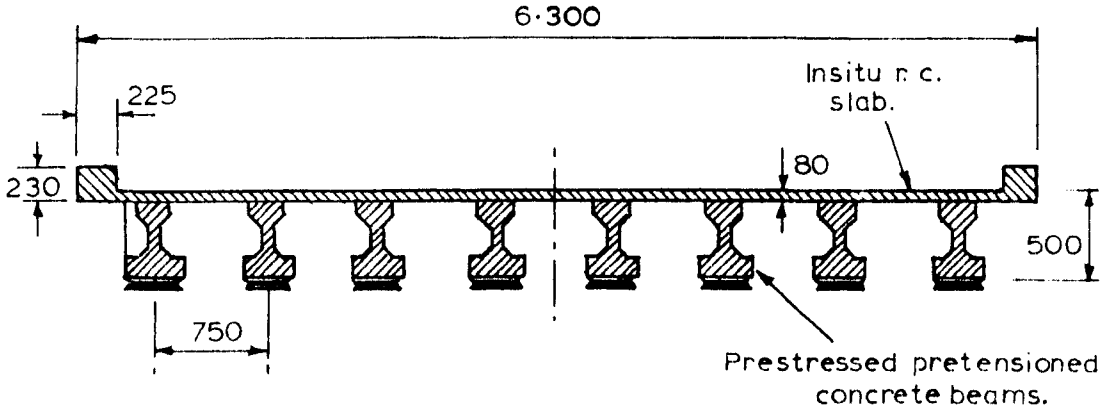

a) Cross Section of Deck.

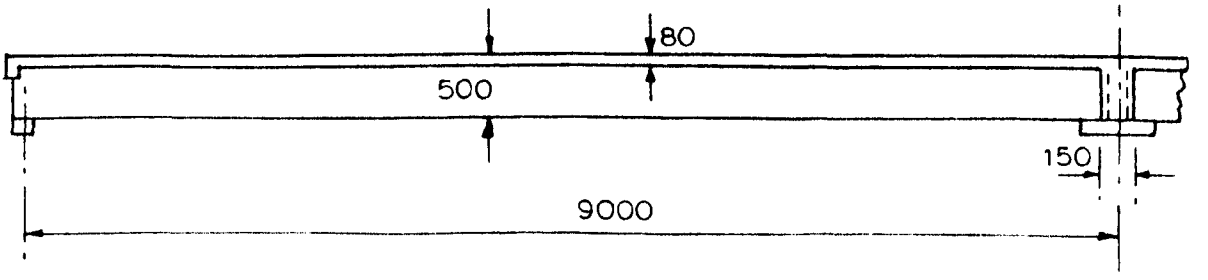

b) Longitudinal Section of Deck.

SCALE 1:50

FIGURE 7.8. HALF SCALE MODEL OF COMPOSITE PRESTRESSED r.c. BRIDGE DECK.

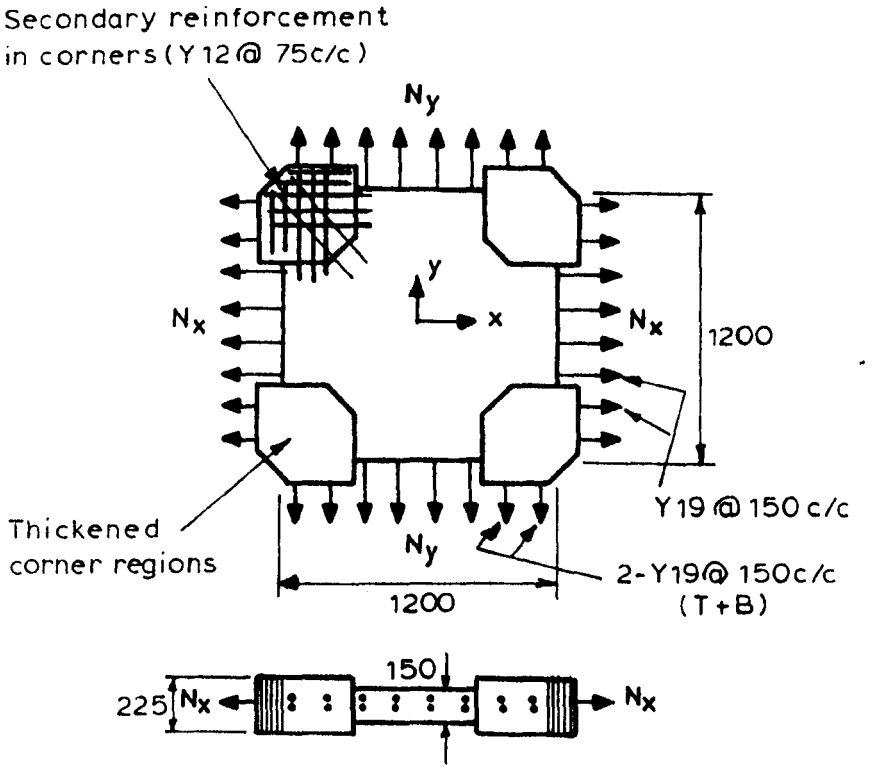

a) Detail of Biaxial Specimen and Tensile Loading.

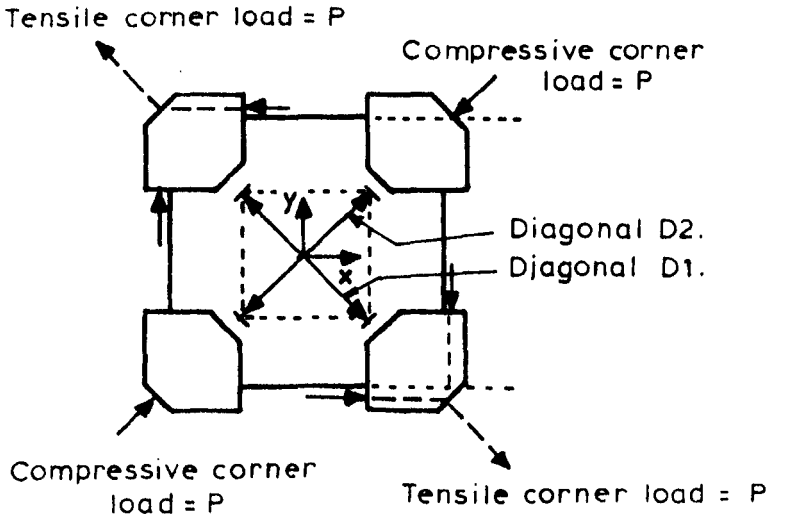

b) Shear Loading.

FIGURE 7.9. DETAILS OF TEST SPECIMEN AND LOADING.
[REF 37]

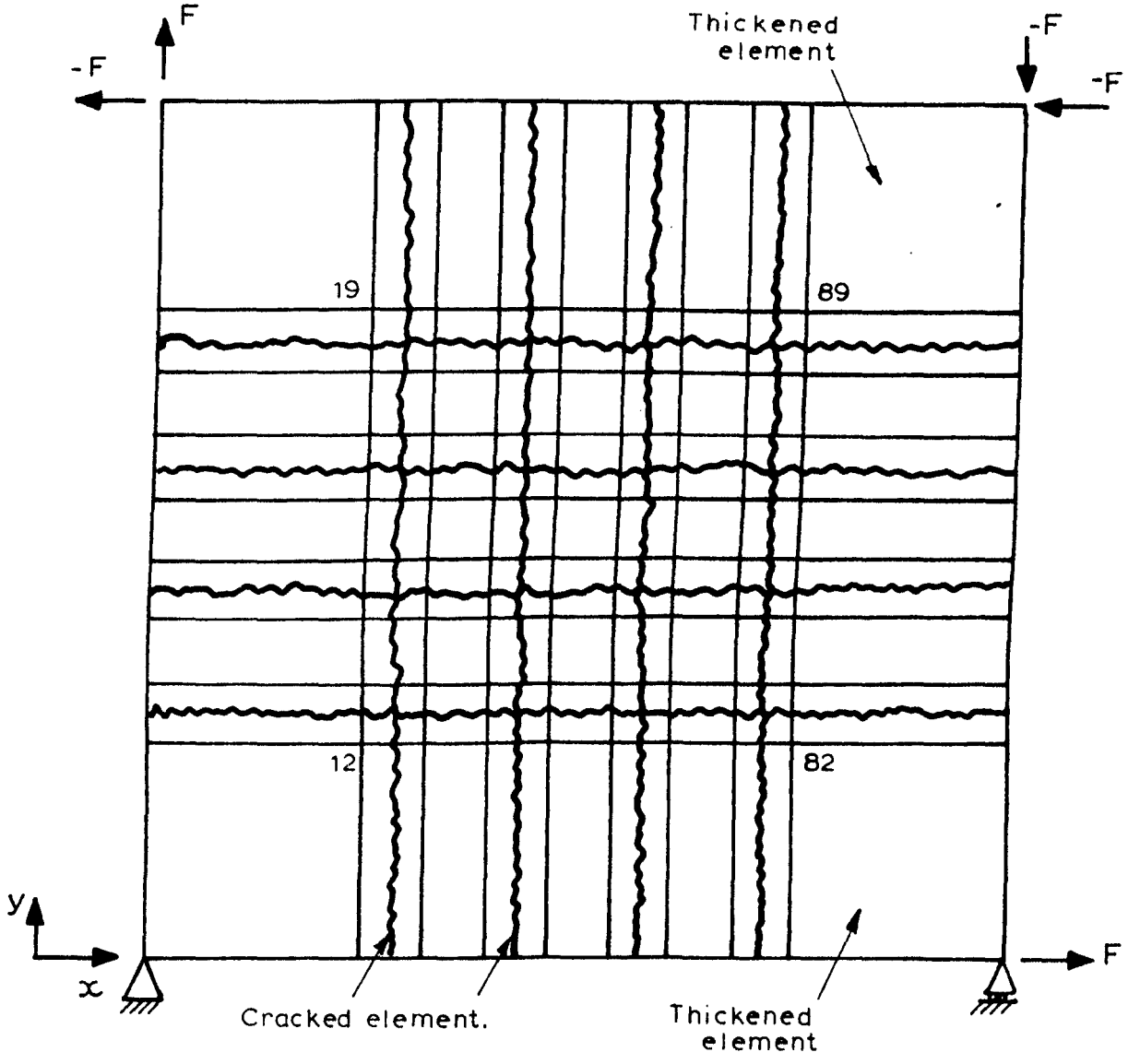

FIGURE 7.10. FINITE ELEMENT MODEL OF SLAB TESTED IN [37]

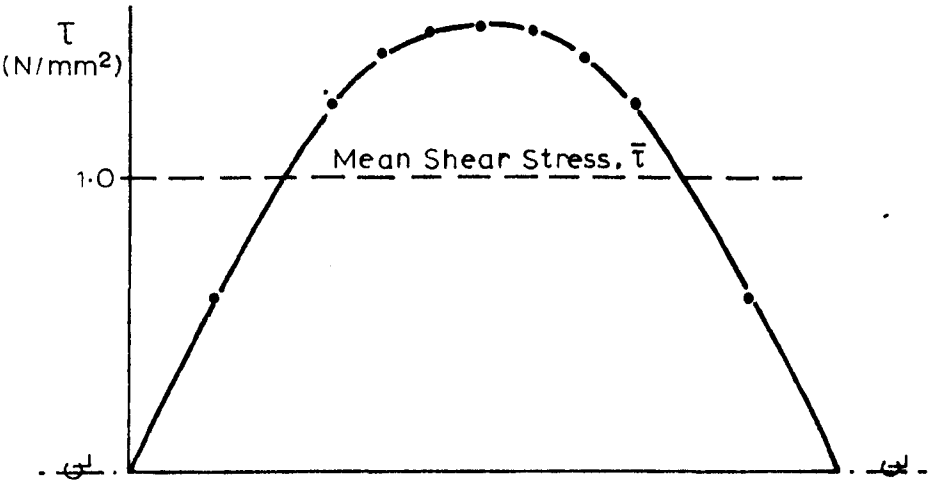

a) Uncracked slab.

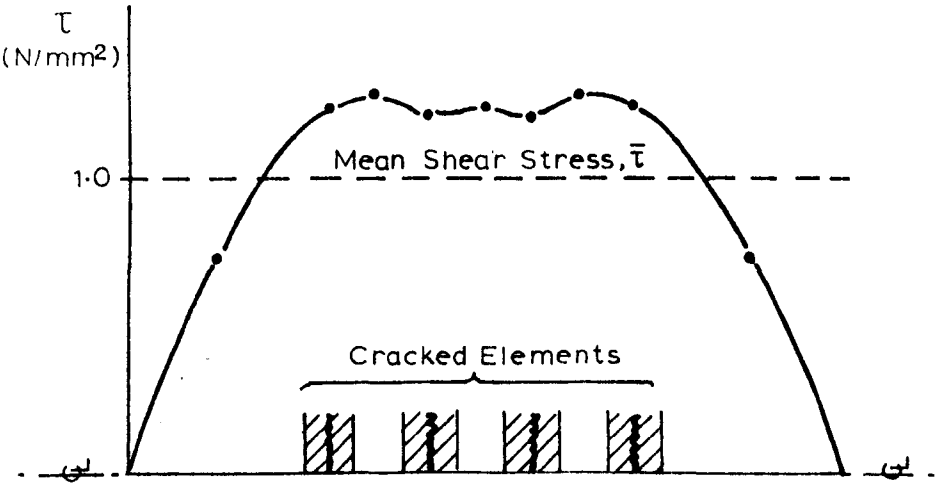

b) Cracked slab.

FIGURE 7.11. SHEAR STRESS DISTRIBUTION FROM F.E.ANALYSIS OF SLAB.

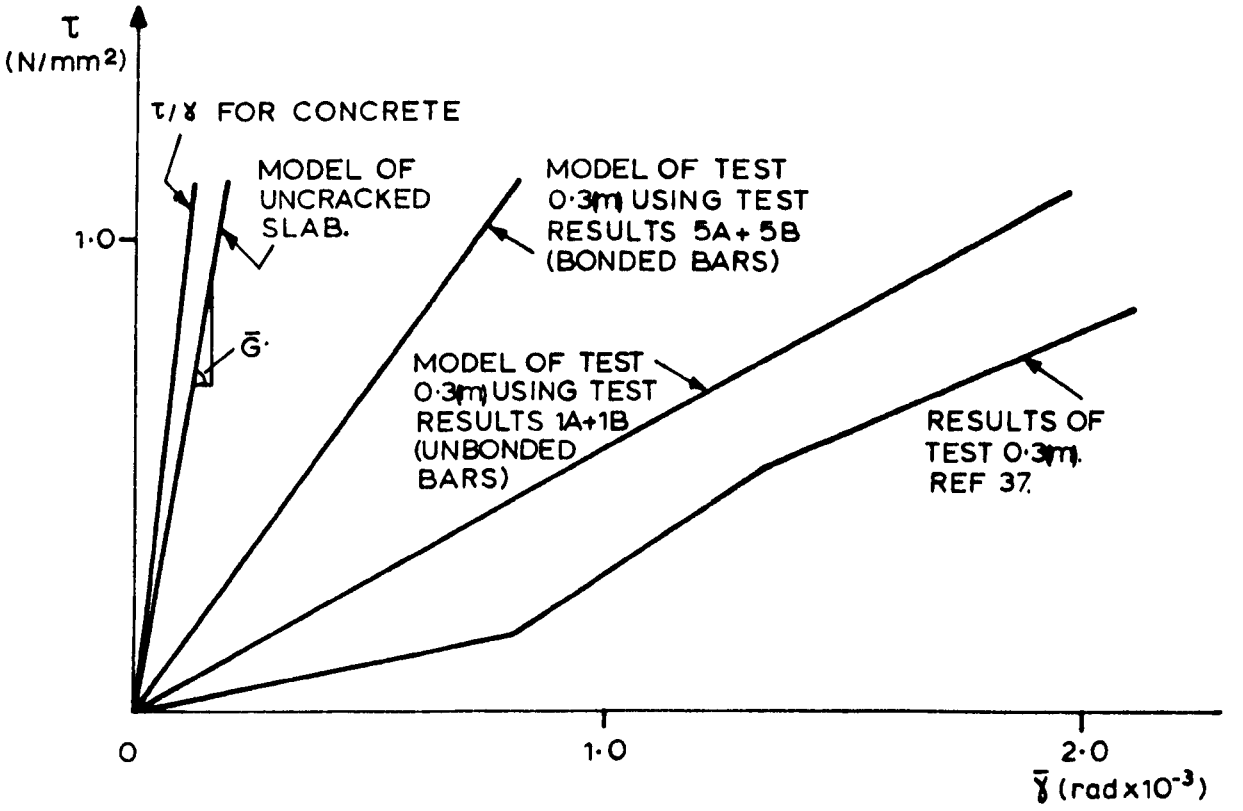

FIGURE 7.12. COMPARISON OF CORNER TEST 0·3(m) WITH FINITE ELEMENT MODEL USING WARWICK RESULTS.

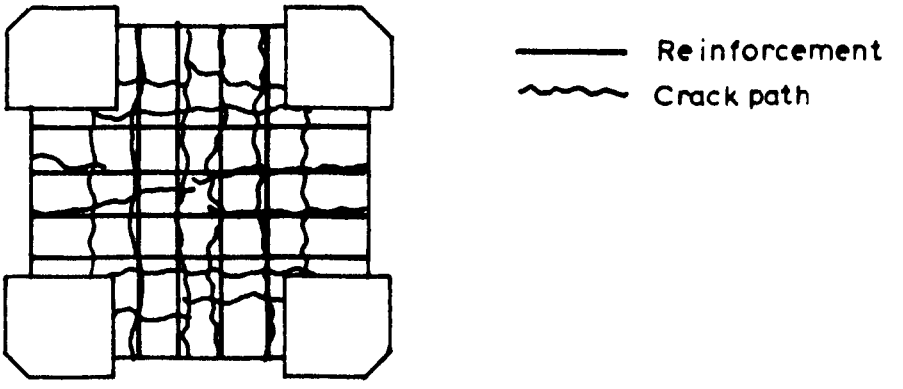

FIGURE 7.13. SPECIMEN 0·3(m): TENSILE LOADING ONLY.

CHAPTER EIGHT

SUMMARY CONCLUSIONS AND RECOMMENDATIONS

8.1 Introduction

There is very little existing information about the non linear behaviour of cracked reinforced concrete under shear loading. A study of the in-plane shear stiffness of reinforced concrete slab elements cracked in tension has been made. The results should allow a more accurate modelling of the behaviour of certain types of reinforced concrete structures to be carried out.

This research has been restricted to the study of a concrete element with a single crack passing orthogonal to the reinforcement. Secondary reinforcement parallel to the plane of cracking was not used. The internal mechanisms of aggregate interlock and dowel action were first examined separately and then the combined effect in reinforced concrete was studied. A detailed presentation of these tests appears in Chapters 3, 4 and 5, and a discussion of the results in Chapter 6. In this Chapter a precis of the important findings is given together with a discussion of the potential use of the results and recommendations for further research.

8.2 Aggregate interlock

The aggregate interlock tests were carried out on specimens which were cracked in direct tension, as might occur in a real structure. The test rig was designed so that the force normal to the plane of cracking could be controlled during shear loading. The shear loading was applied immediately adjacent to the tensile crack, so that shear failure of the uncracked part of the specimen was unlikely to occur. The following

points were observed.

(1) The results of the aggregate interlock tests were found to be repeatable and the trends observed had very little scatter.

(2) The aggregate interlock shear stiffness was found to decrease with increasing shear slip of the crack.

(3) Increasing the initial crack width causes a reduction in the overall shear stiffness and in the ultimate shear stress.

(4) When shear slip occurred there was always a tendency for the aggregate particles protruding across the crack to override and hence for the crack to widen.

(5) An increase in the direct stiffness of the specimen normal to the plane of cracking resulted in a reduction in the tendency of the crack to widen with shear slip. It also resulted in an increase in the shear stiffness and the ultimate shear stress of the cracked specimen.

(6) A change in the strength of the concrete from 35 N/mm^2 to 55 N/mm^2 did not result in any significant difference in the aggregate interlock behaviour.

(7) There was no significant difference in the mode of behaviour between specimens with small or large initial crack widths, other than that discussed above.

An important experimental consideration which became apparent in these

tests is the need to measure rather than to estimate the axial restraint to crack widening when debonded reinforcement is used in aggregate interlock tests. The bedding in effects at the ends of the reinforcement reduced the axial stiffness to up to 50% of the calculated value.

Several conceptual models for the aggregate interlock mechanism were considered. The shear friction model assumed that the two crack faces were rigid and hence shear slip could only occur if overriding of the crack faces also occurred. This model was rejected on the grounds that a realistic simulation of the crack face was too complex and that the predicted results provided a poor qualitative fit to the test results.

The two phase model proposed by Walraven (42) gave a much closer fit to the test results. This model considered concrete to consist of rigid spheres of aggregate, with a range of sizes and embedment depths, located in a softer cement paste. Shear slip caused both crushing of the cement paste and overriding of the crack faces. There were two important limitations to the validity of the model. The cement paste was assumed to be a perfectly rigid-plastic material, which is improbable. Secondly, contact between any two rigid aggregate particles protruding from opposite sides of the crack was not considered. In spite of these drawbacks the model predicted quite closely the non-linear shear stiffness of the aggregate interlock specimens and the tendency for the crack to widen as shear slip occurs.

8.3 Dowel action

The dowel action specimens were similar to the aggregate interlock

specimens and shear loading and axial tension was applied in the same way. This permitted a direct comparison between the test results and those from the aggregate interlock and the reinforced concrete tests.

The following trends were observed from the dowel action tests.

(1) The ultimate shear stress and the shear stiffness of the dowel action specimens was typically between 25% and 50% of those of aggregate interlock specimens.

(2) The shear stiffness of dowel action specimens decreased with increasing shear slip (cf 8.2 (2)).

(3) An increase in the diameter of the reinforcing bars resulted in a higher shear stiffness and ultimate shear stress.

(4) An increase in the initial crack width and hence the axial stress in the reinforcement, resulted in a decrease in the shear stiffness and the ultimate shear stress.

(5) Altering the strength of the concrete from 35 N/mm^2 to 55 N/mm^2 did not significantly influence the behaviour of the specimens (cf 8.2 (6)).

(6) Although the number of specimens tested was quite small, the experimental scatter in the test results was quite small and test results were repeatable.

Two models of the behaviour of the dowel action specimens were studied. The beam-on-an-elastic-foundations (b.e.f.) model has been used by

several researchers (34, 43, 47) to describe the behaviour of dowel bars. The main difficulty is in determining a foundation modulus to represent the stiffness of the concrete. This modulus will diminish as the concrete is damaged, either by shear displacement or axial extension of the reinforcement. The extent and effect of this damage is difficult to quantify. Using a typical value for the foundation modulus determined by Paulay (29), the b.e.f. model predicted quite closely the initial shear stiffnesses of the dowel action specimens. In the absence of further data it was decided not to modify the foundation modulus for the specimens under combined axial tension and shear loading.

It is probable that the crushing of the concrete beneath the reinforcement is too complex to be modelled exactly in a deterministic way. Any void or a hard spot immediately beneath the bar would have a large influence upon the failure of the concrete in compression (74). An exponential decay function was selected as a suitable empirical expression describing the behaviour of the dowel action specimens in the region between the initial response, predicted by the b.e.f. method, and the ultimate failure, obtained by plastic analysis (equation 6.5).

The b.e.f. model could not predict the behaviour of the dowel action specimens after damage to the concrete started to occur. The assumption was then made that ultimate failure occurred due to flexural yielding of the reinforcement at a point remote from the crack face. A plastic analysis provided a close estimate of the ultimate shear strength of dowel action specimens both with and without superimposed axial tension in the reinforcement. However, further tests are necessary to confirm the validity of this model.

The conditions under which the dowel action specimens were tested were probably more simple than would be encountered in a real structure. The model does not represent ultimate failure due to tensile splitting of the concrete. This is usually the mode of dowel failure in a beam and could also occur in other situations. Nor does the model represent the situation where the crack is not normal to the dowel reinforcement. This would be expected to produce a lower dowel stiffness if the crack were so oblique that the support to the reinforcement adjacent to the crack was reduced. The contribution of the axial force in the reinforcement to the shear stiffness across the crack would also need to be included (see Figure 1.1).

8.4 Reinforced concrete

The results of the reinforced concrete tests showed that the effects of local bond upon the behaviour of the cracked specimen under shear loading were substantial. Overriding of the crack faces caused tensile stresses in the reinforcement and hence a gradual breakdown in the local bond between the concrete and the reinforcement. This in turn caused a reduction in the normal stiffness restraining the crack from widening and hence in the shear stiffness due to aggregate interlock.

The strength of the concrete was also observed to affect the local bond. Hence the shear stiffness of reinforced concrete specimens was more sensitive to variations in the concrete strength than either the aggregate interlock specimens or the dowel action specimens.

It was thought initially that local bond would also affect the shear stiffness of the cracked reinforced concrete specimens by restraining the crack from widening adjacent to the reinforcement giving a

crack with varying width beneath the surface of the concrete. However, further investigation showed this not to be so. Both the reinforced concrete and aggregate interlock specimens had a uniform crack width. This result is not in agreement with the results of other research workers (22, 26, 27). The difference is thought to be due to the different types of deformed reinforcement used.

When the effects of local bond upon the stiffness normal to plane of cracking were taken into account, it was found that the stiffness in shear of a cracked reinforced concrete specimen could be predicted quite closely from the aggregate interlock and dowel action models discussed above. The ratio of crack widening to shear slip was also closely predicted.

This result differs from the results of similar tests conducted by Walraven (42). He inferred that an internal strut was present in reinforced concrete specimens which forced the crack to widen at a greater rate than would have been predicted from the basic aggregate interlock theory. This strut was also needed to balance the equilibrium of the internal stress resultants. It was suggested that this strut was provided by interlocking of crushed aggregate, visible adjacent to the crack and the reinforcement after testing.

In the current test series no evidence of an internal strut was seen. Nor did the test results suggest that a strut mechanism was operating. These differences in the observed test results may again be due to the effects of the different types of deformed reinforcement used.

8.5 Numerical modelling of cracked reinforced concrete structures

A smeared crack approach was adopted for modelling the effects of a crack when using the finite element method of analysis. The tendency of the crack to widen with shear slip was included by adding an off-diagonal term in the [D] matrix, relating the direct stress to the shear strain. This resulted in a stiffer overall structural behaviour and also gave a better modelling of the tensile stresses in the reinforcement. An empirical expression was derived for modelling the non-linear shear stiffness of the cracked element.

A slab tested under biaxial tension and subsequent shear loading (37) was selected and an attempt was made to model the behaviour of this slab using the results of the shear tests in specimens with a single tensile crack. This attempt was not very successful for two reasons. For mean shear stresses in excess of 1 N/mm^2 the shear deformation of the slab was accommodated by the formation of new diagonal shear cracks, and sliding across the original tensile cracks became insignificant. This mode of failure was not included in the finite element model and so the analysis was restricted to shear stress levels below 1 N/mm^2. The analysis still did not predict the behaviour of the slab very closely. This was attributed to the different behaviour resulting from testing a biaxially reinforced slab in biaxial tension, compared with that of a specimen reinforced in only one direction and tested in uniaxial tension. Biaxial tension in the slab caused cracks which tended to follow the lines of the reinforcement in both directions. The anchorage stiffness of this reinforcement was much less than in the specimens under uniaxial tension, where the reinforcement was embedded in uncracked concrete on either side of the main tensile crack. Hence the shear stiffness of the slab cracked in two orthogonal directions would be expected to

be less than calculated from the present shear tests. This was found to be so.

8.6 Recommendations for future research

An important question raised by this research is that of the effect of local bond between the reinforcement and the concrete upon the shear stiffness across a crack normal to the reinforcement. It was evident from the aggregate interlock tests that the stiffness normal to the crack, restraining it from widening, had a major influence on the aggregate interlock shear stiffness. This stiffness is usually provided by the reinforcement anchored into the concrete on each side of the crack. It has been shown in previous research (5, 69) that some deformed reinforcement under anchorage loading causes internal crack initiation at each reinforcement rib. Other types of deformed reinforcement tend to cause crushing of the concrete in front of the ribs or longitudinal splitting of the concrete. It has been recently shown (75) that the presence of transverse reinforcement can also influence the anchorage stiffness. In these tests it was apparent that some sliding of the concrete over the ribs was occurring. Until the nature of local bond and its effect upon the anchorage stiffness of the reinforcement are better understood, little further progress can be made on the study of shear across cracks in reinforced concrete.

A second question raised by the research concerns the width of a crack beneath the surface of the concrete. The uniform crack width observed in this study was not observed by other research workers (26, 27). However, little attention has been focussed on this topic and experimental results are sparse. As the aggregate interlock mechanism is sensitive to changes in the crack width, then any

variation in the crack width beneath the surface of the concrete is of prime importance. It is suspected that the local bond mechanism may influence the crack width profile as this would explain the differing findings. The precise relationship between the local bond mechanism, the type of deformed reinforcement used and the crack width profile is the subject of further study by the writer.

Another area of uncertainty concerns the relationship between local bond stresses, internal cracking and the internal strut mechanism reported in reference 42. No evidence of an internal strut was seen (section 8.4) in this study. It is suspected that this was because the type of deformed reinforcement used did not initiate "Goto type" (22) cracks at each reinforcement rib. Kanabar (68) repeated some of Goto's tests, using the same type of deformed reinforcement used in this study, but was unable to find local bond cracks initiated by each reinforcement rib. This finding supports the hypothesis but the topic needs further study to reach a conclusive result.

Finally, the study of shear transfer across cracks in reinforced concrete needs extending to include more complex situations such as cracking oblique to the reinforcement, cracks and/or reinforcement in two directions and the possibility of additional diagonal shear cracking, before the results can be used to predict the expected behaviour of real structures.

REFERENCES

1. Liu, T. Y. C., Nilson, A. H. and Slate, F. O., "Biaxial stress-strain relations for concrete", Jnl. Struc. Div., A.S.C.E., May 1972, pp. 1025-1034

2. Cedolin, L., Crutzen, Y. R. J. and Dei Poli, S., "Triaxial stress-strain relationship for concrete", Jnl. Mech. Div., A.S.C.E., June 1977, pp. 423-439

3. Kotsovos, M. D. and Newman, J. B., "A mathematical description of the deformational behaviour of concrete under complex loading", Mag. of Conc. Res., Vol. 31, No. 107, June 1979, pp. 77-90

4. Gambarova, P. G. and Karakoc, C., "Shear confinement interaction at the bar to concrete interface", Proc. Int. Conf. on Bond in Concrete, Paisley College of Tech., June 1982, pp. 82-96

5. Lutz, L. A. and Gergely, P., "Mechanics of bond and slip of deformed bars in concrete", Jnl. A.C.I., Nov. 1967, pp. 711-721

6. Taylor, H. P. J., "Investigation of the forces carried across cracks in reinforced concrete beams in shear by the interlock of aggregate", C. & C.A. Tech. Rep. 42.447, November 1970

7. Beeby, A. W., "The prediction of crack widths in hardened concrete", The Structural Engineer, Vol. 57A, Jan. 1979, pp. 9-17

8. Broms, B. B. and Lutz, L. A., "Effects of arrangement of reinforcement on crack width and spacing of reinforced concrete members", Jnl. A.C.I., Nov. 1965, pp. 1395-1409

9. Ngo , D. and Scordelis, A. C., "Finite element analysis of reinforced concrete beams", Jnl. A.C.I., Vol. 64, No. 3, Mar. 1967, pp. 152-163

10. Houde, J., "Study of force-displacement relationships for the finite element analysis of reinforced concrete", Ph.D. thesis, McGill University, Montreal, Canada, 1973

11. Nilson, A. H., "Non-linear analysis of reinforced concrete by the finite element method", Jnl. A.C.I., Sept. 1968, pp. 757-766

12. Gergely, P. and White, R. N., "Advanced mechanics of reinforced concrete - applications and experimental verifications", I.A.B.S.E. Colloquium, Delft 1981, Introductory report, pp. 109-135

13. Isenberg, J. and Adham, S., "Analysis of orthotropic reinforced concrete structures", Jnl. Struc. Div., A.S.C.E., Dec. 1970, pp. 2607-2624

14. Lin, C. S. and Scordelis, A. C., "Non-linear analysis of r.c. shells of general form", Jnl. Struc. Div., A.S.C.E., Mar. 1975, pp. 523-538

15. Hand, F. R., Pecknold, D. A. and Schnobrich, W. C., "Non linear layered analysis of plates and shells", Jnl. Struc. Div., A.S.C.E., July 1975, pp. 1491-1505

16. Bresler, B. and Bertero, V., "Behaviour of Reinforced Concrete under Repeated Load", Jnl. Struc. Div., A.S.C.E, June 1968, pp. 1567-1590

17. Clough, R. W. and Rashid, Y., "Finite Element Analysis of Axi-symmetric Solids", Jnl. Mech. Div., A.S.C.E., Feb. 1968, pp. 71-85

18. Nilson, A. H., "Internal Measurement of Bond Slip", Jnl. A.C.I., July 1972, pp. 439-441

19. Houde, J. and Mirza, M. S., "A finite element analysis of thé shear strength of reinforced concrete beams", A.C.I. SP42-5, "Shear in reinforced concrete", Vol. 1, 1974

20. Mirza, M. S. and Houde, J., "A study of the bond stress-slip relationship in reinforced concrete", Jnl. A.C.I., Jan. 1979, pp. 19-46

21. Clark, L. A. and Speirs, D. M., "Tension stiffening in reinforced concrete beams and slabs under short term loads", C. & C.A. Tech. Rep. 42.521, July 1978

22. Goto, Y., "Cracks formed in concrete around deformed tension bars", Jnl. A.C.I., Apr. 1971, pp. 244-251

23. Soretz, S. and Hölzenbein, H., "Influence of rib dimensions of reinforcing bars on bond and bendability", Jnl. A.C.I., Jan. 1979, pp. 111-125

24. Martin, H., "Zusammenhang zwischen oberflächenbeschaffenheit, verbund und sprengwirkung von bewehrrungsstählen unter kurzzeitbelastung", Deutscher Ausschuss für stahlbeton, Heft 228, Berlin 1973

25. Schiessl, P., "Beschränkung der rissbreiten bei zwangsbearrspruchung", Betonwerk & fertigteiltechnik, Heft 6/1976

26. Broms, B. B., "Technique for investigation of internal cracks in reinforced concrete members", Jnl. A.C.I., Jan. 1965, pp. 35-43

27. Illston, J. M. and Stevens, R. F., "Discussion of 'Cracks formed in concrete around deformed tension bars' by Y. Goto", Jnl. A.C.I., Oct. 1971, pp. 798-799

28. Johnson, R. P., "Discussion of 'The prediction of crack widths in hardened concrete' by A. W. Beeby", The Structural Engineer, Vol. 58A, No. 10, Oct. 1980, pp. 326-332

29. Paulay, T., Park, R. and Phillips, M. H., "Horizontal construction joints in cast-in-place reinforced concrete", A.C.I. SP42, "Shear in reinforced concrete", Vol. 2, 1974, pp. 599-616

30. Johansen, K. W., "Yield-line theory", Cement and Concrete Association, London, 1962, pp. 181

31. Wood, R. H., "Plastic and elastic design of slabs and plates", Thames and Hudson, London 1961, pp. 344

32. Kwiecinski, M. W., "Yield Criterion for initially isotropic reinforced concrete slabs", Magazine of Concrete Research, Vol. 17, No. 51, June 1965, pp. 97-100

33. Prince, M. R. and Kemp, K. O., "A new approach to the yield criterion for isotropically reinforced concrete slabs", Magazine of Concrete Research, Vol. 20, No. 62, Mar. 1968, pp. 13-20

34. Mills, G. M., "A partial kinking criterion for reinforced concrete slabs", Magazine of Concrete Research, Vol. 27, No. 90, Mar. 1975, pp. 13-22

35. Morley, C. T., "Experiments on the distortion of steel bars across cracks in reinforced concrete slabs", Magazine of Concrete Research, Vol. 18, No. 54, Mar. 1966, pp. 25-34

36. Friberg, B. F., "Design of dowels in transverse joints of concrete pavements", Transactions, A.S.C.E., Vol. 105, 1940, pp. 1809-1828

37. Jimenez, R., Gergely, P. and White, R. N., "Shear transfer across cracks in reinforced concrete", Cornell Univ. Rep. 78-4, Aug. 1978

38. Stanton, J. F., "An investigation of dowel action of the reinforcement of nuclear containment vessels and their non-linear dynamic response to earthquake loads", M.Sc. thesis, Cornell Univ., Jan. 1977

39. Krefield, W. J. and Thurston, C. W., "Contribution of longitudinal steel to shear resistance of reinforced concrete beams", Jnl. A.C.I., Vol. 63, Mar. 1966, pp. 325-344

40. Taylor, H. P. J., "Investigation of the dowel shear forces carried by the tensile steel in reinforced concrete beams", C. & C.A. TRA.431, Nov. 1969

41. Fenwick, R. C. and Paulay, T., "Mechanisms of shear resistance of concrete beams", Jnl. Struc. Div., A.S.C.E., Oct. 1968, pp. 2325-2350

42. Walraven, J. C., "Aggregate interlock : a theoretical and experimental analysis", Delft University Press, 1980

43. Dulacska, H., "Dowel action of reinforcement crossing cracks in concrete", Jnl. A.C.I., Dec. 1972, pp. 754-757, Digest paper and supplement

44. Dulácskáné, S. I., "A vasbeton repedésein áthaladó acélbetétek ékhátasa", Különlenyomat az Épités, Epiteszettudomány 3, Kötet 1, Számából, Budapest 1971

45. Den Hartog, J. P., "Advanced strength of materials", McGraw-Hill, New York, 1952

46. Elleiot, A. F., "An experimental investigation of shear transfer across cracks in reinforced concrete", M.Sc. thesis, Cornell Univ., June 1974

47. Rasmussen, B. H., "Strength of transversely loaded bolts and dowels cast into concrete", Laboratoriet for Bygningsstatik, Den. Tecn. Høskole, Meddelelee, Vol. 34, No. 2, 1962 (in Danish)

48. White, R. N. and Gergely, P., "Shear transfer in thick walled reinforced concrete structures under seismic loading", Report No. 75-10, Cornell Univ., N.Y., 1975

49. Cope, R. J., Rao, P. V. and Norris, P., "Modelling of reinforced concrete behaviour for finite element analysis of bridge slabs", Numerical methods for non-linear problems, Vol. 1, Proc. Int. Conf., Swansea, 1980, pp. 458-470

50. Paulay, T. and Loeber, P. J., "Shear transfer by aggregate interlock", A.C.I., SP-42, "Shear in reinforced concrete", 1974, Vol. 1, pp. 1-16

51. Bazant, Z. P. and Tsubaki, T., "Slip dilatancy model for cracked reinforced concrete", Jnl. Struc. Div. A.S.C.E., Sept. 1980, pp. 1947-1966

52. White, R. N. and Holley, M. J., "Experimental studies on membrane shear transfer", Jnl. Struc. Div., A.S.C.E., Aug. 1972, pp. 1838-1852

53. Laible, J. P., White, R. N. and Gergely, P., "Experimental investigation of seismic shear transfer across cracks in concrete containment vessels", A.C.I., SP-53, "Reinforced concrete in seismic zones", 1977, pp. 203-226

54. Fardis, M. N. and Buyukozturk, O., "Shear transfer model for reinforced concrete", Jnl. Mech. Div., A.S.C.E., Apr. 1979, pp. 255-275

55. Birkeland, P. W. and Birkeland, H. W., "Connections in precast concrete constructions", Jnl. A.C.I., Vol. 63, No. 3, Mar. 1966, pp. 345-368

56. Hofbeck, J. A., Ibrahim, I. O. and Mattock, A. H., "Shear transfer in reinforced concrete", Jnl. A.C.I., Feb. 1969, pp. 119-128

57. Mattock, A. H. and Hawkins, N. M., "Shear transfer in reinforced concrete - recent research", Jnl. P.C.I., Mar./Apr. 1972, pp. 55-75

58. Mattock, A. H., "Effect of moment and tension across the shear plane on single direction shear transfer strength in monolithic concrete", Report SM 74-3, Dept. of Civil Engineering, Univ. of Washington, U.S.A., Oct. 1974

59. Mattock, A. H., "Effect of aggregate type on single direction shear transfer strength in monolithic concrete", Report SM 74-2, Dept. of Civil Engineering, Univ. of Washington, U.S.A., Aug. 1974

60. Mattock, A. H., "Effect of Reinforcing Bar Size on Shear Transfer across a Crack in Concrete", Report SM 77-2, Dept. of Civil Engineering, Univ. of Washington, U.S.A., Sept. 1977

61. Cambell-Allen and Lau, "Cracks in concrete bridge decks", University of Sydney, Research Report 313, 1978

62. Oehlers, D. J., "Stud shear connectors for composite beams", Ph.D. thesis, Univ. of Warwick, Sept. 1980

63. Desayi, P. and Krishnan, S., "Equation for the stress-strain curve of concrete", Jnl. A.C.I., Vol. 61, No. 3, Mar. 1964, pp. 345-350

64. Perdikaris, P. C., White, R. N., Gergely, P., "Strength and stiffness of tensioned reinforced concrete panels subjected to membrane shear", NUREG/CR-1602, Dept. of Struct. Eng., Univ. of Cornell, July 1980

65. Millard, S. G., "Shear stiffness of cracked reinforced concrete", Internal report 4, Univ. of Warwick, Sept. 1980

66. Oehlers, D. J., "Stud shear connectors for composite beams", Ph.D. thesis, Univ. of Warwick, Mar. 1980

67. Kriz, L. B. and Raths, C. H., "Connections in precast concrete structures - Strength of Corbels", Jnl. P.C.I., Vol. 10, p.16, 1965

68. Kanabar, S. N., "Investigation of internal crack initiation in reinforced concrete", Final year undergraduate project, Univ. of Warwick, 1980

69. Skorobogatov, S. M. and Edwards, A. D., "The influence of the geometry of deformed steel bars on their bond strength in concrete", Proc. I.C.E., Part 2, Vol. 67, June 1979, pp. 327-339

70. Irons, B. M. and Ahmad, S., "Techniques of finite elements", Ellis Horwood, Chichester, 1980

71. Cook, R. D., "Concepts and applications of finite element analysis", Pub. John Wiley & Sons, Inc., 1974

72. Zienkiewicz, O. C., "The finite element method", Pub. McGraw-Hill, 1974

73. Gilbert, R. I. and Warner, R. F., "Tension stiffening in reinforced concrete slabs", Jnl. Struc. Div. A.S.C.E., Dec. 1976, pp. 1885-1900

74. Johnson, R. P. and Oehlers, D. J., "Analysis and design for longitudinal shear in composite T-beams", Proc. I.C.E., Part 2, Vol. 71, Dec. 1981

75. Reynolds, G. C., "Bond strength of deformed bars in tension", C. & C.A., Tech. Rep. 548, May 1982

76. Ford, H. and Alexander, J., "Advanced mechanics of materials", 2nd Edition, Part 4, Ellis Horwood Ltd, 1977

77. Roark, R. J. and Young, W. C., "Formulas for stress and strain", 5th edition, McGraw-Hill, 1975

78. Cedolin, L. and Dei Poli, S., "Finite element studies of shear cirtical r.c. beams", Jnl. Eng. Mech. Div. A.S.C.E., June 1977, pp. 395-410

APPENDIX A1

Analysis of the distribution of stresses within the specimen

A1.1 The model

A finite element analysis of the test specimen was carried out for the following reasons:-

1. To gain expertise in the use of finite elements.

2. To determine why premature failure of the bonded end plates was occurring during tensile loading and hence to resolve this problem.

3. To estimate the shear stress distribution across the crack under shear loading.

The type of finite element initially adopted was the three node, triangular, plane stress element. This element can only model a uniform strain distribution within each element and hence the solution obtained is coarse and sometimes erratic. However its advantages are that it is easy to use and lends itself readily to mesh grading, so that a finer element mesh, giving a more accurate solution can be used in regions where a high stress concentration is expected.

The concrete was assumed to be elastic, homogeneous and isotropic and at this stage the effects of the reinforcement were ignored.

A1.2 Tensile loading

In the early aggregate interlock tests it was found that in spite of meticulous surface preparation and bonding of the steel plates onto

the ends of the specimen, one of the plates would break off under tensile loading, before cracking occurred at the centre of the specimen. It was decided that this was probably due to inadequate flexural stiffness of the steel plates and a finite element analysis was carried out to determine the effects of stiffening the plates.

Figure A1.1 shows the element mesh with smaller elements adjacent to the end plates and the centre region than elsewhere. The central line of elements was given a reduced thickness and the edge elements in this region were given a stiffness close to zero to model the crack initiating slot. It was realised that this would not model the stress concentrations produced by the slot in the immediate vicinity, but it should model the effects of the reduced section at the centre of the specimen upon the stresses at the ends.

The stress distribution produced in the original specimen shows (Figure A1.2) that stress concentrations of up to five times the mean stress occurred at the ends of the specimen due to flexure of the steel end plates. This was particularly noticeable with the larger end plate because, although it was much stiffer, the load was applied to the cantilever tips rather than in the centre region. This correlated with the experimental observation that it was usually the larger end plate which became detached. It was clear from observation of the failure surface that this detachment was due to excessive stresses in the concrete rather than a bond failure of the adhesive.

A similar analysis was then carried out to determine the effects of stiffening the end plates. This stiffening had to be done in a way which would not interfere with the existing test rig fittings. This

was accomplished by welding two box sections to the larger end plate and a channel section to the smaller end plate (Figure A1.3). This caused an increase in the second moment of area of six and seven times respectively.

The results of the second analysis, using these increased stiffnesses, (Figure A1.4) showed that the stresses at the edges of the larger end plate were reduced by a factor of two. The stresses at the other end were also much nearer to uniformity. When the end plates were stiffened in this way, no further problems with premature detachment were encountered in the tests.

A1.3 Shear loading

A finite element analysis was then carried out to determine what the shear stress distribution across the crack face was during shear loading. Initially it was assumed that the concrete was uncracked. The element mesh and loading arrangement are shown in Figure A1.5. The results of this analysis (Figure A1.6) showed a non-uniform shear stress distribution around the centre of the specimen.

This shear stress distribution was compared with an analytical result using the Boussinesq equation. The shear stress produced in a semi-infinite membrane of unit thickness by a concentrated point load P is given (76) by

$$\tau_{xy} = \frac{2\rho}{\pi} \frac{xy}{(x^2 + y^2)^2} \qquad (1)$$

where x and y are the lateral and vertical distances from the point of application of the load to the point of interest. The two point loads nearest to the centre of the specimens cause the shear stress distributions shown in Figures A1.7a and A1.7b. If these figures

are summed, the result is very similar to that given by the finite element analysis. Although it is realised that this is not a rigorous validation of the analysis, it nevertheless confirms that the solution given by the finite element analysis is a reasonable one.

The presence of a crack in the centre of the specimen was then modelled by formulating a new element mesh (Figure A1.8) with a central row of elements simulating the crack. By this stage an automatic mesh generator had been developed to simplify the data input. The shear stiffness of the central row of cracked elements was then reduced until the displacement of the point loads adjacent to the crack was similar to that observed during shear tests. This was achieved when a shear modulus of $G_o/100$ was used for the central row of elements.

From the results of this analysis it was found that the shear stresses in all of the central elements was within ± 2% of the mean shear stress i.e. a uniform shear stress distribution was obtained. This result was consistent with the measurements of shear slip across the crack taken during shear tests. On the early aggregate interlock tests the shear slip was measured at three different locations but the three readings were always the same.

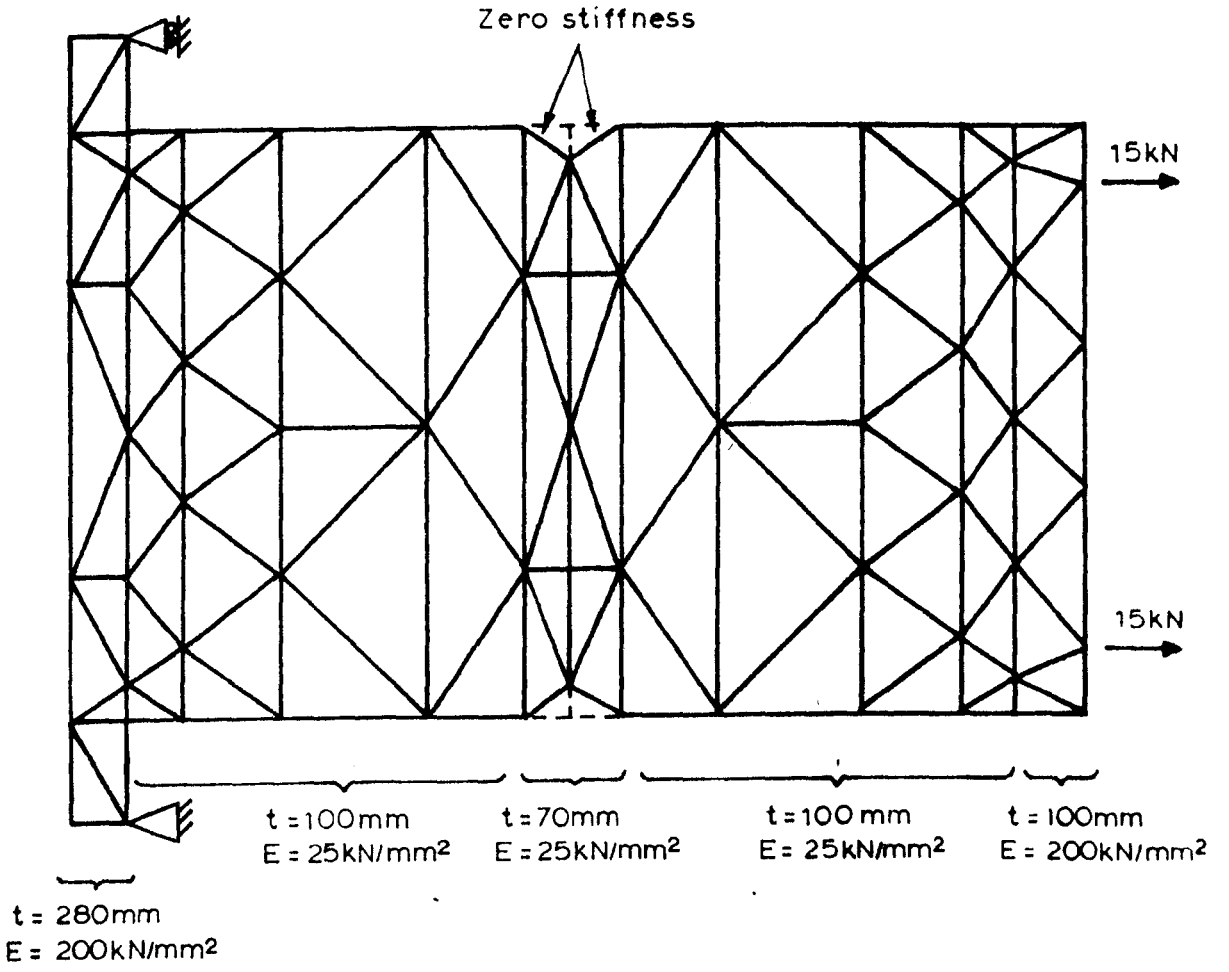

FIGURE A1. 1. ELEMENT MESH.

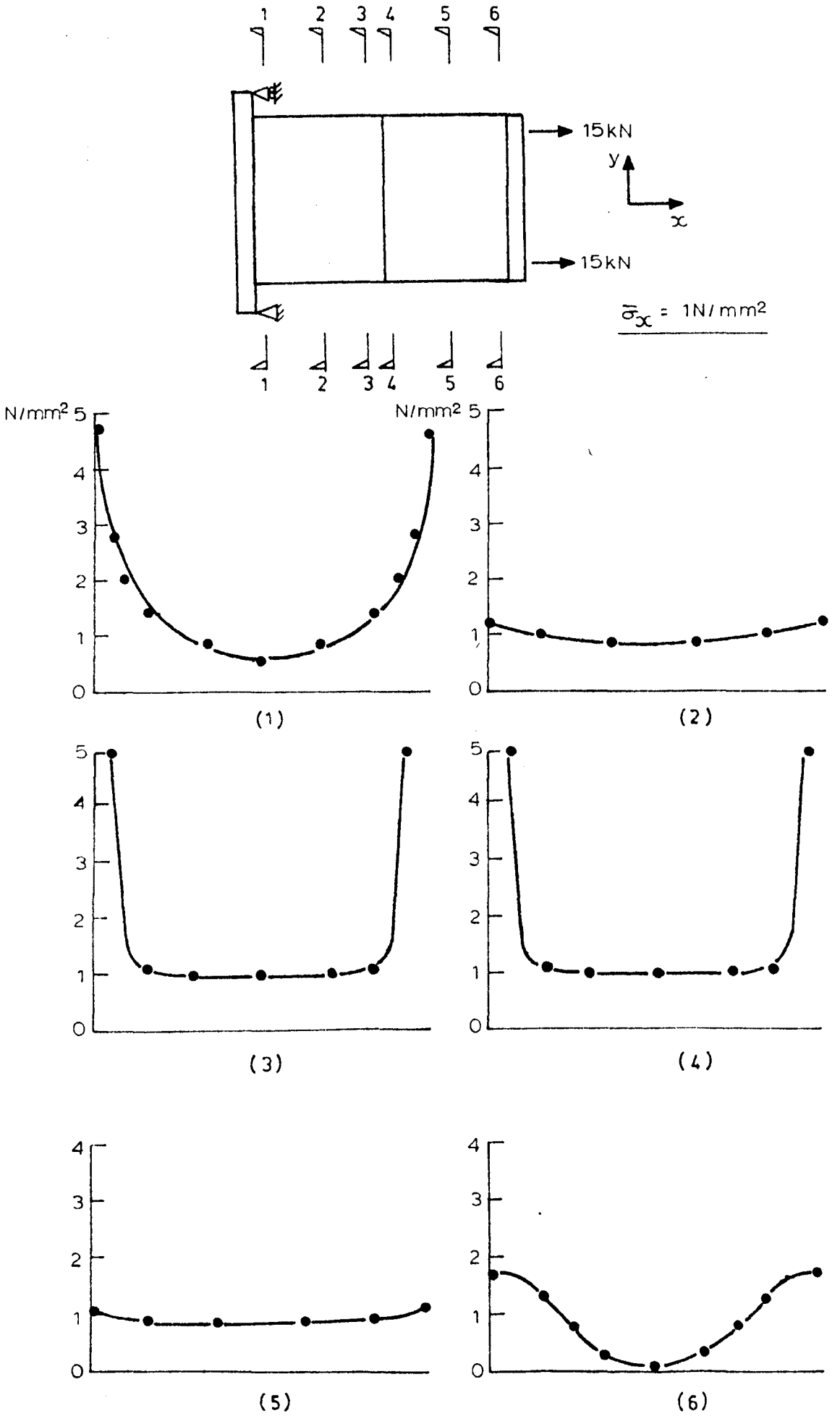

FIGURE A1.2. DISTRIBUTION OF TENSILE STRESS, σ_x, IN SPECIMEN WITH UNSTIFFENED END PLATES.

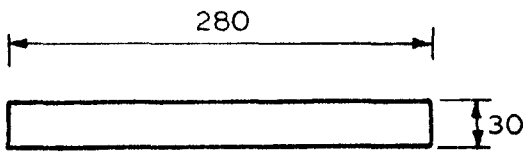

$I_{xx} = 0{\cdot}68 \times 10^6 mm^2$

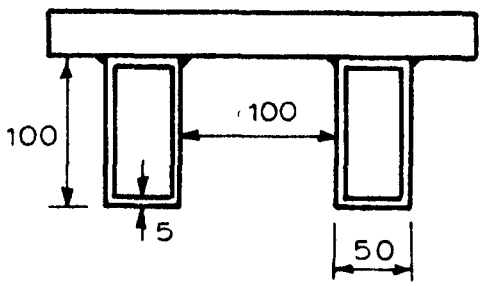

$I_{xx} = 4{\cdot}2 \times 10^6 mm^4$

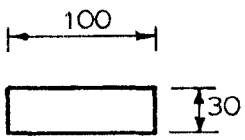

$I_{xx} = 0{\cdot}23 \times 10^6 mm^4$

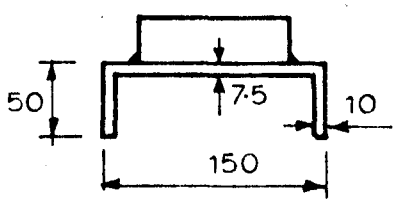

$I_{xx} = 1{\cdot}7 \times 10^6 mm^4$

a) Original plates.

b) Stiffened plates.

FIGURE A1.3. DETAILS OF END PLATES.

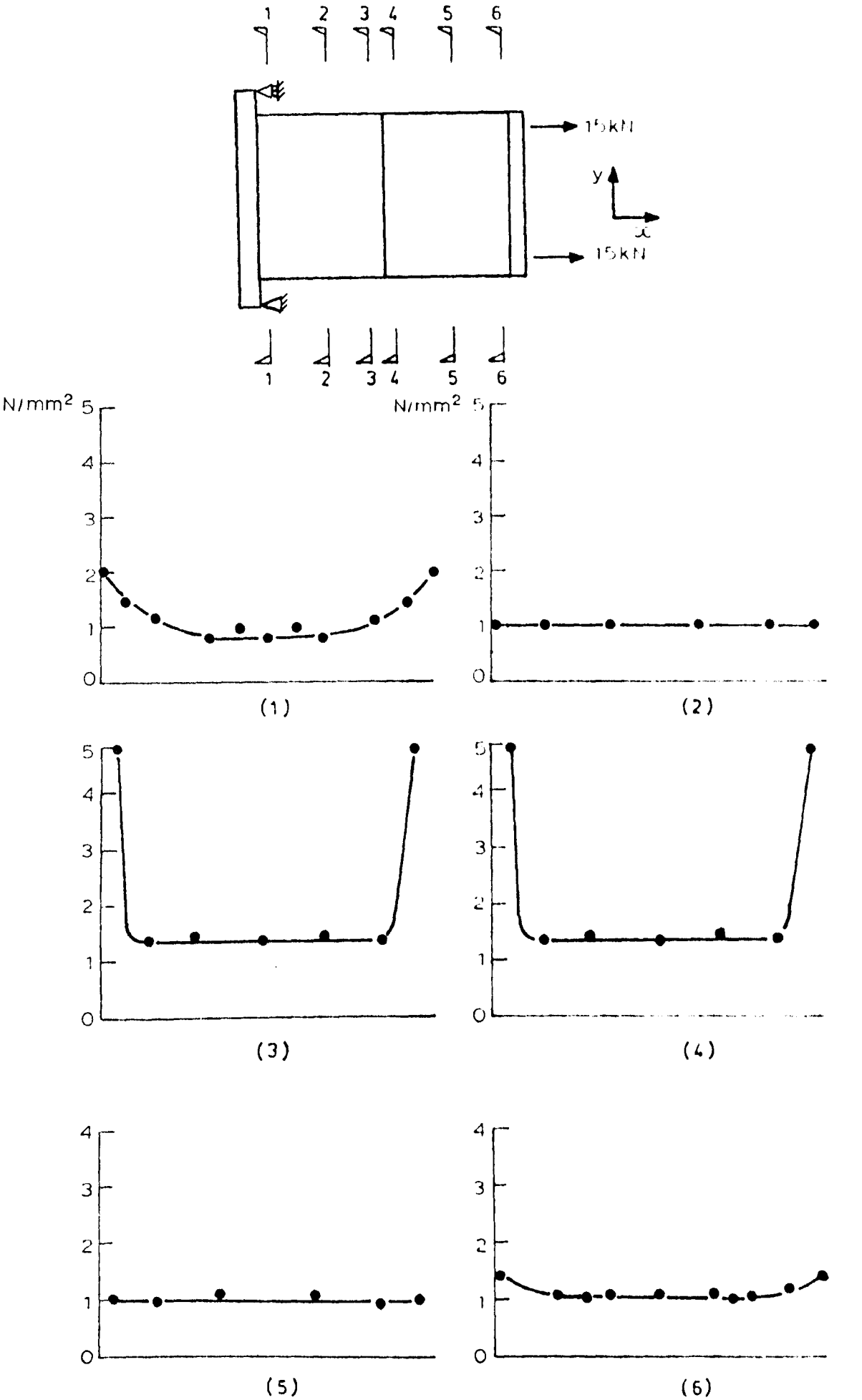

FIGURE A1.4. DISTRIBUTION OF TENSILE STRESS, σ_x, IN SPECIMEN WITH STIFFENED END PLATES.

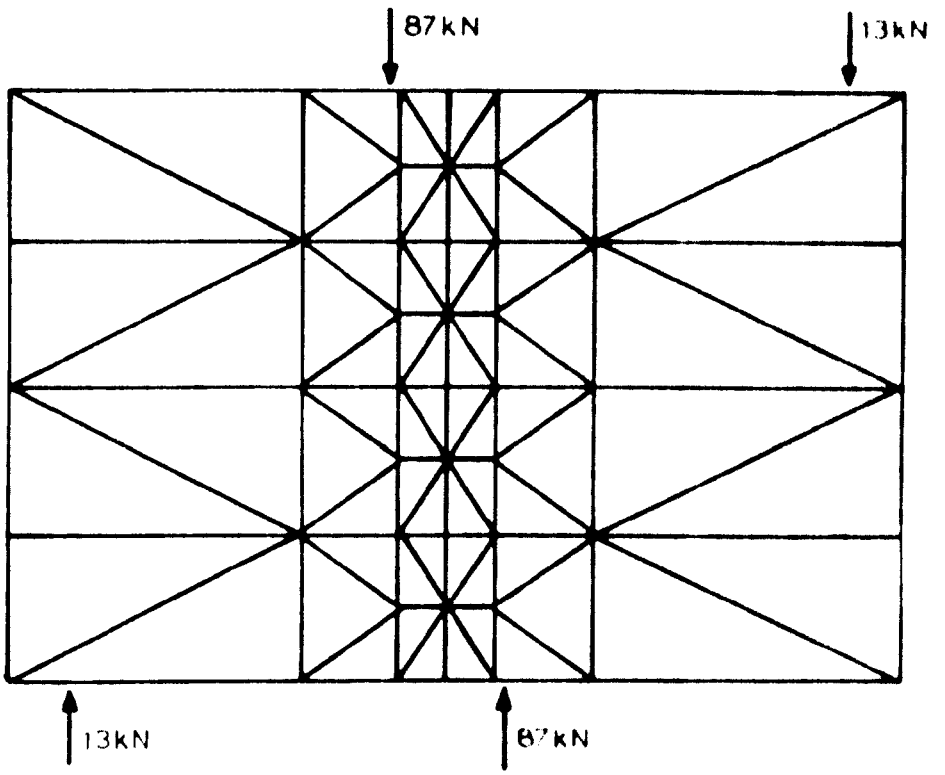

FIGURE A1. 5. ELEMENT MESH AND SHEAR LOADING ARRANGEMENT.

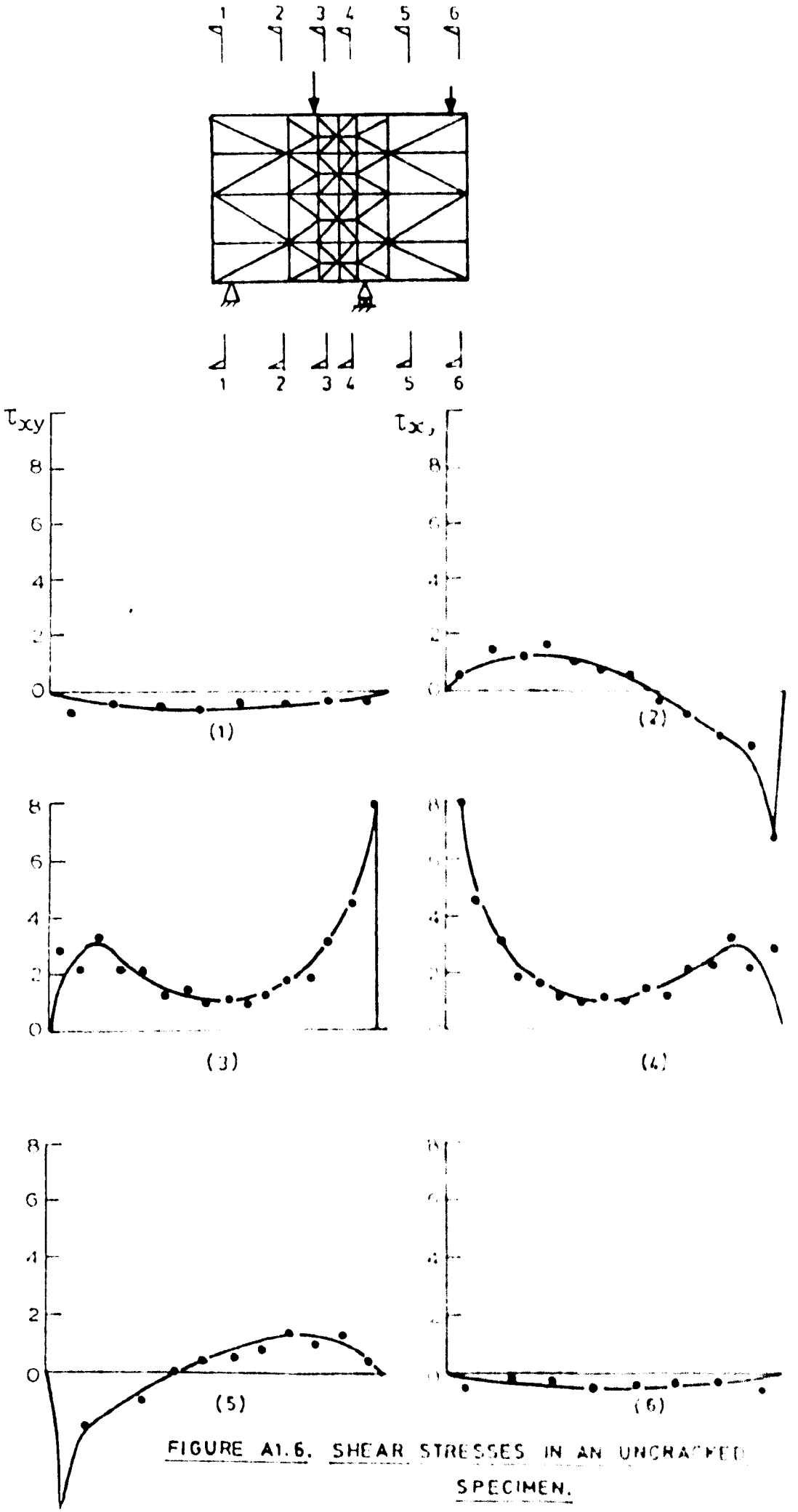

FIGURE A1.6. SHEAR STRESSES IN AN UNCRACKED SPECIMEN.

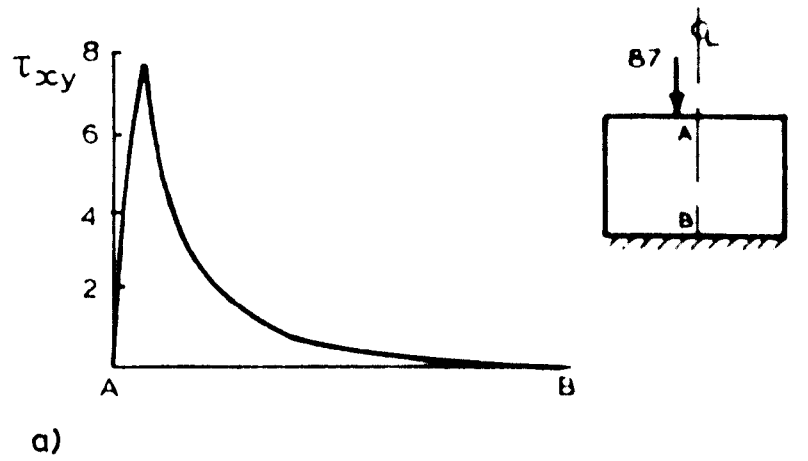

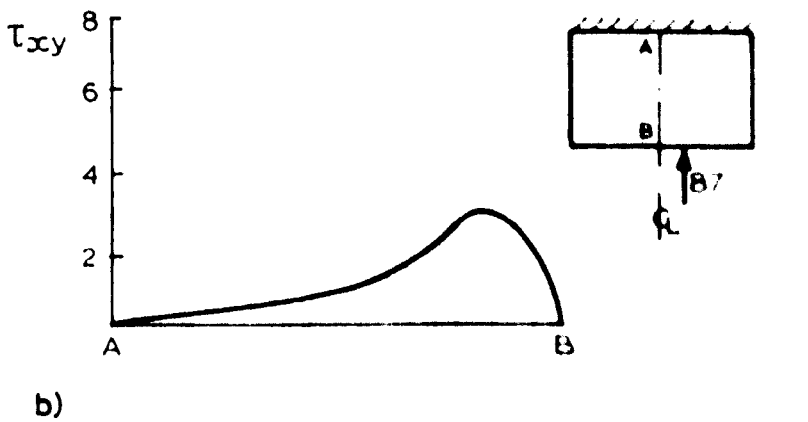

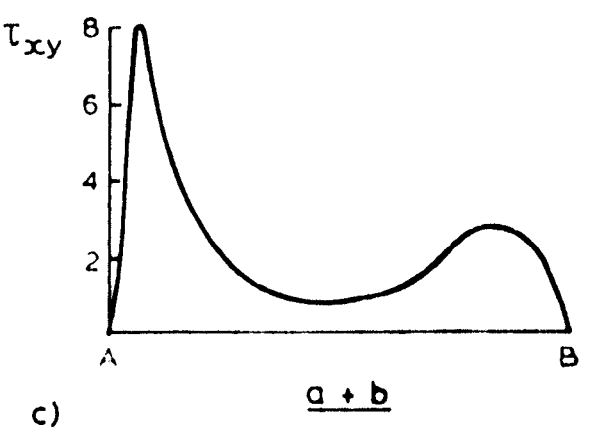

FIGURE A1.7. BOUSSINESQ SOLUTION FOR CONCENTRATED LOADS.

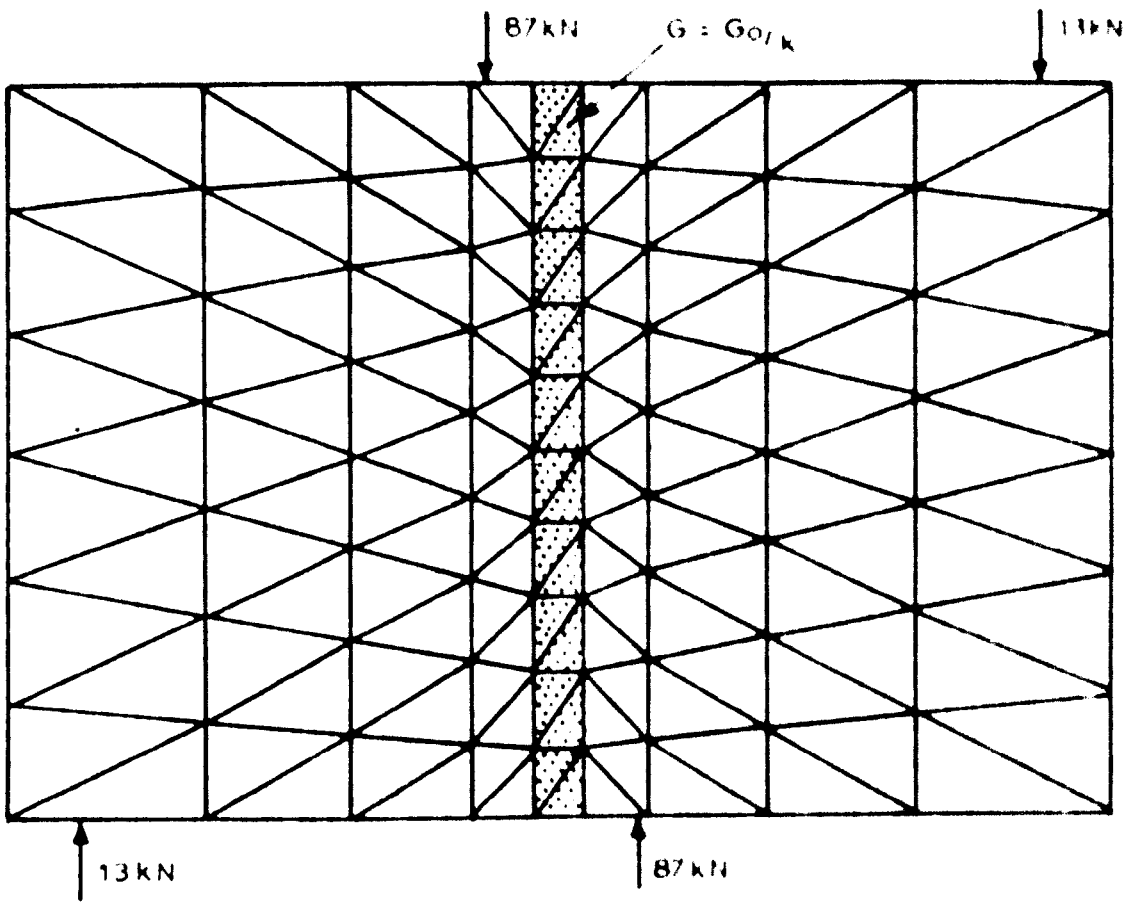

FIGURE A1.8. MODELLING OF A CENTRAL CRACK

APPENDIX A2

The ultimate flexural capacity of a circular prism

A2.1 Simple bending

Under bending, without any resultant axial forces, it can be shown that a prism with an ultimate yield stress of σ_y will have a moment capacity, M_p given by

$$M_p = \frac{1}{6} \phi^3 \sigma_y \qquad \text{(see Figure A2.1)}$$

A2.2 Bending with axial loading

The ultimate bending moment of a circular prism under concurrent axial loading can be determined by considering different areas of the section to be carrying the different types of loading (Figure A2.2).

Hence if the applied tensile load is F_1, the mean axial stress over the entire section, σ_s is given by

$$\sigma_s = k \sigma_y \qquad \text{where } 0 < k < 1$$

$$\text{hence } A_1 = k \pi r^2 = \pi r^2 - 2A_2 \qquad (1)$$

Now if $\frac{\pi}{2} > \alpha > \frac{\pi}{4}$, from Roark (77)

$$A_2 = \frac{2}{3} r^2 \alpha^3 (1 - 0.2 \alpha^2 + 0.019 \alpha^4) \qquad (2)$$

$$\text{and } x_2 - x_1 = 0.2 r\alpha^2 (1 - 0.0619 \alpha^2 + 0.0027 \alpha^4) \qquad (3)$$

Similar expressions may be obtained if $\frac{\pi}{4} > \alpha$

Hence for a given mean axial tensile stress σ_s, the areas A_1, A_2 can first be determined from equation (1). The angle α subtended by the segment A_2 can then be found from equation (2) and the centroid of the segment found from equation (3). The ultimate moment can then be determined. Using a numerical solution procedure this was done for $\sigma_s = \frac{1}{3}\ \sigma_y$ and $\sigma_s = \frac{2}{3}\ \sigma_y$.

Thus if $\sigma_s = \frac{1}{3}\ \sigma_y$,

$$A_1 = \frac{1}{3}\ \pi r^2 = A_2$$

$$\alpha = 1.30$$

$$x_1 = 0.267\ r$$

$$x_2 = 0.572\ r$$

$$\therefore M_{p,\frac{1}{3}} = 0.150\ \phi^3\ \sigma_y$$

Similarly if $\sigma_s = \frac{2}{3}\ \sigma_y$,

$$A_1 = \frac{2}{3}\ \pi r^2\ ,\quad A_2 = \frac{1}{6}\ \pi r^2$$

$$\alpha = 0.984$$

$$x_1 = 0.554\ r$$

$$x_2 = 0.737\ r$$

$$\therefore M_{p,\frac{2}{3}} = 0.096\ \phi^3\ \sigma_y$$

If a rigorous analytical solution of the equations (1), (2) and (3) is carried out, a cumbersome expression can be derived for M_p. However an approximate expression can be found by using an expression similar to that which can be derived for a rectangular section prism. Here,

$$M_{p,k} = \frac{bd^2}{4} \sigma_y (1 - k^2)$$

$$= M_{p,o}(1 - k^2)$$

where $M_{p,o}$ is the ultimate moment capacity with no concurrent axial force and $M_{p,k}$ is the ultimate moment capacity with a concurrent mean axial stress of $k.\sigma_y$

If a similar expression is assumed for a circular prism,

$$M_{p,k} = M_{p,o}(1 - k^2)$$

$$\underline{M_{p,k} = \frac{1}{6} \phi^3 \sigma_y (1 - k^2)} \qquad (4)$$

Comparing this expression with the numerical solutions for $k = \frac{1}{3}, \frac{2}{3}$

$$M_{p,\frac{1}{3}} = 0.148 \ \phi^3 \sigma_y \qquad (\text{cf } 0.150 \ \phi^3 \sigma_y)$$

$$M_{p,\frac{2}{3}} = 0.093 \ \phi^3 \sigma_y \qquad (\text{cf } 0.096 \ \phi^3 \sigma_y)$$

Thus equation 4 is an acceptable approximation.

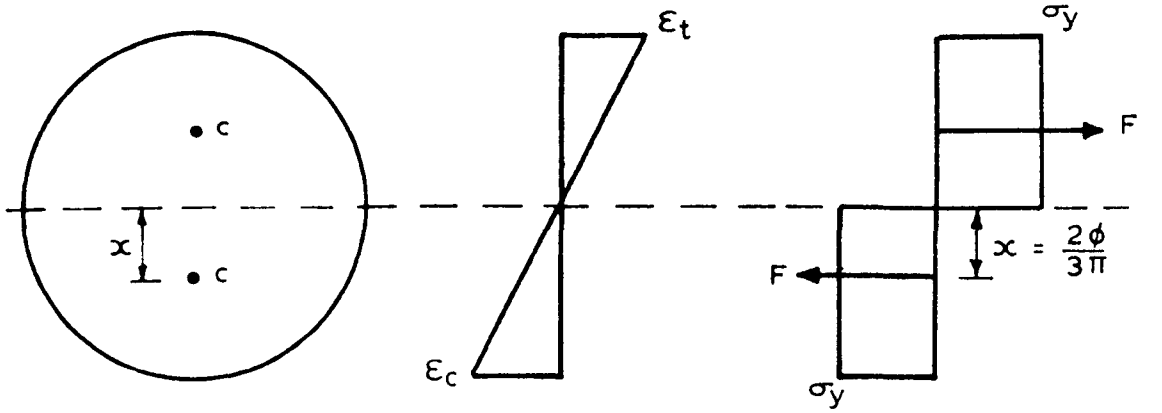

Section. Strain Distribution. Stress Distribution and Stress Resultants.

FIGURE A2.1. PURE BENDING OF A CIRCULAR SECTION.

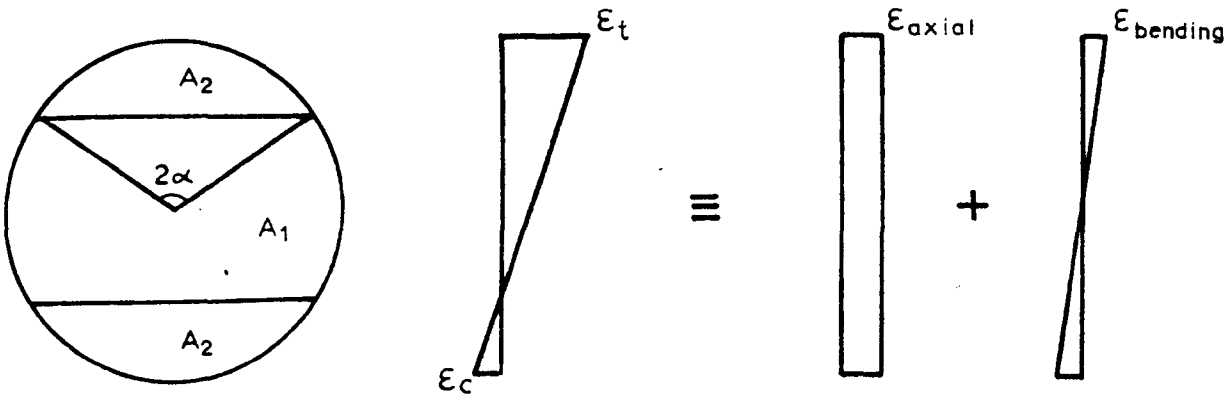

Section. Strain Distribution.

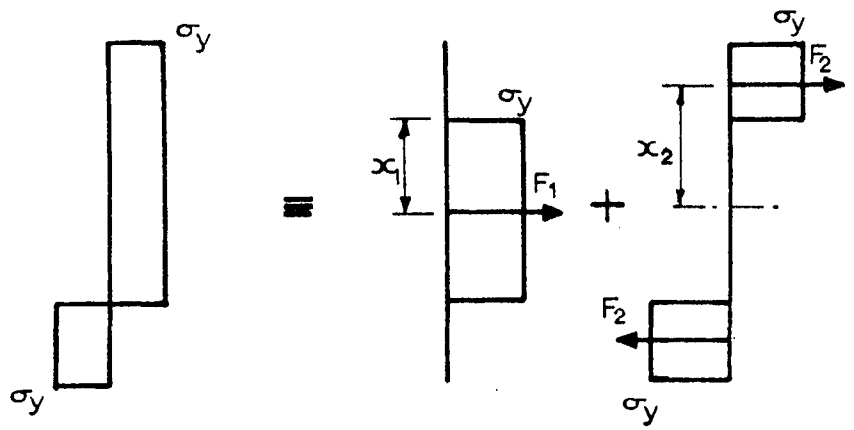

Stress Distribution and Stress Resultants.

FIGURE A2.2. BENDING PLUS AXIAL LOADING OF A CIRCULAR SECTION.